Universitá degli studi di Napoli Federico II
Facoltá di Scienze MM.FF.NN

Dottorato di ricerca Fisica
XXIII ciclo
A.A. 2009/2010

Multiwavelength study of interacting and peculiar galaxies.

Author
Spavone Marilena

Advisors
Prof. G.Longo
Dr. E. Iodice

Co-Advisors
Prof. L. Milano
Dr. O. Pisanti

Ai miei genitori

Contents

INTRODUCTION **1**

1 Cosmic structures formation **4**
1.1 Introduction: basic cosmological facts 5
1.1.1 Basic empirical properties 6
1.1.2 Simple cosmological models 7
1.2 Small-scale structures: how did galaxies form? 8
1.3 The Hot Dark Matter model 10
1.4 The Cold Dark Matter model 11
1.5 Hierarchical structure formation in CDM models 14

2 Galaxy formation **16**
2.1 Morphological classification: the Hubble Sequence for Galaxies 17
2.1.1 Elliptical galaxies 17
2.1.2 Spiral galaxies 18
2.1.3 Lenticular galaxies 20
2.1.4 Irregular galaxies 22
2.2 Peculiar and interacting galaxies 23
2.3 The light distribution in galaxies 24
2.3.1 Elliptical galaxies 26
2.3.2 Spiral and lenticular galaxies 26
2.4 Galactic structure formation 27
2.4.1 Disk formation 27
2.4.2 Spheroid formation 32
2.5 Scaling relations 36

2.5.1 The Faber-Jackson Relation and the Fundamental Plane 37
2.5.2 The Tully-Fisher Relation for Spiral Galaxies 37
2.5.3 Luminosity-Metallicity Relations 39
2.6 The Properties of Galaxies: Correlations Along the Hubble Sequence 41

3 Galaxy interactions: An overview 43
3.1 Galaxy orbits 44
3.2 Gravitational interactions 44
3.2.1 Mergers 44
3.2.2 Tidal destruction 45
3.2.3 Cold accretion 46
3.2.4 Harassment 47
3.3 Hydrodynamical Interactions 48
3.3.1 Ram pressure 48
3.4 Numerical methods for modeling galactic interactions 49
3.4.1 N-Body Methods 49
3.4.2 Gas-Dynamic Methods 51
3.5 Signatures of galaxy interactions 52
3.5.1 Bridges and Tails 52
3.5.2 Wavelike Tidal Spirals 53
3.5.3 Cartwheel galaxies 55
3.5.4 Damaged ellipticals 56
3.6 How galaxies accrete mass? 57
3.6.1 Shells and other fine structures 57
3.6.2 Polar Rings 59
3.6.3 Destruction of satellites 59
3.7 The role of environment 61
3.8 Mergers and morphology 62
3.9 Further questions 64

4 The tidal accretion scenario 65
4.1 Early type galaxies 65
4.1.1 Dynamical subsystems 66
4.1.2 Dust lanes 66
4.1.3 Shells and ripples 67
4.2 Secular evolution by accretion 67
4.3 Revisiting the formation history of the minor axis dust lane galaxy NGC1947 69

5 The cold accretion scenario **97**
5.1 Polar Ring Galaxies 97
5.1.1 Morphology of PRGs 98
5.2 Formation scenarios for Polar Ring Galaxies 101
5.2.1 Accretion scenario 102
5.2.2 Merging scenario 103
5.3 Galaxy Buildup by Gas Accretion 105
5.4 Dynamical models for Polar Ring Galaxies 110
5.5 Chemical abundances in the polar disk of NGC4650A: implications for cold accretion scenario 114
5.6 Chemical abundances of the PRGs UGC7576 and UGC9796: testing the formation scenario 145

6 The merging scenario **168**
6.1 Spherical systems 168
6.2 Disk/Halo systems 171
6.3 Gas dynamics in merging disk galaxies 173
6.4 Compact Groups of Galaxies 174
6.4.1 Spatial distribution and environment 176
6.4.2 Structure and morphology 177
6.4.3 Far Infrared Emission 181
6.4.4 Star formation and nuclear activity 181
6.4.5 Diffuse light 184
6.4.6 Cool gas 184
6.4.7 Hot gas 185
6.5 Hickson 62. I. Kinematics of NGC4778. 186
6.6 Shakhbazian Groups of Galaxies 204
6.6.1 Selection criteria 204
6.6.2 Mean properties 205
6.7 Characterizing Shakhbazian Groups of Galaxies 207
6.8 The role of dry mergers in galaxy formation 219
6.8.1 Morphological signatures 220
6.9 CSL-1: a prototype of dry merger caught in the act 222

7 Conclusions **235**

Publications & Proposals **241**

Bibliography **244**

List of Figures

1.1 The large-scale structure in the local universe, also known as "Fingers of God". 5

2.1 The Hubble sequence of galaxies. 18
2.2 The elliptical galaxy M87, appears near the center of the Virgo cluster of galaxies. 19
2.3 The spiral galaxy M51, also known as the "Whirlpool Galaxy". 21
2.4 The lenticular galaxy M102, located in the constellation Draco. 21
2.5 Barnard's Galaxy or NGC 6822, a small irregular galaxy only 14 degrees East of the galactic plane in Sagittarius. 22
2.6 The peculiar galaxy Centaurus A. 23
2.7 The strange pair of interacting galaxies known as the "Antennae". 24
2.8 A simulation of a close encounter between two disc galaxies which approach each other on prograde orbits. It can be seen that the outer rings of stars are torn off each galaxy, forming the remarkable "Antenna" structures (Toomre & Toomre, 1972). 25
2.9 Fundamental Plane from Djorgovski & Davis (1987). The figure plots a linear combination of surface brightness and log velocity dispersion against log effective radius; thus, the 3-dimensional plane is rotated for an edge-on view. 38

2.10 The stellar mass-gas phase metallicity relation for 53,400 star-forming galaxies from the SDSS. The large black points represent the median in bins of 0.1 dex in mass which include at least 100 data points. The thin line through the data is a best-fitting smooth curve and the solid lines are the contours which enclose 68% and 95% of the data (Tremonti et al., 2004). 40

3.1 These two galaxies are known collectively as Arp 87. The bridge between them is made of stars, gas, and dust. It spans 75,000 lightyears, and shows that there is a gravitational connection between the two galaxies. At one point, the two galaxies came close to each other and a "violent gravitational battle" ensued. This type of connection is relatively common, and it is expected that the two galaxies will eventually join to create one larger galaxy. The blue spots on the galaxy on the right are regions where new stars have recently formed. This was likely a result of the interaction between the two galaxies. 53
3.2 The spiral galaxy Arp 188, the Tadpole Galaxy. Its eye-catching tail is about 280 thousand light-years long and features massive, bright blue star clusters. Probably a more compact intruder galaxy crossed in front of Arp 188 - from left to right in this view - and was slung around behind the Tadpole by their gravitational attraction. During the close encounter, tidal forces drew out the spiral galaxy's stars, gas, and dust forming the spectacular tail. 54
3.3 *Left panel* - Ground based image of the "antennae" galaxies. *Right panel* - Computer model of two identical disk galaxies in interaction (Toomre & Toomre, 1972). 54
3.4 The prototypical shell galaxy NGC 3923. 58

4.1 Color composite image of NGC1947 assembled from EMMI-NTT images in the V (blu channel), J (green channel) and K (red channel) bands. The North is up, while the East is on the left of the image. 72
4.2 Calibrated K (left panel) and V (right panel) images of NGC1947 75
4.3 Ellipticity (ϵ), Position Angle (P.A), mean surface brightness profile and shape parameter a_4/a in the J and K bands. 77

4.4 Light profiles along the minor (top-left panel) and major (bottom-left panel) axis of NGC1947 in the V (stars) and R band (triangles). Light profiles along the minor (top-right panel) and major (bottom-right panel) axis of NGC1947 in the J (stars) and K band (triangles) 79
4.5 V-R color profiles along the minor (top panel) and major (bottom panel) axis of NGC1947. 80
4.6 *Left panel* - V-K color profiles along the major (top panel) and minor (bottom panel) axis. The straight line correspond to the average V-K color for $r \geq 10$ arcsec. *Right panel* - V-K color map. The North is up, while the east is on the left of the image. Darker colors correspond to redder galaxy regions. 81
4.7 *Left panel* - J-K color profiles along the major (top panel) and minor (bottom panel) axis. *Right panel* - J-K color map. The North is up, while the east is on the left of the image. Lighter colors correspond to redder galaxy regions. 81
4.8 Top panel - 2-D fit of NGC1947 light distribution. The observed light profile along the major axis, is compared with those derived by the fit (continuous line). Bottom panel - Residuals between the observed and the fitted light profiles. . 83
4.9 Top panel - 2-D fit of NGC1947 light distribution. The observed light profile along the minor axis, is compared with those derived by the fit (continuous line). Bottom panel - Residuals between the observed and the fitted light profiles. . 84
4.10 2D fit of NGC1947. Left panel - K band image of NGC1947. Middle panel - Model of the galaxy. Right panel - Residual image. 84
4.11 Residuals of the subtraction of the K band model to the V band image. 85
4.12 Stellar (filled points) and gaseous (triangles) rotation curves along the major (bottom panel) and minor axis (top panel) of NGC1947. The dashed line is the velocity of the galaxy center. In the bottom-right corner is plotted the error bar that represents the mean error on the velocity of the gas. . . . 87
4.13 Stellar (filled points) and gaseous (triangles) rotation curves along the minor axis of NGC1947 superposed on the position-velocity plot of the HI along the $P.A. = 127\circ$ presented by Oosterloo et al. (2002). 88
4.14 Image of a field of 25 arcmin around NGC1947. The two boxes on the left show the HI distribution for NGC1947 and ES0 085-GA088 published by Oosterloo et al. (2002). 90

4.15 V-K color measured within 1kpc apertures as a function of the Toomre sequence merger stage. The dotted horizontal line indicates the V-K color for a SSP $10^{10}yr$ population of solar metallicity, which provides a reasonable fit to the measured colors for early-type galaxies. 92
4.16 J-K color measured within 1kpc apertures as a function of the Toomre sequence merger stage. The dotted horizontal line indicates the J-K color for a SSP $10^{10}yr$ population of solar metallicity. 93
4.17 Continuous line shows the prediction of our model (see text); filled squares are V, J, and K integrated data given in sec. 4.3, the other data are from NED, in particular IRAS data at 12, 25, 60 100 μm and ISOPHOT data at 170 μm of Stickel et al. (2004). 95

5.1 Narrow polar ring around the galaxy NGC2685. 99
5.2 Wide polar ring around the galaxy NGC4650A. 99
5.3 Multiple ring galaxy. 100
5.4 Low inclined ring around a galaxy. 100
5.5 Distribution of gas and dark matter in a 2 Mpc wide slice of simulation by Macciò et al. (2006) centered on a galactic mass dark matter halo. The gas temperature is colored purple-white in a logarithmic temperature scale from 10^4 to 10^6 K. The narrow filament of gas flowing into the halo is at a temperature of $\sim 2 \times 10^4$ K. The filament in the dark matter is significantly wider than the gas and consists of a smooth component and many smaller halos. The entire simulation volume is 90 Mpc^3 and is centered on a region forming several galaxies, which are simulated at a higher resolution than the rest of the cube. The masses and softening of the dark matter and gas particles are 4.90×10^5, $9.75 \times 10^4 M_\odot$; and 0.2, 0.15 kpc, respectively. The polar ring would appear face-on in this projection, perpendicular to the filament. 108
5.6 (a) Hubble Space Telescope image of the classic polar ring galaxy NGC 4650A (side length: 24 kpc), courtesy of the Hubble Heritage site, Space Telescope Science Institute. (b), (c) and (d) Smoothed images of the stars and gas of the simulated galaxy in different projections (side length 35 kpc): (b) inclined 20°, (c) with the ring edge-on and (d) face-on. The face-on image shows a clumpy distribution of gas that lies in two slightly offset rings. 109

5.7 Dark Halo shape proposed by Sackett et al. (1994) for NGC4650A; a pseudoisothermal ellipsoid with a vertical-to-radial axis ratio of $0.3 \leq c/a \leq 0.4$, i.e. an E6/E7 flattening and $M_{DH}(R = 10kpc) \sim 4 \times 10^{10} M_{\odot}$ 111
5.8 Dark Halo shape proposed by Combes & Arnaboldi (1996) for NGC4650A; an E7 flattened halo aligned with the polar disk, with $M_{DH}(R = 10kpc) \sim 1.4 \times 10^{10} M_{\odot}$ 112
5.9 Optical image of NGC4650A with superimposed the slits used to acquire data analyzed in this work. 117
5.10 1-D spectrum of the standard star LTT4816, used to flux-calibrate the spectra. The black line represent the spectrum of the star acquired in the blue wavelength range, while the red line is the same star acquired in the red range. 120
5.11 *Top panel* - Spectrum of NGC4650A in the blue wavelength range, corresponding to the region marked as A in the Fig. 6.2. *Middle panel* - Spectrum of the region B in the Fig. 6.2. *Bottom panel* - Spectrum of the region C in the Fig. 6.2, where are clearly visible the absorbing features of the line H_{γ} and H_{β}. 122
5.12 *Top panel* - Spectra of NGC4650A in the red wavelength range, corresponding to the region marked as A in the Fig. 6.2. We divided the spectra in A1 and A2 in order to obtain a better visualization of the lines. *Bottom panel* - Spectrum of the region B (B1 and B2 as explained below) in the Fig. 6.2. . . . 123
5.13 Oxygen abundance, obtained by using the empirical calibration introduced by Pilyugin (2001), versus oxygen abundance parameter R_{23} (see Sec. 5.5). 127
5.14 Oxygen abundance derived with empirical methods proposed by Pilyugin (2001) versus radius. The values in Tab. 5.3 were binned each 5 arcseconds. The superimposed lines are the linear best fit derived by Pilyugin et al. (2006); the red line represents the best fit to the abundance of oxygen-rich spirals, while the blue line is those related to ordinary spirals. The black line is the best fits obtained for NGC4650A. 128
5.15 Electron temperature along the polar disk of NGC4650A. The filled circles correspond to the observed T[OIII], the starred points correspond to the T[OII] estimated by the photoionization model (see Sec. 5.5 for details), the open square corresponds to the average value of T[OII] directly estimated by the ratio $R_{OII} = OII[3727]/[7325]$. In the bottom left side of the plot the mean error is shown. 131

5.16 Oxygen abundance derived with direct method. Squares are the values derived by using the observed $T[OII]$ estimates; stars are those derived by using the $T[OII]$ from photoionization models. See Sec. 5.5 for details. The errors on oxygen abundance is 0.5. 132
5.17 Oxygen abundance vs absolute blue magnitude for CNELGs (yellow filled circles), ELGs (cyan open circles), four field galaxies with emission lines (filled black circles), nearby dwarf irregulars (open triangles), local spiral galaxies (open circles), local HII galaxies (open squares), NGC4650A (star) and the polar disk galaxy IIZw71 (Pérez-Montero et al., 2009). The dashed line indicates the solar oxygen abundance. The arrow indicates the shift of the value of the oxygen abundance if we use the direct methods to evaluate it. The total B-band magnitude for NGC4650A ($M_B = -19.3$) has been evaluated by using the same value of H_0 used by Kobulnicky & Zaritsky (1999) in order to compare NGC4650A with galaxies in their sample 134
5.18 R-band image of the Polar Ring Galaxy UGC7576 150
5.19 Optical image of the Polar Ring Galaxy UGC9796, obtained by the authors at TNG telescope. 151
5.20 Optical image of UGC7576 (left) and UGC9796 (right), with superimposed slits used to acquire data analyzed in this work. 153
5.21 Spectrum of UGC7576. 154
5.22 Spectrum of UGC9796. 155
5.23 Oxygen abundance vs absolute blue magnitude for CNELGs (yellow filled circles), ELGs (cyan open circles), four field galaxies with emission lines (filled black circles), nearby dwarf irregulars (open triangles), local spiral galaxies (open circles), local HII galaxies (open squares), NGC4650A (red star) (Spavone et al. 2010), the polar disk galaxy IIZw71 (Perez-Montero et al.2009), UGC7576 (black star) and UGC9796 (blue star) (this work). The dashed line indicates the solar oxygen abundance. The total B-band magnitude for NGC4650A, UGC7576 and UGC9796 ($M_B = -19.3$, $M_B = -19.8$ and $M_B = -19.4$) have been evaluated by using the same value of H_0 used by Kobulnicky et al. (1999) in order to compare our galaxies with those in their sample 159

5.24 Oxygen abundance derived with P- method, proposed by Pilyugin (2001), versus radius. The superimposed lines are the linear best fit derived by Pilyugin et al. (2006); the red line represents the best fit to the abundance of oxygen-rich spirals, while the blue line is those related to ordinary spirals. The black line is the best fit obtained for NGC4650A, while the magenta line is the best fit obtained for UGC7576. 161
5.25 Optical image of UGC9796 and its two nearest companion galaxies, MCG +07-31-049 (number 1) and CGPG 1514.2+4320 (number 2). 166

6.1 Morphology-velocity correlation for compact groups. 179
6.2 B band image of HCG62 with the slit overlayed. The dashed lines overlayed on the slit represent the directions along which we have extracted the light profiles presented in fig.6.6. 190
6.3 Observed spectrum of NGC4778. The main absorption features used for the kinematical analysis are marked. 191
6.4 Top panel - Ellipticity, position angle (P.A.) and diskiness for NGC4778. The solid line indicates R_e. The trends of all parameters are different from those of $r < R_e$. Bottom panel - The same as above for the nuclear region of NGC4778. The first dashed line indicates the limit over which the data points are not affected by the seeing. The second dashed line marks the region discussed in the text. 193
6.5 Mean B-R color profile of NGC4778. The dashed line indicates the limit of reliability of the photometry. 194
6.6 Top panel - 2-D fit of NGC4778 light distribution. The observed light profiles along the major (open circles), and minor axis (asterisk), are compared with those derived by the fit (continuous line). Bottom panel - Residuals between the observed and the fitted light profiles. 195
6.7 Top panel - Rotation curve and velocity dispersion profile derived for the whole slit length, which include both galaxies NGC4778 and NGC4761 (labelled on the plot as A and C respectively). Bottom panel - Uncalibrated light profile through the slit, which includes both galaxies NGC4778 and NGC4761; the dashed lines indicates the region of the spectrum used to derive the kinematics. 197

6.8 Rotation curve and velocity dispersion profile derived for NGC4778 for the whole galaxy extension (top panel) and for the nuclear regions (bottom panel) The vertical solid lines marks the regions discussed in the text. 199
6.9 Comparison of the uncalibrated light profile along the slit in the NE and SW directions. The data-points were binned to reach a minimum signal-to-noise of 50. 200
6.10 Photometric versus SDSS spectroscopic redshifts for galaxies in the SHK 348 region. The plot shows all objects within 3 Mpc, from the group centroid, with available SDSS spectroscopic redshift. Only a few compact group members, i.e. within the central 200 kpc, have spectroscopic redshift. 208
6.11 **Left panel:** normalized f(E) distributions for the inner regions of the SHKGs (solid line), and of the HCGs (dotted line). **Right panel:** Early-Type fraction distributions for SHKGs in the core ($r < 150$ kpc, solid line), local environment ($150 < r < 1000$ kpc, dotted line) and background ($2 < r < 3$ Mpc, dashed line). 210
6.12 Background subtracted group richness estimated within 150 kpc versus background subtracted richness within 500 kpc. The line shows the expected locus for isolated compact groups. Groups with $f(E) < 0.8$ and $f(E) \geq 0.8$ are plotted, respectively, as grey asterisks and black dots. The size of the symbols is scaled according to the group redshift. **Left panel:** Shakhbazian groups. **Right panel:** Hickson groups. 211
6.13 Extension index vs N_{150} for SHKs (left panel) and HCGs (right panel). Solid line for extension index = 1.5 is plotted. Groups with $f(E) < 0.8$ and $f(E) \geq 0.8$ are plotted, respectively, as grey asterisks and black dots. 211
6.14 We observe a tentative evidence that more concentrated SHK groups (grey filled histogram) have lower velocity dispersion than less concentrated ones (open black histogram), thus suggesting that the total mass plays a significant role in the evolution of these structures. However the small statistics does not allow to draw significant conclusions, especially when groups with less reliable velocity dispersion estimates ($\sim 2/3$ of the total) are removed from the sample. Furthermore the subsample of SHK groups with measured velocity dispersions is strongly biased toward rich/extended structures. 212
6.15 Comparison between our richness measurements and those performed by Tovmassian et al. (2006) 216

6.16 Comparison between the mass to light ratio measurements in our sample and those performed by Tovmassian et al. (2006) . 216
6.17 Extention index versus N_{150} for SHK groups. Solid line for extention index = 1.5 is plotted. 217
6.18 Extention index versus σ for SHK groups. A logarithmic scale on x-axis is used. 218
6.19 Comparison between the velocity dispersion of groups in our sample and those estimated by Tovmassian et al. (2006). . . . 218
6.20 Comparison between the masses of groups in our sample and those estimated by Tovmassian et al. (2006). 219
6.21 Left: The HST image of the CSL-1 region in the F814W band. Right: CSL-1 image in pseudocolor. 224
6.22 Spectra of the E (left) and W (right) components of CSL-1. The raw spectrum is shown on the bottom while a slightly smoothed version is showed above it. Flux normalization is arbitrary. 225
6.23 Flux calibrated spectra of the two components of CSL-1. . . . 226
6.24 Radial profiles of the E (left) and W (right) components of CSL-1. An $r^{1/4}$ profile with the best fit R_e is shown for comparison. 227
6.25 The normalized residuals (residuals/model) obtained by subtracting from the HST images a model consisting of two Sersic light profiles. Crosses mark the centroids of the two galaxies. . 228
6.26 The CSL1 components on the Kormendy (left), adapted from Hamabe & Kormendy (1987) and Faber-Jackson (right), adapted from Faber & Jackson (1976) relations. 230
6.27 The four panels show the age and the metallicity distribution for the E (left) and W (right) galaxies respectively. Quantities were derived by fitting the VLT optical spectra with the software STARLIGHT. 231
6.28 One of our simulations (left two panels) and residuals obtained from a 2D Sersic fit (rightmost panel). 232
6.29 Radial profiles of the E and W components of the simulations shown above, compared with the actual data 233
6.30 One of our simulations (left two panels) and residuals obtained from a 2D Sersic fit (rightmost panel). 233
6.31 Radial profiles of the E and W components of the simulations shown above, compared with the actual data 234
6.32 Galaxy number counts in the CSL-1 field using different SExtractor theresholds, and compared to OAC-DF and HDF counts. 234

List of Tables

4.1 General properties of NGC1947 73
4.2 Magnitudes and Colors for NGC1947 in circular aperture. . . . 83

5.1 Observed and de-reddened emission lines fluxes relative to H_β in the $3300 - 6210$ Å wavelength range. 142
5.2 Observed and de-reddened emission lines fluxes relative to H_β in the $5600 - 11000$Å wavelength range 143
5.3 Oxygen and Sulphur abundance parameters and oxygen abundances for the polar disk in NGC4650A 144
5.4 Oxygen abundances for the polar disk in NGC4650A derived by the T_e method 146
5.5 Global properties of UGC7576 and UGC9796 compared to those observed for NGC4650A. 152
5.6 Oxygen abundances and metallicities of UGC7576 and UGC9796 compared to those observed for NGC4650A. 157
5.7 Discriminant parameters between different formation scenarios 167

6.1 Summary of the properties of the Hickson 62 members. Data are taken from Nasa/IPAC Extragalactic Database. 189
6.2 Main results for SHK's group 215
6.3 General properties of CSL-1 224
6.4 2D fitting results from F814W ACS images 227

ABSTRACT

I present a multiwavelength study of a sample of peculiar galaxies in order to constraint the physics of interacting objects, to study how the physical processes affect the structure of galaxies, and to derive some hints on the formation and evolution history of such galaxies.

One of the major open issues in modern cosmology is to understand how galaxies formed and evolved. Its likely that the formation of galaxies was dominated by two processes: the assembly of luminous and dark matter through accretion and merger, and the conversion of baryonic and non-baryonic matter into stars. This is the reason why the study of galaxy interactions has received an increasing attention both on the observational and the theoretical sides. Several theoretical works based on numerical simulations, have tested different plausible scenarios for the origin of peculiar galaxies, such as "Tidal accretion", "Cold accretion" and "Merging". For this reason, the sample of galaxies to use was selected in order to reproduce all these mechanisms.

The first peculiar object that I studied is the minor axis dust lane galaxy NGC1947. I performed a detailed study of the main properties of this galaxy (Spavone et al., 2009). In NGC1947 are present components with different angular momentum, infact gas and dust rotate along the minor axis while stars rotate along the major one. This is a clear evidence that it cannot be the result of a single protogalactic cloud collapse, but rather the result of an interaction event. I performed a detailed study of the main properties of this galaxy and compared them with the prediction of simulations. Putting together all this evidences it was difficult to disentangle in a non ambiguous way the two possible scenarios, even though some aspects can help us in understanding. First of all, the galaxy does not present clear signs of interaction, such as tidal tails and so on, and this leads to the conclusion that the merger occurred about 10 Gyrs ago, a fact which is not consistent with the fact that, according to my estimate, the last burst of star formation occurred 1 Gyr ago. So I can say that the accretion scenario is favoured.

The second object in my sample is the Polar Ring Galaxy (PRG) NGC4650A. I used high resolution NIR and optical spectroscopy along the North and South side of the polar disk, to measure the metallicity of the HII regions in the polar disk of this galaxy because, if it formed from the accretion of external cold gas from cosmic web filaments, we expect metallicities similar to those of late type galaxies, while if the metallicities are similar to those of early type galaxies, the accretion from a gas rich donor is favoured. I estimated the metallicity by using both direct and empirical methods, the Stellar Formation Rate (SFR), and the metallicity gradient along the disk. The average metallicity for the polar disk of NGC4650A turned out to be $Z = 0.2Z_{\odot}$, which is lower than the typical values found in spiral galaxies, and is instead consistent with the metallicities predicted for the formation of disks by cold accretion processes ($Z \sim 1/10Z_{\odot}$), due to the

accretion of pristine gas in the cold streams. Moreover, also the absence of any metallicity gradient is consistent with the infall of metal-poor gas from outside which is still forming the disk (see Spavone et al. 2010 for details).
As a follow up of this work, I obtained observing time at the TNG telescope to observe the PRGs UGC7576 and UGC9796. I performed the study of the chemical abundances also for these galaxies in order to constrain their formation history (Spavone et al. in preparation). Both PRGs have metallicities (respectively 0.4 $Z_{\odot}$ and 0.1 $Z_{\odot}$) lower than that observed in spiral galaxies of the same total luminosity and, given their present star formation rate, this values is again consistent with the predictions of the cold accretion mechanism for disk formation.

UGC7576 is an isolated galaxy and the absence of close companions led to exclude both the tidal accretion from a donor galaxy and the merging with another galaxy. UGC9796 is instead in a group and has 5 close companions with an amount of HI gas comparable with that of UGC9796. The merging scenario is however ruled out because in order to produce a massive polar disk such as those observed in UGC9796 is required a merging with high mass ratios (7:1 or 10:1) and this would destroy the ordered motion of the central galaxy, transforming it into an elliptical-like, not rotationally supported galaxy. In conclusion, for this object, both the tidal accretion and the cold accretion seem to be plausible scenarios.

Finally, to analyze also another type of merging process, I am studying the pair of interacting galaxies known as CSL-1. By using high resolution spectroscopy (FORS1@VLT) and imaging (HST) I am studying the morphology, light distribution and structural parameters of this system, to test the dry-merger scenario (cf. "A prototype dry-merger caught in the act", M. Paolillo , G. Covone, C. Nipoti, M. Spavone, M. Capaccioli, G. Longo, A.Cimatti, L. Ciotti, in preparation).

In order to investigate also the minor merging processes I also studied the photometric and kinematical properties of a compact group of galaxies belonging to the Hickson's catalogue. The group analyzed in this work was HCG62, one of the nearest group in the celestial Southern hemisphere, which was selected by cross correlating the available X-ray and optical data.

Galaxies in compact groups are in a very dense configuration in the sky, having a mean separation comparable with their dimensions and a very low velocity dispersion. Taking into account that theories on formation and evolution of galaxies predict that the intensity and frequency of interactions strongly depend on the density of the environment, compact groups may be considered the ideal place where to test interaction processes, such as dynamical friction, tidal interaction, collisions, merging and so on.

The main goal of this part of my work was to derive some hints on the formation and evolutionary history of compact groups, in order to address the possible scenario for the formation of structure in the Universe, and to determine the evolutionary status of the studied objects. To this aim, I performed a detailed study of the kinematical properties of HCG62, that revealed the presence of many peculiarities in the dominant galaxy of the group, NGC4778, such as the presence of a

kinematically decoupled and counter-rotating core (KDC), or kinematical profiles strongly perturbed, also in the outer regions of this galaxy.

Moreover, I also performed an analysis of the photometric properties of the whole group, to look for correlations between kinematical and photometric peculiarities. The absence of such correlations in HCG62, can be explained by stating that weak interactions do not perturb the rotation curves but produce morphological deformations in the outer regions, while the so called minor mergers perturb the rotation curves in the inner regions, without producing morphological peculiarities. The results obtained in this work are in good agreement with similar studies performed on the same group and with its observed X-ray properties (Spavone et al., 2006).

I was also Co-Investigator in two accepted proposals to observe, with the TNG telescope, a sample of Shakhbazian galaxy groups, with the aim of building a larger statistical sample and obtain redshift informations which are lacking for most Shakhbazian groups, and are needed to establish on firm grounds their physical nature. Groups of galaxies have been extensively studied in the past decades. Despite this effort, their evolution is yet not well understood. Loose groups are almost certainly still collapsing and are therefore crucial to uncover the formation processes shaping cosmic structures. As it was already mentioned, in compact groups a few member galaxies are compressed in a small volume of space with low relative velocities. Early theoretical studies suggested that in such high density environments the low velocity dispersion of compact galaxy groups would favor strong interactions and mergers, leading to rapid evolution (within $\sim 10^9$ yrs) into a single massive merger remnant. The best studied sample of compact groups to date is the one included in the Hickson catalogue; this sample however, is biased towards extremely high values of matter density and therefore it allows to investigate only the "close-to-final" stage of the complex dynamical evolution of groups. The density range bridging the field to these almost coalesced structures is still poorly explored, mainly due to the difficulties encountered in constructing reliable samples of 'physically bound', low multiplicity groups.

Shakhbazian Groups of galaxies (SHKGs) in spite of having been originally selected as "compact groups of compact galaxies", have been shown to sample a large range of spatial densities. To properly characterize the properties of these groups and their evolutionary path, I obtained more accurate redshift determination for a sample of 10 SHK, so almost doubling the sample of SHK groups, with detailed spectroscopic data. Main goals of this work are: i) obtain redshift estimates for groups without literature data, sampling the different sub-populations; ii) confirm the galaxy membership of the groups, which is currently based on photometric estimates for most of the objects; iii) study the dynamical status of the group and derive dynamical mass estimates; iv) study the stellar population of the member galaxies through comparison with population synthesis models, and the degree of activity from emission line measurements.

INTRODUCTION

This thesis discusses the formation and evolution scenarios for galaxies. I focus on interacting and peculiar galaxies, in order to constrain the physics of interacting objects, to study the processes at work and to try to understand how the structure of galaxies can be modified by them. Finally, I wish to derive some hints on the formation and evolution history of such galaxies.

The study of interacting galaxies is of crucial importance; in fact, despite the fast development of scientific instrumentation and analysis methods, one of the major open issues in modern cosmology is to understand how galaxies formed and evolved. Since 1950 it was clear that galaxies are not island universes and that they interact with their neighbors. The observations in fact show that about 6% of galaxies are peculiar, in the sense that they cannot be associated with any standard galaxy type. Most of these peculiarities can be understood in terms of disruptions or deformations induced by the tidal pulls experienced during close interactions with nearby objects. It has been shown that gravitational interactions and mergers affect the morphology and dynamics of galaxies from the Local Group to the high-redshift universe (e.g. Conselice et al. 2003a; Bundy et al. 2004; Lin et al. 2004; Kartaltepe et al. 2007; De Propris et al. 2007; Lotz et al. 2008).

Furthermore, the hierarchical, merger-dominated picture of galaxy formation is based on the Cold Dark Matter (CDM) model (Cole et al., 2000a), which predicts that observed galaxies and their dark halos (DH) were formed through a repeated merging process of smaller systems (De Lucia et al. 2006; Genel et al. 2008).

In this framework, major and minor mergers of disky systems do play a major role in the formation of spheroid and elliptical galaxies (Naab et al. 2007; Bournaud et al. 2007), in all environments and from the Local Group to high-redshift universe (Conselice et al., 2003b); in fact the observational results support the scenario in which the merging of two disk galaxies produces spheroidal merger remnants with physical characteristics, such as density profiles, mean velocity dispersion

and surface brightness, quite similar to those observed for E and S0s (Toomre & Toomre 1972; Barnes & Hernquist 1992; Bekki 1998a; Bournaud et al. 2005a).

The gas fraction is a key parameter in the physics of such gravitational interactions. Galaxies can get their gas through several interacting processes, such as smooth accretion, stripping and accretion of primordial gas, which are equally important in the growth of galaxies. The relative share of all gravitational interactions depends on the environments and it drives many morphological features observed in galaxies, such as bars, polar rings and shells (see Malin & Carter 1980) and highly inclined or even counter-rotating rings/disks (see Galletta 1996 for a review).

In the present work I will present an overview of the main interaction processes: *Tidal accretion, Cold accretion* and *Merging*. I will focus on the main properties of the studied objects and in particular on the tracers of their formation history, through pointed and archival data of the Very Large Telescope (VLT) and Telescopio Nazionale Galileo (TNG). I choose galaxies showing the features typical for all the interaction mechanism cited above, in order to reproduce all of them. I also compared the results of our works with the predictions of numerical simulations in order to try to address the most plausible formation scenario for each studied object.

The thesis is organized as follows:
- in chapter 1 I give some basic concepts on cosmic structure formation;
- in chapter 2 I present a review of the different interaction processes proposed so far. I then focus on the three main processes analyzed in the present work;
- in chapter 3 I discuss about the various formation scenarios proposed for both ordinary and peculiar galaxies;
- in chapter 4 I focus on the tidal accretion scenario, present the data analysis concerning the galaxy NGC1947 and discuss the results (Spavone et al., 2006);
- in chapter 5 I present the results of the analysis performed on the Polar Ring Galaxies (PRGs) NGC4650A (Spavone et al., 2010), UGC7576 and UGC9796 and discuss the results obtained for each object separately and on their implications for the cold accretion scenario;
- in chapter 6 I present the results of the study of HCG62 (Spavone et al., 2006), CSL-1 and SHK groups, and discuss the different kind of merging between galaxies.

Acknowledgment

I would like to start with very special thanks to my mother, my sisters, my brother and my brothers-in-law; even if the life gave us a big pain, we hanged together helping each other. I would also like to thank Francesco, for his patience, loving care, aid and moral support.

I would like to thank my supervisors, Prof. Giuseppe Longo and Dr. Enrichetta Iodice, for their scrupulous help and support during the realization of this work

and also for their friendship. Thanks also to my co-advisors, Prof. Leopoldo Milano and Dr. Ofelia Pisanti, for their careful reading of my thesis and for the useful suggestions and discussions that lead to improve this work.

Special thanks are given to Dr. Magda Arnaboldi, Prof. Ortwin Gerhard and all their group of students and collaborators for the assistance and friendship given me while I was in Munich, Germany.

I'm very grateful to my friends Rosa Calvi, Adriana Gargiulo, Gabriele Minervini, Enrico Cascone, Nicola Napolitano and Maurizio Paolillo for many useful discussions and mainly for their friendship and moral support.

This work is to my nephew and my nieces, that will be born soon, and to their guardian angel: my father!

CHAPTER 1

Cosmic structures formation

This Chapter reviews the dominant paradigm for the formation of galaxies and larger structures in the universe: *gravitational instability*. The observed universe appear to be almost spatially uniform on scales larger than about 10^{26} cm. On these scales, given that gravitational dynamics is almost linear, it is relatively easy to relate to observations of large-scale structure. On the other hand, on smaller scales the study of cosmic structure formation is complicated not only by nonlinear gravitational clustering but also by nonlinear nongravitational gas dynamical processes. The complexity of these phenomena makes galaxy formation one of the major open issues of the physical sciences. Significant progress has been made during the last few years, but no fully satisfactory theory can account in detail for the observed cosmic structure.

The currently standard theory of cosmic structure formation assumes that the present day clumpy appearance of the universe developed through gravitational amplification of the matter density fluctuations which were generated in the very early universe. The energy content of the universe and the basic statistics of the initial density field have been determined with a reasonable accuracy from recent observations of the cosmic microwave background, large-scale structure, and distant supernovae. Progress in observations and theory makes now possible to make accurate predictions based on the standard model. Cosmology is now at the stage where we can rigourously test the model against various observations of large- and small-scale structure. In what follows, I review the latest observations and the recent progress in the theory of structure formation at low and high redshifts. Results from state-of-the-art cosmological simulations are also presented.

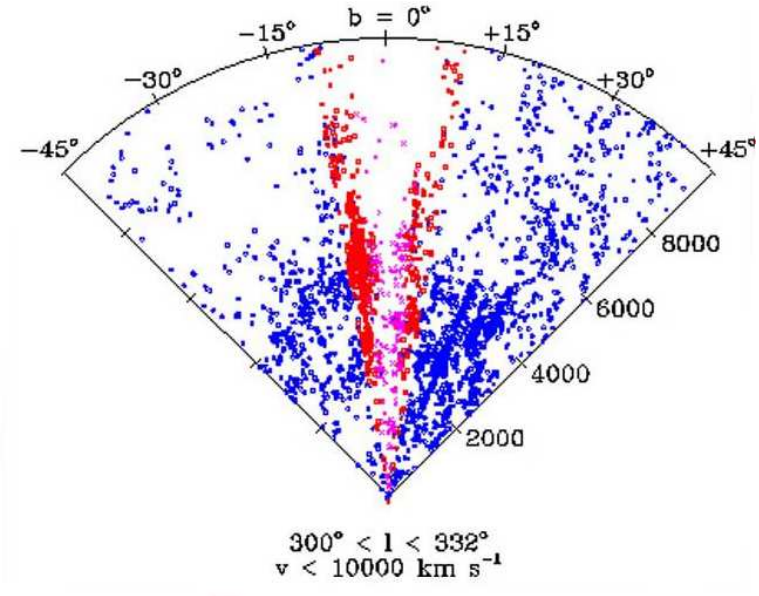

Figure 1.1: The large-scale structure in the local universe, also known as "Fingers of God".

1.1 Introduction: basic cosmological facts

The almost perfectly isotropic feature in the cosmic background radiation temperature shows that the universe "was" homogeneous and isotropic, while a variety of clumpy structures are seen in the local universe, such as galaxies and galaxy clusters. We also find that there are some patterns or prominent "structures" which extend over tens of mega-parsecs (see Fig. 1.1).

If the universe began in a state of near-perfect homogeneity and isotropy, then how did it become so inhomogeneous on small scales? This is the puzzle facing cosmologists sorting through the fossil relics of the early universe: the cosmic microwave background radiation, the chemical elements, the mass both visible and invisible, and the complex patterns - galaxies, clusters and superclusters of galaxies, voids, filaments, and fluctuations - that organize these ingredients. Apparently the universe has undergone a rapid transition from a smooth initial state to the clumpy state as we see today, but details remain largely unknown. Understanding the origin and evolution of the structure of the universe is hence a major goal in modern cosmology. The so-called standard theory of structure formation claims that the present-day clumpy appearance of the universe developed through gravitational amplification of the initial matter density fluctuations together with other physical processes. This basic picture is now supported by an array of observations, including the measurement of the cosmic microwave background anisotropies by the WMAP satellite (Spergel et al., 2003).

1.1.1 Basic empirical properties

Models of structure formation must take into account basic empirical properties of the universe averaged over large scales. Five sets of empirical facts seem especially relevant:

1. **The isotropy of distant objects.** Galaxies are not randomly distributed in space, but rather they gather in groups, clusters, or even larger structures. This means that the probability of finding a galaxy at location $\mathbf{x}$ is not independent on whether there is a galaxy in the vicinity of $\mathbf{x}$. Infact, it is more probable to find a galaxy in the vicinity of another one than at an arbitrary location. A standard statistical measure of this anisotropy is the angular 2-point correlation function $w(\theta)$, giving the relative excess number of pairs of objects separated by angle θ compared with the mean number for a Poisson distribution. Since the Universe is considered statistically homogeneous $w(\theta)$ can only depend on the separation between the objects and not on their individual positions. From the measured correlations we know that for θ in the range of 1° to 3°, $w(\theta) \leq 10^{-3}$ for faint radio sources, while for $\theta = 10^\circ$, $w(\theta) \leq 10^{-4}$ for X-ray sources. Hence, the correlation function provides a means to characterize the structure of the matter distribution in the Universe.

2. **Hubble's linear velocity-distance relation.** The discovery of cosmic expansion was made by Hubble (1929). Galaxies display well known spectral lines, whose wavelengths are found to be shifted relative to their laboratory values, due to the Doppler effect, in rough proportion to the distance r:

$$c\Delta\lambda/\lambda \simeq H_0 r \tag{1.1}$$

where c is the speed of light and H_0 is the Hubble constant. The linear relation is modified for distances so large that $H_0 r/c$ approaches 1. The Doppler interpretation of cosmological redshifts is well established, and $v = cz[1 + f(z)]$ is the recession speed. The most commonly accepted value for H_0 is 72 km $s^{-1}Mpc^{-1}$.

3. **The cosmic microwave background radiation.** In 1965, Penzias & Wilson discovered that the sky glows brightly and uniformly in the microwave at wavelengths of a few cm. The spectrum and isotropy of this radiation have been found to match a blackbody with temperature of $T_0 = 2.73K$. The Cosmic Microwave Background (CMB) anisotropies reflect the conditions in the Universe at the epoch of recombination, thus at $z \sim 1000$. Over the last few years, sensitive and significant measurements of the CMB anisotropy have also been carried out using balloons and ground-based telescopes. In 1992 the *COsmic Background Explorer* satellite (COBE) has placed limits on the deviations from the Planck spectrum of less than 3×10^{-4} relative to the peak intensity.

4. **The abundance of light nuclei.** The most abundant nuclei in the universe are *H* and *He*. All heavier elements - primarily carbon, nitrogen, and oxygen - are grouped together and called "metals". The relative abundances of the metals - but not the light nuclei - can be explained by "nucleosynthesis" occurring in stars

and supernovae. In older stars the mass fraction of He is less than in the Sun, but in no case is convincingly below 0.22. Nucleosynthesis in massive stars produces a much larger ratio of metals to He than 1:10, and stars effectively destroy H and Li. Thus, the light nuclei could not have been produced in stars. The only satisfactory explanation known was proposed by Gamow, Alpher and Herman in the late 1940s (Gamow 1946; Alpher & Herman 1950): the light elements were produced by nucleosynthesis at relatively low temperatures ($\sim 10^9 K$) and high densities for a duration of several tens of seconds.

5. **The existence of large amounts of dark matter.** In the 1930's it was recognized by Zwicky (1933) that galaxies in clusters move too rapidly for the clusters to remain bound, assuming that the galaxies weight no more than the visible stars and gas they contain. In the 1980's, Rubin et al. (1980) discovered that stars and gas clouds in the outskirts of spiral galaxies also orbit too quickly around the center to be held in place by the gravity of the visible matter. The simplest, even though puzzling, explanation of these behaviors being that there is unseen mass present in galaxies and clusters. A wide range of evidence supports the conclusion that most (perhaps 90-99%) of the mass in the universe is much less luminous (per unit mass) than stars. Ordinary luminous matter dominates in the central regions of galaxies, with the dark matter forming an extended "halo" around the luminous parts. Unfortunately, little else is known about the dark matter. Three outstanding questions are: (1) What is the dark matter? (2) How much of it is there? (3) How is it distributed through space?
The dark matter problem posed by these three questions is currently one of the most outstanding puzzles in all of science.

1.1.2 Simple cosmological models

The five sets of facts summarized above need to be justified by any cosmological models considered tenable by astrophysicists. In particular, the first two points, large-scale isotropy and the Hubble expansion, motivate the *Cosmological Principle*: the universe is approximately homogeneous and isotropic on large scales with a uniformly expanding mass distribution. Spatial homogeneity is difficult to establish, however it is a natural extension of the Copernican principle[1]. If the universe is isotropic (in the large) around every point, then it is necessarily homogeneous. The available data are consistent with large-scale homogeneity.

Uniform expansion means that galaxies separate with time with all distances scaling in proportion to a universal expansion scale factor $a(t)$ where t is the proper time measured by observers in each galaxy.

Simple models of a homogeneous and isotropic, uniformly expanding universe were introduced during the period 1917-1940 by de Sitter, Friedman, Lemaître,

[1]The Copernican principle, named after Nicolaus Copernicus, states that the Earth is not in a central, specially favored position. More recently, the principle has been generalized to the relativistic concept that humans are not privileged observers of the universe.

Robertson, Milne, and others. Although Einstein proposed the first cosmological model as a solution to his field equations of general relativity in 1917, he assumed, incorrectly, that the universe was static. To force his field equations to yield a static (as opposed to expanding or contracting) solution he added an extra term called *the cosmological constant*. After the discovery of an expanding universe by Hubble, in all models, all separations between objects scale with time in proportion to the universal scale factor $a(t)$. Thus, the position of each galaxy relative to some origin may be written as $\vec{r} = a(t)\vec{x}$, where $\vec{x}$ is a constant vector for that galaxy, called the *comoving position*. The Hubble law follows at once: $\vec{v} = d\vec{r}/dt = H\vec{r}$ where $H(t) = d(lna)/dt$. This result implies that H need not be independent of time; only its present value, H_0, is called the *Hubble constant*. There are in fact quite strong evidences that $a(t)$ is presently increasing with time and will double in about 10^{10} years. Therefore it was smaller in the past, and may have been very small (possibly even zero) at some finite proper time in the past. In fact, points (3) and (4) of section 1.1.1 support the notion that about 1.5×10^{10} years ago, the expansion scale factor was very much smaller than it is now, and that the universe began expanding tremendously rapidly in an event that has come to be called the *big bang*. The reasoning is that the temperature of an expanding gas (such as fills the universe) decreases adiabatically if there is no heat input. The heat content of the microwave background radiation is far too large to have been produced at low energies, therefore the mass and radiation in the universe must have been hotter and denser in the past.

When the temperature was above 10^{10} K, atomic nuclei were dissociated into protons and neutrons. The universe expanded and cooled rapidly, requiring only a few minutes to cool through the era of cosmic nucleosynthesis. About 3×10^5 years later the temperature dropped below 3500 K, the temperature at which hydrogen ionizes at cosmic density. After this epoch the protons and electrons combined to form neutral hydrogen gas, which is almost completely transparent to radiation.

At the present time, we can look out in distance, and therefore back in time, to see the radiation left over from this "recombination" era. Because of the large distance and relativistic recession velocity, the radiation is redshifted by a factor of about 1100, so that we detect it as the microwave background radiation.
The big bang theory accurately predicts both the nuclear abundances and nearly perfect Planck spectrum and isotropy of the cosmic microwave background radiation in an approximately homogeneous and isotropic expanding universe.

1.2 Small-scale structures: how did galaxies form?

Gravity is responsible for cosmic structure formation, but the nonlinear evolution can make very complex the determination of the initial conditions, having as starting point only the present day distribution of mass. On large scales, spatially

averaging the mass, this problem is not present because if smoothed sufficiently, the density fluctuations have small amplitude and then they evolve in a simple way. For this reason, the relation between the density, velocity and potential fields immediately after the recombination (considered as initial), and the present ones, is approximately linear on large scales.

On small scales instead, cosmic gravitational dynamics is strongly nonlinear and chaotic. Even if we could specify the position and velocity of every particle in the universe today, due to the strong chaos of gravitational dynamics, it becomes impossible to integrate the trajectories backwards in time. A possible solution proposed by cosmologists to this problem consists in try different theories for the initial conditions and then, rather than go backwards, integrate forward in time using gravitational N-body simulations in which each particle represents a cloud of dark matter. Moreover, more recently some peoples have also begun to include gas dynamics in their simulations in order to follow the baryonic matter.

Simulations of galaxy formation are not a trivial matter. First of all, in these simulations large dynamic ranges are required, both in length and mass scales (from $1g/cm^3$ and $10^7 cm$ for the Earth, to $10^{-30}g/cm^3$ and $10^{28}cm$ for the Universe). Individual luminous galaxies are smaller than 10^{23} cm but they reside in structures thousands of times larger. Realistic simulations would therefore require a dynamic range of at least 10^4 in length and 10^9 in mass.

Moreover, to model galaxy formation in a realistic way, one has to take into account the complexity of gas dynamical processes. Impressive calculations of cosmological gas dynamics have recently been made, but the greater computational cost of gas dynamics relative to gravitational simulation has greatly limited the dynamic range in mass and/or length. Even if some of these problems can be circumvented by using much more powerful computers, the complexity of radiative processes, magnetic fields, etc., are still a challenge for computational astrophysicist. Furthermore, star formation, which is known to be important in determining the appearance and evolution of galaxies, can be treated only in a phenomenological manner at best.

However, even if the theory of galaxy formation is so complex, we can still use it to test theories of cosmic structures formation. In fact, since all theories of the initial conditions are stochastic, it is then unnecessary for calculations to correctly reproduce every detail of the evolution beginning from a specific state. In particular, we only want that the distribution of mass, averaged over galactic or larger scales, have the correct statistical properties.

Moreover, it is plausible that gas dynamical effects are important only within galaxies and that galaxies form in the minima of the gravitational potential field of the dark matter. If these assumptions are correct, we need only the gravity to identify the sites of galaxy formation, and also the global properties of the galaxies themselves.

Finally, analytical arguments suggest several simple scaling relations for the evolution of self-gravitating dark matter, that are also confirmed by simulations.

We can then use these relations to extend the dynamic range of simulations in a statistical sense.

1.3 The Hot Dark Matter model

Let us outline how structure formation comes about in rather different dark matter scenarios, namely the hot and cold dark matter. I consider first the hot dark matter scenario which is to some extent of historical interest, but the presence of hot dark matter has observable consequences in the nowadays preferred cold dark matter scenario.

If the dark matter was in the form of known types of neutrino with rest masses of the order 10 eV, these particles became non-relativistic at an energy $m_\nu c^2 = 3kT$, which corresponds to a redshift of $z \approx 10^4$, assuming $\Omega_0 = 1$. The fact that the particles were highly relativistic when they decoupled, means that this epoch also corresponded to the epoch at which the Universe changed from being radiation- to matter-dominated.

It is assumed that all perturbations of astrophysical interest were set up on a very wide range of scales which far exceeded their particle horizons in the very early Universe. These perturbations then grew, until they came through their particle horizons. If the neutrinos remained relativistic when they came through the horizon, the perturbations on these scales were rapidly damped out by free-streaming. This process continued until the epoch of equality of the matter and radiation energy densities at $z \approx 10^4$ and wiped out all perturbations in the dark matter with masses less than $M = 4 \times 10^{15}(m_\nu/30eV)^{-2}M_\odot$.

At this epoch, the perturbations in the neutrinos, baryons and dark matter had more or less the same amplitude, but immediatly after the perturbations in the dark matter became dynamically dominant and, since they were not coupled to the radiation-dominated plasma, they continued to grow in amplitude. In contrast, when the perturbations in the radiation-dominated plasma came through the horizon, they were very quickly stabilised and oscillated with more or less constant amplitude between the epoch when they came through the horizon to the epoch of recombination. The amplitudes of the perturbations in the dark matter became progressively greater than those in the plasma, and, by the epoch of recombination, the perturbations in the dark matter with masses $M \sim 4 \times 10^{15}(m_\nu/30eV)^{-2}M_\odot$ were greater than those in the plasma.

The perturbations in the plasma were subject to the dissipation processes, and so baryonic perturbations with masses up to about $10^{12}M_\odot$ were damped out, but this is not such an important feature: the perturbations which determined the structures in the present epoch Universe are those in the dark matter which survived to the epoch of equality of matter and radiation energy densities, that is, $M \geq 4 \times 10^{15}(m_\nu/30eV)^{-2}M_\odot$. After the epoch of recombination when the matter and radiation were decoupled, the baryonic matter collapsed into the dark matter perturbations. The density perturbations in the matter then grew rapidly

to the same amplitude as those in the dark matter, which continued to grow until they became non-linear.

At this point, the perturbations separated out as discrete entities and began to form the large-scale structures we observe today. The hot dark matter scenario avoids creating excessively large fluctuations in the cosmic background radiation because, at the last scattering surface, the amplitude of the perturbations in the plasma were significantly less than those in the dark matter.

A key prediction of the hot dark matter model is that the first structures to form are those on the largest scales in the Universe and that smaller-scale structures such as galaxies and their contents, formed by fragmentation and instabilities once the structures on the scales of clusters of galaxies and greater began to form.

A success of this picture was that it accounted naturally for the large-scale "cellular" structure in the distribution of galaxies. Indeed the theory is too successful in producing structure on the very largest scales. The problem with this scenario is that galaxies can only form once the large-scale structures have collapsed, and so it is inevitable that galaxies and their contents formed rather late in the Universe. This poses problems for topics such as the early heating and ionisation of the intergalactic gas and the early chemical enrichment of that gas.

1.4 The Cold Dark Matter model

The modern theoretical framework for understanding galaxy formation is fundamentally different from the classical approach, which attempts to work backwards from the present time by using our understanding of stellar evolution and stellar dynamics. Instead, the modern picture works forward from prescribed initial conditions by using the physics of structure formation and attempts to understand galaxy formation as a natural consequence of the growth of mass fluctuations by gravitational instability. The change in thinking about galaxy formation benefited from a growing appreciation that: *i*) the universe is dominated by dark matter whose presence is inferred only through its gravitational interaction with visible matter, and *ii*) from the improved understanding of initial conditions in the early universe, which produced the gravitational seeds from which structure would grow. Much of this insight came through improved limits on fluctuations in the cosmic microwave background. The hypothesis that gravity is responsible for producing structure on all scales made it straightforward to follow the evolution of what would become galaxies in an ab initio sense. Theoretical arguments and numerous observations suggest that initial conditions imposed in the early universe, together with gravitational instability, will result in a universe in which the smallest mass fluctuations collapse first and merge into progressively larger structures as time goes on.

The theoretical models that are currently favored are all variations on this general framework, which usually is referred to as "hierarchical structure formation". The basic premise is that dark matter dominates the overall mass density

and interacts only gravitationally with normal matter but ultimately dictates the underlying structure of all matter, determining where normal baryonic matter will end up and thus where visible galaxies will form.

The cold dark matter (CDM) model was the most popular specific model for cosmic structure formation. First proposed by Peebles (1982), it soon replaced the pancake model (Zel'Dovich, 1970) with light massive neutrinos as the leading theory for structure formation.

It is worth spending a few words about the "pancake scenario". In it, formation of clusters took place first and it was followed by their fragmentation into galaxies due to adiabatic fluctuations. According to the non-linear gravitational instability theory, a growth of small inhomogeneities leads to the formation of thin, dense, and gaseous condensations that are called 'pancakes'. These condensations are compressed and heated to high temperatures by shock waves causing them to quickly fragment into gas clouds. The later clumping of these clouds results in the formation of galaxies and of their clusters. Thermal, hydrodynamic, and gravitational instabilities arise during the course of evolution. It leads to the fragmentation of gaseous proto-clusters and, subsequently, clustering of galaxies takes place. The pancake scheme therefore follows three simultaneous processes: first, gas cools and new clouds of cold gas form; secondly, these clouds cluster to form galaxies; and thirdly, the forming galaxies and, to an extent, single clouds cluster together to form a cluster of galaxies.

The standard cold dark matter scenario has become the most common model for studies of structure formation in the standard Big Bang. The cold dark matter particles decoupled early in the Universe not too long after they became non-relativistic at $t \sim 10^{-9}$ s, and the mass within the horizon at these times was very small, $M \ll M_{\odot}$. Free streaming was unimportant as soon as the particles became non-relativistic and so the cold dark matter scenario begins with the big advantage that dark matter perturbations on all scales of astrophysical interest survived from the early Universe.

Cold dark matter must be the dominant form of mass at the present epoch and the ingredients of the CDM model include the standard big bang theory plus nonbaryonic dark matter with:

1. $\Omega_0 = 0.3$ and $\Omega_B = 0.05$ (inflation predicts $\Omega = 1$, while primordial nucleosynthesis models favor small baryonic abundance), $\Omega_\lambda = 0.7$;

2. $h = 0.7$ (small Hubble constant, implying for $\Omega = 1$ a cosmic age of 13.2 billion years);

3. scale-invariant gaussian density fluctuations.

For these reference values, the epoch of equality of matter and radiation energy densities occurred at a redshift of $z = 2.4 \times 10^4 \Omega_0 h^2 \approx 3500$. Up to this epoch, the perturbations in the dark matter hardly grew at all. After this epoch, the dark matter became dynamically dominant and the perturbations in the dark matter grew

independently of the behaviour of the perturbations in the radiation-dominated plasma. As in the standard baryonic picture, adiabatic baryonic fluctuations came through the horizon and were quickly stabilised by the pressure of the plasma.

The diffusion of photons from these perturbations led to damping of masses up to about $M = 10^{12}(\Omega_B h^2)^{-5/4} M_\odot \sim 10^{14} M_\odot$ by the epoch of recombination. Perturbations with greater masses survived as oscillating sound waves up to the epoch of recombination, when they imprinted their signature on the last scattering surface, just as in the case of the hot dark matter and baryonic scenarios. However, because perturbations on all mass scales survived in the cold dark matter throughout these epochs, baryonic perturbations on all scales were regenerated by collapse into the cold dark matter perturbations very soon after the epoch of recombination when the coupling of matter and radiation ended.

Cold dark matter models for galaxy and structure formation have been studied in great detail by computer simulation. Once a spectrum of initial curvature perturbations has been adopted, their evolution can be followed rather precisely. The lowest-mass objects formed first soon after the epoch of recombination, and these then clustered and coalesced under the influence of the spectrum of perturbations on larger scales. Just like the baryonic isothermal model, this process can be thought of as a "bottom-up" scenario in which small-scale structures formed first and subsequently clustered to form galaxies and clusters.

The model is remarkably successful in accounting for the observed power spectrum of the spatial distribution of galaxies and for the spectrum of fluctuations in the cosmic microwave background radiation. Furthermore, the formation of stars and the other contents of galaxies can begin soon after the epoch of recombination, and so there is no problem in accounting for the early heating and reionisation of the intergalactic gas and the early chemical enrichment of the gas by the products of stellar nucleosynthesis. The success of the model in accounting for the large-scale distribution of galaxies has persuaded most theorists that this is the correct framework for studying the processes of galaxy formation.

Recent observations have set stringent constraints on the values allowed for the fundamental parameters of the CDM model. Studies of the temperature anisotropies in the CMB strongly suggest that the universe is flat, $\Omega_0 \simeq 1$, with a matter contribution of $\Omega_m = 0.10 - 0.36$. The latter values are derived from the local abundance of galaxy clusters, their redshift evolution, mass-to-light ratio of groups of galaxies, X-ray gas mass fraction of clusters of galaxies, and high-z supernovae. The baryon contribution to matter, $\Omega_B h^2 = 0.020 - 0.030$, is derived through measurements of CMB anisotropies, and all the estimates of the Hubble constant are based on secondary distance indicators, such as the Tully-Fisher relation, the fundamental plane of elliptical galaxies, Type Ia supernovae and surface brightness fluctuations, and give $h = 0.5 - 0.8$. Local and high-z evolution of galaxy clusters is used to set a limit to the rms relative fluctuation $\sigma_8 = 0.7 - 1.2$. Finally, studies of the temperature anisotropies in the CMB give $n = 1.01 - 1.08$. These parameters have been confirmed by the CMB data from WMAP, although

there is an indication for a possible running spectral index, with $n > 1$ on large scales and $n < 1$ on small scales.

At present, the most popular model is a ΛCDM with $\Omega_0 = 1.02 \pm 0.02$, $\Omega_\lambda = 0.73 \pm 0.04$, $\Omega_m = 0.27 \pm 0.04$,$\Omega_b = 0.044 \pm 0.004$, $h = 0.71^{+0.04}_{-0.03}$,$\sigma_8 = 0.84 \pm 0.04$ and $n = 0.93 \pm 0.03$. The above parameter set, determined from CMB experiments, is impressively in good agreement with that obtained independently by experiments based on high-redshift Type Ia supernovae and galaxy cluster evolution data.

1.5 Hierarchical structure formation in CDM models

As already mentioned, in hierarchical galaxy formation, the early history of the universe begins with a spectrum of fluctuations imposed as initial conditions by the physics of the very early universe. Gravity acts over time to alter this spectrum and to increase the amplitude of the fluctuations; large gravitationally bound density enhancements such as galaxies and clusters of galaxies are made over a protracted period of time through successive merging or accretion of smaller lumps of matter. Within this framework, it is much easier to build small galaxies than large ones, and the characteristic mass of the largest gravitationally bound dark-matter "halos" is an increasing function of time, with the time scale to produce a given mass set by the details of the cosmological model, most notably the mean density of matter.

The primordial density fluctuations predicted by popular inflation models have simple characteristics. They are described by a random Gaussian field, and have a nearly scale-invariant power spectrum $P(k) \propto k^n$ with $n \sim 1$. Subsequent growth of perturbations in the radiation-dominated and then in the matter-dominated era results in a modified power spectrum, but the final shape is still simple and monotonic in CDM models; the power spectrum has a feature that it has progressively larger amplitudes on smaller length scales. Hence structure formation is expected to proceed in a *bottom-up* manner, with smaller objects forming earlier.

It is useful to work with a properly defined mass variance (σ) to obtain the essence of non-linear evolution and collapse in the CDM model. At $z = 20$, the mass of the halos which correspond to 3σ fluctuation is just about $10^6 M_\odot$. This mass scale coincides with the characteristic mass of the first objects in which the primordial gas can cool and condense. It is worth noting that the mass variance is sensitive to the initial power spectrum. In warm dark matter models in which the power spectrum has an exponential cut-off at the particle free-streaming scale, or in models in which the primordial power spectrum has a 'running' feature, the corresponding mass variance at small mass scales is reduced. In such models, early structure formation is effectively delayed, and hence nonlinear objects form later than in the CDM model. Thus the formation epoch of the first objects and hence that of cosmic reionization have a direct link to the nature of dark matter and the primordial density fluctuations.

One of the key concepts of the hierarchical clustering scenario is that cosmic structures form by a process of continuous mass aggregation, opposite to the monolithic collapse scenario, in which large galaxies formed through a rapid gravitational collapse that would have resulted in huge bursts of star formation at early epochs, leaving behind galaxies that had rapidly exhausted their fuel to age quiescently until the present; these galaxies appear now as large collections of old, red stars, such as elliptical galaxies and the central bulges of spiral galaxies.

The mass assembly of CDM halos is characterized by the mass aggregation history (MAH), which can alternate *smooth mass accretion* with *violent major mergers*. By using the ΛCDM model, several studies showed that most of the mass of the present-day halos has been aggregated by accretion rather than major mergers. Major merging was more frequent in the past, and it is important for understanding the formation of massive galaxy spheroids and the phenomena related to this process like QSOs, supermassive black hole growth, obscured star formation bursts, etc. Both the mass aggregation rate and major merging rate histories depend strongly on environment: the denser the environment, the higher is the merging rate in the past. However, in the dense environments (group and clusters) form typically structures more massive than in the less dense regions (field and voids). Once a large structure virializes, the smaller, galaxy-sized halos become subhalos with high velocity dispersions: the mass growth of the subhalos is truncated, or even reversed due to tidal stripping, and the merging probability strongly decreases. Halo assembling (and therefore, galaxy assembling) definitively depends on environment.

CHAPTER 2

Galaxy formation

The formation and evolution of galaxies is one of the most hotly debated topics in modern astronomy. The question to answer is: why do we see different types of galaxies?

Galaxy formation is not a trivial matter because normal galaxies are complex, many-body systems. Typically, a galaxy consists billions of stars, it can contain considerable quantities of interstellar gas and dust and can be subject to environmental influences through interactions with other galaxies and with the intergalactic gas, and star formation takes place in dense regions of the interstellar gas. Moreover, it is now certain that dark matter is present in galaxies and in clusters of galaxies and the dynamics of galaxies is largely dominated by this invisible dark component, that complicates further the study of galaxy formation.

Until the advent of the massive surveys of galaxies, like the 2dF Galaxy Survey undertaken by the Anglo-Australian Telescope and the Sloan Digital Sky Survey (SDSS), the typical properties of galaxies were defined by meticulous visual morphological studies of large samples of bright galaxies. Given that in this way it was possible to analyze only bright and relatively nearby galaxies, the morphological classification schemes contain a vast amount of detail and this was reflected in Hubble's pioneering studies as further elaborated by de Vaucouleurs, Kormendy, Sandage, van den Bergh and others.

In contrast, the size of the new galaxy samples, which each encompass about 200,000 galaxies, has pointed out that classification schemes had to be based upon parameters which could be derived from computer analysis of the galaxy images and spectra[1]. What the new approach loses in detail, it more than makes up for

[1] A possible exception being Galaxy Zoo project

in the huge statistics involved and in the less subjective nature of the classification procedures.

These recent developments have changed the description of the properties of galaxies. While the new samples provide basic global information about the properties of galaxies, the old schemes describe many features which need to be incorporated into the understanding of the detailed evolution and internal dynamics of particular classes of galaxy. To summarize, until a better method comes out, we need to develop in parallel both the traditional and more recent approaches to obtain a reasonable classification of galaxies.

2.1 Morphological classification: the Hubble Sequence for Galaxies

I will start describing the traditional approach to the classification of galaxies, outlining at the same time, the points of contact with more recent statistical approaches. We can observe galaxies in a large variety of different shapes and forms. From this consideration arise the necessity to put some order into this diversity; this was done by computing classification schemes, in which galaxies were ordered on the basis of their visual appearance, or morphologies, originally on photographic plates but nowadays from digital images taken with CCD cameras.

The basis of the traditional morphological schemes remains the *Hubble Sequence of Galaxies* (Hubble, 1936). The Hubble sequence, sometimes referred to as a "tuning-fork" diagram, arranges galaxies into a continuous sequence of types with elliptical galaxies at the left-hand end, ordered on the basis of their ellipticity, and ordinary and barred spirals at the right-hand end (Fig. 2.1)

The spiral galaxies are ordered into two branches named "normal" and "barred" spirals. Conventionally, galaxies towards the left-hand end of the sequence are referred to as "early-type" galaxies and those towards the right as "late-type" galaxies, reflecting Hubble's original idea concerning their evolution from one type to another. Despite the fact that these ideas have long outlived their usefulness, the terms are still in common use, even in the era of the massive surveys of galaxies.

Morphological classification schemes such as the Hubble sequence become an integral part of astrophysics when independent properties of galaxies are found to correlate with the morphological classes. This has been found to be the case for a number of the overall properties of galaxies such as their integrated colors, the fraction of the mass of the galaxy in the form of neutral and molecular gas, and so on.

2.1.1 Elliptical galaxies

These galaxies show no clearly defined structure in their brightness distributions but have an elliptical appearance (see Fig. 2.2), as if they were spheroids or ellip-

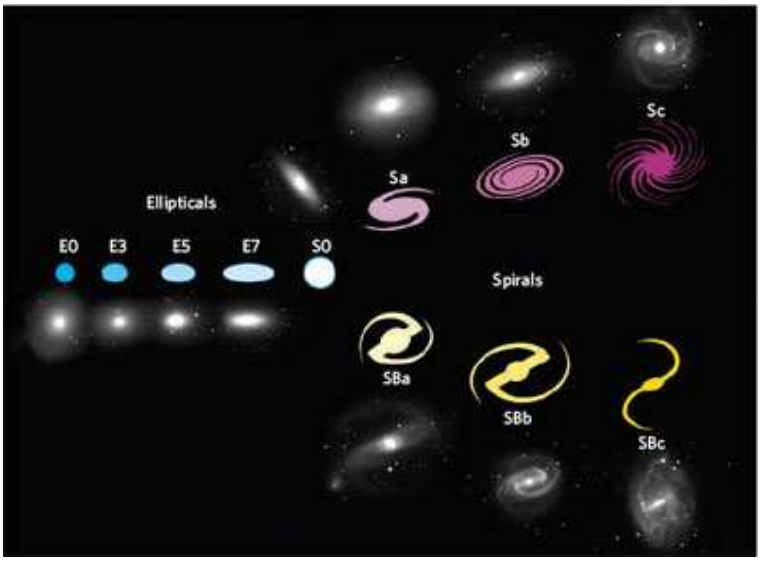

Figure 2.1: The Hubble sequence of galaxies.

soids of revolution, and have nearly elliptical isophotes[2]. In absolute magnitude, elliptical galaxies range from the most luminous galaxies known, having $M_B \approx 24$, to dwarf ellipticals (dE), having magnitudes in the range $-18 < M_B < -14$, which are found in the Local Group of galaxies. In Hubble's notation, the observed ellipticity of the galaxy is included in the morphological designation according to the rule that the number $10 \times (a - b)/a$ was written after the letter E, where a and b are the observed major and minor axes of the ellipse. Thus E0 galaxies have circular isophotes and E6 galaxies, the most extreme ellipticities found in elliptical galaxies, have $b/a = 0.4$. Galaxies flatter than E6 all show a distinct disc and bulge structure and hence are classified as lenticular (S0) rather than E galaxies[3].

2.1.2 Spiral galaxies

The characteristic feature of spiral galaxies is their disk-like appearance with well-defined spiral arms protruding from their central regions (Fig. 2.3). Very often the spiral pattern is double with a remarkable degree of symmetry with respect to the center of the galaxy, but many more complicated configurations of spiral structure are known. The light distribution of what Hubble termed "normal" spiral galaxies (or SA galaxies) can be decomposed into a *central bulge* or *spheroidal component*,

[2]Isophotes are contours along which the surface brightness of a sources is constant. If the light profile of a galaxy is elliptical, then its isophotes are ellipses.

[3]In the original classification scheme there was also an E7 class which has now been recognized as being formed by close to edge on lenticulars.

Figure 2.2: The elliptical galaxy M87, appears near the center of the Virgo cluster of galaxies.

similar to an elliptical galaxy, and a *disk component*, within which the spiral arms lie. In the case of the *barred spirals* (or SB galaxies), the central bulge has an elongated or ellipsoidal appearance, the spiral arms originating from the ends of the bar. There are as many "barred" spiral galaxies as "normal" spirals and, furthermore, there are just as many spirals intermediate between these two classes.

Both types of spiral galaxies are divided in subclasses, classified as Sa, Sb, Sc according to the following criteria, in decreasing order of importance:

1. the openness of the winding of the spiral arms,
2. the degree of resolution of the arms into stars,
3. the size of the spheroidal component or central bar relative to the disk component.

Sa galaxies have tightly wound spiral arms which are smooth and show no resolution into stars. The central bulge or bar is dominant, shows no structure and is unresolved into star clusters.
Sb galaxies have more open spiral arms, which show resolution into stars. The central spheroidal component or bar is generally smaller than in Sa galaxies.
Sc galaxies have very open spiral arms which are patchy and resolved into star clusters and regions of ionized hydrogen. The spheroidal component is very small. In barred spiral galaxies, the bar is resolved into clusters and HII regions and is not as prominent as in classes Sa or Sb.

The *revised Hubble scheme* extends this classification beyond Sc to include "nearly chaotic" structures which would have been classified as very late Sc spirals in the standard sequence but are now classified as Sd spirals.

2.1.3 Lenticular galaxies

All galaxies with smooth light distributions and axial ratios $b/a < 0.3$ show evidence of a disk-like component and these are called *lenticular* (lens-like) or S0 galaxies (Fig. 2.4). They are similar to spiral galaxies in that their light distributions can be decomposed into a central bulge, similar in properties to elliptical galaxies, and an extensive disk. The lenticular galaxies appear an intermediate class of objects in morphological type between elliptical and spiral galaxies.

In many cases, the central bulges of the S0 galaxies have a bar-like appearance and hence, as in the case of the spirals, they can be divided into "ordinary" and "barred" lenticulars as well as in intermediate types. In a number of lenticular galaxies, there is evidence for obscuring matter, often in the form of rings. In the revised Hubble classification, lenticular galaxies which are free of obscuring matter are termed "early" $S0^-$ with stages $S0^0$ and $S0^+$ representing "later" stages with increasing amounts of obscuring material. By the intermediate stage between lenticular and spiral galaxies, $S0/a$, the obscuring matter begins to show what is referred to as "incipient spiral structure".

Figure 2.3: The spiral galaxy M51, also known as the "Whirlpool Galaxy".

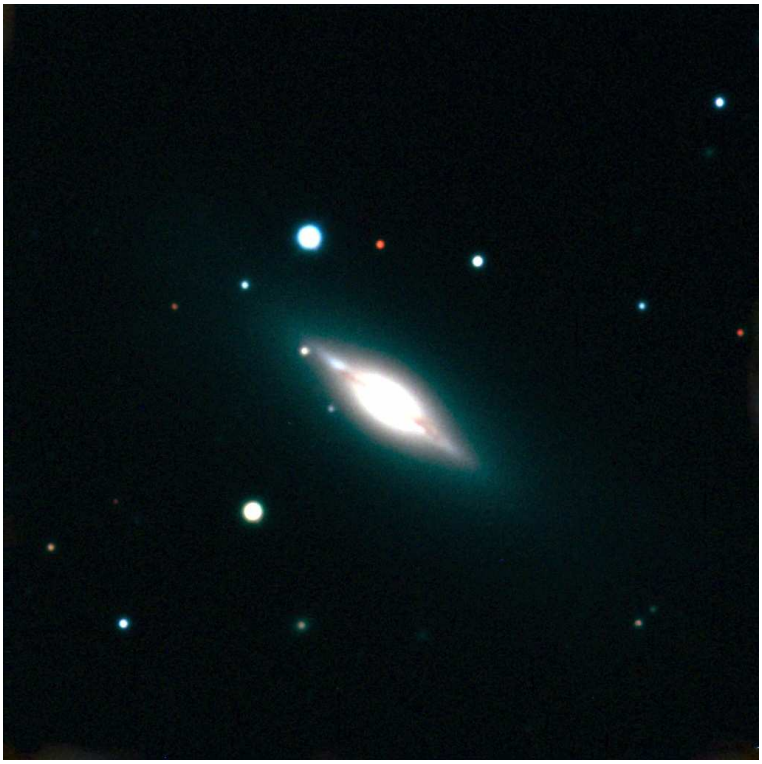

Figure 2.4: The lenticular galaxy M102, located in the constellation Draco.

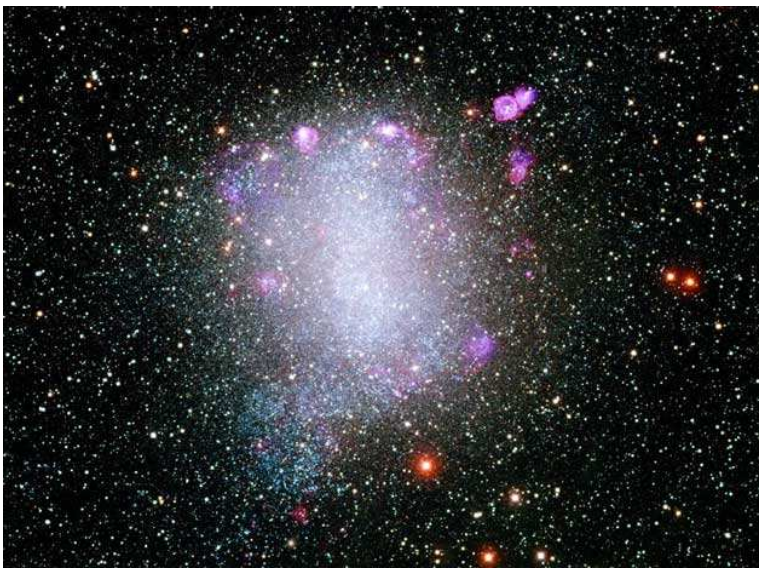

Figure 2.5: Barnard's Galaxy or NGC 6822, a small irregular galaxy only 14 degrees East of the galactic plane in Sagittarius.

2.1.4 Irregular galaxies

In Hubble's original classification, irregular galaxies were systems "lacking both dominating nuclei and rotational symmetry" and the class included everything which could not be readily incorporated into the standard Hubble sequence. Many of these irregulars were similar to the companion galaxies of our own Galaxy, the Magellanic Clouds, and these were designated Irr I or Magellanic irregulars, and are characterized by a very weak regular structure. There remained a small class of irregulars consisting of galaxies such as M82 , NGC 520 and NGC 3077, in which there was no evidence of resolution into stars and of any regular structure; these galaxies were classified Irr II galaxies.

Evidence that the Irr I galaxies form a natural extension of the Hubble sequence was provided by de Vaucouleurs' discovery of weak but definite spiral structure in the Large Magellanic Cloud (LMC). Galaxies like the LMC can be considered to belong to stages in the Hubble sequence later than Sd and are denoted Sm. The Irr II systems find no natural place in the revised sequence and are designated I0 by de Vaucouleurs. The characteristics of the I0 irregular galaxies are that they are very rich in interstellar matter and contain young stars and active regions of star formation; a number of these would be classified as starburst galaxies.

Figure 2.6: The peculiar galaxy Centaurus A.

2.2 Peculiar and interacting galaxies

The revised Hubble classification encompasses the forms of almost all galaxies. There are, however, a number of galaxies with very strange appearances (Fig. 2.6) and these are referred to as *peculiar galaxies* (Arp, 1966), to indicate that they cannot be associated with any standard galaxy type. A few galaxies are known, for example, in which the stellar component is in the form of a ring rather than a disc or spheroid, the Cartwheel being a beautiful example of this type of galaxy, known as *ring galaxies*.

Most of these remarkable structures are due to strong gravitational interactions, or collisions, between galaxies. In the early 70's, Toomre and Toomre, by performing a numerical integration of the restricted three body problem, carried out pioneering computer simulations of close encounters between galaxies which showed how such events could modify the structure of the galaxies involved in the process, giving rise to remarkable asymmetric structures (Toomre & Toomre, 1972). In Fig. 2.7, a deep image of the pair of interacting galaxies known as the "Antennae" is shown, revealing the extraordinary long "tails" which seem to be emanating from a pair of closely interacting spiral galaxies in which a great deal of recent star formation has occurred.

The Toomres showed how such elongated "tails" could be accounted for by a gravitational interaction between two spiral galaxies. In the simulation shown in Fig. 2.8, the two spiral galaxies pass close to each other on prograde orbits, that is, the rotational axes of the two discs are parallel and also parallel to the rotational axis of the two galaxies about their common center of mass. The spiral galaxies

Figure 2.7: The strange pair of interacting galaxies known as the "Antennae".

are represented by differentially rotating discs of stars and, while they are at their distance of closest approach, the stars in the outermost rings feel the same mutual force acting upon them for a very much longer time than if the passage had been in, say, the retrograde direction. As a result, the outer rings of stars feel a coherent force for an extended period and are stripped off to form the tails, the extended structure observed in the Antennae. Many of the features of strong gravitational interactions were described in the pioneering papers by the Toomres (Toomre & Toomre, 1972).

Interactions between galaxies play a central role in many aspects of galactic evolution. From the observational point of view, the IRAS satellite showed that colliding galaxies are among the most luminous extragalactic far-infrared sources. In fact, when galaxies collide, their interstellar media are compressed to high densities and the rate of star formation is greatly enhanced, resulting in intense far-infrared emission. Collisions between galaxies have also assumed a central role in models of galaxy formation. In the preferred scenarios of structure formation, galaxies are built up by the process of hierarchical clustering in which larger galaxies are formed through the repeated aggregation of smaller galaxies. In this picture, strong gravitational encounters between galaxies are essential in forming the structures we observe today.

2.3 The light distribution in galaxies

Morphological classification is obviously affected by projection effects; for instance, if the spatial shape of an elliptical galaxy is a triaxial ellipsoid, then the observed ellipticity will depend on its orientation with respect to the line-of-sight. To solve

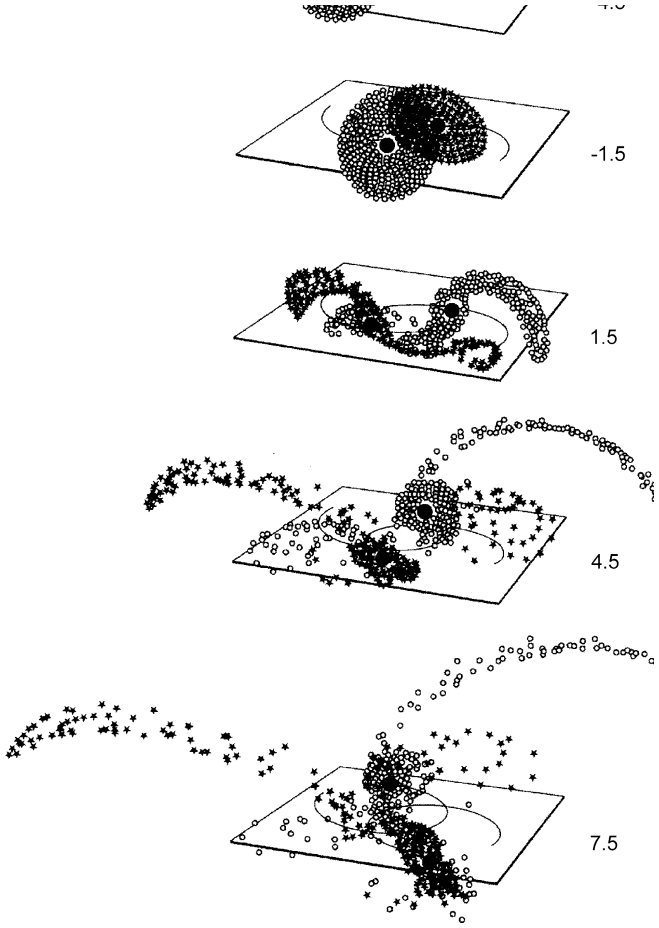

Figure 2.8: A simulation of a close encounter between two disc galaxies which approach each other on prograde orbits. It can be seen that the outer rings of stars are torn off each galaxy, forming the remarkable "Antenna" structures (Toomre & Toomre, 1972).

this problem, we shall adopt another approach to the classification of galaxies based on their light distributions, since it is found that these are somewhat different for bulge-dominated and disc-dominated systems. Let us first summarize the results of studies of bright galaxies and then show how these can be adapted for the study of large samples of galaxies.

2.3.1 Elliptical galaxies

The earliest expression for the observed surface brightness distribution of elliptical galaxies as a function of radius r is commonly referred to as *Hubble's law*:

$$I(r) = I_0 \left(\frac{r}{r_c} + 1 \right)^{-2} \tag{2.1}$$

where r_c is the *core radius* of the galaxy. This expression provides a reasonable description of the intensity distribution in the central regions of elliptical galaxies but is a poor fit in the outer regions. A much better description of the surface brightness distribution of elliptical galaxies and the bulges of spiral galaxies is the empirical law proposed by de Vaucouleurs which is usually referred to as the $r^{1/4}$ law:

$$\log \left[\frac{I(r)}{I(r_e)} \right] = -3.3307 \left[\left(\frac{r}{r_e} \right)^{1/4} - 1 \right] \tag{2.2}$$

This expression provides a good representation of the luminosity profile over many decades of surface brightness. The expression has been normalized so that r_e, the *effective radius*, is the radius within which half the total luminosity is emitted and $I(r_e)$ is the surface brightness at that radius. The corresponding total luminosity of the galaxy is

$$L = 7.215 \pi I_e r_e^2 \left(\frac{b}{a} \right) \tag{2.3}$$

where b/a is the apparent axis ratio of the elliptical galaxy.

2.3.2 Spiral and lenticular galaxies

Given that in disk galaxies we can distinguish two components, the light distributions in most spiral and lenticular galaxies can be decomposed into two components, a spheroidal component associated with the central bulge and a disc component. The luminosity profile of the spheroidal component is the same as that of an elliptical galaxy and may be described by the de Vaucouleurs $r^{1/4}$ law discussed above. In almost all galaxies in which there is evidence of a disc component, including spirals, barred spirals and lenticulars, the luminosity profile of the disc may be represented by an exponential light distribution

$$I(r) = I_0 \exp(-r/h) \tag{2.4}$$

where h is called the *disc scale length*. The total luminosity of the disc is then $L = 4\pi h^2 I_0$, and this luminosity profile is also found in very late-type galaxies, such as the Magellanic irregulars which show evidence of a disc in rotation.

A convenient way of combining the light distributions of elliptical and spiral galaxies is to adopt the formulation proposed by Sérsic which can be thought of as a generalization of de Vaucouleurs' $r^{1/4}$ law:

$$\log\left[\frac{I(r)}{I(r_e}\right] = -b_n\left[\left(\frac{r}{r_e}\right)^{1/n} - 1\right] \tag{2.5}$$

where r_e is the radius within which half of the total light is emitted and the b_n is a normalization constant to ensure that the total light sums to L_{tot} for a given value of n, which is also called "Sersic index". It can be seen that the value n = 4 results in de Vaucouleurs' $r^{1/4}$ law and n = 1 in the exponential law found in the discs of spiral galaxies. This formalism can be used to discriminate between disc-dominated and bulge-dominated galaxies.

2.4 Galactic structure formation

The preceding sections describes what is known about the properties of galaxies. The next significant question is what structure that galaxy will have. In the following section I will review the process of disk and spheroid formation and make quantitative estimates of the sizes of these structures.

2.4.1 Disk formation

Disks are a common astrophysical phenomenon and galactic disks owe their origins to the same fundamental process as other astrophysical disks: conservation of angular momentum in a system collapsing under gravity eventually leading to arrest of the collapse by rotational support. Understanding the physical properties of galactic disks therefore requires knowledge of their angular momentum content and the gravitational potential in which they form.

The angular momentum of the gas which will eventually form a galactic disk arises in the same way as that of dark matter halos, namely from tidal torques from surrounding large scale structure. The magnitude of the angular momentum content of the baryonic component of a halo is close to being a scaled version of that of the dark matter, for example the distributions of spin parameters and angular momentum distributions within individual halos for dark matter and non-radiative gas are very similar and numerical hydrodynamical studies show that the angular momenta vectors of galactic disks are well aligned with the angular momenta of the inner regions of dark matter halos (Hahn et al., 2010).

We have assumed so far that the angular momentum of the pre-galactic gas is conserved during collapse. This may not be precisely true and indeed did not seem

to be in earlier generations of hydrodynamical simulations which typically found that disk galaxies lost significant fractions of their angular momentum and, as a result, were too small. However, more recent simulations do show approximate conservation of angular momentum (most likely due to the inclusion of effective feedback in these later generations of simulations) and, furthermore, conservation of angular momentum leads to disks with sizes comparable to those observed. Confirmation has recently been obtained by Zavala et al. (2008) who convincingly show in N-body+hydrodynamical simulations that the particular feedback prescription used can lead to the formation of a disk dominated or spheroid dominated galaxy in the same dark matter halo, with stronger feedback leading to a disk galaxy. The angular momentum of the mass in the disk galaxy tracks that of the dark matter halo as a whole, growing as expected during the linear regime and remaining nearly constant after halo collapse. With weaker feedback a spheroid forms instead. Its angular momentum also grows during the linear regime but then declines rapidly (as does that of the inner regions of the dark matter halo) due to angular momentum transfer from dense, progenitor blobs to the surrounding, diffuse dark matter.

The disk mode of galaxy formation is motivated by the gravitational instability of gas-rich disks. Disk galaxies form late, slowly and inefficiently. The inefficiency is plausibly interpreted in terms of momentum input into the interstellar medium from expanding supernova shells. Supernovae provide the quantitative amount of feedback required to account for the star formation rate observed in disk galaxies. Star formation is sustained by a combination of disk self-gravity and supernova feedback. The self-gravity drives large-scale instability provided the disk is cold. Continuing accretion of cold gas guarantees the gaseous disk continues to fragment into large molecular cloud complexes.

These accrete smaller clouds, cool and themselves fragment into stars. Calculation of the star formation rate is complicated by the role of magnetic fields, whose pressure also plays a role in supporting clouds against collapse and decelerating star formation. The magnetic fields themselves are ionization-coupled to the cold gas, and the ionization fraction is itself due to radiation from massive stars. The situation is further complicated by the fact that many clouds are supported by turbulent pressure, and the turbulence driver is not well understood.

Despite these non-linear complications, the global star formation rate in galactic disks is described by a remarkably simple formula:

$$SFR = 0.02\frac{\Sigma_{gas}}{t_{dyn}} \tag{2.6}$$

where Σ_{gas} is the surface density of the gas and t_{dyn} the dynamical time scale. This simple model fits a wide range of data, including quiescent and star-bursting galaxies. Evidence for local cold gas feeding is found in nearby disk galaxies that have extensive HI envelopes.

While one can phenomenologically understand star formation in disks, there is no successful model for disk formation. All attempts to date lead to overly

massive or concentrated bulges. Detailed studies of self-gravitating hydrodynamic collapse with realistic initial conditions find that while the initial specific angular momentum matches that of observed disks, some 90% is lost to the halo during collapse. Late infall implies gas-rich halos, which in turn require large SN-heating efficiencies and result in predicted large X-ray luminosities. The implied large amounts of hot gas are at best only rarely seen for massive disk galaxies, where coronal absorption lines set strong constraints.

In fact, the HI "beards" found in nearby spiral galaxies such as NGC 891 and NGC 2403 are analogous to galactic high-velocity clouds and are signposts of a substantial and otherwise mostly hidden halo gas accretion rate that interacts with supernova-driven galactic fountains. While the required accretion rate is consistent with lambda cold dark matter (LCDM) expectations and is comparable to the star formation rate, the infalling gas is required to have low angular momentum in contrast with the expectations from simulations.

Sizes

Once the angular momentum distribution of that part of the baryonic component of the halo which cools to form the galaxy is known, finding the structure of the resulting rotationally supported disk is reduced to solving the following equation:

$$\frac{j^2(M)}{R^3(M)} = \frac{\partial}{\partial R}\Phi(R) \tag{2.7}$$

where $j(M)$ is the specific angular momentum enclosing the mass M and this equation is solved for $R(M)$. The potential is the sum of the self-gravity of the disk and that of any external potential (dark matter halo and bulge for example) which may have responded adiabatically to the formation of the disk. Knowing the functional form of $j(M)$ it is possible to solve for $R(M)$ and therefore the density profile of the disk. Often, for simplicity, a particular form for the density (e.g. exponential) is assumed which leaves a single free parameter (the scale length) to be solved for.

A significant complication to this picture arises from the fact that the external potential in which the disk forms is likely to change in response to the formation of the disk. If the disk forms slowly, so that the timescale for changes in the potential greatly exceeds the dynamical time of the dark matter halo, then we can use adiabatically invariant quantities to estimate the response of the halo to the forming disk. In this simplified picture, the dark matter particles are considered to be on circular orbits in a spherical potential. In this case, the only adiabatic invariant whose corresponding angle variable has a non-infinite period is the magnitude of the angular momentum, L_ϕ. Prior to the formation of any galaxy, this angular momentum is given by:

$$L_\phi^2 = (1 - f_b)^{-1} G M_{DM}(r_0) r_0 \tag{2.8}$$

where G is the gravitational constant, $M_{DM}(r)$ is the mass of dark matter within the radius r, r_0 is the initial radius of the circular orbit and we have assumed that baryons are present in the halo at the universal fraction, f_b ($\equiv \Omega_b/[\Omega_b + \Omega_{CDM}]$) and distributed as the dark matter. If L_ϕ is conserved during the formation of a galaxy, then, at any point after galaxy formation has begun we have:

$$L_\phi^2 = (1 - f_b')^{-1} G[M'_{DM}(r_f) + M_{gal}(r_f)]r_f \tag{2.9}$$

$M'(r)$ is the mass of dark matter enclosed within radius r after responding to the forming galaxy, M_{gal} is the mass of the galaxy within the same radius, f_b' is the baryon fraction remaining uncondensed into the galactic phase and r_f is the radius of the new circular orbit for this dark matter particle. Given a knowledge of the mass and density distribution of the galaxy this allows us to solve for r_f as a function of the initial radius r_0.

This approach makes several simplifying assumptions, including adiabatic growth, a spherical halo and circular orbits for dark matter particles. Many of these assumptions have yet to be adequately tested. However the process of halo response to galaxy growth is more complicated than is captured by these simple models, perhaps because the assumed invariants are not precisely invariant in non-spherical potentials or perhaps because galaxy growth is not sufficiently slow to be truly adiabatic.

Galaxy disks are, of course, not razor thin. The origins of the vertical extent of galaxy disks remain a topic of active research but various possibilities are currently considered seriously:

1. External origin (accretion):

   (a) The hierarchical nature of galaxy formation implies that a galactic disk can expect to accrete pre-existing, smaller stellar systems frequently during its life. The stars from these smaller galaxies are often found in numerical simulations to form a thickened disk structure, in the same plane as the pre-existing disk of the galaxy. This is to be expected as dynamical friction will tend to drag orbiting satellites into the plane of the disk where tidal forces will proceed to shred the satellite, leaving its stars orbiting in the plane of the disk.

   (b) Early, chaotic gas accretion: In a slightly different scenario, Brook et al. (2004) find, in numerical simulations of a forming galaxy, that many of the thick disk stars form from accreted gaseous systems during an early, chaotic period of merging.

2. Internal origin (dynamical heating):

(a) Dark matter substructure: In recent years there have been numerous studies focused on the question of whether relatively thin galactic disks can survive in the rather violent environment of a hierarchically formed dark matter halo. A careful treatment of dark matter substructure orbital evolution and the build-up of the substructure population over time is required to address this problem. The conclusion from these studies is that galactic disks can survive in the currently accepted cold dark matter cosmogony, but that interactions with orbiting dark matter substructure must be a significant contribution to the thickening of galaxy disks. The heating is dominated by the most massive dark matter substructures and so is a rather stochastic process, depending on the details of the merger history of each galaxy's dark matter halo and the orbital properties of those massive substructures.

(b) Molecular clouds: Massive molecular clouds can gravitationally scatter stars that happen to pass by them, effectively transforming some of their orbital energy in the plane of the galaxy disk into motion perpendicular to that plane, thereby effectively thickening the disk.

(c) Spiral arms: Spiral density waves can also act as scatterers of stars, but predominantly increase the stellar velocity dispersion in the plane of the galaxy, resulting in little thickening.

Most likely, a combination of these processes is at work.

Stability

Spiral arms and other non-axisymmetric features such as bars in galactic disks are a visually impressive reminder that these systems possess interesting dynamics. The basic theory of spiral arms, that they are density waves, was first proposed by Lin & Shu (1964) and has come to be widely accepted. From our current standpoint, the question in which we are interested in is whether these perturbations to an otherwise smooth disk are stable or unstable and, if unstable, how they affect the evolution of the galaxy as a whole.

Toomre (1964) derived an expression for the local stability of thin disks to axisymmetric modes in the tight-winding approximation which turns out to be extremely useful (and often approximately correct even in regimes where its assumptions fail). Disks will be unstable to axisymmetric modes if $Q < 1$ where

$$Q = \frac{k\sigma_{gas}}{\pi G \Sigma_{gas}} \tag{2.10}$$

where

$$k = (R\frac{d\Omega^2}{dR} + 4\Omega^2)^{1/2} \tag{2.11}$$

is the epicyclic frequency and Ω is the angular frequency of the disk, for a gaseous disk of surface density Σ_{gas} and velocity dispersion σ_{gas}.

Toomre's criterion applies to local perturbations. Perturbations on the scale of the disk can occur also. Study of these global instabilities is less prone to analytic treatment (since one can no longer ignore contributions from distant parts of the disk). However, global instabilities most likely lead to the formation of a very strong bar which effectively disrupts the disk leaving, after a few dynamical times, a boxy/peanut bulge or a disky bulge. This may therefore be a possible formation scenario for pseudo-bulges, i.e. bulges formed through secular processes in the disk rather than as the result of a merger event.

Bars and spiral arms

The presence of perturbations in the disk can also affect its structure in less dramatic but still significant ways. For example, numerical simulations by Roškar et al. (2008) show that a significant fraction of stars in galaxy disks undergo large migrations in radius due to resonant scattering from spiral arms. The resonant scattering of a star initially on an approximately circular orbit tends to change its energy and angular momentum in such a way as to keep it in a circular orbit, but to change the radius of that orbit. As such, stars initially on circular orbits near the corotation resonance will tend to be scattered into approximately circular orbits. Roškar et al. (2008) show that this phenomenon can lead to the formation of an outer stellar disk with a steeper exponential decline than the inner disk and formed entirely of stars scattered from the inner regions of the galaxy. This process also smooths out age and metallicity gradients in disks that otherwise form inside out and so tend to be older and less metal rich in the center.

2.4.2 Spheroid formation

There is a long-standing debate about how early-type galaxies formed. Was the process primarily monolithic or hierarchical? The response seems to centre on understanding star formation as opposed more simply to mass assembly.

The following observations argue for a monolithic origin:

- $[\alpha/Fe]$: the ratio of type II supernova (SNII)-generated alpha elements to iron, mostly produced by SNIa, is a powerful clock that demonstrates star formation in massive galaxies proceeded more rapidly than in lower-mass systems.

- *Star formation time*: SED (spectral energy distribution) analysis of distant galaxies favours systematically lower specific star formation rates for increasing stellar mass. This supports downsizing: massive galaxy formation preceded low-mass galaxy formation. Star formation in massive galaxies was complete before the peak in cosmic star formation history at $z \sim 1.5$

- *Fundamental plane*: the low dispersion in the fundamental plane for elliptical galaxies indicates a narrow spread in ages at a given stellar mass.
- *Colour-magnitude relation*: the low dispersion argues for a conspiracy between age and metallicity.

A hierarchical origin is supported by the following arguments:

- *Environment*: the dependence of morphological type on environment, especially mean density and cluster membership, argues for formation via a merging history.
- *Major mergers*: ultraluminous infrared and submillimetre galaxies invariably show evidence of triggering by major mergers.
- *Morphological evolution*: deep surveys show that the Hubble sequence is essentially unchanged to $z \sim 1$, but rapid evolution in both size and morphology occurs at higher redshift.
- *Star formation history*: the colour-magnitude relation conspiracy may be broken with GALEX data, which, however, leads to new issues concerning the gas supply needed to account for the residual star formation found in 30% of nearby early-type galaxies. Significant minor mergers provide a plausible explanation.

The reality most likely is a combination of both hierarchical and monolithic scenarios. The former controls disk formation, the latter seems appropriate to massive spheroid formation. However, even monolithic star formation is reconcilable with hierarchical assembly of dark matter and gas, although stars could only track hierarchical aggregation to a much lesser extent. Most stars in massive early-type galaxies must be formed over a period of order of the dynamical timescale and hence monolithically. However, a pure monolithic scenario is incompatible with the observed cosmic star formation and galaxy assembly history at high redshift.

The formation of galactic spheroids (which we take here to mean both the bulges of disk galaxies and isolated elliptical galaxies) can proceed via two distinct routes. The first, through the destruction of pre-existing stellar systems in violent mergers, is a natural consequence of hierarchical galaxy formation. The second, secular evolution of galactic disks, is a natural consequence of the dynamics of self-gravitating disk systems. It is worth noting that, observationally, it has been proposed that bulges be divided into two broad classes: "classical" bulges (those which look like ellipticals in terms of their light distribution and kinematics but happen to live inside a disk) and "pseudo-bulges" (those which do not look like ellipticals. Typically, pseudo-bulges are better fit by a Sersic profile with index $n \simeq 1$, as opposed to the $n = 4$ profiles of classical bulges, have significant rotation and may show signs of disk phenomena such as bars or spiral features).

There is good evidence that ellipticals (and therefore presumably classical bulges also) form through major mergers, and suggestions that pseudo-bulges are the result of secular evolution of galactic disks.

Major mergers

In the context of the ΛCDM scenario, spheroids are expected to be formed as the result of major mergers of disks.

Dissipative processes can lead to gravitationally bound interactions between galaxies. When the masses of the galaxies in question are comparable we may expect significant changes in their structure and the formation of a merger remnant which is very different from either of the merging galaxies. Such *major mergers* are thought to be responsible for the formation of spheroidal (i.e. elliptical) galaxies from pre-existing galaxies (which could be, in principle, disk galaxies, other spheroidals or something intermediate).

The process of violent relaxation, in which the energy of orbits undergoes order unity changes due to significant time-variable fluctuations in the gravitational potential, leads to a randomization of the orbits leading to a Maxwellian distribution of energies but with temperature proportional to stellar mass. This can turn the ordered motions of disks into the random motions seen in spheroids. This process is, however, rather poorly understood: it seeks an equilibrium state which maximizes the entropy of the system, but the usual entropy is unbounded in gravitating systems implying no equilibrium state exists.

The remnants of major mergers of purely stellar disk systems, while spheroidal, do not look like elliptical galaxies, in fact, their phase space densities turn out to be too low in the central regions compared to observed ellipticals. This implies that mergers between reasonably gas rich (gas fractions of around 25%) galaxies are required: the presence of gas allows for dissipation and the formation of higher phase-space density cores. Similar gas fractions and the subsequent dissipation are required to produce the observed tilt in the fundamental plane of elliptical galaxies. Mergers of purely stellar systems instead follow the expected virial scalings.

Mergers are often separated into *major* (mergers between galaxies of comparable mass) and *minor* (mergers in which one galaxy is significantly less massive than the other). Numerical simulations (Bournaud et al., 2005b) show that mergers with a mass ratio $\mu \equiv M_2/M_1 \geq 0.25$ are able to destroy any disks in the ingoing galaxies and leave a spheroidal remnant, while mergers with lower mass ratio tend to leave disks in place (although somewhat thickened). Moreover, mergers are expected to trigger a possibly very large enhancement in the star formation rate in the merging system.

It has recently become clear that not all major mergers lead to the formation of a spheroid. Under certain conditions, major mergers of very gas rich systems can lead to the reformation of a disk after the merger is over (Barnes 2002, Springel & Hernquist 2005). This requires a high gas fraction (greater than about 50%) just

prior to the final coalescence of the merging galaxies and therefore may preferentially occur under conditions which prevent the rapid depletion of gas after the first passage of the galaxies.

Secular evolution

Major mergers are not the only way to form a spheroid. Internal, secular processes (generically, any internal dynamical process operating on a timescale significantly longer than the dynamical time) in galaxies can also disrupt the cold and relatively fragile disks. In particular, bars (a disk phenomenon) can efficiently redistribute mass and angular momentum and lead to the build-up of dense central mass concentrations, reminiscent in many ways of bulges formed through mergers. To distinguish such secularly formed bulges from their merger-formed (or "classical") counterparts, they are referred to as "pseudo-bulges".

Such secular processes are the result of quite generic dynamical considerations and so most likely operate in all galaxies. Whether or not they are important depends upon their timescale. For example, relaxation due to star-star encounters in a galaxy operates on a timescale many orders of magnitude longer than the age of the Universe and so can be safely neglected. Instead, most relevant secular processes involve the interaction of stars (or gas elements) with collective phenomena such as bars or spiral arms.

A general picture of how secular evolution leads to the formation of pseudo-bulges has emerged. As a bar spontaneously begins to form[4] it transfers angular momentum to the outer disk and increases in amplitude. The response of gas to this bar is crucial: gas accelerates as it enters the bar potential and decelerates as it leaves. This leads to shocks forming in the gas which lay approximately along the ridge line of the bar. These shocks lead to dissipation of orbital energy and, consequently, to the inflow of the gas. The enhancement in the gas density (since it is concentrated towards the galactic center) inevitably leads to star formation and to the build-up of a pseudo-bulge. Bars eventually destroy themselves in this way: the increase in the central mass of the galaxy effectively prevents the bar instability from working.

[4]The bar instability involves the joint actions of the swing amplifier and a feedback mechanism. A randomly occurring leading spiral density wave in a disk will unwind and, as it does so, will rotate faster. As it swings from leading to trailing it reaches a maximum rotation speed which is close to the average orbital speed of stars in the disk. This leads to a resonance condition, in which the wave can strongly perturb the orbits of those stars, the self-gravity of which enhances the bar further, leading to an amplification of the wave. If there is some mechanism to convert the amplified trailing wave that results into a leading wave once more (e.g. if the wave can pass through the center of the galaxy and emerge as a leading wave, or if nonlinear couplings of waves can generate leading waves) the whole process can repeat and the wave will grow stronger and stronger.

Sizes

The sizes of spheroidal galaxies formed through major mergers can be determined given the properties of the progenitor galaxies and their orbit and some knowledge of the extent to which mass and energy is conserved through the merging process. If the galaxies are dissipationless, purely stellar, systems (a so-called *dry merger*) then energy is at least approximately conserved. In a gas rich (or *wet*) merger the gaseous component is likely to radiate significant amounts of energy prior to forming stars.

A simple model to compute the size of a galaxy formed via a major merger was described by Cole et al. (2000a), who assumed perfect conservation of mass and energy. The size of the merger remnant, r_f, is then given by:

$$\frac{c_f G(M_1+M_2)^2}{r_f} = \frac{c_1 G M_1^2}{r_1} + \frac{c_2 G M_2^2}{r_2} + \frac{f_{orbit} G M_1 M_2}{r_1 + r_2} \tag{2.12}$$

The left-hand side represents the gravitational binding energy of the final system while the first two terms on the right represent the gravitational binding energy of the two merging galaxies, which have masses M_1 and M_2 respectively and half-mass radii r_1 and r_2 respectively. The "c" coefficients relate the actual binding energy to the characteristic value of GM^2/r and depend on the density distribution of the galaxy. The final term in Eq. 2.12 represents the orbital energy of the two merging galaxies just before the merging and is parameterized in terms of their gravitational binding energy when separated by the sum of the half-mass radii. Cole et al. (2000a) adopt $F_{orbit} = 1$ so that this orbital term corresponds to a circular orbit. According to this approach, a merger of two identical galaxies of radii r_1 results in a remnant of size $r_f = (4/3)r_1$.

More recently, Covington et al. (2008) performed numerical simulations of merging galaxies including gaseous components, and found significant deviations from the simple model of Cole et al. (2000a) as a result of energy loss due to radiative processes in merging galaxies containing gas. Covington et al. (2008) propose an improved model which accounts for this energy loss and results in a merger remnant size given by

$$E_{int,f} = E_{int,i} + E_{rad} + E_{orb} \tag{2.13}$$

where $E_{int,f}$ is the internal binding energy of the final galaxy, $E_{int,i}$ is the internal binding energy of the initial galaxies and E_{orb} is the orbital energy of the galaxies just prior to the merger.

2.5 Scaling relations

The kinematic properties of spiral and elliptical galaxies are closely related to their luminosity. As I will discuss below, spirals follow the *Tully-Fisher relation*, whereas

elliptical galaxies obey the *Faber-Jackson relation* and are located in the *fundamental plane*. These scaling relations express relations between galaxy properties which any successful model of galaxy evolution must be able to explain. In the following I will describe these scaling relations and discuss their physical origin.

2.5.1 The Faber-Jackson Relation and the Fundamental Plane

Extensive studies have been made of correlations between various properties of elliptical galaxies, specifically, their luminosities, their sizes, as described by the de Vaucouleurs radius r_e , their central velocity dispersions, their surface brightnesses, the abundance of heavy elements, and so on. Among these, two results are of particular importance. The first is the analysis of Faber and Jackson who found a strong correlation between luminosity L and central velocity dispersion σ of the form $L \propto \sigma^x$ where $x \approx 4$. This correlation has been studied by other authors who have found values of x ranging from about 3 to 5. The significance of this relation is that, if the velocity dispersion σ is measured for an elliptical galaxy, its intrinsic luminosity can be found from the Faber-Jackson relation and hence, by measuring its observed flux density, also its distance can be found.

This procedure for measuring distances was refined by Dressler and his colleagues and by Djorgovski and Davis who discovered the so called *fundamental plane* (Fig. 2.9) for elliptical galaxies. The fundamental plane lies in a three-dimensional space in which luminosity L is plotted against the central velocity dispersion σ and the mean surface brightness Σ_e within the half-light radius r_e, that is, $\Sigma_e = L(\leq r_e)/\pi r_e^2$. Dressler and his colleagues found an even stronger correlation than the Faber-Jackson relation when the surface brightness was included, $L \propto \sigma^{8/3}\Sigma_e^{-3/5}$.

2.5.2 The Tully-Fisher Relation for Spiral Galaxies

The masses of spiral galaxies can be estimated from their rotation curves. In 1975, Tully and Fisher discovered that, for spiral galaxies, the widths of the profiles of the 21-cm line of neutral hydrogen, once corrected for the effects of inclination, are strongly correlated with the galaxy intrinsic luminosities. In their studies, they correlated the total B luminosities with the corrected velocity width ΔV of the 21-cm line and found the relation $L_B \propto \Delta V^\alpha$, where $\alpha = 2.5$. A much larger survey found a somewhat steeper slope, $\alpha = 3.5$, for luminosities measured in the optical B waveband and an even steeper slope, $\alpha = 4.3$ in the near-infrared H waveband at $1.65\mu m$.

The correlation was found to be much tighter in the infrared as compared with the blue waveband, because the luminosities of spiral galaxies in the blue waveband are significantly influenced by interstellar extinction within the galaxies themselves, whereas, in the infrared waveband the dust becomes transparent.

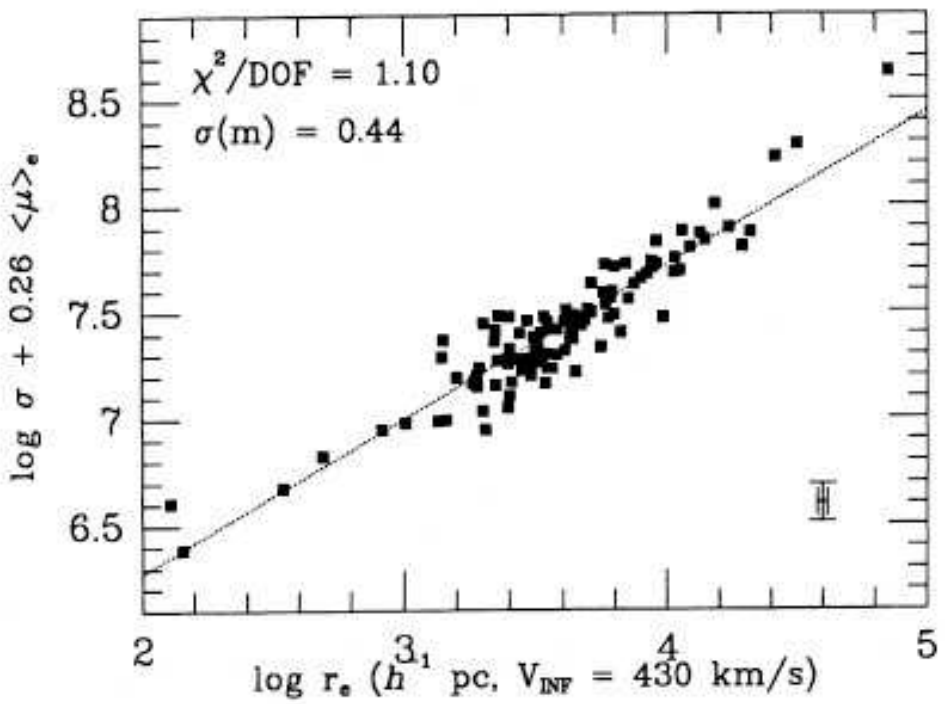

Figure 2.9: Fundamental Plane from Djorgovski & Davis (1987). The figure plots a linear combination of surface brightness and log velocity dispersion against log effective radius; thus, the 3-dimensional plane is rotated for an edge-on view.

What has come to be called the infrared Tully-Fisher relation is very tight indeed. As a result, measurement of the 21-cm velocity width of a spiral galaxy can be used to infer its absolute H magnitude and hence, by measuring its flux density in the H waveband, its distance can be estimated. This procedure has resulted in some of the best distance estimates for spiral galaxies and has been used in programmes to measure the value of Hubble's constant.

2.5.3 Luminosity-Metallicity Relations

An important aspect of the physics of galaxies which plays an important role in understanding their formation is the relation between their luminosities, masses, colors and the abundances of the heavy elements, the last being referred to as their *metallicities*. The observations are well controlled, but their interpretation is subject to many caveats and uncertainties.

For elliptical galaxies, it has been shown that there is a correlation between their luminosities and the strength of the magnesium absorption lines. In subsequent analysis, a similar relation was established over a wide range of luminosities and between the central velocity dispersion of the elliptical galaxy and the strength of the Mg_2 index[5], that is also strongly correlated with the (B - V) colors of the bulges of these galaxies and so the correlation referred to the properties of the galaxy as a whole.

A similar relation was found for elliptical galaxies in groups and clusters of galaxies in the sense that the more luminous the galaxy, the redder it is. The prime interest was in using this correlation in groups and clusters of galaxies to estimate their distances, but the sense of the correlation is the same as that found by Faber and her colleagues since galaxies with greater metallicities have greater line blanketing in the blue and ultraviolet regions of the spectrum and hence are redder than their lower metallicity counterparts. These studies laid the foundation for the analysis of the huge databases of galaxies available from the Sloan Digital Sky Survey.

Tremonti et al. (2004), rather than using luminosity, worked directly with the stellar mass of the galaxy. This approach has become feasible thanks to the development of efficient and reliable codes for determining the stellar and gaseous masses of galaxies from their optical spectra (Bruzual & Charlot, 2003a). It turns out that the correlation with stellar mass is stronger than that with luminosity. Figure 2.10 shows the strong correlation between metallicity, estimated by using the oxygen abundance, and the total stellar mass of star-forming galaxies. These observations provide important constraints on the physics of the evolution of galaxies. With the advent of 8-10-meter class telescopes, these studies have been extended to samples of high redshifts galaxies and so constrain directly the evolution of the stellar and gaseous content of galaxies of different masses.

[5] Mg_2 is a metallicity indicator based on the prominent absorption feature around 518 nm of the Magnesium line.

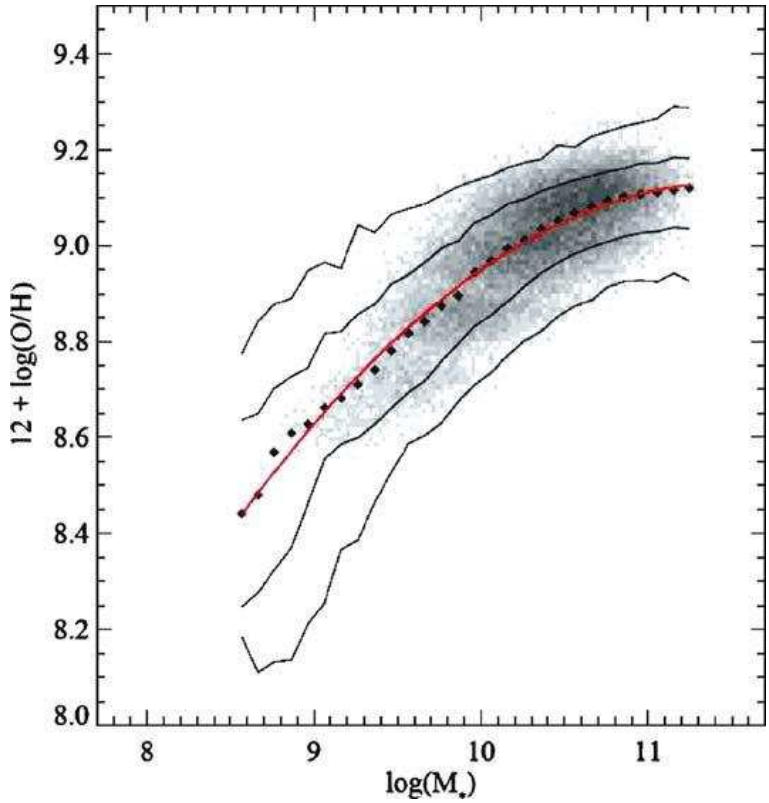

Figure 2.10: The stellar mass-gas phase metallicity relation for 53,400 star-forming galaxies from the SDSS. The large black points represent the median in bins of 0.1 dex in mass which include at least 100 data points. The thin line through the data is a best-fitting smooth curve and the solid lines are the contours which enclose 68% and 95% of the data (Tremonti et al., 2004).

2.6 The Properties of Galaxies: Correlations Along the Hubble Sequence

What gives the Hubble classification physical significance is the fact that a number of physical properties are correlated with position along the sequence. Although there are clear trends, there is a wide dispersion about these correlations at any point along the sequence. Some of the more important correlations are listed in the following:

- *Total masses and luminosities.* The average masses and range of masses are roughly constant for galaxies in classes S0 to Scd. At later stages beyond Scd, the mass of the galaxies decreases monotonically. The mass-to-luminosity ratios of the galaxies in the sample are roughly constant and so it is no surprise that the average luminosity for the S0 to Scd galaxies is roughly constant, whilst it decreases monotonically beyond Scd. These relations again quantify van den Bergh's remark that the classical Hubble types refer primarily to luminous, and consequently, massive galaxies.

- *Neutral hydrogen.* There is a clear distinction between elliptical and spiral galaxies in that very rarely is neutral hydrogen observed in ellipticals while all spiral and late-type galaxies have significant gaseous masses. The upper limit to the mass of neutral hydrogen in elliptical galaxies corresponds to $M_{HI}/M_{tot} \leq 10^{-4}$. For spiral galaxies, the fractional mass of the galaxy in the form of neutral hydrogen ranges from about 0.01 for Sa galaxies to about 0.15 at Sm, the increase being monotonic along the revised Hubble sequence. The fractional hydrogen mass is more or less independent of the mass of the galaxy at a particular point along the Hubble sequence. A consequence of the constancy of the M_{tot}/L_B ratio for the galaxies in the sample is that there is also a significant trend for the ratio M_{HI}/L_B to increase along the sequence.

- *Total surface density and surface density of neutral hydrogen.* These quantities change in opposite senses along the Hubble sequence. The total surface density, as determined by the total mass of the galaxy and its characteristic radius, decreases monotonically along the sequence, whereas the surface density of neutral hydrogen increases along the sequence.

- *Integrated color.* Elliptical galaxies are red whereas late-type galaxies are blue. Despite the systematic trend, there is a significant dispersion about the relation at each point in the sequence. For example, there are red Sc galaxies.

- *Luminosity function of HII regions.* In a pioneering study, Kennicutt et al. (1989) determined the luminosity function of HII regions in different galaxy types. Normalizing to the same fiducial mass, it was found that there is a much greater frequency of HII regions in the late-type galaxies as compared with early-type galaxies and that the relation is monotonic along the sequence.

An obvious interpretation of these correlations is that there are different rates of star formation in different types of galaxy. The various correlations provide

information about the past, current and future star formation rates in galaxies. The correlation with color along the sequence is related to the past star formation history of the galaxy; the changes in the luminosity function of HII regions refer to star formation rates at the present epoch; the large fraction of the mass of neutral hydrogen and its large surface density at late stages in the sequence show that these galaxies may continue to have high star formation rates in the future.

CHAPTER 3

Galaxy interactions: An overview

The original concept of galaxies as "island universes" is, of course, not the whole truth. While many galaxies do seem to be evolving in isolation, there are clear indications that some galaxies are interacting strongly with other galaxies or their larger scale environment. In fact, a number of galaxies does not find a place in the Hubble sequence and cannot be associated to any standard galaxy type.

Collisions and mergers are cited as culprits in the production of a large range of morphological phenomena observed in galaxies. Galactic interactions may generate faint structures, such as arcs and rings, or create an entirely different type of galaxy, depending on the types of galaxies involved and their orbital geometry.

In the early days of Hubble's original classification, it was common to classify all galaxies that were neither spiral nor elliptical as irregular, but today it is more common to make a further distinction between "normal irregular" galaxies and "peculiar" galaxies, which have unusual shape, size, structure and composition. Most of these objects have been tidally distorted by interaction with another galaxy.

Peculiar galaxies are not an exception in the universe, in fact it is thought that about one fifth of all galaxies are peculiar in some way.

The study of these types of galaxies has gradually put more emphasis on the important evolutionary influence of interactions between galaxies. Astronomers are now convinced that this process plays a fundamental role in establishing the different galaxy shapes. These interactions are also important in stimulating the formation of stars and star clusters.

Galaxies can interact with their neighbors in many different ways. In the following sections (3.2 and 3.3) I shall describe some of the more common mechanisms of interaction.

3.1 Galaxy orbits

A consequence of the hierarchical nature of structure formation in a cold dark matter universe is that dark matter halos are built through repeated merging of earlier generations of less massive halos. While for a long time numerical simulations indicated that all traces of earlier generations of halos were erased during the merging process, it was understood on analytical grounds that this was likely a numerical artifact rather than a physical result. Beginning in the late 90's, N-body simulations clearly demonstrated that this was indeed the case. Unlike earlier generations of simulations, they found that halos can persist as *subhalos* within larger halos into which they merge. Each subhalo may, in principle, have acted as a site of galaxy formation and so may contain a galaxy which becomes a satellite in the host potential.

These subhalos are gravitationally bound to their host halo and, as such, they will orbit within it. A subhalo's orbit can take it into regions where interactions affect the properties of any galaxy that it may contain. I begin, therefore, by considering the orbits of subhalos.

At the point of merging, which we shall define as the time at which the center of mass of a subhalo first crosses the virial radius of its future host halo, we expect the orbital parameters (velocities, energy etc.) to be of the order of the unity when expressed in units of the characteristic scales of the host halo. This distribution of velocities reflects the influence of the host halo (infall in its potential well) but also of the surrounding large scale structure which may have torqued the infalling subhalo. Such orbits will typically carry subhalos into the inner regions of halos. Most orbits initially reach to 40% of the virial radius, but a significant tail have orbits which carry them into the inner 10% of the halo.

The collisionless dark matter is affected only by gravity, while the baryonic content of galaxies (and their surrounding atmospheres of gas) can be strongly affected by hydrodynamical forces. For this reason, in the following I will divide the possible interactions between galaxies in two classes: *gravitational* (sec. 3.2) and *hydrodynamical* (sec. 3.3) interactions.

3.2 Gravitational interactions

3.2.1 Mergers

Orbiting subhalos are gravitationally bound to their host halos and, as such, they rarely encounter other subhalos at velocities resulting in a bound interaction.

To cause gravitationally bound interactions between subhalos and their galaxies typically requires a dissipative process to reduce their orbital energies. *Dynamical friction* fulfills this role and tends to drag subhalos down towards the center of their host halo, where they may merge with any other galaxy which finds itself there. When a massive object moves through a cloud of smaller lighter bodies

the effect of gravity causes the light bodies to accelerate and gain momentum and kinetic energy. From the conservation of energy and momentum, we may conclude that the heavier body will be slowed in order to compensate. Since there is a loss of momentum and kinetic energy for the body under consideration, the effect is called dynamical friction. Another equivalent way of describing this process is that the light bodies are attracted by gravity toward the larger body moving through the cloud, and therefore the density at that location increases and is referred to as a gravitational wake. In the meantime, the object under consideration has moved forward and, therefore, the gravitational attraction of the wake pulls it backward and slows it down. Of course, the mechanism works the same for all masses of interacting bodies and for any relative velocities between them. However, while the most probable outcome for an object moving through a cloud is a loss of momentum and energy, as described intuitively above, in the general case it might be either loss or gain.

The classic derivation of dynamical friction acceleration from Chandrasekhar (1943) has been used extensively to estimate dynamical friction timescales within dark matter halos, but besides the fact the dark matter halos are not isothermal, there are a number of other reasons why this simple approach is not accurate. For instance, Chandrasekhar's derivation assumes an infinite, uniform medium, and not a dark matter halo with a radially varying density profile. Moreover, subhalos will experience mass loss as they orbit changing the timescale, and the host halo itself is constantly evolving and is non-spherical with a non-isotropic velocity dispersion. While some of these limitations can be overcome (e.g. mass loss can be modeled) others are more problematic.

When two galaxies of similar mass collide at a speed that is comparable with the internal velocities of the galaxies, the dynamical friction approximation is no longer valid. In these cases numerical simulations suggest that a slow encounter between galaxies often leads to the merging of two systems one.

The consequences of merging for the galaxies involved, the ranges of initial velocities and impact parameters for which the encounter leads to a merger and other observational properties (e.g. velocity dispersion, rotation curves etc.), will be discussed in Chapter 6.

3.2.2 Tidal destruction

An orbiting subhalo and its galaxy can experience tidal forces which may strip away the outer regions or, in extreme cases, can entirely disrupt the galaxy resulting in a stellar stream.

In a rotating frame in which an orbiting satellite instantaneously has zero tangential velocity, the effective tidal field felt by the satellite is:

$$\Phi = -\frac{d}{dr}\left(\frac{GM_h(r)}{r^2}\right) + \omega^2 r \tag{3.1}$$

where $M_h(r)$ is the mass enclosed within radius r in the host halo and ω is the

instantaneous angular velocity of the satellite. An estimate of the radius, r_t , in the satellite subhalo/galaxy system beyond which tidal forces become important can be obtained by equating the tidal force to the self-gravity of the subhalo:

$$\Phi r_t = \frac{GM_s(r_t)}{r_t^2} \tag{3.2}$$

Beyond this *tidal radius* the material becomes unbound from the satellite, forming a stream of dark matter and, potentially, stars which continue to orbit in the host potential.

This simple estimate ignores the fact that particles currently residing in the inner regions of a subhalo may have orbits which carry them out to larger radii where they may be more easily stripped. As such, the degree of tidal mass loss should depend not only on the density profile of the satellite but also on the velocity distribution of the constituent particles. Attempts to account for this phenomenon find that particles in an orbiting satellite that are on prograde orbits are more easily stripped than those on radial orbits which are in turn more easily stripped than those on retrograde orbits. Additionally, some material will be stripped from within the classical tidal radius, as particles which contribute to the density inside that radius may be on orbits which carry them beyond it. This can lead to more extensive and continuous mass loss as the reduction in the inner potential of the satellite due to this mass loss makes it more susceptible to further tidal stripping.

Observational examples of *Tidal accretion* will be discussed in Chapter 4.

3.2.3 Cold accretion

Evidence for the accretion of cold gas in galaxies from the environment has been rapidly accumulating in the past years. HI observation of galaxies and their environment have brought to light new facts and phenomena which are evidence of ongoing or recent accretion:

1. A large number of galaxies are accompanied by gas-rich dwarfs or are surrounded by HI cloud complexes, tails and filaments. This suggests ongoing minor mergers and recent arrival of external gas. It may be regarded, therefore, as direct evidence of cold gas accretion in the local universe.

2. Considerable amounts of extra-planar HI have been found in nearby spiral galaxies. While a large fraction of this gas is undoubtedly produced by galactic fountains, it is likely that a part of it is of extragalactic origin.

3. Some spirals are known to have extended and warped outer layers of HI. It is not clear how these have formed, and how and for how long the warps can be sustained. Gas infall has been proposed as a possible origin.

4. The majority of galactic disks are lopsided in their morphology as well as in kinematics. Also here, recent accretion of cold gas from the environment has been advocated as possible cause.

To be more precise, accretion takes place both through the arrival and merging of gas-rich satellites and through gas infall from the intergalactic medium (IGM). The new gas could be added to the halo or be deposited in the outer parts of galaxies and form reservoirs for replenishing the inner parts and feeding star formation. The infall may have observable effects on the disk such as burst of star formation and loopsidedness.

Gas accretion plays a fundamental role in the evolution of galaxies. Fresh supplies of gas are needed for the ongoing process of star formation. Such a process of galaxy "nurture" is expected to continue to the present day. The importance and role of gas infall for the evolution of disk galaxies have been recognized for many years.

The rate of star-formation in the solar neighborhood has been remarkably constant over the Milky Way's life, which suggests that the gas consumed by star formation has been replaced by accretion. Steady accretion of metal-poor gas would also explain the discrepancy between the observed stellar metallicity distribution in the solar neighborhood and that predicted by closed-box models[1] of chemical evolution. It is not clear how much new gas is needed to sustain star formation.

Several arguments suggest that most of the baryons in the local universe still reside in the intergalactic medium. Out of this medium, galaxies are expected to grow through a series of infall events ranging from a small number of major mergers down to an almost continuous infall of dwarf galaxies and gas clouds, the latter being more and more important at low redshifts. Recent, high-resolution cosmological simulations show that there are two modes of accretion: *hot accretion*, mainly around massive structures, and *cold accretion* (clouds, streams or filaments) for galaxies with lower halo masses, which correspond to the population of star forming galaxies.

In Chapter 5 I will show some examples of galaxy formation through cold gas accretion from cosmic web filaments.

3.2.4 Harassment

A less extreme form of tidal interaction arises when tidal forces are not strong enough to actually strip material from a galaxy. The tidal forces can, neverthe-

[1]The closed-box model for the chemical evolution of a galaxy is the simples possible model. It assumes that in the period under study no material enters or leaves the galaxy. Initially the material is entirely gaseous and free of heavy elements. As the times goes on, stars are formed from the interstellar gas and massive stars return hydrogen, helium and heavy elements to the interstellar medium. The supply of interstellar gas is gradually consumed, and the remaining gas becomes steadily more polluted with heavy elements.

less, transfer energy from the orbit to the internal motions of stars in the galaxy, effectively heating the galaxy. As a generic result of such heating the galaxy expands and the cold, ordered structures such as disks are destroyed. Interactions involving high-speed galaxies and their satellites are often referred to as *galaxy harassment*. Harassment can disturb, or even radically change, the morphologies of the galaxies involved, often inducing new bursts of star formation. Asymmetrical galaxies, disturbed galaxies, warps, bars and tidal tails can all be produced through galaxy harassment. Research into the nature of galaxies is aided by the study of harassed galaxies for two reasons: 1) the effects of harassment (tidal tails, asymmetry, warps etc) can often be used to probe the distribution of matter (both visible and dark) within the galaxies involved; 2) current research suggests that harassment, and other interactions, may play an important role in shaping the evolution of galaxies.

The harassment process works via *tidal shocking* in which the stars in a galaxy experience a rapidly changing tidal field along their orbits and gain energy in the form of random motions, thus leading to a system which is expanding and becoming dynamically hotter.

3.3 Hydrodynamical Interactions

3.3.1 Ram pressure

The orbital motion of a subhalo through the hot atmosphere of a host halo leads to a large ram pressure. Ram pressure stripping is the removal of a galaxy gaseous disc due to its motion through the intracluster medium. The characteristic magnitude of that pressure $P_{ram} = \rho_{host} V_{orbit}^2$ can greatly exceed the binding energy per unit volume of both hot gas in subhalos and interstellar medium (ISM) gas in their galaxies. As such, ram pressure forces may be expected to quite efficiently remove the hot atmospheres of satellite galaxies, a process with several aliases including *strangulation*[2] and *starvation*[3], and the ISM of the galaxy.

The first quantification of this process showed that the ram pressure force could remove material from a galactic disk if it exceeded the gravitational restoring force per unit area. The mass loss caused by this ram pressure can, in many cases, be further enhanced by related effects, such as turbulent viscous stripping. The process of ram pressure stripping has been incorporated into some semi-analytic models of galaxy formation where it plays an important role in mediating the

[2]Galaxy fuel supply is stripped away as it encounters the other objects. Starved of the raw material needed to form new stars, it will slowly change color from blue to red as its existing stars age.

[3]Induces a decrease of the stellar surface brightness of the perturbed disc by removing any extended gaseous halo surrounding the galaxy and preventing further infall of such gas onto the disc. The galaxy becomes anemic simply because it exhausts the gas reservoir through on-going star formation.

transition of cluster galaxies from the blue cloud of star-forming galaxies to the red sequence of passively evolving galaxies.

Ram pressure stripping is a good candidate to explain observations such as the HI deficiency of cluster disc galaxies and the truncated star forming discs in the Virgo cluster. A distinct feature of ram pressure stripped galaxies is that their gas discs are distorted or truncated while their stellar discs appear undisturbed, because ram pressure stripping affects only the gaseous components of the galaxy. In addition to the effect on the galaxy, ram pressure stripping plays an important role in the evolution of the ICM because the gas lost by galaxies enriches the ICM with metals.

3.4 Numerical methods for modeling galactic interactions

Interacting galaxies encompass a wide range of phenomena; indeed, if events during galaxy formation are counted, there are probably few galaxies that were not shaped by interactions or even outright mergers (Toomre, 1977).

Simple estimates imply that relaxation times of galaxies are many orders of magnitude longer than a Hubble time (Binney & Tremaine, 1987). Consequently, the dynamics of stars in galaxies is well described by the collisionless Boltzmann equation:

$$\frac{\partial f}{\partial t} + v\frac{\partial f}{\partial x} - \bigtriangledown\Phi\frac{\partial f}{\partial v} = 0 \tag{3.3}$$

where $f = f(x, v, t)$ is the distribution function normalized so that $fdxdv$ is the number of stars in the phase-space volume $dxdv$ centered on the point (x, v). The potential Φ includes the self-consistent field generated by the stars as well as the gravitational influence of the dark matter and gas. Even if the nature of the dark matter remains enigmatic, observational constraints suggest that it too obeys equation 3.3.

3.4.1 N-Body Methods

In the purely stellar-dynamic limit, the interaction of galaxies is a well posed problem, in the sense that the evolution is determined entirely by the collisionless Boltzmann equation, that states that the flow of stellar phase points through phase space is incompressible, or the phase space density around the phase point of any star remains constant. Unfortunately, we don't know how to obtain relevant analytic solutions to this partial differential equation obeyed by a function of six dimensions, except in the limit of weak interactions or for rather special systems, so numerical methods must be used.

Rather than solve the collisionless Boltzmann equation with a finite difference technique in six dimensions, a Monte-Carlo approach is usually employed. The initial $f(x, v)$ is used as a probability distribution function to pick phase-space coordinates x_i and v_i for particles $i = 1, \cdots, N$; these particles are then integrated along the characteristic curves of equation 3.3:

$$\frac{dx_i}{dt} = v_i \tag{3.4}$$

$$\frac{dv_i}{dt} = - \bigtriangledown \Phi_i \tag{3.5}$$

Despite the enormous simplification introduced by equations 3.4 and 3.5, the evolution of interacting galaxies is quite costly to compute, owing mainly to the difficulty of calculating the self-consistent potential. In practice, the mass in real galaxies is much more finely divided than in any computer model, so the model's self-consistent potential is much noisier than that of actual galaxies. This gives rise to an unwanted diffusion in phase space which can alter the structure of simulated galaxies on short time scales.

The various known algorithms for computing the potential of a system of N particles can be categorized as either "action-at-distance" or "field" methods. The former explicitly treat interactions between individual particles while the latter do so only indirectly through the contributions of particles to the global gravitational field. The simplest action-at-distance technique is the *direct summation.* A common expression for the gravitational potential at the location of particle i is:

$$\Phi(r_i) = -G \sum_{j \neq i} \frac{m_j}{[|r_i - r_j|^2 + \epsilon^2]^{1/2}} \tag{3.6}$$

where ϵ is the "softening parameter". Some early investigations of dynamics of mergers were performed using this algorithm and larger simulations with $N > 10000$ may be feasible.

A variety of methods have been proposed to reduce the computing cost of the self-consistent potential. For some problems, it is expedient to neglect the self-gravity and evolve the system in a potential which is known a priori, such as in test-particle methods, the restricted three body method or semi-restricted N-body codes. However, the dynamics of interacting galaxies will not be represented faithfully without including self-gravity.

The majority of the known self-consistent methods have historically not been useful for studying systems with small filling factors in three dimensions such as interacting and merging galaxies. An exception is the technique known as the "hierarchical tree" method, which has had significant impact on the study of colliding galaxies. All variants of this technique retain the essential ingredients of the action-at-distance formulation. Particles are processed similarly to direct summation, but the potential from distant groups of particles is approximated using low-order multipole expansions. A distinct approach used in "expansion

codes", relies on the uses of basis function expansion to compute potential from the known density field sampled by particles.

However, the choice of method is largely dictated by considerations of efficiency. Action-at-distance and field methods suffer from comparable degrees of relaxation for the same spatial resolution and particle number. Therefore, there is no objection in principle against using direct methods to evolve collisionless systems, provided that a sufficiently large N can be used to suppress relaxation effects to the extent required.

3.4.2 Gas-Dynamic Methods

While present-day galaxies typically contain less than 10% of their luminous mass in this form, gas is critical to our understanding of many galactic phenomena such as starburst and active galactic nuclei. Galactic gas obeys the ordinary conservations laws for a compressible fluid. However, given our present level of understanding of the interstellar medium, the dynamics of galactic gas is not well-posed. Because of cooling and feedback from supernovae, interstellar gas is highly inhomogeneous and comprises several distinct phases. It is difficult to model the different phases simultaneously, and some compromises must be necessarily be made.

One strategy is to focus on global issues where the detailed small-scale structure of the gas is probably not crucial. In the limit where the gas can be represented as a continuous medium, its equations of motion can be solved either by finite-difference algorithms or by particle-based techniques. A good example of the latter is the method known as *smoothed particle hydrodynamics* (SPH). This is a computational method used for simulating fluid flows. It has been used in many fields of research, including astrophysics, ballistics, volcanology, and oceanography. It is a mesh-free Lagrangian method (where the coordinates move with the fluid), and the resolution of the method can easily be adjusted with respect to variables such as the density. The smoothed-particle hydrodynamics (SPH) method works by dividing the fluid into a set of discrete elements, referred to as particles. These particles have a spatial distance (known as the *smoothing length*), over which their properties are smoothed by a kernel function. This means that the physical quantity of any particle can be obtained by summing the relevant properties of all the particles which lie within the range of the kernel.

Since SPH is Lagrangian, it does not suffer from limitations on spatial resolution or global geometry and is specially well-suited for studying interacting systems. In addition, SPH can be generalized so that it is adaptive in both space and time.

A phenomenological treatment is sometimes useful in the opposite extreme when the gas is modeled as a set of discrete clouds. In the "sticky-particle" method, particles representing the gas evolve similarly to collisionless particles but undergo inelastic collisions amongst themselves, thereby dissipating kinetic energy. Computationally, this approach is simpler than those which solve the equations of motion

for continuum gas, but requires a number of ad hoc parameters whose relationship to actual physical processes is problematic. Given our ignorance of the true state of interstellar gas it is difficult to argue for or against one of the two extremes represented by the SPH or sticky-particle formalism.

3.5 Signatures of galaxy interactions

Although the peculiar appearance of galaxies in a few double and multiple systems had been noticed much earlier, it was Zwicky (1956) who first called attention to the enormous variety of extended structures seen in such objects. Zwicky described these features as "clouds, filaments and jets of stars which are ejected massively from galaxies in collision" by "large scale tidal effects".

Many astronomers, however, where skeptical that certain remarkably narrow appendages could be blamed on tidal forces, and Zwicky himself suggested that "electromagnetic actions contribute to the internal viscosity of stellar systems".

3.5.1 Bridges and Tails

Bridges and *tails* are common in interacting disk galaxies. The former often appear to link large galaxies to small companions (see Fig. 3.1), while the latter stretch far away from the galaxy causing perturbation (Fig.3.2).

That gravity could extract these narrow structures was illustrated by Toomre & Toomre (1972). These calculations usually treated each galaxy as a point mass surrounded by a disk of test particles: a simple but adequate numerical method. Only close, relatively slow passages, parabolic or even sub-parabolic, produce convincing bridges and tails, while faster passages produce smaller disturbances. As Toomre & Toomre (1972) noted, such slow passages would naturally result between pairs of galaxies which, bound gravitationally since their formation, have fallen together for the first time along extremely eccentric orbits.

With varying degrees of success, the calculations reproduced bridges and tails as thin, curving ribbons stripped away from the disk by violent tidal forces. Such features are clearly *relics* of recent collisions rather than signs of ongoing interactions. The most impressive examples arise in direct passages where the orbital angular speed of the companion temporarily matches that of the stars within the disks, creating a quite broad resonance.

The tidal hypothesis gained additional credibility from Toomres' simple models of some well known interacting systems (see for example Fig. 3.3).

Further studies of these and other galaxies continue to support the tidal picture. For example, kinematic studies of interacting galaxies have revealed velocity fields quite consistent with tidal models.

Early test particle models raised many questions which could only be addressed with self-consistent calculations. One such question concerns effects of self-gravity in structuring tidal bridges and tails. Once launched, such features develop in an

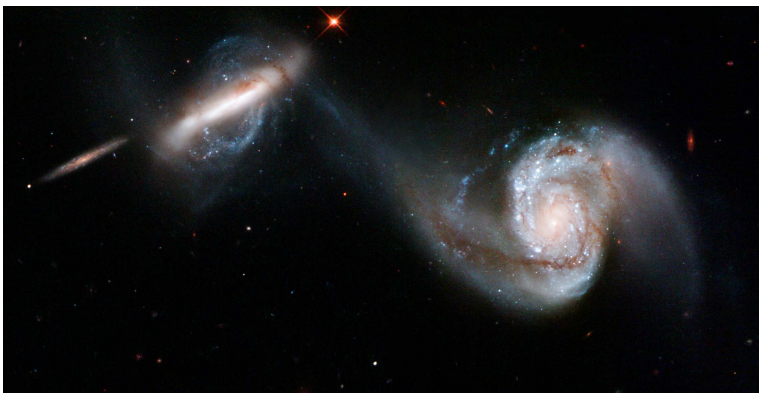

Figure 3.1: These two galaxies are known collectively as Arp 87. The bridge between them is made of stars, gas, and dust. It spans 75,000 lightyears, and shows that there is a gravitational connection between the two galaxies. At one point, the two galaxies came close to each other and a "violent gravitational battle" ensued. This type of connection is relatively common, and it is expected that the two galaxies will eventually join to create one larger galaxy. The blue spots on the galaxy on the right are regions where new stars have recently formed. This was likely a result of the interaction between the two galaxies.

essentially *kinematic* manner, and deep exposures of the antennae (NGC4038/9) reveal thick tails consistent with free expansion both parallel and perpendicular to the direction of extension. On the other hand, self-gravity may create small-scale structure within tails. Zwicky noticed a concentration of luminosity near the end of the southern tail of NGC4038/9 and speculated that such objects might evolve into dwarf galaxies. Models indicate that dwarf galaxies formed in this manner can incorporate considerable gas from the disks but very little material from the halos of their parent galaxies, and so should have unusually low mass-to-light ratios.

Another such question concerned the conjecture that tails extracted from disks might be unable to climb out deep halo potential wells. This raised the possibility that the long observed tails could contradict the large masses proposed for invisible halos. However, encounters between self-consistent disk/halo models indicate that galaxies with halos of four times the mass of their luminous components can nonetheless produce tails as long as those of NGC4038/9. Since the energy required to climb out is provided by falling in, mere length is probably not an effective constraint on halo masses.

3.5.2 Wavelike Tidal Spirals

Self-gravity plays an important role in structuring the *inner* disks of some interacting galaxies. Toomre & Toomre (1972) noted that galaxies with bisymmetric spiral

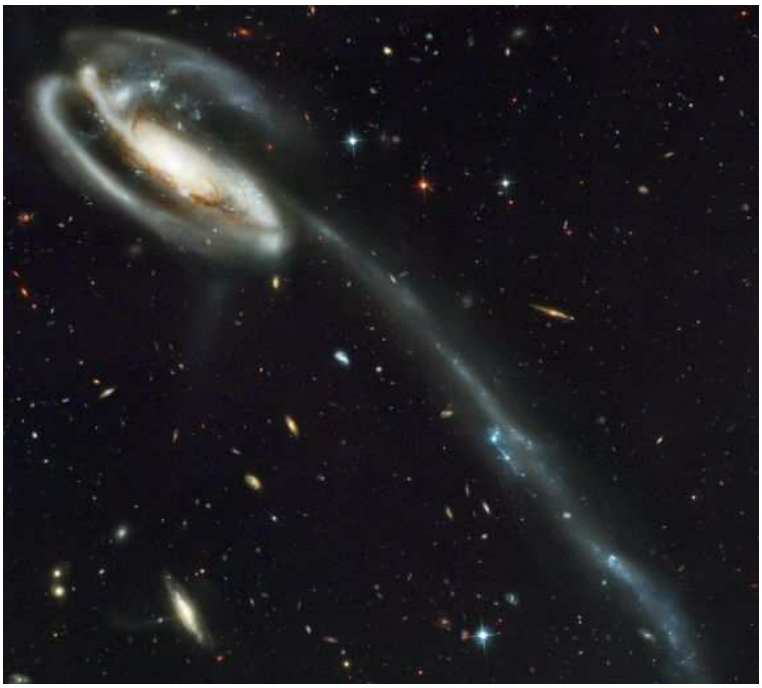

Figure 3.2: The spiral galaxy Arp 188, the Tadpole Galaxy. Its eye-catching tail is about 280 thousand light-years long and features massive, bright blue star clusters. Probably a more compact intruder galaxy crossed in front of Arp 188 - from left to right in this view - and was slung around behind the Tadpole by their gravitational attraction. During the close encounter, tidal forces drew out the spiral galaxy's stars, gas, and dust forming the spectacular tail.

Figure 3.3: *Left panel* - Ground based image of the "antennae" galaxies. *Right panel* - Computer model of two identical disk galaxies in interaction (Toomre & Toomre, 1972).

patterns often have close companions, and suggested that these spirals have a tidal origin. N-body models of galactic disks abundantly illustrate the development of tidally excited spirals. In a self-gravitating disk of stars, perturbations can grow by factors $\gg 10$ while swinging around to become trailing spiral patterns. Such "swing amplification" occurs because the shearing of the spiral pattern temporarily matches the epicyclic motions of individual stars, permitting a modified form of Jeans instability to develop. This mechanism can amplify tidal perturbations in situ, rapidly bringing forth a trailing spiral over much of the disk. The calculations show that such spirals, although manifested as density waves as well as material arms, do not survive long but wind up tightly over a few rotation periods.

Perturbations strong enough to generate the large scale tidal features originally modeled by Toomre & Toomre (1972) also give rise to a "grand-design" spiral density wave in the inner disk.

3.5.3 Cartwheel galaxies

Some galaxies with pronounced rings appear to be the result of collisions. As shown in simple N-body simulations (Lynds & Toomre, 1976), rings develop when a companion galaxy makes a close and nearly normal incidence passage through the plane of the victim, exciting large epicyclic oscillations in the target disk. Initially, all these oscillators are in phase, but since their periods increase with mean radius, the oscillations drift out of phase and orbits crowd together radially to produce an expanding ring.

Indeed, kinematics studies of several ring galaxies find velocities consistent with the collision model. Even the "folded ring" galaxy Arp 144, once interpreted as a collision between a galaxy and an intergalactic HI cloud, is now know to include two bodies with infrared colors typical of evolved stellar populations.

Not all ring-making collisions are described by the simplest models. The "Cartwheel galaxy" itself presents a modest puzzle or two; the putative companion does not seem massive enough to produce the very strong ring observed, and the spoke-like features giving this galaxy its name are not well understood. Self-consistent three dimensional models might help account for all these systems.

Only head-on collisions leave the bulge of the victim at the center of the ring; if the perturber is somewhat off-center, the bulge can be yanked to one side, producing an empty ring. More off-center passages, although presumably more common, may not retain their ring-like appearance for as long as a direct hit; the resulting morphology changes smoothly from a ring to an open tidally-induced spiral as the pericentric separation is increased. Ring-like shapes resulting from off-center passages are more common than generally thought.

3.5.4 Damaged ellipticals

Tidal interactions involving elliptical galaxies are more subtle than those involving spirals, since encounters in rich clusters tend to be fast and disturbed ellipticals produce diffuse sprays of stars instead of narrow filaments. Nonetheless, a number of interacting ellipticals have been identified by their luminosity profiles, distorted and off-center isophotes, and peculiar kinematics.

The effects of hyperbolic encounters on the luminosity profiles of spherical galaxies have been studied both analytically and numerically. Such encounters do not tidally truncate the target; on the contrary, they promote stars to loosely-bound orbits, creating extended halos with $\rho \propto r^{-4}$ density profiles, closely following a de Vaucouleurs law. Stars which have not yet phase-mixed produce transient, outward-moving luminosity excesses. This provide a natural explanation for the distended profiles of galaxies with nearby companions.

Photometric decomposition techniques provide further evidence of interactions among elliptical galaxies. In these reductions a smooth, concentric luminosity model is simultaneously fit to each galaxy in the field; the residuals reveal nonconcentric isophotes and elongated features referred to as "dynamical friction wakes". These studies find little evidence for *strong* interactions among most multiple nucleus cluster galaxies, in general accord with the view that such systems are either optical doubles or extremely fast, plunging encounters. Some points of confusion remain; some astronomers report that only pairs with velocity differences smaller than their internal dispersions show signs of interaction, while others found evidences for interactions in pairs with velocity differences in excess of 1000 km/s.

Surface photometry and long-slit velocity data of several interacting elliptical galaxies have been used to construct semi-restricted 3-body models. These models do a fairly convincing job of reproducing the tidally disturbed morphology and "U-shaped" velocity profiles of their subjects, but it is difficult to assess their claimed uniqueness since they do not seem to be overconstrained by the data. Fully self-consistent models including dark halos are probably needed to reliably predict the future evolution of these systems.

An interesting exception to most of the rules for interacting ellipticals are "dumbbell" systems. These are comparable pairs of giant elliptical galaxies with projected separations of $\sim 10h^{-1}kpc$, found at the centers of some rich clusters. The distorted morphologies and relatively small pairwise velocity differences observed in these objects imply that many are bona fide interacting systems. Tremaine (1990) suggested that dumbbell galaxies are the last stage in the merger of rich clusters, each containing a D or cD galaxy. This proposal provides a reasonable account of many features of dumbbell systems, including their morphology, separations, velocity differences and overall frequency.

3.6 How galaxies accrete mass?

Galaxies can acquire material from passing companions via mass transfer or accrete much less-massive neighbors, such as satellites, suffering only relatively minor damage. Although individual events like these add only a modest amount of mass to large galaxies, their consequences can have a significant effect on observable properties of galaxies and provide indications as to the frequency and importance of galaxy collisions.

3.6.1 Shells and other fine structures

Beginning with Arp's (Arp, 1966) classic study of peculiar galaxies, "fine structures" such as *shells, ripples, plumes, boxy isophotes and X-features* have been detected in an ever larger fraction of S0's and ellipticals. The actual percentage of all galaxies exhibiting such fine structure is rather uncertain, owing to the difficulty of determining if the faint features detected are bona fide. This complication is especially acute for late-type disks, which often possess diffuse spiral patterns that mimic these structures, e.g. shells.

Simulations employing restricted methods support the view that the accretion of material by large galaxies provide a natural explanation for the origin of fine structures. Shells can form either by the "phase-wrapping" of debris on nearly radial orbits or by the "spatial-wrapping" of matter in thin disks. Actually, further studies demonstrated that the shell-forming material need neither reside initially in a thin disk nor be on precisely radial orbits. Shells can be produced during the accretion of spheroidal companions by larger galaxies, provided that the total phase-space volumes they occupy are sufficiently different, and in nonradial collisions through mass transfer, eliminating concerns that an improbable geometry would be needed to produce them.

Other types of fine structure develop in encounters which simultaneously produce shells. Plumes consisting of debris on unbound or weakly-bound orbits occur frequently in shell-forming collisions. Moreover, material accreted by nonspherical potentials can produce X-structures and features that appear boxy in projection.

In spite of the general acceptance of the accretion model, a number of difficulties remain. The numerical studies mostly ignore self-gravity and the consequences of dynamical friction. While the self-gravity of the victim does not appear crucial to the issue of whether or not fine structures will form, it is impossible to predict, e.g. the radial distribution of shells formed by a close collision without including dynamical friction. Indeed, if the accretion scenario is correct, it appears that dynamical friction probably played a significant role in structuring some of these objects since many contain extremely tightly bound shells. Self-consistent calculations indicate that the disruption of satellites can indeed inject material onto tightly bound orbits, populating inner shells. However, even these models are not sufficiently detailed to explain objects such as NGC3923 (Fig. 3.4), which contains

Figure 3.4: The prototypical shell galaxy NGC 3923.

more than 20 shells distributed regularly around the galaxy.

The restricted simulations are deficient in other regards. In some galaxies, the intensity of shells increasingly far from the galaxy drops similarly to that of the elliptical, suggesting that these shells may be of *internal origin*: shells are induced in a thin disk component of an elliptical by a tidal encounter with another galaxy. The existence of such disks in ellipticals is problematic, but the inability of restricted calculations to explain the radial luminosity of shell systems emphasizes the need for more physical models.

It should also be noted that boxy or X-shaped structures need not arise through accretion events; these features simply reflect phase-mixed populations of stars in certain kinds of orbits which may have been created by a variety of processes.

3.6.2 Polar Rings

Many S0 galaxies possess rings of gas-rich material that appear to be kinematically distinct from the galaxy proper. The survey by Whitmore et al. (1990) implies that $\sim 0.5\%$ of all S0s have *polar rings*, i.e. rings of gas, dust and young stars with axes aligned perpendicular to the major axis of the disk. The actual fraction of S0s with such features may be even larger when observational selection effects and ring lifetimes are taken into account.

Searches for similar features in elliptical galaxies have met with mixed success. Obscuring dust lanes (Spavone et al., 2009) and diffuse, extended disks and rings of gas (Spavone et al., 2010) are seen in many ellipticals, but few ellipticals with rings as substantial as those of classical polar rings in S0s are known. A notable exception is the galaxy AM2020-5050, which is classified as Hubble type E4. However, this object rotates rapidly and appears somewhat intermediate between an elliptical and a S0 galaxy.

Since the rings often appear kinematically distinct from their hosts, it is generally assumed that they are of external origin. Different scenarios have been proposed for the formation of polar rings: accretion of gas-rich dwarfs, capture of material from a passing galaxy by mass transfer and, more recently, accretion of cold gas by cosmic web filaments. I will discuss this point in more details in chapter 4.

Theoretical studies of polar rings have instead focused mainly on determining the equilibrium states accessible to material on closed orbits in axisymmetric or triaxial potentials. These calculations have shown that the "settling time", which is the time for gas in an axisymmetric or triaxial potential to settle into steady state, is small compared to the age of the universe, and so there is sufficient time for accreted gas to form polar rings.

However, all these studies are limited by their neglect of self-gravity and time-dependent effects and their use of unrealistic initial conditions. The role of initial conditions in ring-forming events is not likely to be elucidated without resort to calculations that treat the dynamics of galaxy collision and mergers in detail, including dynamical friction and dissipation. Such models may eventually determine why rings are most common in S0 galaxies, largely avoiding other galactic types, and also explain why fine structures such as shells should be more common than rings if all result from accretion of external matter.

3.6.3 Destruction of satellites

Dynamical friction will cause the orbits of satellites around massive galaxies to decay. Eventually, the victims will be destroyed tidally and/or cannibalized by the primary galaxy. Galaxies like the Milky Way have probably accreted a non-negligible amount of mass in the form of discrete objects over a Hubble time. Although it is difficult to make precise estimates of this effect, owing to the absence of a complete theory of galaxy formation and large scale structure, simple argument

implies that galaxies do not age pacefully in isolation, even if they do not experience a strong encounter with a neighbor of comparable mass.

In the limit of weak encounters, perturbation theory can be used to compute torques on satellites and predict their decay paths. More generally, there is a little alternative to numerical simulations, particularly if the details of the tidal disruption of the companion and/or the self-consistent response of the primary to large perturbations are of interest. Numerical studies have included the orbital decay of satellites around spherical galaxies and disks. The results are supported by quasi-analytic calculations, implying that simulations yield reliable decay rates. Fully self-consistent calculations show that the torque on a satellite near a disk is derived in roughly equal measure from the disk and halo, provided that galaxies possess dark matter halos similar to those inferred in external spirals.

However, it seems likely that a variety of phenomena may be blamed on satellite accretions. Some ellipticals contain cores that are kinematically distinct from the surrounding galaxies (Spavone et al., 2006). One possible explanation for these peculiar velocity fields is the accretion by the host galaxy of a spinning dwarf galaxy. This idea has been tested by using N-body simulations, with models in which angular momentum is transferred from the orbit of the dwarf to the primary by gravitational torques during a merger. If the satellite's orbit is retrograde, the angular momentum deposited can partly cancel the primary's original rotation and even reverse it near the center where the rotation curve is rising, so the central regions of the primary galaxy can display distinct velocity fields from the outlying regions.

Satellite mergers may also alter the structure of disk galaxies. In fact, decaying satellites can excite transient warps in the outer parts of disks that may be sufficiently long-lived to explain some stellar warps in external spirals. Moreover, dynamical heating by these satellite accretions produce disturbed, featureless disks possessing little or no large scale spiral structure. Tidal debris from cannibalized satellites may account for a number of peculiar features in our Galaxy, including retrograde halo stars and the Magellanic Stream[4].

More generally, the consequences of satellite accretions are important for theories of the formation of galaxies and large-scale structure. Schweizer et al. (1990) proposed that the bulges of spiral galaxies may be the relics of past accretion events. A similar suggestion has been made for thick disk components of external, edge-on systems. Such processes may be responsible for many aspects of galactic structure that were once attributed to events at the time galaxies were born. If so, then it is impossible to relate the observed properties of galaxies to cosmological models without considering late and ongoing evolutionary effects.

[4]The Magellanic Stream is a high-velocity cloud of gas connecting the Large and the Small Magellanic Clouds. It came into existence by a near-collision of both galaxies some 2.5 billion years ago.

3.7 The role of environment

Evidence that galactic mergers play a significant cosmological role comes from a simple argument presented by Toomre & Toomre (1972). Out of the $\sim$ 4000 galaxies in the NGC catalog, there are at least a dozen which are either close pairs of disk galaxies strongly interacting or recent merger remnants with prominent double tails. Adopting a nominal age of 5×10^8 yr for these objects, Toomre (1977) concluded that we should expect to find roughly 250 old relics of mergers among the NGC system alone, provided that the present rate of those intense encounters is at all typical of the 10-15 billion years that galaxies have existed. In fact, the present merger rate probably underestimates the average rate over the past $\sim 10^{10}$ yr. The pairs we find in violent interactions and mergers today presumably spent most of the last 10^{10} yr moving near apogalacticon[5], and have only recently fallen back together (Toomre & Toomre, 1972). Almost any reasonable assumption for the distribution of binding energies for an ensemble of such pairs yields a merger rate that declines with time (Toomre, 1977).

Besides the relatively isolated pairs which appear to account for most of the objects listed by Toomre (1977), violent interacting galaxies are also found in other settings. Galaxies in compact groups frequently exhibit strong tidal distortions (Hickson, 1997) and kinematics peculiarities (Spavone et al., 2006). Numerical simulations indicate that such groups experience on the order of one merger per crossing time as a result of low velocity encounters. This view gains further support from observations indicating that $\sim$ 6% of compact group members have colors characteristic of recent merger remnants (Zepf et al., 1991). Such mergers might not be as easily recognized as those involving isolated pairs since the tidal forces of other group members tend to shred extended tidal tails. It remains difficult to estimate how many merger remnants are being produced in compact groups, largely because characteristic lifetimes are not well known for many of these systems.

Rich clusters provide another possible setting for interactions and mergers. Initially, attention focused on "cannibalism" as a mechanism for forming extremely luminous galaxies found at the centers of rich clusters. In these early models, dynamical friction was invoked to bring massive galaxies into the core of the cluster, where they would merge to form a D or cD galaxy. However, more detailed studies showed that the victim galaxies would be deprived of much of their halo mass by the cluster's tidal field, and therefore would not spiral in rapidly enough to contribute much more than $\sim$ 10% of the luminosity of the central giant. This result has been substantiated by observational studies which show that most of the "secondary" nuclei in cD galaxies are merely passing through with velocities typical of the cluster as a whole. Such high speed collisions also occur elsewhere in rich clusters and their effects can be studied using analytic approximations; in general, however, it seems unlikely that these collisions cause significant damage to a large

[5]The point in the orbit of a star at which it is furthest from the center of its local galaxy

number of galaxies or contribute a substantial amount of stripped luminosity to a cluster-wide background.

Galactic interactions may have played a more important role during the formation of rich clusters. Within the context of "hierarchical clustering" models for the growth of large scale structure, rich clusters are expected to form by the aggregation of smaller ones. Before collapsing, such a system probably resembles a hierarchical federation of compact groups. Taking into account that frequency and intensity of interactions strongly depend on the density of the environment where they are, such systems are favorable sites for violent interactions since most of galaxies reside in pockets of substructure with relatively high densities and low velocity dispersions. A toy model for dynamical evolution of a hierarchy of 128 core/halo galaxies illustrate how such system passes through stages resembling irregular clusters before relaxing to form a regular, centrally concentrated cluster with substantial population of merger remnants (Barnes & Hernquist, 1992). It remains to be shown that more realistic initial conditions can produce enough mergers to account for the elliptical populations of rich clusters without also depositing more than $10 - 15L_*$ in a central star-pile.

These considerations suggest a plausible explanation for the overall correlation between spatial density and types of galaxies. Merger remnants are formed in regions of intermediate density which are undergoing gravitational collapse, and are caught up by the subsequent growth of larger-scale structure. Thus the products of interactions are found in the regions of higher density than the regions where interactions are now taking place. If so then rich clusters are heaps containing nearly a Hubble time worth of galactic collisions.

3.8 Mergers and morphology

The above arguments imply that at least a fair fraction of elliptical galaxies acquired their present forms as a result of mergers. But merging is only one process shaping galaxies, and the origin of ellipticals is only a part of the larger problem of the formation and evolution of all galaxies. For example, elliptical galaxies share many properties with the bulges of disk galaxies; it seems unlikely that this is a coincidence, Indeed, the success of numerical simulations in producing elliptical-like merger remnants can be partly attributed to the presence of fairly substantial bulges in the victim disk galaxy models. Are bulges merely ellipticals which have subsequently acquired disks, or are the central parts of ellipticals instead merged bulges dressed in the remains of their attendant disks?

Purely collisionless mergers are constrained by conservation of phase-space density; if they are to produce remnants with small cores, the victims must have had small cores to begin with. But mergers of gas rich galaxies could develop cores of much higher phase-space densities through dissipative processes. This is indeed what appears to be happening in many starburst galaxies, and the central concentrations of gas found in these galaxies have characteristic masses and scales

consistent with the cores of ellipticals. The simulations indicate that galactic collisions can *"bring deep into a galaxy a fairly sudden supply of interstellar material"* (Toomre & Toomre, 1972). Core formation from this material has many features in common with "dissipative collapse" pictures for galaxy formation, but two new points need to be stressed. First, merging galaxies in our neighborhood offer an hint of the formation of spheroidal systems in general. Second, the large collapse factors invoked in the dissipative picture may require strong gravitational torques exerted during a merger-like process to get rid of excess angular momentum of the gas.

If this approach to galaxy formation is fruitful, then models of galactic mergers including gas dissipation and star formation might be expected to reproduce the color and metallicity profiles of elliptical galaxies as well as their kinematic properties. Although such models will probably have a number of free parameters reflecting our relative ignorance about the process of star formation, it need not follow that their realization would teach us nothing about events leading up to the formation of real galaxies. On the other hand, real galaxies also have features that may prove difficult to account for in any numerical model feasible with present-generation computers.

Recent observations suggest that nearby galaxies may harbor black holes with masses of 10^7 to $10^9 M_\odot$. The formation of such massive black holes is attended by a substantial release of energy which would presumably manifest as an active galactic nucleus. There is considerable circumstantial evidence linking nuclear activity to violent interactions and mergers. If massive black holes turn out to be common features of galactic spheroids then it seems plausible that spheroidal systems and their central holes were formed as a result of mergers between gas-rich galaxies. This hypothesis has the potential to link galactic activity at redshift $z \sim 2$ with the formation of bulges and elliptical galaxies.

Perhaps one of the greatest puzzles associated with a dissipative merger picture for spheroid formation is the origin of globular clusters. The number of globular clusters in a galaxy is well correlated not with *total* luminosity but rather with the luminosity of the spheroidal component alone. Mergers of disk galaxies, however, are expected to produce remnants with fewer globular clusters per unit luminosity than typical ellipticals. In fact, the specific frequency of globular clusters in elliptical galaxies seems to be somewhat environment dependent, and field ellipticals are perhaps no richer in globulars than typical disk galaxy merger remnants. But still unexplained are the tremendous numbers of globular clusters in some galaxies (like M87); if such galaxies formed as the result of mergers, their progenitors may well have systematically differed from present epoch disk galaxies in other respects besides globular cluster content.

3.9 Further questions

Most astronomers would agree that galaxies interact and gravity plays the leading role in the dynamics of such encounters. At present, however, there is a considerable controversy over the significance of interactions in shaping galaxies. The point of view adopted in this thesis is that interactions provide important examples of galaxy transformations.

Numerous questions remain: How much satellite accretion can disk galaxies stand? How much has occurred? What are realistic parameters for merger progenitors and remnants? What range of remnant dynamics and orbital structure are permitted by the merger process? What distributions of axial ratios, minor axis rotation, and non-elliptical isophote shapes are expected of mergers? Does long term dynamical evolution play a role? How does gas lose angular momentum during interactions and mergers? What effects will star formation have? What photometric, kinematic and enrichment signatures of starburst events should we look for in older merger remnants? What is the origin of density-morphology relationship? How often are compact groups formed in evolving loose groups?

In the following chapters I will address some of these open issues.

CHAPTER 4

The tidal accretion scenario

4.1 Early type galaxies

Given their dominance of the stellar mass density in the local universe, understanding the formation and the subsequent evolution of early type galaxies is a key element of the modern galaxy evolution theories.

The morphology and structure of galaxies carry important information on their formation and evolution history. The most prominent components of a galaxy are its bulge and disk; they have quite different structural and dynamical properties and, for this reason, are considered to have followed different formation histories.

After the introduction of the morphological classification of galaxies by Hubble (1936), the elliptical and lenticular galaxies, grouped into one class called "early-type galaxies", were considered the simplest stellar system, given the lack of disks or internal structures. When CCD detectors[1] become of common use and observations with higher resolution and sensitivity become available, it has been revealed that even elliptical galaxies have internal structures such as dust, shells, and dynamical subsystems. Observations have in fact confirmed that a large portion of elliptical galaxies do host embedded disk components and there are indications suggesting that 1/3 to 2/3 ellipticals may have disks, but they are too faint to be detected.

[1]Charge Coupled Device is a device for the movement of electrical charge, usually from within the device to an area where the charge can be manipulated, for example conversion into a digital value. This is achieved by "shifting" the signals between stages within the device one at a time. CCDs move charge between capacitive bins in the device, with the shift allowing for the transfer of charge between bins.

In the early research, bulge/disk light decomposition was usually performed with a classical de Vaucouleurs' $R^{1/4}$ law profile bulge plus an exponential profile disk. Recently, such decompositions are often substituted by a generalization of the $R^{1/4}$ law (Sersic, 1968) by generalizing the $1/4$ to $1/n$. The Sersic profile accounts for part of the observed deviation from the $R^{1/4}$ law for the bulges of galaxies (Caon et al., 1993). However, a possible way to check if the detected exponential components in this two component decompositions of early type galaxies are really connected to the disks existing in the galaxies, is to verify if these disks are rotationally supported as the disks in spiral galaxies.

In the context of the standard cosmological model, in which mergers play a major role in the build-up of present day galaxies, it is fundamental to investigate the role of galaxy interactions, by estimating the structural properties of close pairs. The signatures of interactions can be most efficiently studied in early type galaxies that exhibit morphological peculiarities such as systems of shells, interpreted as remnants of recent merging, or the presence of dust lanes in spheroidal systems (Spavone et al., 2009), that are thought to be the result of accretion of cold material from gas rich companions within the last few Gyr.

4.1.1 Dynamical subsystems

There have been growing evidences in recent years that galaxies accrete significant amounts of material in the form of gas and small companions. In fact, in galaxies classified as "normal ellipticals" have been detected small cores of higher surface brightness with respect to the principal core (Efstathiou et al. 1982, Spavone et al. 2006). In NGC5813, for example, the inner core rotates more rapidly than the outer, and has a smaller velocity dispersion, thus suggesting a merger between a low and a high luminosity elliptical galaxies; the robust core of a small elliptical, in fact, can survive a merger with a giant elliptical and form a distinct subsystem at the center.

4.1.2 Dust lanes

According to classical definition, elliptical galaxies contain no dust. However this definition is no longer valid, since observations have shown that even classical ellipticals often contain dust. Most of the observed dusty ellipticals have dust lanes along their minor axes and therefore may be prolate. Moreover, most bright ellipticals are dynamically supported not by rotation but by velocity dispersion anisotropy, which suggests that they are triaxial.

However, the estimates of the percentage of ellipticals containing dust give us a lower limit, since the dust is usually in well-defined, nearly edge-on disks; this implies that many face-on dust distributions are going undetected. Typical dust masses are $\sim 10^5 \div 10^6 M_\odot$ and, for canonical gas-to-dust ratios, this corresponds to $\sim 10^7 \div 10^8 M_\odot$ of cold gas.

In early type galaxies, some gas is acquired by accretion, and some is expected from mass loss during stellar evolution. The most clear evidence for the gas accretion comes from the kinematics: the gas and dust are usually in disks rotating at random orientations with respect to the optical major axis. Minor-axis dust lanes rotate at right angles to the stars and sometimes dust lanes and stars even rotate in opposite directions. Moreover, the accretion is also suggested by the morphology: at large radii,in fact, dust lanes often show S-shaped warps or transitions from regular disks to irregular distributions. Such behavior is expected for material just settling into equilibrium. It is however important to note that accretion does not require cannibalism, because gas can be donated by a galaxy that gets away.

The geometry of the dust in elliptical galaxies can, in principle, be used to study their intrinsic shape. Gas in a spheroidal or triaxial potential settles into certain preferred planes through differential precession and dissipation; in the simplest case in which the shape of the potential does not rotate, the gas settles into one of two planes, i.e. perpendicular to the shortest or to the longest axis. In a spheroidal galaxy, only the equatorial orbits are stable; if we knew that ellipticals are spheroids, then those with minor-axis dust lanes would be prolate and those with major-axis dust lanes would be oblate. But ellipticals can be also triaxial systems, then, for some infall angles and galaxy shapes, gas is captured into polar orbits. Therefore, a dust lane along a particular axis is consistent with either oblate or prolate structure. For this reason, there is no unique relationship between galaxy shape and dust-lane geometry.

4.1.3 Shells and ripples

Shells or ripples are faint, arc-shaped structures in galaxy halos. that can result from the accretion of small galaxies. These structures are made of stars similar in color to or slightly bluer than the underlying elliptical and their outer edges are sharp and often edge brightened. Such structures form when a small accreted galaxy falls almost radially into a smooth and stationary potential.

Shell detection frequencies show that accretion of small companions is a normal event in the life of a galaxy, but not all encounter geometries and viewing angles produce visible shells, so the real percentage is larger. Shells may give us informations about galaxy shapes; Dupraz & Combes (1985) in fact suggest that when shells are short arcs bisected by the major axis, the elliptical is likely to be prolate and edge-on, when instead are aligned with the minor axis, the elliptical is oblate and edge-on, while when they are randomly distributed in azimuth and the elliptical is nearly round, it is likely to be oblate and face-on.

4.2 Secular evolution by accretion

The properties summarized above are clear evidences that galaxy structure may be altered significantly by the accretion of gas and small companions. In the past,

galaxies showing clear signs of interactions were classified as "peculiar"; now we know that accretion happens often enough in a typical galaxy that even modest events can add up to a significant effect. However, this is secular evolution and not like the more violent mergers that may completely destroy a disk and convert two spirals into one elliptical.

Since typical masses of dust and gas ($10^7 \div 10^8 M_\odot$) are not much less than the mass of stars in a core, significative changes in core properties could result. Moreover, enough material can be accreted to make disks that would change a galaxy's apparent morphological type, and many shell galaxies have blue colors and early-type spectra implying recent bursts of star formation.

All these evidences have changed the traditional picture in which early type galaxies were believed to form on a gravitational collapse time scale and with little subsequent evolution, favoring a more gradual formation as in disk galaxies, where gas infall and disk building are still going on today. So, tidal accretion and the rearranging of mass in ellipticals may be a significant evolutionary process.

4.3 Revisiting the formation history of the minor axis dust lane galaxy NGC1947

Authors: Marilena Spavone, Enrichetta Iodice, Rosa Calvi, Daniela Bettoni, Giuseppe Galletta, Giuseppe Longo, Paola Mazzei and Gabriele Minervini

Published on Montly Notices of the Royal Astronomical Society, 393, 317

Abstract

In this paper we present a detailed study of the peculiar early-type galaxy NGC1947. The main goal of this work is to constrain the dynamical status and the formation history of NGC1947 by comparing the observed properties with the predictions derived from different galaxy formation scenarios. To this aim, we derived the photometric and kinematical properties of NGC1947. Due to the presence of an extended dust-lane, which crosses the galaxy center along the photometric minor axis, we used near-infrared images (J and K bands) to derive an accurate analysis of the stellar light distribution. Optical images (in the V and R bands) are used to derive the color profiles and color maps to study the structure of the dust-lane. The observed kinematics confirm the presence of two components with decoupled angular momentum: gas and dust rotate along the minor axis, while the rotation velocities of the stars are observed along the major axis. The complex structure observed in NGC1947 support the hypothesis that some kind of interactions happened in the evolution of this object. We analyzed two alternatives: a merging process and an accretion event. We discussed how the observed properties strongly suggest that the decoupled ring of gas and dust have been accreted from outside.

Introduction

One of the major open issues in modern cosmology is to understand how galaxies formed and evolved. It is likely that the formation of galaxies is dominated by two processes: the assembly of luminous and dark matter through accretion and mergers, and the conversion of baryonic and non-baryonic matter into stars. The Cold Dark Matter (CDM) scenario for galaxy formation is based on the hierarchical mass assembly (Cole et al., 2000b) which predicts that the observed galaxies and their dark halo were formed through a repeated merging process of smaller systems. This is the reason why the study of galaxy interactions and merging has received an ever increasing attention in recent years, both on the observational and theoretical sides.

It has been shown that gravitational interactions and mergers affect the morphology and dynamics of galaxies from the Local Group to the high-redshift universe (e.g. Conselice et al. 2003a; Bundy et al. 2004; Lin et al. 2004; Kartaltepe et al. 2007; De Propris et al. 2007; Lotz et al. 2008). These observational results support the scenario in which the merging of two disk galaxies produces spheroidal merger remnants with physical characteristics, such as density profiles, mean velocity dispersion and surface brightness, quite similar to those observed for E and S0s (Toomre & Toomre 1972; Barnes & Hernquist 1992; Bekki 1998a; Bournaud et al. 2005a). However, other types of interactions, such as smooth accretion and stripping seem to be equally important in the growth of galaxies and the relative weights of the various processes depends on the environment, which drive many morphological features observed in galaxies, such as bars, shells (see Malin & Carter 1980) and highly inclined or even counter-rotating rings/disks (see Galletta 1996 for a review). Concerning the latter morphology, different degrees of evolution of these peculiar rings/disks are seen: some cases the decoupled matter is composed by stars and gas, and regions of recent star formation are also observed (Iodice et al. 2002b, Iodice et al. 2002c; Reshetnikov et al. 2005); other cases show rings with a particularly smooth structure (Iodice et al., 2004), or formed only by gas (Bettoni et al., 2001). In general, these peculiar galaxies have very large amount of gas (Richter et al. 1994 and Galletta et al. 1997) and dust which lies in the same plane of the decoupled ring/disk (e.g. Arnaboldi et al. 1997; Bettoni et al. 2001; van Driel et al. 2002a; Cox et al. 2006). The decoupling of the angular momentum between the two components cannot be explained by the collapse of a single protogalactic cloud, thus a "second event" must have happened in the formation history of these systems. Given all the above, such peculiar galaxies turn out to be the ideal laboratory where to derive detailed information about many of the physical processes controlling galaxy interactions and merging.

Several theoretical works based on numerical simulations, have tested two plausible scenarios for the origin of the decoupled matter: either gas accretion from infall processes, or merging between gas-rich galaxies (Thakar & Ryden 1996, Thakar & Ryden 1998; Reshetnikov & Sotnikova 1997; Bekki 1998b; Bournaud & Combes 2003a, Bournaud et al. 2005a). In both cases, the decoupled material forms a ring (Quinn 1991, Hernquist & Weil 1993) which after a while settles into one of the principal planes of the gravitational potential associated with the host galaxy (Heisler et al. 1982; Bertola et al. 1991; Bournaud & Combes 2003a). Multiple accretion events may also account for more complicated objects, like NGC2685 where two orthogonal rings are observed around the main galaxy body (Schinnerer & Scoville 2002; Bournaud & Combes 2003a).
The unequal-mass merging of two disk galaxies is the other way to build a galaxy with an highly inclined ring/disk: the morphology and kinematics of the merger remnants depends on the initial orbital parameters and the initial mass ratio of the two galaxies involved in the process (e.g. Bournaud & Combes 2003a, Bournaud et al. 2005a).

External gas can also be accreted from cosmic web filaments with high inclined angular momentum relative to the main disk plane (Davé et al. 2001; Semelin & Combes 2005; Macciò et al. 2005) and recent theoretical work has argued that this might even be the most realistic way by which galaxies get their gas (Kereš et al., 2005). Finally, in the standard CDM scenario, recent high-resolution cosmological simulations of galaxy formation have shown that angular momentum misalignment during the hierarchical structure formation can also lead to the formation of highly inclined ring/disk (Brook et al., 2008a).

Although most of the formation scenarios proposed so far seem able to account for many of the observed morphologies and kinematics for this class of peculiar galaxies, the relative weight of the two main processes, i.e. the merging of two galaxies or external gas accretion, remains still uncertain. The reasons for such an uncertainty mainly reside in the poor understanding of many processes which are at work during gravitational interactions such as, for instance, gas dissipation, star formation efficiency, feedback, gas re-heating, etc., phenomena that all strongly affect the dynamical history of galaxies. Detailed photometric and kinematical observations of systems in different dynamical states, both in the local universe and at higher redshift, can help better constraining the physics of such processes. To this aim, we present a detailed study of the peculiar early-type galaxy NGC1947, that can be considered as a prototype of minor-axis dust-lane galaxy (see Fig.4.1).

In 1978 Bertola & Galletta (1978) made the first study of a small sample of peculiar galaxies (including NGC1947) that all showed a dust-lane crossing perpedicularly the central spheroidal body: the similarities in observed properties let them to conclude that, by a morphological point of view, these objects should be considered as a new class of galaxies. A larger sample of dust-lane galaxies, including objects similar to NGC1947, have been studied by Hawarden et al. (1981), and they found that galaxies with a minor axis dust-lane form a dominant group among all dust-lane galaxies. The difference of the angular momenta of the stellar, gaseous and dusty components is a clear proof that the three components have not all the same origin, and an accretion of new material from outside was addressed as possible formation mechanism for such class of objects (Hawarden et al., 1981).

This work is a part of an ongoing research project aimed to select a sample of peculiar and interacting galaxies, for which both multiwavelength photometric and kinematical data are available, and to compare the observed properties with the predictions derived from different galaxy formation scenarios.

The main properties of NGC1947 are listed in Tab.6.3. The morphological classification of this galaxy is somewhat controversial. In fact, NGC1947 was initially classified as S0 peculiar by de Vaucouleurs et al. (1976) and $S0_3$ peculiar by Sandage & Tammann (1987) while, due to the absence of a photometrically detectable disk, Bertola et al. (1992) and Oosterloo et al. (2002) classified it as an E1 crossed by a series of dust lanes along the optical minor axis. As shown by Bertola et al. (1992) the peculiarity of NGC1947 resides in the presence of three parallel minor-axis dust lanes, which appear as concentric rings, in addition to the

Figure 4.1: Color composite image of NGC1947 assembled from EMMI-NTT images in the V (blu channel), J (green channel) and K (red channel) bands. The North is up, while the East is on the left of the image.

Table 4.1: General properties of NGC1947

Parameter	Value	Ref.
Morphological type	S0 peculiar	NED[a]
R.A. (J2000)	05h26m47.6s	NED
Dec. (J2000)	-63d45m36s	NED
Helio. Radial Velocity	1100 km/s	NED
Redshift	0.0037	NED
Distance	15 Mpc	
Axial ratio$_K$	0.98	
$(J-K)_T$	0.931	2MASS[b]
Total m$_J$ (mag)	8.445 $\pm$ 0.02	2MASS
Total m$_K$ (mag)	7.510 $\pm$ 0.03	2MASS
$M(HI)(M_\odot)$	$3.4 \times\ 10^8$	Oosterloo et al. (2002)
$M_{dust}(M_\odot)$	$15.3 \times\ 10^5$	Oosterloo et al. (2002)
$L_K(L_\odot)$	$2.65 \times\ 10^{11}$	
$M/L_K(M_\odot/L_\odot)$	0.2	

[a]NASA/IPAC Extragalactic Database
[b]2 Micron All Sky Survey

central one, which is typical of the dust-lane galaxies. The main dust lane crosses the center along the SW direction, while the others, less pronounced and parallel to the central one, are detected in the NE side. The galaxy also exhibits a ring of molecular gas (Sage & Galletta, 1993) and a disk-like distribution of ionized gas centered on the nucleus and at the same position angle of the dust lane. Moreover, the stars in NGC1947 rotate along the galaxy's major axis, perpendicular to the gas rotation axis (Bertola et al., 1992).
A considerable amount of HI was detected by Oosterloo et al. (2002): the HI gas is distributed in a warped disk, which is aligned with the dust lane and it rotates in the same sense; the HI mass is about $3.4 \times\ 10^8 M_\odot$.

This paper is structured as follows: in Section 6.9 we describe the observations and data reduction procedures. The morphology in the NIR and optical bands and the light and color distribution of the galaxy are described in Section 4.3, while in Section 6.9 we present a 2-dimensional model of the light distribution. In Section 4.3 we discuss the star and gas kinematics along the two principal photometric axes of the galaxy, and in Section 4.17 is presented and discussed the spectral energy distribution derived for NGC1947. Finally, in Section 5.6 we draw our conclusions. Throughout this paper we shall adopt for NGC1947 a distance of about 15 Mpc based on $H_0 = 75\, km\, s^{-1}\, Mpc^{-1}$ and an heliocentric radial velocity $V = 1100\, km\, s^{-1}$, which implies that 1 arcsec = 0.07 kpc.

Observations and data reduction

Near-Infrared data - NGC1947 belongs to a selected sample of peculiar galaxies observed (December 2002) in the Near-Infrared (NIR) J and K bands with the SofI infrared camera at the ESO-NTT telescope. The field of view was 4.92×4.92 $arcmin^2$ with a pixel scale of 0.292 arcsec/pixel. Images were acquired in the offsetting mode: a cycle was defined by several images on the target, interspersed with sky frames and with an integration time of 60 seconds; each object frame was taken with a small offset from the galaxy center and the sky frames were taken before and after each galaxy frame. More cycles were obtained in the K band than in the J band, in order to have a better estimate of the background level. A total exposure time of 720 sec was obtained on the target in the J band and of 2760 sec in the K band. The average seeing during the observing time is about $FWHM \simeq 1.1$ arcsec.

The data reduction was carried out using the CCDRED package in the IRAF[2] (*Image Reduction and Analysis Facility*) environment. The main strategy adopted for each data-set included dark subtraction[3], flatfielding correction, sky subtraction and rejection of bad pixels. Finally, all frames were registered and co-added to form the final science frames. Several standard stars, from Persson et al. (1998), observed at the beginning, middle and end of each observing night, were used to transform instrumental magnitudes into the standard J and K band systems.
The calibrated K band image of NGC1947 is shown in Fig. 4.2 (right panel).

Optical data - CCD images of NGC1947 in the Johnson V and R bands were extracted from the European Southern Observatory (ESO) Public Archive. They had been obtained with the red arm of EMMI at ESO-NTT telescope and the detector used for the observations consisted of two MIT/LL CCDs, with a scale of 0.332 arcsec/pixel (with a 2×2 binning) and a field of view of 22.7×22.7 $arcmin^2$. The average seeing was $FWHM \sim 0.99 \pm 0.03$ arcsec for the V band, and $FWHM \sim 0.94 \pm 0.03$ for the R band. There were seven exposures available in the V band with an integration time of $100s$, and five exposures in the R band with an integration time of $60s$. The raw frames were pre-processed using the standard IRAF tasks for de-biasing and flat-fielding. The flat-field was performed using normalized sky flat. Each CCD was reduced independently: the images were dithered and shifted in order to obtain a complete image of both the galaxy and its surroundings. The frames of each CCDs were combined, after de-biasing and flat-fielding, to filter out cosmic ray hits. Finally, we used the IRAF task IRMOSAIC to obtain a mosaic of the images. Multiple exposures of identical fields were aligned using several stars present in the images and then co-added to produce a final median averaged image. An average value of the background emission was

[2]IRAF is distributed by the National Optical Astronomy Observatories, which is operated by the Associated Universities for Research in Astronomy, Inc. under cooperative agreement with the National Science Foundation.

[3]Bias frame is included in the Dark frame.

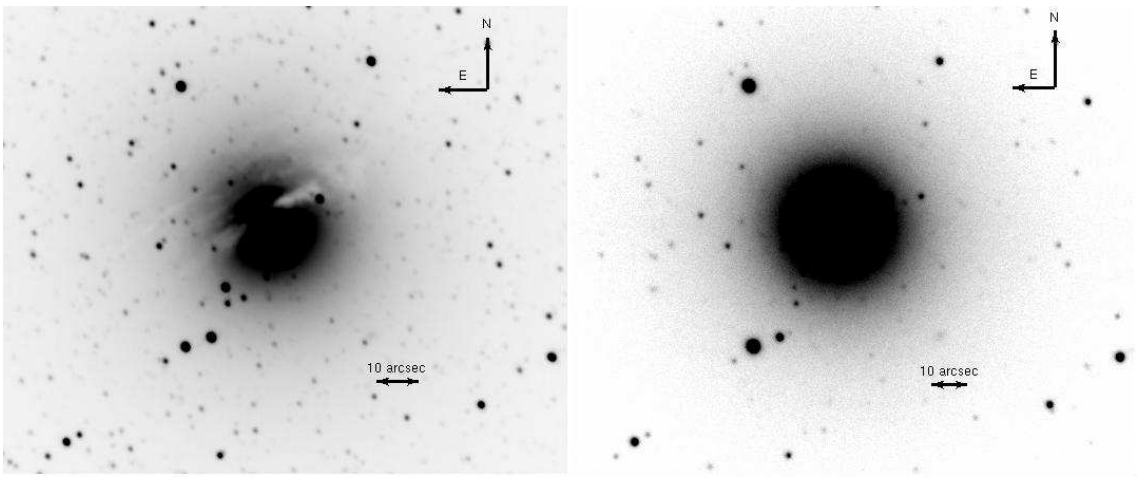

Figure 4.2: Calibrated K (left panel) and V (right panel) images of NGC1947

estimated in several regions of the sky far from the galaxy light.
In order to perform the photometric calibration, several Landolt standard stars were observed in the same bands.
The final, calibrated V band image of NGC1947 is shown in Fig. 4.2 (left panel).

Spectroscopic data - The spectroscopic data were extracted from the European Southern Observatory (ESO) public archive[4]. They have been obtained with the EMMI spectrograph at ESO-NTT in the RILD mode. The data, consisting of four set of spectra, were acquired with a slit 1.0″ wide, using the GR♯5 grism with a dispersion of 5.5 nm mm^{-1}, corresponding to 0.83 Å pxl^{-1}, in the $380 - 700$ nm wavelength range. The spectra were acquired along both the photometric major ($P.A. = 40°$) and minor ($P.A. = 130°$) axis of NGC1947. The total integration time of both spectra is 600 s; the average seeing turned out to be $FWHM = 1$ arcsec. A set of spectra of standard template $K0III$ stars were also acquired with the same configuration.
Individual frames were pre-reduced using the standard IRAF image processing package; the wavelength calibration was made using the IRAF TWODSPEC.LONGSLIT package and a set of He-Ar-Ne lamp spectra taken for each observing night. Sky subtraction was performed with the IRAF BACKGROUND package, by using a narrow region at both edges of the slit where the galaxy contamination is minimum. Finally, all the exposures for both axis were co-added in the final median averaged 2D spectra, which were used to derive the central velocity dispersion and the rotation curve along both axes. The velocity dispersion and the radial velocity were derived with the Fourier Quotient Technique (Sargent et al. 1977; Bertola et al. 1984), using the standard stars as templates. One of the main source of sta-

[4]http://archive.eso.org/

tistical and systematics errors is the template mismatching; so we performed tests to verify if the standard star we used to derive the kinematics of the galaxy was the best one. These tests showed no template mismatching. In both spectra some extended emission lines are well visible, in particular [OIII] λ5007Å, H_α, [NII] $\lambda\lambda$6548,6583 and [SII] $\lambda\lambda$6717,6731. These lines allowed us to measure the gas rotation curves also. To measure the rotation curves, every record of each galaxy spectrum was fitted with a Gaussian function on the emission line using the task SPLOT of IRAF package. The H_α line was not measured due to the presence of a strong absorption component, for this reason only the more extended [NII] λ 6583 line with a signal to noise ratio ≥ 2 was fitted. Taking into account the average seeing and the EMMI pixel scale, the final stellar and gaseous rotation curves were derived by adopting a binning factor of 3 along the spatial direction to obtain independent data points. They will be presented in Fig.6.5 and described in the sec.4.3. Due to the low signal-to-noise ratio (which is about 20 in the center and decreases to about 10 towards the outer regions), the kinematic profiles are about 4 times less extended than the light profiles (Fig.4.3).

Photometry: morphology, light and color distribution

The most prominent feature of NGC1947 is the extended dust-lane, which crosses the galaxy center along the photometric minor axis. Since the dust optical depth decreases toward longer wavelengths, NIR photometry is necessary to reduce as much as possible the dust absorption, that strongly affects the starlight distribution in the galaxy. Thus, we used near-infrared images (J and K bands) to easily identify the inner structures of NGC1947 and accurate analyse the stellar light distribution. On the other hand, optical images (in the V and R bands) are used to derive the optical versus NIR color profiles and color maps to study the structure of the dust-lane.

Isophote analysis - We used the IRAF-ELLIPSE task on the NIR images to perform the isophotal analysis for NGC1947 and the results are shown in Fig.4.3. The average surface brightness extends up to about 80 arcsec from the galaxy center (see Fig.4.3); in the K band, the half-light radius is $R_e = 24.4 \pm 2$ arcsec $\sim 1.86 \pm 0.15$ kpc. For a semi-major axis r, in the range $10 \leq r \leq 40$ arcsec, the ellipticity and P.A. are almost constant and equal to 0.05 and 40°, respectively, that indicates that in this regions the isophotes are almost round and co-axial. For $r \leq 20$ arcsec the dust lane perturbs the ellipticity and P.A. profiles and also the shape parameters a_4/a, which are shown in Fig.4.3. This effect is even more evident in the J than in the K band. For $10 \leq r \leq 25$ arcsec, the shape parameters are all consistent with zero, thus the isophotes do not significantly deviate from purely elliptical shape, while at larger distances (out to $\sim$ 40 arcsec) they tend to be more disky (see Fig.4.3). In Tab.4.2 we give the integrated magnitudes and

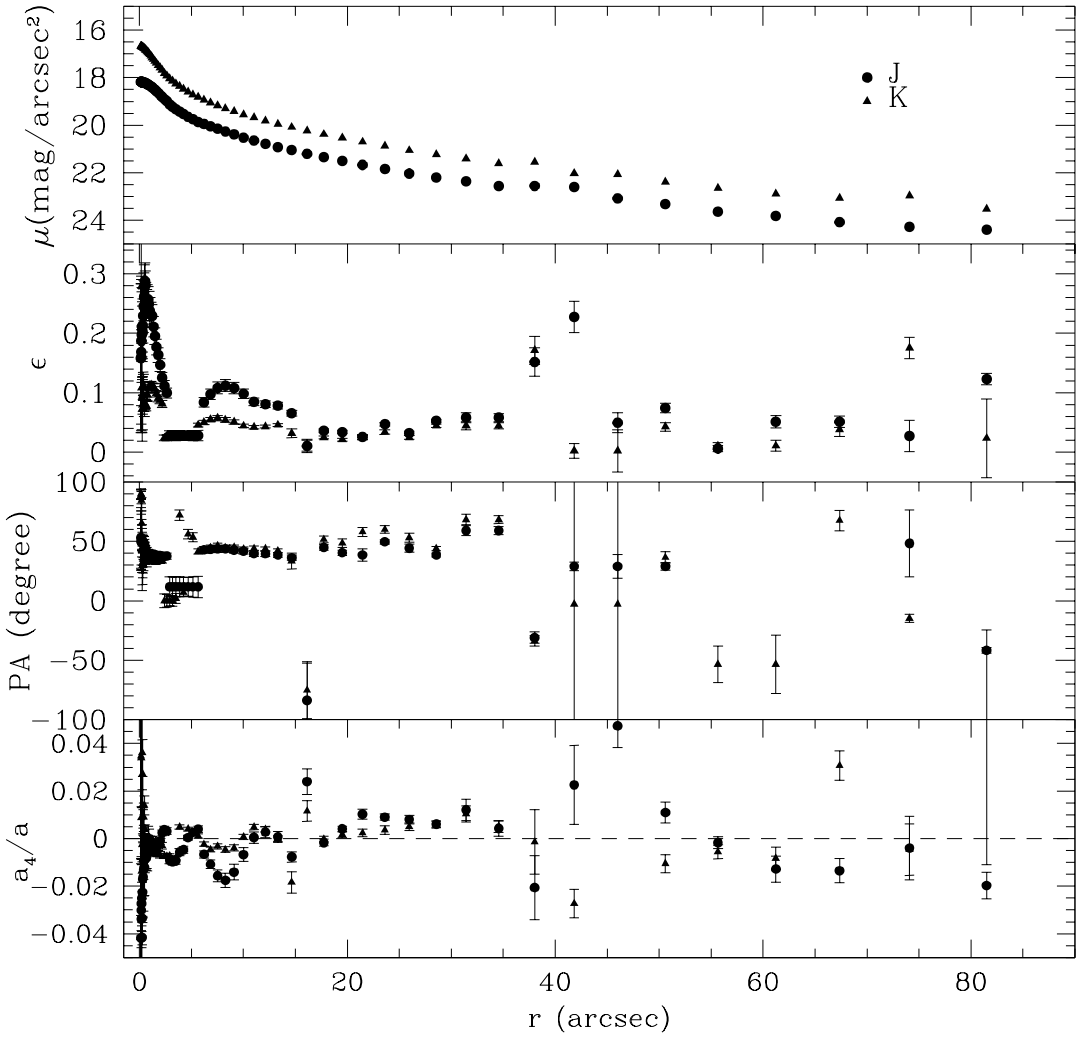

Figure 4.3: Ellipticity (ϵ), Position Angle (P.A), mean surface brightness profile and shape parameter a_4/a in the J and K bands.

average colors within two circular apertures, derived for the NIR J and K bands, and optical V and R bands. The apertures were chosen in order to make the comparison easier with the magnitudes of NED.

Light and color distribution - In Fig.4.4 we show the light profiles along the major ($P.A. = 40°$) and minor ($P.A. = 130°$) axis in the NIR and in the optical bands respectively. The light distributions in the optical V and R bands are very much perturbed by the presence of the dust-lane, in the regions between 10 and 30 arcsec on the NE side of the major axis, and for $r < 20$ arcsec on the SE side of the minor axis. Except for this, neither NIR nor optical profiles show any significant feature.
We have derived the $V - R$ (Fig.4.5), $J - K$ (Fig.4.7, left panels) and $V - K$ (Fig.4.6, left panels) color profiles along both photometric axes of NGC1947, and the 2-dimensional $V - K$ and $J - K$ color maps (Fig.4.6 and Fig.4.7 right panels, respectively). On average, the central regions of the galaxy have redder colors, with a maximum value of $V - R = 1.05$, $J - K = 1.5$ and $V - K = 5$. At larger radii the colors are bluer. In all color profiles, on the NE side of the major axis, between 10 to 30 arcsec, double red peaks are observed, at r=18 arcsec and r=30 arcsec where V-R=0.85 and V-K=4: such features are due to the ring-like structure of the dust-lane, already suggested by Bertola et al. (1992) and described in Sec.5.6, which stands out very clearly in the 2-dimensional V-K color map (Fig.4.6). The dust-lane perturbs only the SE side of the minor axis color profile, within 10 arcsec from the center: this suggests that the dust-lane is slightly misaligned with respect to the photometric minor axis. This is also confirmed by the 2-dimensional J-K color map (see Fig.4.7, right panel): with respect to the nucleus, which is very red, there are two "thin" and redder structures which do not lie on the same direction. In particular, the one on the NW side is on a parallel direction towards North. The full extension of the inner dust-lane is about 27 arcsec.

Stellar population ages - We derived the integrated V-K and J-K colors in two circular apertures: one including the nuclear regions of the galaxy inside a radius of 1 kpc $\sim 0.54R_e$, where $V-K = 3.2$ and $J-K = 1.02$, and one out to $1.5R_e \sim 2.85$ kpc, where $V - K = 2.84$ and $J - K = 0.99$. The stellar population synthesis model by Bruzual & Charlot (2003b) were used to reproduce the integrated colors in these regions, in order to derive an estimate of the stellar population ages. We adopted a star formation history with an exponentially decreasing rate, that produces a reasonable fit of the photometric properties of early-type galaxies in the local Universe. It has the following analytical expression: $SFR(t) = \frac{1}{\tau} \exp(-t/\tau)$, where the τ parameter quantifies the "time scale" when the star formation was most efficient. Adopting $\tau = 1$ Gyr, the correspondent evolutionary tracks were derived for both solar metallicity, $Z = 0.02$, and for a higher value, $Z = 0.05$; both values were assumed constant with age. In every model it has been assumed that stars form according to the Salpeter (1955) IMF, in the range from 0.1 to $125M_\odot$. To account for the V-K and J-K colors the best model is that obtained for $Z = 0.05$, from which we derived an age of about 3.9 Gyrs for the inner region

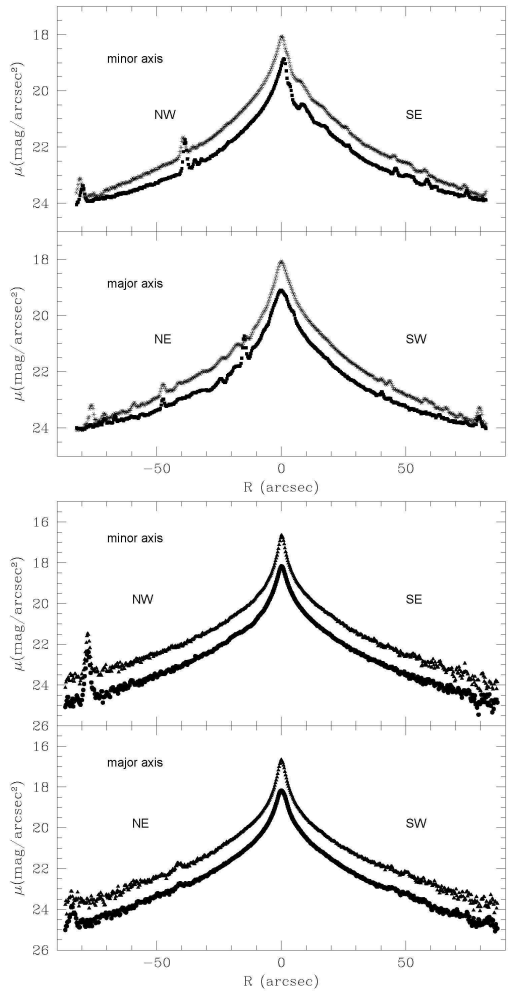

Figure 4.4: Light profiles along the minor (top-left panel) and major (bottom-left panel) axis of NGC1947 in the V (stars) and R band (triangles). Light profiles along the minor (top-right panel) and major (bottom-right panel) axis of NGC1947 in the J (stars) and K band (triangles)

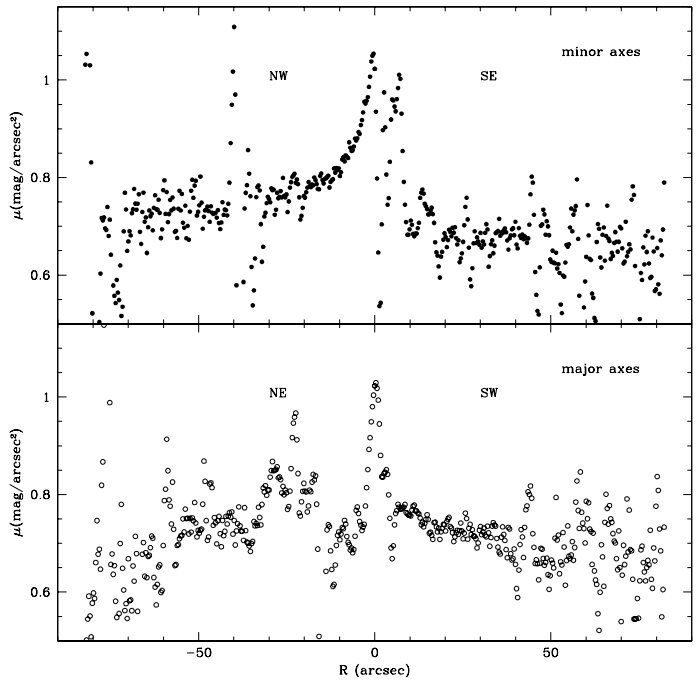

Figure 4.5: V-R color profiles along the minor (top panel) and major (bottom panel) axis of NGC1947.

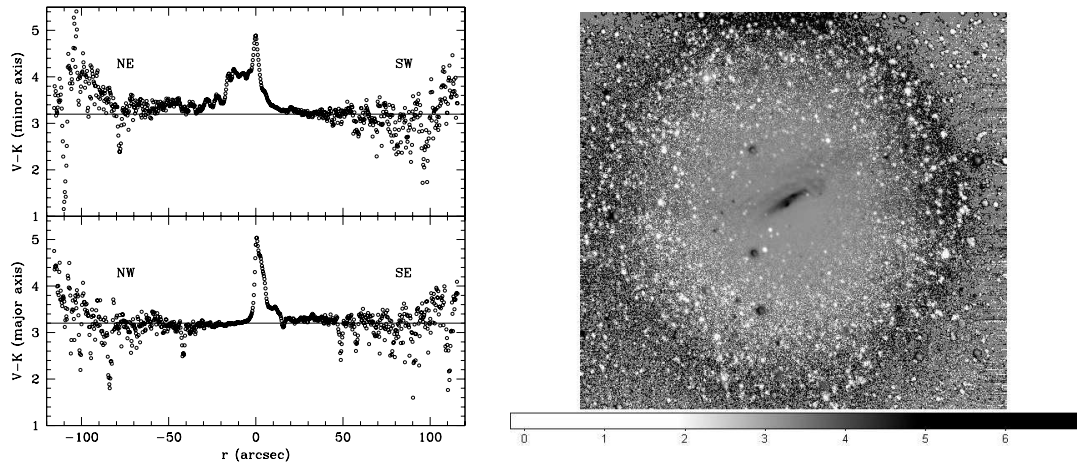

Figure 4.6: *Left panel* - V-K color profiles along the major (top panel) and minor (bottom panel) axis. The straight line correspond to the average V-K color for $r \geq 10$ arcsec. *Right panel* - V-K color map. The North is up, while the east is on the left of the image. Darker colors correspond to redder galaxy regions.

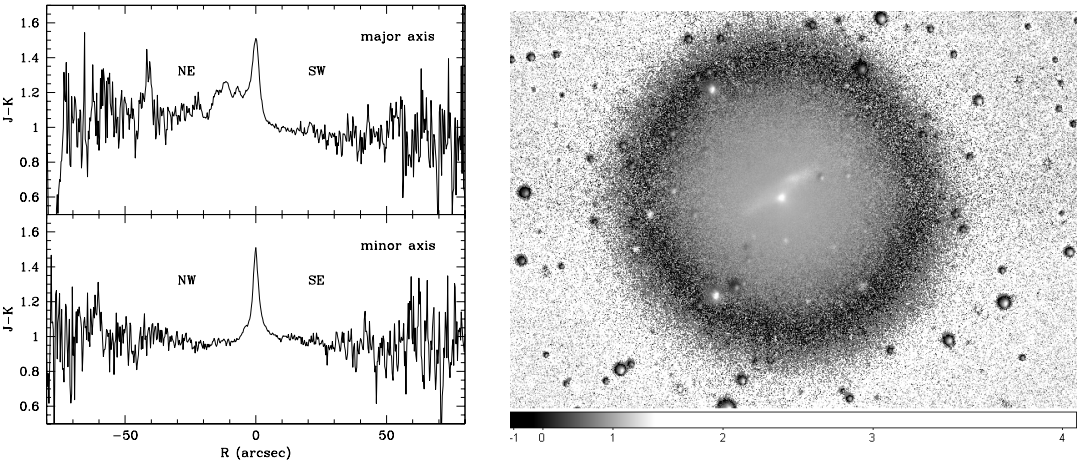

Figure 4.7: *Left panel* - J-K color profiles along the major (top panel) and minor (bottom panel) axis. *Right panel* - J-K color map. The North is up, while the east is on the left of the image. Lighter colors correspond to redder galaxy regions.

and of about 2.3 Gyrs for the outer one. These estimates have to be considered as an upper limit to the last burst of star formation. These constraints will turn to be fundamental in the discussion on the formation scenarios (Sec.5.6).

2-Dimensional model of the light distribution

We performed a 2-dimensional model of the light distribution in the K band, where the effect of dust absorption is weaker, and stars are accurately masked. To this aim, we used the GALFIT task (Peng et al., 2002). As a first attempt and according to the morphological classification given for NGC1947 in the previous work (see Tab.6.3) as an Elliptical, the galaxy light is modelled through a single Sersic law (Sersic, 1968): the fit is very poor, suggesting the presence of an additional component in the outer regions. Therefore, we adopted a double-component model as the superposition of a Sersic law (Sersic, 1968) plus an exponential profile (Freeman, 1970a). The fit improves considerably; the fitted light profiles for the major and minor axis of NGC1947 are shown in Fig.4.8 and Fig.4.9. The structural parameters derived from the fit are: the bulge total magnitude $m_b = 17.7 \pm 0.01\ mag$, the bulge scale length $r_e = 74.0 \pm 0.7$ arcsec, the disk total magnitude $m_d = 17.0 \pm 0.02\ mag$, the disk scale length $r_h = 121.1 \pm 0.3$ arcsec and the Sersic exponent $n = 2.83 \pm 0.01$, leading to a bulge total luminosity-to-disk total luminosity ratio, $L_B/L_D \simeq 0.43$.

Along both axes, inside a 30 arcsec radius from the galaxy center, the residuals reflect the presence of the dust-lane, which is more pronounced along the NE region of the major axis, where the galaxy appears to be less luminous than the model. Such an effect is much more clear in the residual image (see Fig.4.10) obtained by subtracting the 2D model to the galaxy. In order to analyze the structure of the dust-lane in NGC1947, we used the 2D model obtained in the K band, which is less perturbed by dust absorption, to match the light distribution in the V band. To this aim, the V band image of NGC1947 was scaled to the K band, by accounting for the average V-K color (see Sec.4.3). In the residuals (Fig.4.11) two main features stand out very clearly: *i*) the concentric ring-like structure of the dust-lane, superposed to *ii*) a bright region (within 20 arcsec from the center) which is more luminous on the SW side with respect to the NE side. The existence of such luminous "counterpart" is reliable due to the fit interpolation, which is an average of the whole galaxy light (see Fig.4.8 and Fig.4.9): this is also confirmed by the absence in the V-K color profile (see Fig.4.6) of any bluer component on the SW region, which should have appeared in the V-band residual image respect to the K band one. By this analysis, we estimate that the dust-lane extends by 49.6 arcsec from SE to NW, with a thickness of about 23 arcsec.

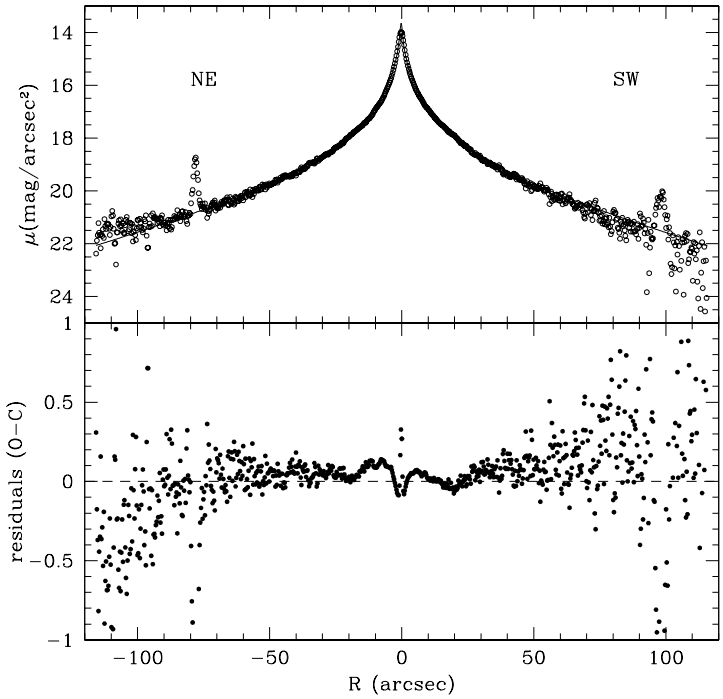

Figure 4.8: Top panel - 2-D fit of NGC1947 light distribution. The observed light profile along the major axis, is compared with those derived by the fit (continuous line). Bottom panel - Residuals between the observed and the fitted light profiles.

Table 4.2: Magnitudes and Colors for NGC1947 in circular aperture.

aperture radius (arcsec)	m_J ± 0.05	m_K ± 0.04	m_V ± 0.01	m_R ± 0.01	J-K ± 0.09	V-R
15.7	10.44	9.35	13.20	11.81	1.09	1.39
81.2	8.91	7.90	11.26	9.99	1.01	1.27

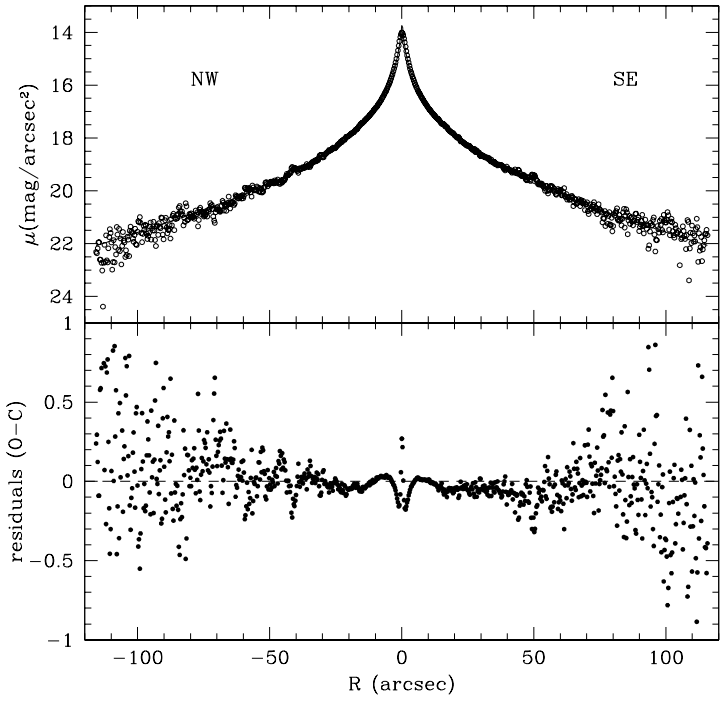

Figure 4.9: Top panel - 2-D fit of NGC1947 light distribution. The observed light profile along the minor axis, is compared with those derived by the fit (continuous line). Bottom panel - Residuals between the observed and the fitted light profiles.

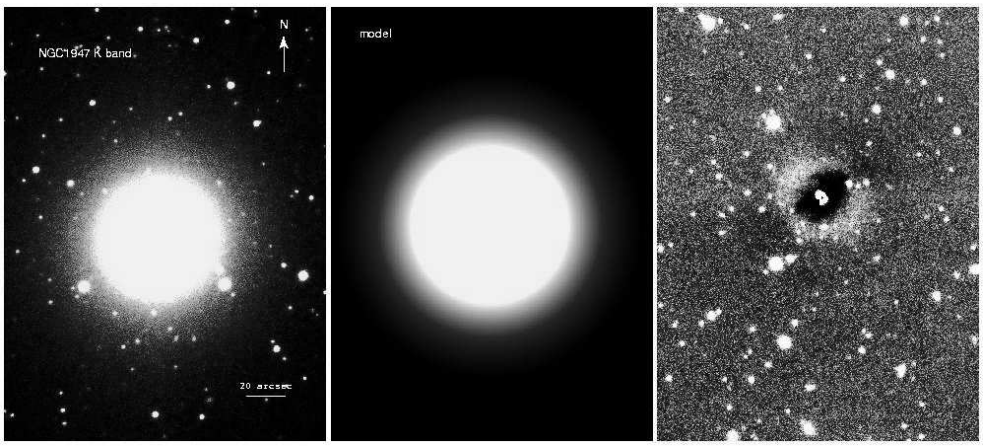

Figure 4.10: 2D fit of NGC1947. Left panel - K band image of NGC1947. Middle panel - Model of the galaxy. Right panel - Residual image.

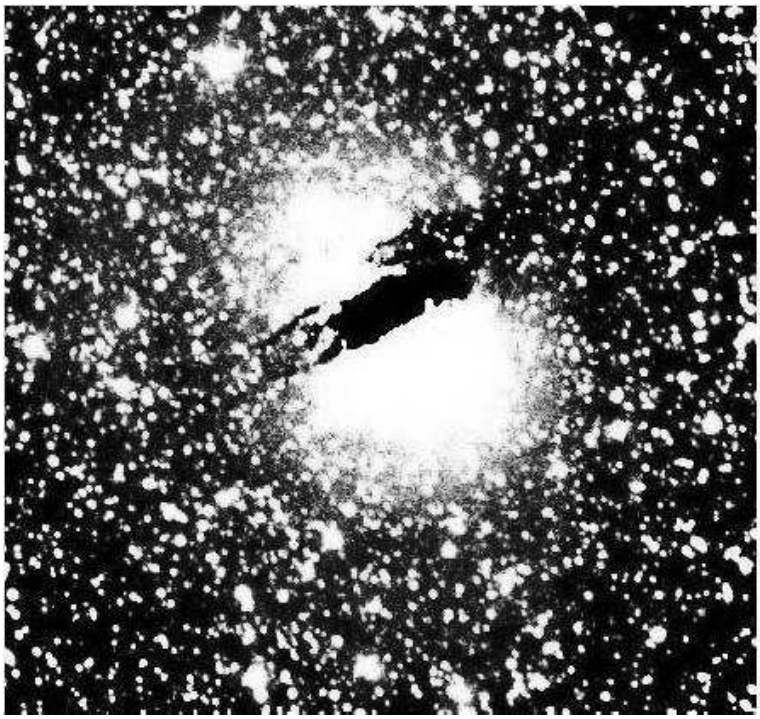

Figure 4.11: Residuals of the subtraction of the K band model to the V band image.

Stellar and gaseous kinematics along the principal photometric axes of NGC 1947

Major axis - The stellar kinematics is more extended on the SW side with respect to the NE and it is measured out to $20''\sim 1.4$ kpc (Fig. 6.5, bottom panel), which corresponds to a surface brightness of ~ 21.7 mag arcsec^{-2} in the V band. The rotation curve is not symmetric with respect to the galaxy center: in the range $2'' < r < 14''$ NE, rotation increases, up to a maximum value between 55 and 80 km/s, to be compared with the corresponding distance range on the SW side, where almost no rotation is measured. The kinematics along NE side, for $r > 6''$, is strongly perturbed by the dust-lane, as suggested by the V-K color profiles (Fig.4.6).
The velocity dispersion remains almost constant within the uncertainties at an average value of $\sim 133\pm 31$ km/s, out to 10 arcsec from the center. Both the rotation velocity profile and the average velocity dispersion turns out to be consistent with those published by Bertola et al. (1992).
The gas component too shows some rotation along this direction, and the rotation curve has the same extension as the stellar rotation curves (see Fig. 6.5): it shows a very steep inner gradient, reaching a maximum velocity of ~ 100 km/s on the NE side and ~ 80 km/s on SW side, between $2''$ and $4''$ from the center. Velocities remain almost on these values up to the last measured point. These data (both for emission and absorption) are consistent with, and extend those of Moellenhoff (1982). However, the measured rotation for the gas was not so evident in the data of Moellenhoff (1982).

Minor axis - The stellar kinematics is measured out to the same distance from the galaxy center, i.e. $20''$ (Fig. 6.5, top panel). On average, stars do not rotate and the velocity dispersion has the mean weighted value of $\sim 146\pm 37$ km/s within $5''$ from the center.
The gas rotation curve is more extended (up to about $30''$) and better resolved with respect to the stellar rotation curves. Along the major axis, the gas shows a very steep inner gradient, reaching a maximum velocity of ~ 200 km/s between $10''$ and $20''$ from the center. The full extension of the gas rotation curve is of about 60 arcsec, which is about 2 times wider than the dust-lane (see Sec. 4.3).
The gas velocity curve presented in this work, even though more extended on the SE side, is consistent with the one published by Moellenhoff (1982).
The observed kinematics led us to conclude that the minor axis is the principal rotation plane of the gaseous disk. Moreover, for this component some rotation is observed even in the direction of the major axis: this implies that the disk is warping towards the inner regions (Arnaboldi & Galletta, 1993) and suggests that this component has not reached a stable configuration yet. The average velocity dispersion turns out to be consistent also with values derived by Carollo et al. (1993), according to the kinematics derived along two intermediate directions.

In Fig. 4.13 we show the stellar and gaseous rotation curves along the minor

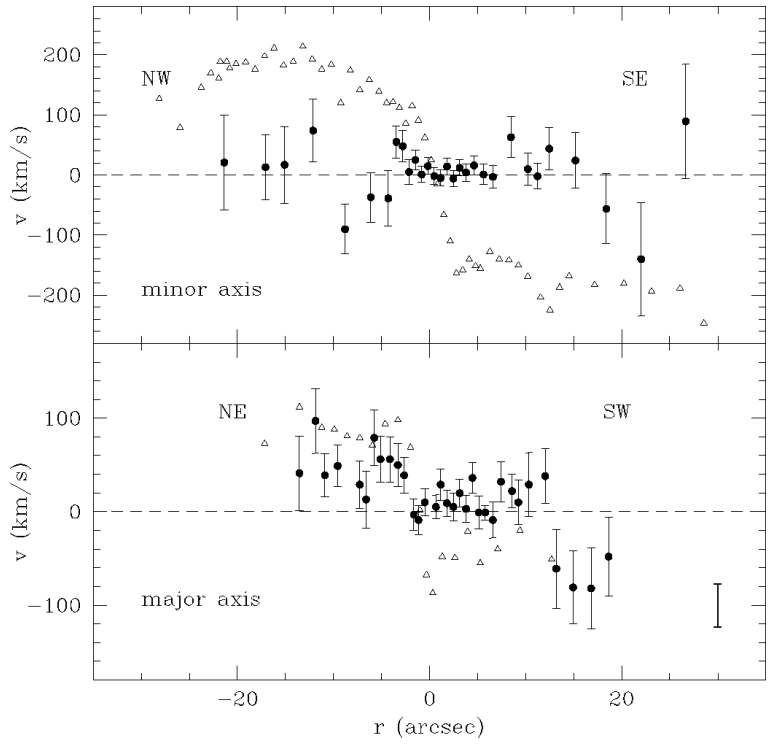

Figure 4.12: Stellar (filled points) and gaseous (triangles) rotation curves along the major (bottom panel) and minor axis (top panel) of NGC1947. The dashed line is the velocity of the galaxy center. In the bottom-right corner is plotted the error bar that represents the mean error on the velocity of the gas.

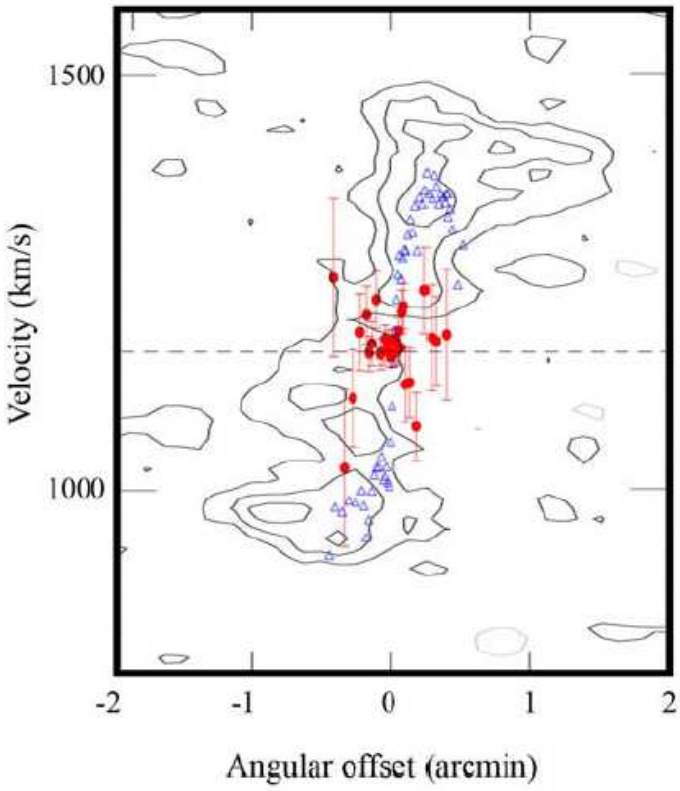

Figure 4.13: Stellar (filled points) and gaseous (triangles) rotation curves along the minor axis of NGC1947 superposed on the position-velocity plot of the HI along the $P.A. = 127\circ$ presented by Oosterloo et al. (2002).

axis of NGC1947 superposed on the position-velocity plot along the $P.A. = 127^\circ$ of the HI distribution presented by Oosterloo et al. (2002). The HI distribution is more extended than the stellar rotation curve: the HI extends out to about 90 arcsec, while the stellar rotation curve extends up to about 20 arcsec. The HI and gas in the dust-lane rotates in the same sense and with the same amplitude (see Fig.4.13): this confirms that the HI is in a warped rotating disk associated with the dust-lane, as already suggested by Oosterloo et al. (2002).

Discussion and conclusions

In the present work we performed a detailed analysis of the structure of the minor-axis dust-lane galaxy NGC1947, and in what follows we will discuss the implications of our findings on the formation and evolution history of this peculiar object.

In particular, we will discuss how the observed properties for NGC1947 presented in this work, compare with the predictions from different formation scenarios for such kind of systems. The main observed properties for NGC1947 that the most likely formation scenario has to account for are *i)* the high-inclined ring of gas and dust which rotates in the perpendicular direction with respect to the stars in the major axies of the S0-like host galaxy, and *ii)* the photometry and kinematics observed for the two decoupled components (stars and gas), in particular, the warp observed for the gas towards the inner regions (sec. 4.3), which suggests that the inner rings of gas has not settled yet in the equilibrium plane; *iii)* the estimated timescale of the formation mechanism has to be consistent with the age estimates of the different stellar populations.
The presence of two components with different angular momenta, gas and dust along the minor axis and stars along the major axis, suggests that NGC1947 could not be the result of a single protogalactic cloud collapse and that it may have experienced an interaction event. In this framework, the possible formation scenarios which may account for a galaxy with high inclined ring/disk of gas, stars and dust (discussed in the Sec.5.6) are *i)* the tidal accretion of gas by outside, and *ii)* the unequal-mass merging of two disk galaxies. In the following we will discriminate between these two scenarios for NGC1947. Furthermore, we will discuss how Smoothed Particles Hydrodynamic (SPH) simulations of isolated collapsing triaxial systems, presented by Mazzei & Curir (2003), may account for peculiar galaxies like NGC1947.

- *Tidal accretion* -

The features observed in NGC1947 lead to the possibility of considering the galaxy as a tidal accretion remnant. The tidal accretion scenario accounts for a large variety of polar structures; many simulations show that the accretion produces warped rings and transient features (see Bournaud & Combes 2003a), with processes similar to those leading to the formation of Polar Ring Galaxies (PRGs). Differently from PRGs, in the polar ring of NGC1947 there are not detected stars associated to the gas and dust. Such Interstellar Medium (ISM) could be accreted by a gas-rich donor galaxy during a close passage of a pre-existing S0 galaxy near this companion galaxy. In order to consider the accretion hypothesis, we studied the field around NGC1947 (shown in Fig.4.14) to see if there are any objects from which the galaxy could have accreted material: inside a radius of about 5 times the diameter of the galaxy, which correspond to about 16 arcmin, (as suggested by Brocca et al. 1997) there is the early-type spiral galaxy ESO 085-GA088, which is at the same redshift of NGC1947, with a radial velocity of 1164 km/s. As discussed by Oosterloo et al. (2002), NGC1947 shows a warped HI disk at the same position angle as the dust lane, while the HI emission of ESO 085-GA088 extends in a direction perpendicular to that of NGC1947: this is the orbital configuration needed to form a polar ring (of gas) through an accretion event (Bournaud & Combes, 2003a). These observed features may suggest that the donor galaxy could be ESO 085-GA088: in fact, taking into account the linear relative distance

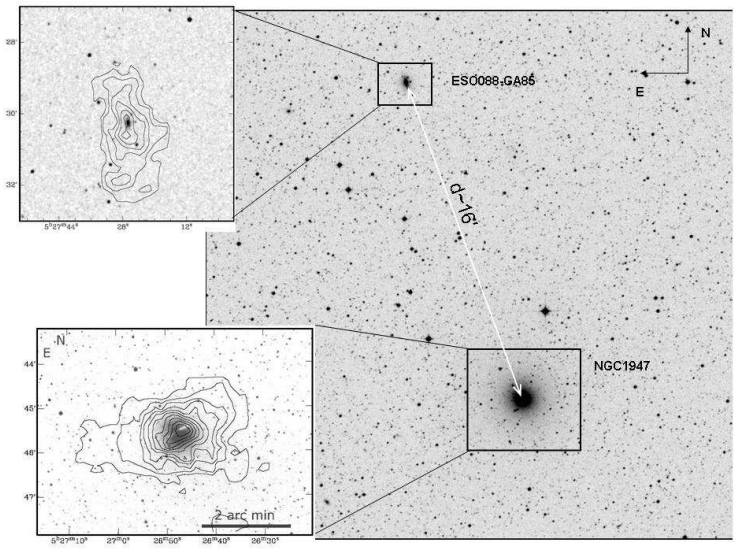

Figure 4.14: Image of a field of 25 arcmin around NGC1947. The two boxes on the left show the HI distribution for NGC1947 and ES0 085-GA088 published by Oosterloo et al. (2002).

of about $16' \sim 70$ kpc, and the relative velocities of the two systems, we estimate the time at which the interaction happened, to be about 1 Gyr ago. Such value estimated in the case of a parabolic orbit has to be considered a lower limit. In the case of a parabolic orbit a longer time is expected, which should be consistent with the upper limit to the last burst of star formation in NGC1947 (estimated in Sec. 4.3).

- *Merging* -

Unequal-mass merging of two disk galaxies may build a spheroidal galaxy with an high inclined ring/disk of gas, stars and dust. In order to test such formation mechanism, we will compare the observed properties with those expected from simulations performed by Bournaud et al. (2005a). To do so, we computed the following quantities:

- the fitted light profile for this galaxy is consistent with a Sersic plus exponential luminosity profile, with bulge/disk=0.43 and bulge/total=0.57 (see Sec.4.3);

- according to Bournaud et al. (2005a), we evaluated the isophotal shape parameters of the galaxy, in the range $[0.55R_{25th}, R_{25th}]$, which is the range between the bulge and the disk optical radius. In this range the ellipticity is almost constant, ~ 0.11, and the $a_4 \simeq -0.004$ suggests a bulge with a moderate boxiness;

- we have taken into account the global kinematical properties of NGC1947 by deriving the v/σ ratio along the major axis: in the range $[0.55R_{25th}, R_{25th}]$ $v/\sigma \sim 0.15$, while the ratio v_{max}/σ_0 is about 0.62.

Such quantities have been compared with those predicted by numerical simulations for galaxy mergers with various mass ratios (see Tab.2 in Bournaud et al. 2005a): we found that they turn to be consistent with those expected for a merging with initial mass ratios 3:1 or 4:1 (Bournaud et al. 2005a). This is a mass ratio for which Bournaud et al. 2005a found stable and long lived polar or high-inclined rings of gas, returning to the galaxy along tidal tails, and equatorial rings, that appears as "dust lanes" when they are seen edge-on. Such unequal-mass merger has been proven to be the most likely scenario for another peculiar galaxy: the double-ring ESO 474-G26 (Reshetnikov et al., 2005).

In the hypothesis that NGC1947 may be the result of a merging event, we compare the observed properties of NGC1947 with those of the galaxies that have certainly experienced a merging, such as the galaxies belonging to the Toomre Sequence (hereafter TS, Toomre 1977).
The first step was to place NGC1947 on the TS, to determine at which merger state we are looking at. To this aim, we studied the position of NGC1947 on the plot of the total K band magnitude versus the magnitude within a radius of 1 kpc for the galaxies belonging to the TS, performed by Rossa et al. (2007) (see Fig.25 in that paper). Thus, for NGC1947 we estimated the total K band magnitude and the V, J and K magnitudes within a radius of 1kpc, which are respectively $M_K = -23.3$ mag, $m_V = 12.37$ mag, $m_J = 9.79$ mag and $m_K = 8.74$ mag. The nucleus of NGC1947 lies in the region between the nuclei of the late-stage mergers and the normal early-type galaxies. This leads to the reasonably conclusion that NGC1947 could be considered a very late-stage merger remnant. As a second step, we compared the V-K and J-K nuclei colors obtained by Rossa et al. (2007) for the galaxies belonging to the TS with those derived for NGC1947 (see Sec.4.3), by classifying it as late-stage merger (Fig.4.15 and 4.16). The J-K colors for NGC1947 are consistent with those of TS galaxies, while in the V-K color plot NGC1947 turns to be bluer relative to the TS galaxies: since no clumps of star forming galaxies are observed in NGC1947, this difference could reasonably due to the presence of a larger amount of dust in the TS galaxies.

- *Formation of NGC1947 through SPH simulations* -

We derive a suitable match of the dynamical and photometric properties of NGC1947 with a SPH simulation: Mazzei & Curir (2003) implemented SPH simulations with chemo-photometric evolutionary population synthesis models providing the SED from ultraviolet to near-IR wavelengths. The simulation includes self-gravity of gas, stars and dark matter (DM), radiative cooling, hydrodynamical pressure, shock heating, artificial viscosity, star formation and feedback from evolved stars and type II SNe, as described in Mazzei & Curir (2003). The starting point is a triaxial collapsing system initially composed of 30000 particles, 15000 of gas and 15000 of DM with a relative mass ratio of 0.01. The total mass, M, of the

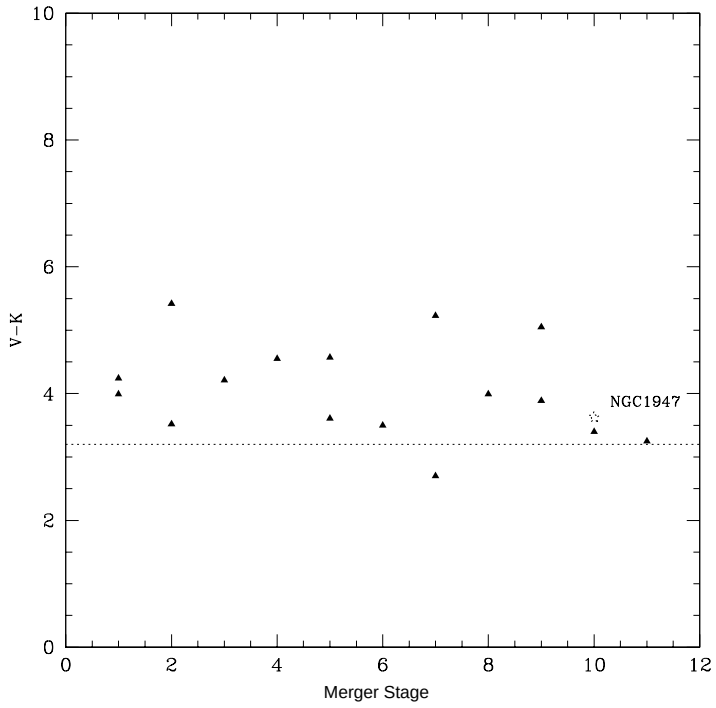

Figure 4.15: V-K color measured within 1kpc apertures as a function of the Toomre sequence merger stage. The dotted horizontal line indicates the V-K color for a SSP $10^{10}yr$ population of solar metallicity, which provides a reasonable fit to the measured colors for early-type galaxies.

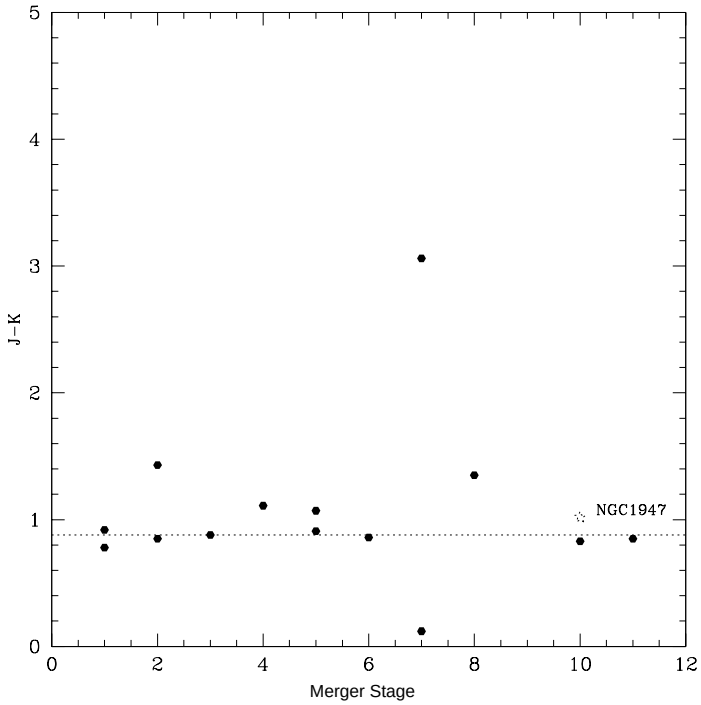

Figure 4.16: J-K color measured within 1kpc apertures as a function of the Toomre sequence merger stage. The dotted horizontal line indicates the J-K color for a SSP $10^{10}yr$ population of solar metallicity.

collapsing system is $10^{13} M\odot$. The system is built up as described by Mazzei & Curir (2003), i.e., with a spin parameter, λ, given by $|\mathbf{J}||E|^{0.5}/(GM^{0.5})$, where E is the total energy, J the total angular momentum and G the gravitational constant, equal to 0.06, and it is aligned with the shorter principal axis of the DM halo. It is also assumed a triaxiality ratio of the DM halo, $\tau = (a^2 - b^2)/(a^2 - c^2) = 0.84$, where $a > b > c$, which corresponds to an average radius of about 1 Mpc. Under these conditions, as found out by Mazzei & Curir (2003), the morphology of the resulting galaxy is highly related to the initial properties of the halo, which drive the galaxy formation and evolution. In particular, the dynamical timescales of stars and gas are quite different and, as a consequence, the two components become decoupled during the evolution of the system.
Here, we present the synthetic SED which accounts for chemical evolution, stellar emission, internal extinction and re-emission by dust in a self-consistent way, as described in (Mazzei et al., 1992, 1995). This allows us to extend the SED over four orders of magnitude in wavelength, i.e., from 0.1 to 1000 μm. So the model self-consistently provides morphological, dynamic and chemo-photometric evolution. Fig. 4.17 compares the predicted SED with the available data for NGC1947. Such a model suggests that star formation started about 14.5 Gyrs ago, and that the maximum was reached about 9 Gyrs ago. The average age for the inner stellar generations is dated at about 3 Gyrs: this could be due to the still efficient inflow of the gas and is consistent with the findings by Serra et al. (2007), which included such a galaxy in the sample of centrally-rejuvenated objects.
Dynamical predictions of such SPH simulations agree with kinematical features observed for NGC1947 (see Sec. 4.3): in particular, the model predicts a maximum rotation velocity of about 20 km/s for the stars and of 120 km/s for the gas, and a velocity dispersion in the central regions of about 130 km/s.

- *Conclusions* -

Putting all the above evidences together, we now try to address which are the observational aspects that can help to disentangle in a non ambiguous way the possible formation scenarios for NGC1947 discussed above.

We have found that an unequal-mass merging of two disk galaxies, with a mass ratio in the range 3:1 - 4:1, could account for the average structure and kinematics observed for NGC1947. But this scenario fails to reconcile *i*) the epoch of the merging event with the estimates of stellar population ages in NGC1947; and *ii*) the gas kinematics. According to the simulations (Bournaud et al. 2005a), after 3 Gyrs from the merging event, the outer regions of the remnant are characterized by typical signs of the past interaction, like tidal tails and/or shells. Such features are not observed in NGC1947. To account for this, the merger would have occurred very long ago ($\sim$ 10 Gyrs) and the ring should be very long-lived: these predictions are not consistent with both *i*) the upper limit to the epoch at which the interaction happened for NGC1947, i.e. $\sim$ 3 Gyrs (see Sec.4.3) and *ii*) the warped structure of the ring, which suggests that the polar component has not reached a stable configuration yet (see sec.4.3). Therefore, we can reasonably rule out the merging

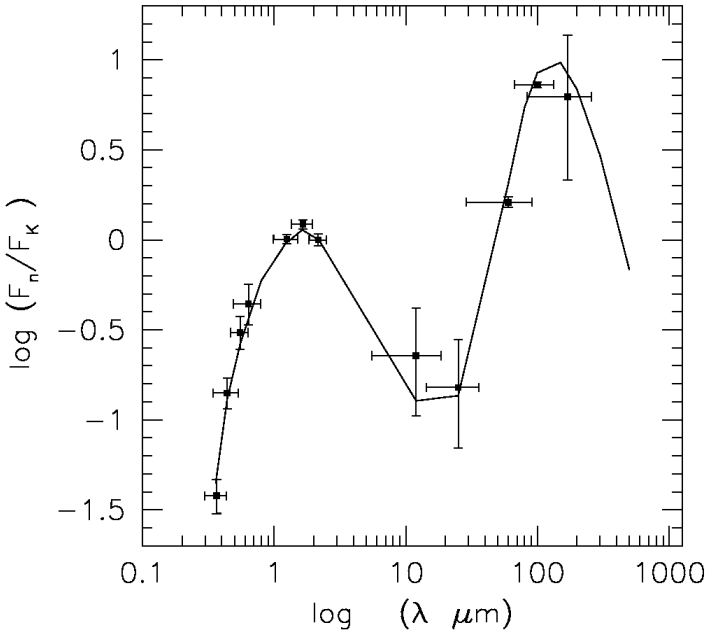

Figure 4.17: Continuous line shows the prediction of our model (see text); filled squares are V, J, and K integrated data given in sec. 4.3, the other data are from NED, in particular IRAS data at 12, 25, 60 100 μm and ISOPHOT data at 170 μm of Stickel et al. (2004).

scenario for the formation of NGC1947 and we can regard the recent polar accretion from a gas rich donor galaxy as one of the most probable interaction event in the formation history of this galaxy.
We have also discussed how such a peculiar object may be the result of processes of galaxy formation and evolution under particular initial conditions, linked to the ratio between baryonic and dark matter: the SPH simulations by Mazzei & Curir (2003) can reasonably account for the observed photometry and kinematics of the galaxy. We aim to further investigate in detail such aspect by comparing the predictions of such a model and observations, but they are beyond the aims of the present work and they will be the subject of a forthcoming paper.

CHAPTER 5

The cold accretion scenario

5.1 Polar Ring Galaxies

Gravitational interactions and mergers affect the morphologies and dynamics of galaxies. Both the Hubble Space Telescope (HST) and the Very Large Telescope (VLT) make it possible to observe the early universe and to show that these processes become even more common as redshift increases.

From this kind of studies, there are growing evidence that mergers play a major role in the formation of early type galaxies (Ellipticals and S0s), both in the field and in clusters. These observational results support the scenario firstly proposed by Toomre & Toomre (1972), in which the merging of two disk galaxies produce an elliptical galaxy. Furthermore, detailed numerical simulations have shown that mergers between two spiral galaxies of comparable mass lead to form spheroidal merger remnants with physical characteristics, such as density profiles, mean velocity dispersion and surface brightness, that are quite comparable to those of observed ellipticals.

If merger occurs between two unequal-mass spiral galaxies, named as "minor mergers", it does not completely destroy their disks. Numerical simulations for this kind of mergers are able to produce an early-type object with morphology, structure and kinematics quite similar to those observed in S0 galaxies. The disk-disk merger is also able to form peculiar morphologies, such as disky/boxy shape, fine structures (loops, shells, X-structures) and counterrotating cores like those observed in present-day early-type galaxies.

If two gas rich disk galaxies with unequal mass merge with each other under an high perpendicular relative inclination and with relative collisional velocity smaller than the escape velocity of the system, the merger remnant becomes a *Polar Ring*

Galaxy (Bekki 1998a and Bekki 1998b).

These peculiar objects are composed by a central spheroidal component, the "host galaxy" (HG), surrounded by an outer "ring", made up by gas, stars and dust, which orbits in a nearly perpendicular plane to the equatorial one of the central galaxy (Whitmore et al., 1990). In the dissipative disk merging scenario for the formation of early type galaxies, PRGs may be considered as an extreme samples of minor merger remnants: in fact, they form under very particular initial physical conditions related to the orbit configuration of the two galaxies and to the mass ratio of the two progenitors. However, the origin of PRGs is still an open field of study: the scenario proposed by Bekki (1998a) is substantially different from the standard picture for the formation of PRGs, which on the other hand, suggests that a pre-existing early type galaxy either accreted gas by a gas-rich dwarf galaxy or by stripping it from a nearby gas-rich object during high speed encounter (Reshetnikov & Sotnikova, 1997).

The discovery of PRGs has provided an unexpected but very welcome opportunity to study galaxies in a new way: in these galaxies in fact, the two merging components remain relatively distinct, rather than quickly mixing together into a single system where most evidence of the progenitors is lost. Moreover, the unique geometry of PRGs allows to study also the three dimensional shape of their dark matter halo. Constraints on the best scenario describing the polar ring formation can be derived from a detailed study of the observational properties of PRGs, such as their morphology, kinematics, HI and dust content, integrated colors and metallicity.

5.1.1 Morphology of PRGs

According to the ring morphology, PRGs can be divided into two broad classes (Whitmore et al., 1990):

1) *Narrow polar rings* (Fig. 5.1), where the ring is not extended in radius;
2) *Wide polar rings* (Fig. 5.2), which show disk-like polar structures.

Inside the class of PRGs are also observed peculiar ring morphologies, such as *multiple rings* (Fig. 5.3) and *low inclination rings* (Fig. 5.4).

Roughly two-thirds of PRGs show a warped ring whose shape looks like an "integral sign", with the two sides warped in opposite directions, or a "banana" where both sides are bending in the same direction. In almost all PRGs the morphology of the host galaxy resembles that of an early type object: kinematical studies of some PRGs have confirmed that this component is rapidly rotating (Whitmore et al., 1990).

PRGs are characterized by a large amount of HI gas, which is in some cases comparable with the total mass of the host galaxy, and it is closely associated with the stellar component in the polar ring (Arnaboldi et al., 1997). The integrated

Figure 5.1: Narrow polar ring around the galaxy NGC2685.

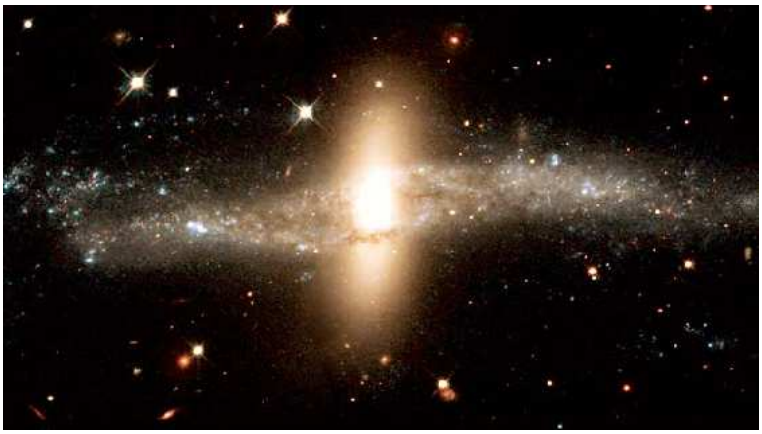

Figure 5.2: Wide polar ring around the galaxy NGC4650A.

Figure 5.3: Multiple ring galaxy.

Figure 5.4: Low inclined ring around a galaxy.

colors and gas to dust ratio, together with the large HI/L_B ratio, suggest that PRGs may be quite similar to the late type spirals.

5.2 Formation scenarios for Polar Ring Galaxies

Polar ring galaxies are usually considered dynamically peculiar systems, since they show the coexistence of two luminous components (the central host galaxy and the ring) in two nearly orthogonal plane. The presence of two almost perpendicular angular momentum vectors, of comparable size, cannot be explained through the collapse of a single protogalactic cloud. In the local universe, the frequency of early type galaxies with polar rings is only about 0.5% and this suggests that a very particular and relatively rare mechanism is required to form PRGs.

In the last years, a growing number of theoretical and observational studies have been produced, in order to provide even more informations about the origin of PRGs. The "best scenario" to describe the PRGs formation should be able to predict most of the observed properties of polar ring systems. In particular, it should explain:

1. why the morphology of the host galaxy resembles that of an S0 galaxy;
2. why PRGs are rare objects;
3. why the ring component shows different morphologies (i.e. narrow or wide rings etc, see Sec.5.1.1);
4. why the rings are found close to the polar plane of the host galaxy;
5. the large amount of HI gas observed in polar structures.

The two possible formation mechanisms for PRGs involve the interaction of two galaxies and can be grouped into two main scenarios:

1. **tidal accretion** of a gas-rich dwarf galaxy by an early type system or gas stripped from a nearby gas rich object (Bournaud & Combes, 2003b);
2. **major dissipative merging** of two disk galaxies (Bekki, 1998a).

Both scenarios are able to account for the main morphologies of PRGs and to produce a central galaxy similar to an early-type. The accretion scenario fails in reproducing the extended disk-like polar structure of some PRGs, while the merging scenario fails to form massive polar disk around an HG with rotation velocity. In fact in the merging scenario, a high mass ratio is required to form a massive polar disk, and according to simulations of galaxy mergers this would convert the intruder in an elliptical-like, not rotationally supported, stellar system,

on the contrary to what we observe in some PRGs. Recent theoretical works have argued that the most realistic way to form some PRGs might be the accretion of external gas from cosmic web filaments.

In the next sections these proposed scenarios will be discussed in detail, focusing the attention on how well these models perform in reproducing polar rings around early type galaxies.

5.2.1 Accretion scenario

In the standard scenario, the formation of PRGs is the result of a *secondary event* involving a pre-existing S0 galaxy. In this context, the mechanisms which are able to create ring-like structures around early type galaxies are the following: accretion of matter from a nearby system or capture and merging of a gas rich companion; delayed inflow of a primordial intergalactic cloud; polar ring formation from the return of tidal material during the merging of two gas rich spirals. The accreted material would then form a ring, which settles into one of the principal plane of the gravitational potential associated with the host galaxy.

The final structure of the accreted gas depends on the relative amount of gas present in the main galaxy at the intersecting radii, so only in relative gas-free galaxies the resistance to form a tilted disk is minimum. The evolution of the accreted gas depends strongly on the gravitational field of the galaxy, dissipation and self-gravity. On the relative importance of each of these factors are based the different evolutionary models.

The *preferred orientation model* (Steiman-Cameron, 1991) is based on the hypothesis that the potential of the host galaxy is triaxial rather than axisymmetric. Thus, the accreted material could settle in one of the preferred directions (the so called "principal planes"): the equatorial plane or the polar one, if the ring capture occurs respectively at small or high inclinations relative to the galaxy principal plane. The differential precession, caused by the quadrupole momentum of the potential, induces the migration of the ring forward the nearest of these two directions.

The *self-gravitating model* (Sackett & Sparke 1990 and Arnaboldi & Sparke 1994) explains the polar structure as the result of the accretion of a massive ring captured at high inclination in an axisymmetric galaxy. If the mass of the ring exceeds a minimum value, the self gravity of the ring makes it precess as a rigid body. The really massive PRGs are stable at whatever angle and evolve independently from the potential, while for intermediate values of the mass they are stable near either 90° or 0°.

Both these models require an high inclination angle for the accretion process and predict the formation of a stationary polar ring. On the contrary, in the *statistical selection model* (Schweizer et al., 1983) the polar rings are transient features and they are seen at these higher inclinations because the timescales on which the differential precession acts are long.

Given that observations of several interacting pairs of galaxies, of comparable luminosities, show ring-like structures, Reshetnikov & Sotnikova (1997) studied in detail the gas stripping scenario for the formation of PRGs. They analyzed the different morphologies generated through smoothed particle hydrodynamic simulations (SPH)in high speed encounters between either an elliptical or an S0 galaxy, and a comparable mass spiral. They presented a description of the full history of the gas stripping from the spiral galaxy outskirts and its consequent capture by a satellite during a parabolic encounter.

Following a parabolic trajectory, the accreting galaxy passes in a zero inclination in the plane of the donor galaxy disk: the orbital parameters are set in such a way that the orbit regarding the accreting galaxy is polar, i.e. the equatorial plane is taken to be perpendicular to that of the orbital motion. In these conditions, the gas stripped by the accreting galaxy from the outskirts of the donor galaxy is accreted and will form a polar ring. The total amount of the accreted gas is about 10 % of all gas in the donor galaxy ($\sim 10^9 M_\odot$).

The average time scale of ring formation is about 10^8 years, but this value becomes shorter for rings forming around bulge-dominated galaxies and larger when the accreting galaxy is disk-dominated. The interesting result of these simulations concerns the morphology of the ring: with the same impact parameters, rings formed around bulge-dominated galaxies are on average much less extended ($\sim$ 7 kpc in diameter) than rings formed around disk-dominated galaxies, which are 13 kpc wide.

Reshetnikov & Sotnikova (1997) also built a more complete model that takes into account the presence of a dark matter halo around the accreting galaxy. They assumed that the halo mass distribution is a spherical isothermal sphere with a mass to light ratio M/L = 2 inside a radius of 15 kpc. The timescale of the ring formation is larger than in the case of haloless systems, and it reaches up to a few Giga years. On the other hand, the masses of the ring structure obtained in the two kind of models, are comparable (about $2.2 \times 10^9 M_\odot$), while the size of the ring changes significantly, in fact the estimated diameter of this structure is about 30 kpc.

5.2.2 Merging scenario

A quite different approach to the formation of polar ring galaxies was proposed by Bekki (1998a). In this scenario, the polar ring results from a "polar" merger of two disk galaxies with unequal mass. The "intruder", placed on a polar orbit with respect to the "victim" disk, passes through it near its center: it is slowed down, and pulled back toward victim's gaseous disk. The two galaxies have the same density profiles for the disk and rotational curve profile, whereas they have different initial gas mass fraction: zero for the intruder and 0.2 for the victim. The adopted value of 0.2 is usually observed in gas rich spiral galaxies. The nature of the interstellar medium is considered to be collisional and dissipative.

In this scenario, a rather simplified star formation model is also taken into account: only the gas-to-star conversion is considered, and important effects from feedback by type II supernova are not included. Two types of trajectories are considered: 1) *polar collision*, where the two objects move along the x-axis, and 2) *parabolic collision*. The initial spin axis of the victim is set to be in the $x - z$ plane, and several angles between this direction and z-axis are considered (form 30° to 90°); the initial spin axis of the intruder is fixed to be parallel to the x-axis.

In this type of encounters, the two galaxies, whose initial separation is about 40 kpc, must have a small relative velocity (V_{rel}), so that the intruder is brought to the rest at the center of the victim's disk. The values for the relative velocity varies in the range $32.6 \leq V_{rel} \leq 326$ km s^{-1}. The most important parameter, which varies from model to model, is the initial mass ratio of the two progenitors and it is shown that it controls the final morphology of the merger remnant. This ratio varies from 2.0 to 0.1.

Then: which is the mechanism of polar ring formation? While the intruder is piercing the victim, its initially thin stellar disk becomes thicker and ticker: this is due to the strong dynamical heating during such violent gravitational interaction. Then the intruder is pulled again back through the victim and, at the same time, its stellar disk suffers violent relaxation. At this time ($t \sim 1.12 \times 10^9$ yrs), the intruder's morphology is very similar to that of an S0-like system. The density profile of this component deviates from the initially exponential behavior and it is more concentrated toward the center; furthermore the intruder shows an appreciably larger amount of global rotation, even after galaxy merging.

The polar ring surrounding this central spheroid is formed by the victim disk: the central part of the victim tends to be pushed out as the intruder goes through it and, simultaneously, propagating density wave are excited in the outer regions. The violent relaxation caused by the galaxy merging yields the stellar component in the victim disk to become dynamically relaxed and to form a diffuse spheroidal component. The density waves generate a cloud-cloud collision in the gas medium, which tends to form compressed layers with higher density; as a consequence, star formation and further dissipation start in correspondence of such layers. These last phenomena transform the victim disk into a polar ring made by gas and new stars. The typical timescale for the S0-like host galaxy and polar ring to form is about 3×10^9 yrs.

Bekki's scenario successfully reproduces many of the observed morphologies for polar ring galaxies, such as the existence of wide and narrow rings, helical and multiple rings. Narrow polar rings are formed through the merging of two disk galaxies, colliding in a polar orbit, when 1) the relative velocities are small ($V_{rel} \sim 33 kms^{-1}$) and 2) the intruder disk is more massive than the victim one.

The only different initial condition from the previous one, which let to the formation of wide polar rings is the mass ratio of the two merging galaxies: the victim disk must be 10 times more massive than the intruder one. When wide polar rings are produced, they are more similar to a disk-like structure, rather

than a polar annulus, characterized by a hole in the center.

Both narrow and wide polar ring galaxies have the following properties:

1. mass distributions in the central component and ring become more centrally concentrated after the encounter; an $R^{1/4}$ profile can develop if the "intruder" disk is much more massive than the "victim"

2. the central component is nearly gas-free, similar to an S0-like system, while the density wave triggered by the intruder into the victim disk causes rapid star formation, within $\simeq 10^9$ yr, so that the polar structure is characterized by a very young stellar population.

One uncertainty related to thee Bekki's model is whether the polar rings formed in this way are stable and for how long these objects can preserve the polar morphology after the merger remnant reaches virial equilibrium.

Both the tidal accretion and the merging scenario explain why PRGs are rare: they are formed in particular initial conditions for the encounter. Furthermore, they explain why the central host galaxy resemble an S0. Moreover, the orbital parameters, considered in both of them are able to explain why the rings are found close to the polar plane of the host galaxy.

The accretion scenario fails in reproducing massive disk-like polar structures, and it may account for the narrow polar annuli only. Moreover, the total amount of accreted gas can be of the order of $10^9 M_\odot$ at most, which is the typical amount of HI in a gas rich dwarf. On the other hand, the merging scenario would also explain the presence of wide and massive polar disks as well as other observed peculiar morphologies in the class of Polar Ring Galaxies. When extended polar structures are formed, depending on the intruder/victim mass ratio, they may be characterized by an high content of HI gas (up to $10^{10} M_\odot$), which originally was in the victim disk: this is a value comparable to the HI observed in late-type spirals. This scenario, however, fails in reproducing very massive polar disks; in these cases in fact, high mass ratios are required for the merging galaxies, and this would convert the central galaxy in a not rotationally supported, elliptical-like object.

Recent theoretical works have argued that a possible formation scenario for this kind of PRGs could be the cold accretion scenario (Macciò et al., 2006), described in the following section.

5.3 Galaxy Buildup by Gas Accretion

How galaxies acquire their gas is a major uncertainty in models of galaxy formation,and recent theoretical work has argued that cold accretion might play a major

role. This idea is also supported by numerical simulations (e.g. Macciò et al. 2006). Galaxy formation is a major unsolved problem that brings together many aspects of astrophysics. Observations across many scales and redshifts, from the cosmic microwave background to the large-scale clustering of galaxies, has defined a standard cosmological model that sets the background cosmology and initial conditions within which we can try to understand the formation of cosmic structures. Within this framework, it is well understood how the dark matter structures collapse and form galactic halos, but much more complex is the behavior of the baryons. Many questions remain unanswered, such as how the gas settles into the centers of dark matter halos.

According to the conventional picture of galaxy formation, gas falling into a dark matter potential well is first heated to the halo virial temperature behind an expanding virial shock. It is then supported by pressure in a quasi-static equilibrium while it is cooling radiatively and is slowly contracting to a centrifugally supported disc where it can eventually form stars. Mergers of disks can scatter stars onto disordered orbits, producing spheroidal systems, which may regrow disks if they experience subsequent gas accretion.

The cooling process thus determines important galaxy properties such as the star-formation rate and the metal enrichment, so it is necessarily an important ingredient in the galaxy formation process.

However, in the absence of a virial shock, the gas is not heated to the virial temperature until it falls all the way onto the disc, where the collapse stops and the gas is heated in a thin layer. This may alter some of the assumed processes of disc formation and in particular its star formation rate.

More recently, a wealth of observational evidence suggests that a significant reservoir of cold gas exists within galactic halos and groups of galaxies. This cold material may be stripped from infalling satellites or infalling directly via a smooth cold flow focused along filamentary structures. There are, however, many unsettled issues such as, for instance: how do filaments that are driving the cold mode accretion connect to galaxies and halos? How do these connections depend on halo mass and redshift?

Recent simulations show that the classical picture of galaxy formation needs some revisions: roughly half of the gas accreted by the simulated galaxies is never shock heated close to the halo virial temperature but instead radiates its acquired gravitational energy from $T \leq 2.5 \times 10^5$ K (often $T \leq 5 \times 10^4$ K). This *cold mode* of gas accretion dominates for lower mass galaxies (baryon mass $M_{gal} \leq 2 \times 10^{10} M_{\odot}$), while the conventional, *hot mode* of gas accretion dominates the growth of high mass systems. As a result, cold mode accretion dominates at high redshift ($z \geq 3$) and in low density environments today, while hot mode accretion dominates in group and cluster environments at low redshift.

Early studies suggested that cold accretion could be an important element of galaxy formation, showing that the amount of shock heating could be small for plausible physical conditions, with only a fraction of the gas reaching temperatures

$T \sim T_{vir}$. Katz & White (1993) and Katz et al. (1994) showed the importance of filamentary structures as channels for gas accretion in simulations with cold dark matter (CDM) initial conditions. Although both analytic and semi-analytic studies of galaxy formation usually assume spherical symmetry, numerical simulations show different geometries. In fact, as the matter in the Universe collapses, it forms a network of sheets and filaments, the so-called "cosmic web". Galaxies form in the densest regions, the most massive galaxies where filaments intersect. These structures can have an important effect on gas accretion. If a galaxy is being fed along filaments, the average density of the accreting gas will be higher. The cooling time will thus be smaller and it will be easier to radiate away the gravitational binding energy. Filaments may therefore feed galaxies preferentially through cold accretion.

Birnboim & Dekel (2003) by using high resolution, spherically symmetric collapse calculations, found that a virial shock fails to develop if the gas cooling time is shorter than the local dynamical time, so in these cases, gas shells fall far inside the halo virial radius without ever being heated to high temperature, and the cooling time condition corresponds approximately to a threshold in the galaxy's halo mass, with little dependence on redshift.

In addition to being an important aspect of the physics of galaxy formation, the existence of distinct cold and hot modes of gas accretion could have interesting observational implications, for example cold accretion allows much of the cooling radiation associated with galaxy formation to emerge in the $Ly\alpha$ line instead of the X-ray continuum. A reduced role for hot accretion might help explain why diffuse X-ray emission from late-type galaxy halos is well below the predictions of standard semi-analytic calculations.

In order to better understand the origin of the hot/cold distinction, it is useful to look for differences in the physical state of gas before it is accreted in one of these two modes. Cold mode particles initially have higher overdensities than hot mode particles, at least on average. Because of the correlation between density and temperature in the photoionized medium, cold mode particles also start at slightly higher temperature. This suggests that cold mode particles experience much of their heating in filamentary structures, while hot mode particles are heated at halo virial shocks.

Recently Macciò et al. (2006) proposed that the formation of Polar Ring Galaxies can occur naturally in a hierarchical universe where most low-mass galaxies are assembled through the accretion of cold gas infalling along megaparsec-scale filamentary structures (Fig. 5.5). Within a large cosmological hydrodynamical simulation, they find a system that closely resembles the classic polar ring galaxy NGC 4650A (Fig. 5.6).

In these simulations the ring forms from cold gas that flows along the extended $\sim$ 1 Mpc filament into the virialized dark matter halo. The gas streams into the center of the halo on an orbit that is slightly offset from purely radial infall and is "braked" by ram pressure drag from the ionized halo gas. As it reaches the

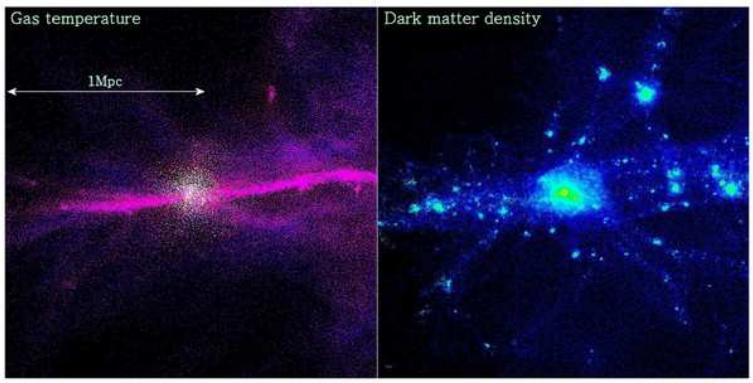

Figure 5.5: Distribution of gas and dark matter in a 2 Mpc wide slice of simulation by Macciò et al. (2006) centered on a galactic mass dark matter halo. The gas temperature is colored purple-white in a logarithmic temperature scale from 10^4 to 10^6 K. The narrow filament of gas flowing into the halo is at a temperature of $\sim\ 2 \times\ 10^4$ K. The filament in the dark matter is significantly wider than the gas and consists of a smooth component and many smaller halos. The entire simulation volume is 90 Mpc^3 and is centered on a region forming several galaxies, which are simulated at a higher resolution than the rest of the cube. The masses and softening of the dark matter and gas particles are $4.90 \times\ 10^5$, $9.75 \times\ 10^4 M_\odot$; and 0.2, 0.15 kpc, respectively. The polar ring would appear face-on in this projection, perpendicular to the filament.

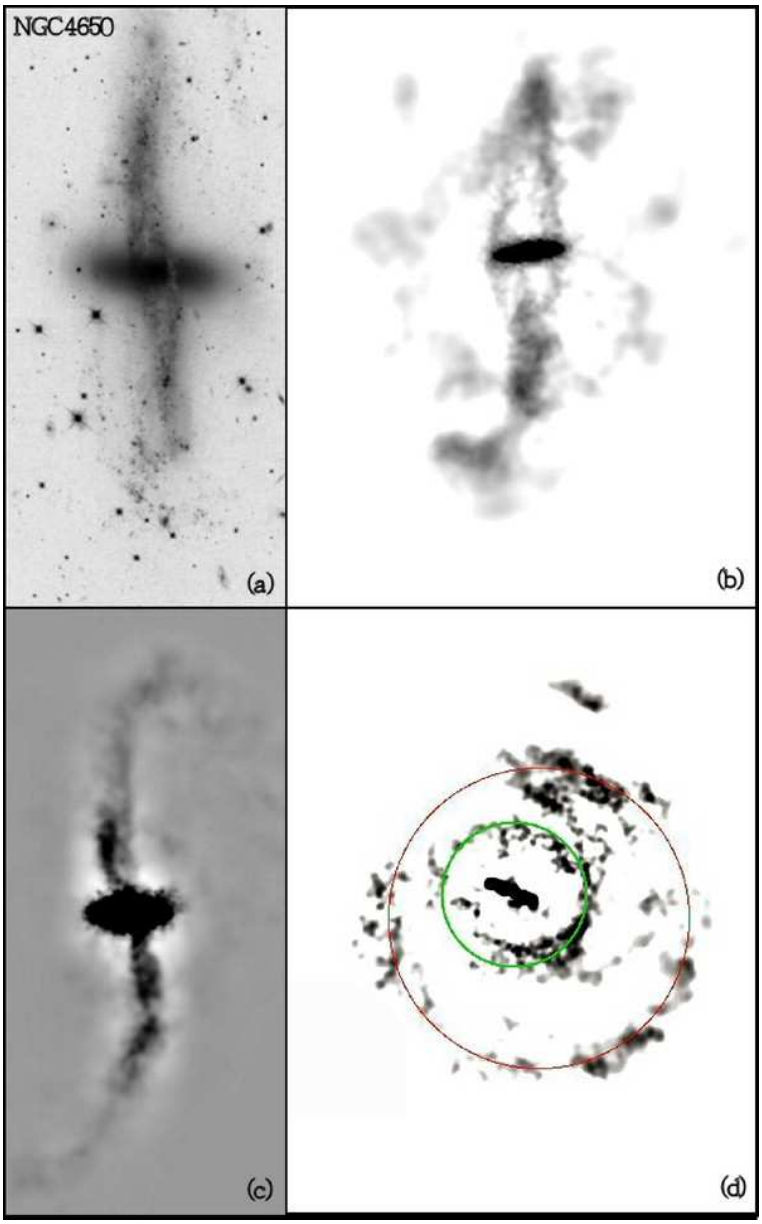

Figure 5.6: (a) Hubble Space Telescope image of the classic polar ring galaxy NGC 4650A (side length: 24 kpc), courtesy of the Hubble Heritage site, Space Telescope Science Institute. (b), (c) and (d) Smoothed images of the stars and gas of the simulated galaxy in different projections (side length 35 kpc): (b) inclined 20°, (c) with the ring edge-on and (d) face-on. The face-on image shows a clumpy distribution of gas that lies in two slightly offset rings.

center, it impacts with gas in the halo of the existing galaxy and with the warm gas flowing along the opposite filament. The small impact parameter is sufficient to leave the gas with sufficient angular momentum that it can rotate at the halo circular velocity at 10-20 kpc. The ring is clumpy, and where it has a high enough density it can fragment and form stars.

Any gas falling away from the perpendicular symmetry axis will rapidly precess into the plane of the disk. Only gas accreting perpendicular to the major axis of the oblate potential will survive for more than a few dynamical times. Indeed, the ring is long-lived in simulations by Macciò et al. (2006). This mode of gas accretion will usually be off-axis and provides a source of material from which the disk can grow and form new stars. Gas accreting onto a bulge or a spheroid would likely produce an S0 galaxy. Accretion of cold gas could also explain other strange kinematical features in galaxies, such as counterrotating stellar and gaseous disks.

5.4 Dynamical models for Polar Ring Galaxies

The existence of two orthogonal components of the angular momentum let the PRGs be the ideal laboratory to put limits on the 3-D shape of the dark matter haloes. The question of the Dark Halo (DH) shape is important because cosmological simulations (Navarro et al., 1997) predict the distribution of the DH shapes and the universal radial dependence of the matter distribution in the dark halos (NFW), but divergence have been found (de Blok et al. 2003 and Napolitano et al. 2005). By deriving the most likely dark halo flattening distribution from polar ring dynamics, test can be performed on the likelihood of the differen cosmological models.

The first attempts to derive the dark halo shape in polar ring galaxies were made by Schweizer et al. (1983) and Whitmore et al. (1987); by comparing the ratio between ring and disk speeds at the same galactocentric radius, they derived a wide range of flattening for the mass distributions. Among the objects studied, the prototype polar ring galaxy NGC4650A has been the best investigated. In their work Whitmore et al. (1987) concluded that the dark matter halo for this object was spherical. On the other hand, the analysis of the S0 and outer polar ring rotation curve, let Sackett & Sparke (1990) to conclude that the observed kinematics was well reproduced by adopting dark halo flattenings in the range E3-E7.

Sackett et al. (1994) proposed a dynamical model, based on the observations of the rotation and velocity dispersion of the central disk obtained at the ESO 3.6 m telescope, which ruled out the spherical dark halo. Their best fit model was given by a dark halo with an E6 to E7 flattening, whose axis are aligned with those of the S0 (see Fig. 5.7).

In 1996, the observed similarities between the wide polar rings and the late-

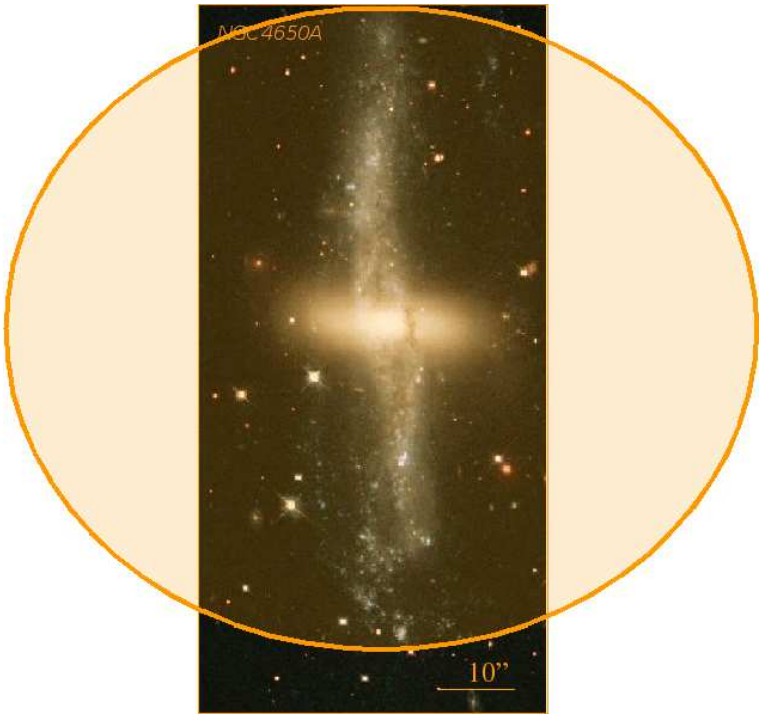

Figure 5.7: Dark Halo shape proposed by Sackett et al. (1994) for NGC4650A; a pseudoisothermal ellipsoid with a vertical-to-radial axis ratio of $0.3 \leq\ c/a \leq\ 0.4$, i.e. an E6/E7 flattening and $M_{DH}(R = 10kpc) \sim 4 \times\ 10^{10} M_{\odot}$

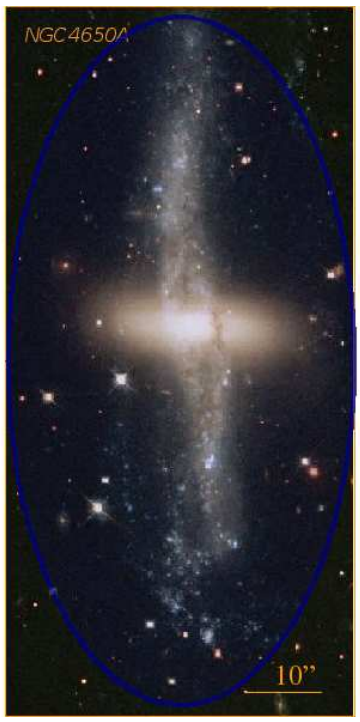

Figure 5.8: Dark Halo shape proposed by Combes & Arnaboldi (1996) for NGC4650A; an E7 flattened halo aligned with the polar disk, with $M_{DH}(R = 10kpc) \sim\ 1.4 \times\ 10^{10} M_{\odot}$

type spiral disks led Combes & Arnaboldi (1996) to develop a radically different dynamical model for NGC4650A. By knowing that 1) the HI component lies entirely in the polar ring, 2) their B-R and R-K integrated colors are very similar to those of late type systems (Arnaboldi et al., 1995), and 3) that there is an empirical relationship between the dark matter and the HI surface density, Combes & Arnaboldi (1996) proposed a dark component flattened in the plane of the polar ring itself (see Fig. 5.8)

The biggest uncertainties in the mass models proposed until 1996 are due to the low resolution of the HI data and to the difficulty in measuring the velocity dispersion along the spheroid and S0 major axis. The new high resolution CaT[1] spectra (Iodice et al., 2006) are better tracers of the kinematics for the NGC4650A spheroid than what was available before: since they allowed the authors to measure a flat velocity dispersion profile along the spheroid major axis, while previous measurements were too scattered to reliably establish any trend with radius.

These new velocity dispersion profiles show that both the linear decreasing fit proposed by Sackett et al. (1994) and the exponential empirical law proposed

[1]Calcium triplet lines.

by Combes & Arnaboldi (1996) do not reproduce well the observed trend with radius. By using the new spectroscopy available for the HG (Iodice et al., 2006) and rotation curves of stars and gas in the polar disk (Arnaboldi et al. 1997 and Iodice et al. 2008), Iodice et al. are currently developing a new dynamical model for NGC4650A (Iodice, Napolitano, Arnaboldi et al. in preparation).

As a first step they fitted the kinematics of the two components (HG and polar disk) separately: 1) they have assumed a centrifugal equilibrium along the polar disk, $V_c^2(R) = GM(R)/R$, where the circular velocity $V_c^2 = V_{star}^2 + V_{gas}^2 + V_{DH}^2$; 2) they have performed an axisymmetric Jeans analysis on the equatorial plane of the spheroid. The best fit for the polar disk was obtained with M/L = 0.25 (K band) by adding to an exponential disk a DH with a NFW radial profile, with a scale radius $r_s^{PD} = 54$ kpc and a DH mass of about $5.910^{10} M_\odot$ inside a radius of 25 kpc. To fit the rotation velocity and velocity dispersion along the spheroid equatorial plane, they assumed a NFW DH, with virial mass and the concentrations fixed from the polar axis, and isotropy of the velocity ellipsoid: the best fit was obtained with a scale radius $r_s^{HG} = 18$ kpc for the DH. By such a simple analysis they have obtained that the two scale radii are different $r_s^{HG}/r_s^{PD} = 0.3$ which suggests a DH flattened along the polar axis with a flattening of the potential $(c/a)_\phi \sim 0.7$ (E7). This preliminary result, together with the DH mass, are consistent with the DH content and flattening given by Combes & Arnaboldi (1996).

In the following section I will show new results about the formation scenario for NGC4650A.

5.5 Chemical abundances in the polar disk of NGC4650A: implications for cold accretion scenario

Authors: Marilena Spavone, Enrichetta Iodice, Magda Arnaboldi, Ortwin Gerhard, Roberto Saglia and Giuseppe Longo

Published in The Astrophysical Journal, 714.1081

Abstract

The aim of the present study is to test whether the cold accretion of gas through a "cosmic filament" (Macciò et al., 2006) is a possible formation scenario for the polar disk galaxy NGC 4650A. If polar disks form from cold accretion of gas, the abundances of the HII regions may be similar to those of very late-type spiral galaxies, regardless of the presence of a bright central stellar spheroid, with total luminosity of few $10^9 L_{\odot}$.

We use deep long slit spectra obtained with the FORS2 spectrograph at the VLT in the optical and near-infrared wavelength ranges for the brightest HII regions in the disk polar disk of NGC 4650A. The strongest emission lines ([OII] H_{β}, [OIII], H_{α}) were used to derived oxygen abundances, metallicities and the global star formation rates for the disk. The deep spectra available allowed us to measure the Oxygen abundances $(12 + log(O/H))$ using the *Empirical method* based on intensities of the strongest emission lines, and the *Direct method*, based on the determination of the electron temperature from the detection of weak auroral lines, as the [OIII] at 4363 Å.

The Oxygen abundance measured for the polar disk is then compared with those measured for different galaxy types of similar total luminosities, and then compared against the predictions of different polar ring formation scenarios.

The average metallicity values for the polar disk in NGC 4650A is $Z = 0.2 Z_{\odot}$, and it is lower that the values measured for ordinary spirals of similar luminosity. Moreover the gradient of the metallicity is flat along the polar disk major axis, which implies none or negligible metal enrichment from the stars in the older central spheroid.

The low metallicity value in the polar disk NGC 4650A and the flat metallicity gradient are both consistent with a later infall of metal-poor gas, as expected in the cold accretion processes.

Introduction

The hierarchical, merger-dominated picture of galaxy formation is based on the Cold Dark Matter (CDM) model (Cole et al., 2000a), which predicts that the observed galaxies and their dark halo (DH) were formed through a repeated merging process of small systems (De Lucia et al. 2006; Genel et al. 2008). In this framework, major and minor mergers of disky systems do play a major role in the formation of spheroid and elliptical galaxies (Naab et al. 2007; Bournaud et al. 2007), in all environments and from the Local Group to high-redshift universe (Conselice et al., 2003b). The gas fraction is a key parameter in the physics of such gravitational interactions: if it is high enough, an extended and massive disk structure can survive (Springel & Hernquist 2005; Robertson & Bullock 2008). Galaxies can get their gas through several interacting processes, such as smooth accretion, stripping and accretion of primordial gas, which are equally important in the growth of galaxies. Recent theoretical works have argued that the accretion of external gas from the cosmic web filaments, with inclined angular momentum (Davé et al. 2001, Semelin & Combes 2005), might be the most realistic way by which galaxies get their gas. This process may also explain the build-up of high redshift disk galaxies (Kereš et al. 2005, Keres 2008, Brook et al. 2008b, Dekel et al. 2009b, Bournaud & Elmegreen 2009). The relative share of all gravitational interactions depends on the environments and it drives many morphological features observed in galaxies, such as bars and polar rings.

Galaxies with polar rings (PRGs) generally contain a central featureless stellar spheroid and an elongated structure, the "polar ring" (made up by gas, stars and dust), which orbits in a nearly perpendicular plane to the equatorial one of the central galaxy (Whitmore et al., 1990). The decoupling of the angular momentum of the polar structure and the central spheroid cannot be explained by the collapse of a single protogalactic cloud: thus a "second event" must have happened in the formation history of these systems. This is the reason why studying PRGs promise to yield detailed information about many of the processes at work during galaxy interactions and merging (Iodice et al. 2002c, Iodice et al. 2002b, Reshetnikov & Combes 1994, Reshetnikov et al. 2002, Bournaud & Combes 2003b).

The debate on the origin of PRGs is still open and two main processes have been proposed *i)* a major dissipative merger or *ii)* gas accretion. In the merging scenario, the PRG results from a "polar" merger of two disk galaxies with unequal mass, (Bekki 1997; Bekki 1998a; Bournaud et al. 2005b): the morphology of the merger remnants depends on the merging initial orbital parameters and the initial mass ratio of the two galaxies. In the accretion scenario, the polar ring may form by a) the disruption of a dwarf companion galaxy orbitating around an early-type system, or by b) the tidal accretion of gas stripping from a disk galaxy outskirts, captured by an early-type galaxy on a parabolic encounter (Reshetnikov & Sotnikova 1997; Bournaud & Combes 2003b; Hancock et al. 2009). In the latter case, the total amount of accreted gas by the early-type object is about 10% of

the gas in the disk donor galaxy, i.e. up to 10^9 $M_\odot$. Both major merger and accretion scenarios are able to account for many observed PRGs morphologies and kinematics, such as the existence of both wide and narrow rings, helical rings and double rings (Whitmore et al., 1990).

Very recently, a new mechanism has been proposed for the formation of wide disk-like polar rings: a long-lived polar structure may form through cold gas accretion along a filament, extended for ~ 1 Mpc, into the virialized dark matter halo (Macciò et al., 2006). In this formation scenario, there is no limits to the mass of the accreted material, thus a very massive polar disk may develop either around a stellar disk or a spheroid. Brook et al. (2008b), by using high-resolution cosmological simulations of galaxy formation, have confirmed and strengthened the formation scenario proposed by Macciò et al. (2006). In this case polar disk galaxies can be considered as extreme examples of angular momentum misalignment that occurs during the hierarchical structure formation. In the merging history, an inner disk formed first after the last major merger of two galaxies with a 1:1 mass ratio, then, due to the high gas fraction, the galaxy rapidly forms a new disk whose angular momentum depends on the merger orbital parameters. At later times, gas continues to be accreted along the disk which may be also in a plane perpendicular to the inner disk. The morphology and kinematics of one simulated object, in both simulations, are similar to those observed for NGC4650A: in particular, Brook et al. (2008b) found that such formation mechanism can self-consistently explain both morphology and kinematics of central spheroid and polar structure, and all the observed features (like colors and colors gradient, longevity, spiral arms, HI content and distribution).

NGC 4650A is the prototype for PRGs (see Fig. 6.2). Its luminous components, inner spheroid and polar structure were studied in optical and near-infrared (NIR) photometry, spectroscopy, and in the radio emission, HI 21 cm line and continuum (Arnaboldi et al. 1997, Gallagher et al. 2002, Iodice et al. 2002c, Swaters & Rubin 2003, Iodice et al. 2006). The polar structure in NGC 4650A is a disk, very similar to that of late-type spirals or LSB galaxies, rather than a ring. The polar disk stars and dust can be reliably traced to ~ 1.2 kpc radius from the galaxy nucleus, and the surface brightness profiles have an exponential decrease (Iodice et al. 2002b, Gallagher et al. 2002). Furthermore, the rotation curves measured from the emission and absorption line optical spectra are consistent with those of a disk in a differential rotation rather than that of a narrow ring (Swaters & Rubin, 2003). This is also confirmed by the HI 21 cm observations (Arnaboldi et al., 1997) which show that the gas is five times more extended than the luminous polar structure, with a position-velocity diagram very similar to those observed for edge-on disks. The polar disk is very massive, since the total HI mass is about $10^{10} M_\odot$, which added to the mass of stars, makes the mass in the polar disk comparable with the total mass in the central spheroid (Iodice et al., 2002c). The morphology of the central spheroid resembles that of a low-luminosity early-type galaxy: the surface brightness profile is described by an exponential law, with

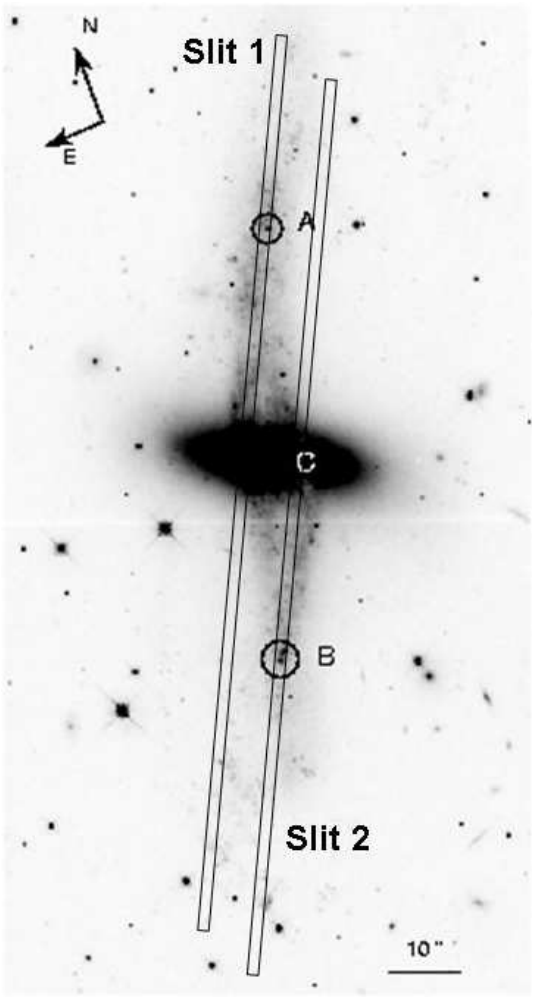

Figure 5.9: Optical image of NGC4650A with superimposed the slits used to acquire data analyzed in this work.

a small exponential nucleus; its integrated optical vs. NIR colors are similar to those of an intermediate age stellar population (Iodice et al. 2002b, Gallagher et al. 2002). New high resolution spectroscopy in NIR on its photometric axes suggests that this component is a nearly-exponential oblate spheroid supported by rotation (Iodice et al., 2006).

These new kinematic data, together with the previous studied, set important constraints on the possible formation mechanisms for NGC4650A.

Because of the extended and massive polar disk, with strong H_α emissions, NGC 4650A is the ideal candidate to measure the chemical abundances, metallicity and star formation rates (SFR) via spectroscopic measurements of line emissions along the major axis of the polar disk. The goal is to compare the derived values for the metallicity and SFR with those predicted by the different formation scenarios. As we shall detail in the following sections, if the polar structure forms by accretion of primordial cold gas from cosmic web filament, we expect the disk to have lower metallicities of the order of $Z \sim 1/10 Z_\odot$ (Agertz et al., 2009) with respect to those of same-luminosity spiral disks.

We shall adopt for NGC4650A a distance of about 38 Mpc based on $H_0 = 75\ km\ s^{-1}\ Mpc^{-1}$ and an heliocentric radial velocity $V = 2880\ km\ s^{-1}$, which implies that 1 arcsec = 0.18 kpc.

Observations and data reduction

Spectra were obtained with FORS2@UT1, on the ESO VLT, in service mode, during two observing runs: 078.B-0580 (on January 2007) and 079.B-0177 (on April 2007). FORS2 was equipped with the MIT CCD 910, with an angular resolution of $0.25''$ pixel^{-1}. The adopted slit is $1.6''$ wide and $6.8'$ long. Spectra were acquired along the North and South side of the polar disk, at $P.A. = 152°$ (see Fig. 6.2), in order to include the most luminous HII regions in polar disk. The total integration time for each direction is 3 hours, during the 078.B-0580 run and 2.27 hours during 079.B-0177 run, respectively, with an average seeing of $1.2''$.

At the systemic velocity of NGC 4650A, to cover the red-shifted emission lines of the $[OII]\lambda3727$, $[H_\gamma]\lambda4340$, $[OIII]\lambda4363$, $[OIII]\lambda\lambda4959, 5007$, $[H_\beta]\lambda4861$, $[NII]\lambda5755$ the grism GRIS-600B+22 was used in the $3300 - 6210$ Å wavelength range, with a dispersion of 50 Å/mm (0.75 Å/pix). In the near-infrared $5600 - 11000$Å wavelength range, the grism GRIS-200I+28 was used, with a dispersion of 162 Å/mm (2.43 Å/pix) to detect the fainter $[SII]\lambda\lambda6717, 6731$ and $[SIII]\lambda\lambda9068, 9532$ emission lines, with a $S/N \geq 20$ and the brighter $[H_\alpha]\lambda6563$ emission line, with a $S/N > 150$. In this wavelength range, where the sky background is much more variable and higher with respect to the optical domain, to avoid the saturation of the sky lines a larger number of scientific frames with short integration time (850 sec) were acquired.

The data reduction was carried out using the CCDRED package in the IRAF[2] (*Image Reduction and Analysis Facility*) environment. The main strategy adopted for each data-set included dark subtraction[3], flat-fielding correction, sky subtraction and rejection of bad pixels. Wavelength calibration was achieved by means of comparison spectra of Ne-Ar lamps acquired for each observing night, using the IRAF TWODSPEC.LONGSLIT package. The sky spectrum was extracted at the outer edges of the slit, for $r \geq 40$ arcsec from the galaxy center, where the surface brightness is fainter than $24 mag/arcsec^2$, and subtracted off each row of the two dimensional spectra by using the IRAF task BACKGROUND in the TWODSPEC.LONGSLIT package. On average, a sky subtraction better than 1% was achieved. The sky-subtracted frames, both for North and South part of the polar disk, were co-added to a final median averaged 2D spectrum.

The final step of the data-processing is the flux calibration of each 2D spectra, by using observations of the standard star LTT4816 and the standard tasks in IRAF (STANDARD, SENSFUNC and CALIBRATE). The flux calibration is very important in the present study because we need to "align" two spectra, which cover different wavelength range and taken in different times. Thus, we checked and obtained that the calibrations for the spectra in both spectral range were consistent. Fig. 5.10 shows the 1D flux calibrated spectra of the spectrophotometric standard star used to calibrate the spectra in the whole range $3300 - 11000$ Å. To perform the flux calibration we extracted a 1-D spectrum of the standard star to find the calibration function; then we extracted a set of 1-D spectra of the galaxy summing up a number of lines corresponding to the slit width. Since the slit width was $1.3''$ and the scale of the instrument was $0.25''/pix$, we collapsed seven lines to obtain each 1-D spectrum. Finally we applied the flux calibration to this collection of spectra. Furthermore, we compared our flux calibrated spectra with others acquired at the Siding Spring Observatory with the Double Beam Spectrograph (DBS) (Buttiglione et al., 2006). The DBS has a dichroic that slits the light in a red and a blue arm, therefore the flux calibration with standard stars can be done simultaneously for the red and the blue arms. We used these spectra to check for any difference in the flux calibrations, finding that our flux calibrated spectra, both of the template star and of the galaxy, turn out to be consistent with them.

The wavelength and flux-calibrated spectra are shown in Fig. 5.11 and 5.12. In the blue spectrum (top panel) are clearly visible a number of emission lines: H_β, H_γ, $[OII]\lambda 3727$ and $[OIII]\lambda\lambda 4959, 5007$, while in the red one (bottom panel) we have H_α (blended with the $[NII]\lambda 6583$ line appearing in the red wing of H_α), $[SII]\lambda\lambda 6717, 6731$ and $[SIII]\lambda\lambda 9069, 9532$. From a two-Gaussian fit to the combined emission, we estimate the line ratio $[NII]\lambda 6583/(H_\alpha + [NII]\lambda 6548 \simeq 0.1$. For this reason the H_α flux is that measured as the total flux in the line reduced by

[2]IRAF is distributed by the National Optical Astronomy Observatories, which is operated by the Associated Universities for Research in Astronomy, Inc. under cooperative agreement with the National Science Foundation.

[3]Bias frame is included in the Dark frame.

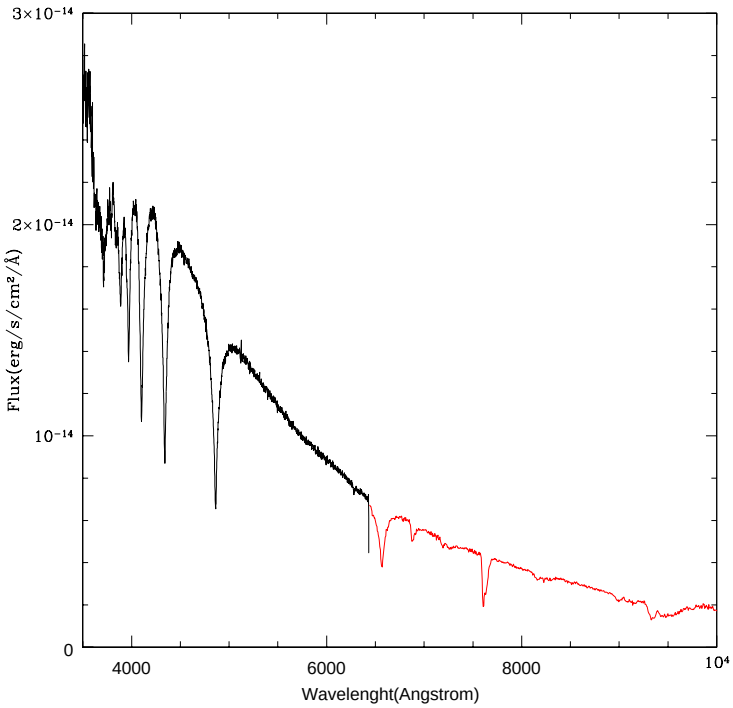

Figure 5.10: 1-D spectrum of the standard star LTT4816, used to flux-calibrate the spectra. The black line represent the spectrum of the star acquired in the blue wavelength range, while the red line is the same star acquired in the red range.

the contribution of $[NII]\lambda6583$. The observed emission lines and their uncorrected and reddening-corrected fluxes relative to H_β are listed in Tab. 5.1 and Tab. 5.2.

Since ground-based near-infrared spectroscopy is affected by the strong and variable absorption features due to the Earth's atmosphere, we accounted for this effect in our spectra, in which the telluric absorption bands are clearly visible around 7200, 8200 and 9300 Å. In order to perform this correction we used the "telluric standard star" LTT4816, near both in time and air mass to the object, and the IRAF task TELLURIC; by fitting the continuum, telluric calibration spectra are shifted and scaled to best divide out telluric features from data spectra. The ratios of the uncorrected fluxes relative to those obtained applying the average telluric correction are the following: $\frac{[SII]\lambda6717_{uncorrected}}{[SII]\lambda6717_{corrected}} = \frac{[SII]\lambda6731_{uncorrected}}{[SII]\lambda6731_{corrected}} = 1.7$ and $\frac{[SIII]\lambda9069_{uncorrected}}{[SIII]\lambda9069_{corrected}} = \frac{[SIII]\lambda9532_{uncorrected}}{[SIII]\lambda9532_{corrected}} = 0.6$.

Measurement of emission-lines fluxes

The fluxes of the above mentioned emission lines were measured using the IRAF SPLOT routine, that provides an interactive facility to display and analyze spectra. The H_β is evaluated for $r \geq 10$ arcsec, where only the emission line is present; for lower distances, i.e. where stars relative to the spheroid also contributes to the spectra, the H_β is also in absorption. We evaluated flux and equivalent width by marking two continuum points around the line to be measured. The linear continuum is subtracted and the flux is determined by simply integrating the line intensity over the local fitted continuum. The errors on these quantities have been calculated, following Pérez-Montero & Díaz (2003), by the relation $\sigma_1 = \sigma_c N^{1/2}[1 + EW/(N\Delta)]^{1/2}$, were σ_1 is the error in the line flux, σ_c is the standard deviation in a box near the measured line and represents the error in the continuum definition, N is the number of pixels used to measure the flux, EW is the equivalent width of the line and Δ is the wavelength dispersion in Å/pixel. The errors relative to each emission line fluxes are listed in Tab. 5.1 and Tab. 5.2.

Reddening correction

Reduced and flux calibrated spectra and the measured emission line intensities were corrected for the reddening, which account both for that intrinsic to the source and to the Milky Way. By comparing the intrinsic Balmer decrements, $H_\alpha/H_\beta = 2.89$ and $H_\gamma/H_\beta = 0.468$, predicted for large optical depth (case B) and a temperature of 10^4 K, with the observed one, we derived the visual extinction $A(V)$ and the color excess $E(B-V)$, by adopting the mean extinction curve by Cardelli et al. (1989) $A(\lambda)/A(V) = a(x) + b(x)R_V$, where $R_V[\equiv\ A(V)/E(B-V)] = 3.1$ and $x = 1/\lambda$. In order to estimate reddening correction for all the observed emission lines, we used the complete extinction curve into three wavelengths regions (Cardelli et al. (1989)): *infrared* ($\lambda \geq 0.9\mu m$), *optical/NIR* ($0.9\mu m \geq \lambda \geq 0.3\mu m$) and *ultraviolet* ($0.125\mu m \geq \lambda \geq 0.10\mu m$), which are characterized by different relations of a(x)

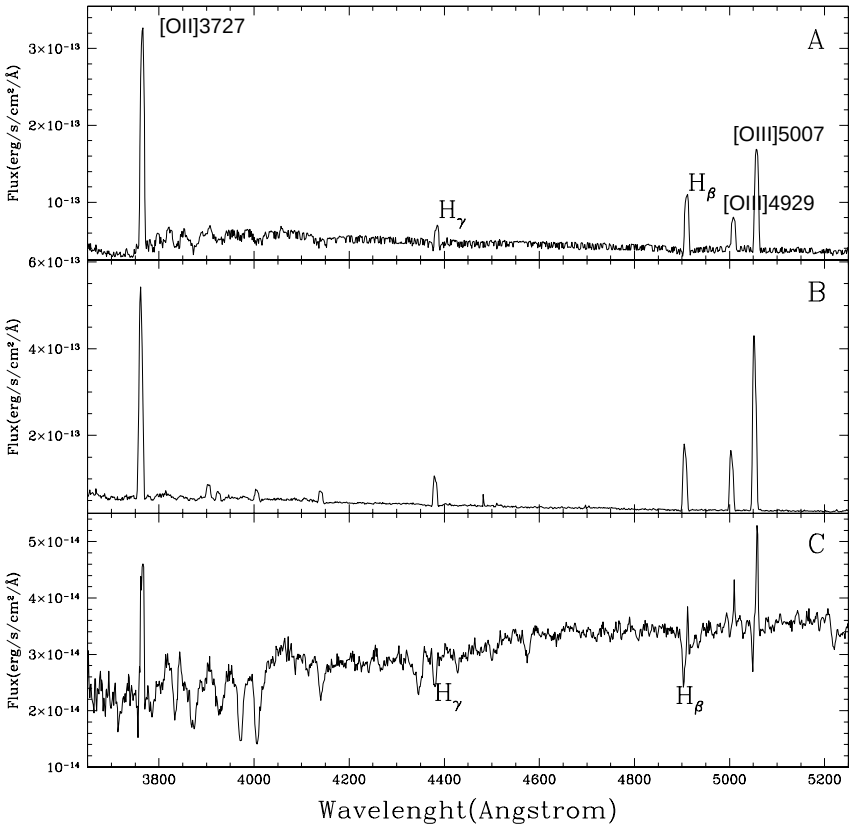

Figure 5.11: *Top panel* - Spectrum of NGC4650A in the blue wavelength range, corresponding to the region marked as A in the Fig. 6.2. *Middle panel* - Spectrum of the region B in the Fig. 6.2. *Bottom panel* - Spectrum of the region C in the Fig. 6.2, where are clearly visible the absorbing features of the line H_γ and H_β.

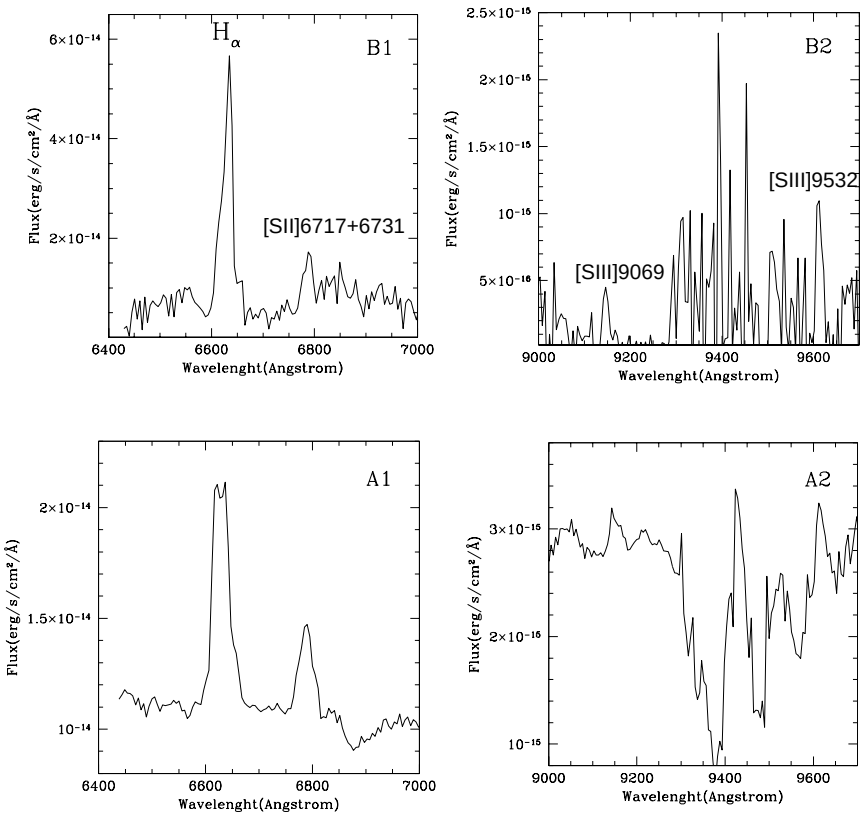

Figure 5.12: *Top panel* - Spectra of NGC4650A in the red wavelength range, corresponding to the region marked as A in the Fig. 6.2. We divided the spectra in A1 and A2 in order to obtain a better visualization of the lines. *Bottom panel* - Spectrum of the region B (B1 and B2 as explained below) in the Fig. 6.2.

and b(x). All the emission lines in our spectra are in the *optical/NIR* range, except for the $[SIII]\lambda 9532$, that falls in the *infrared* range, so we used the average R_V-dependent extinction law derived for these intervals to perform the reddening correction.
We measured the fluxes of H_β, H_γ and H_α lines at each distance from the galaxy center and for each spectra (North slit and South slit), than we derived the average observed Balmer decrements, which are the following:
$H_\alpha/H_\beta = 2.40 \pm\ 0.01$
$H_\gamma/H_\beta = 0.41 \pm\ 0.01$
while the color excess obtained by using these observed decrements are:
$[E(B-V)]_{H_\alpha/H_\beta} = 0.20 \pm\ 0.004$
$[E(B-V)]_{H_\gamma/H_\beta} = 0.25 \pm\ 0.012.$
Such values of E(B-V) are used to derive the extinction A_λ, through the Cardelli's law; in particular, the $[E(B-V)]_{H_\gamma/H_\beta}$ and $[E(B-V)]_{H_\alpha/H_\beta}$ are used respectively for the reddening correction in optical and NIR wavelength range. The corrected fluxes are given by $F^\lambda_{int}/F^{H_\beta}_{int} = F^\lambda_{obs}/F^{H_\beta}_{obs} 10^{0.4[A_\lambda - A_{H_\beta}]}$. Observed and reddening-corrected emission line fluxes are reported in Tab. 5.1 and Tab. 5.2.

Oxygen abundances determination

The main aim of the present work is to derive the chemical abundances in the polar disk of NGC4650A: in what follow we evaluate the oxygen abundances following the methods outlined in Pagel et al. (1979), Díaz & Pérez-Montero (2000) and Pilyugin (2001), referring to them as *Empirical methods*, and those introduced by Osterbrock (1989) and Allen (1984), or *Direct methods*.

The large dataset available (presented in Sec. 6.9) let us to investigate both the *Empirical methods*, based on the intensities of easily observable lines (Sec. 5.5), and the *Direct method*, based on the determination of the electron temperature, by measuring the intensities of the weak auroral lines (Sec. 5.5).
As described in details in the next sections, we have derived the oxygen abundance parameter $12 + log(O/H)$ along the polar disk, by using both the *Empirical* and *Direct* methods.

Empirical oxygen and sulphur abundance measurements

The *Empirical methods* are based on the cooling properties of ionized nebulae which translate into a relation between emission-line intensities and oxygen abundance. Several abundance calibrators have been proposed based on different emission-line ratios: among the other, in this work we used R_{23} (Pagel et al., 1979), S_{23} (Díaz & Pérez-Montero, 2000) and the P-method (Pilyugin, 2001). The advantages of different calibrators have been discussed by several authors (Díaz & Pérez-Montero 2000, Kobulnicky & Zaritsky 1999, Kobulnicky & Kewley 2004,

Pérez-Montero & Díaz 2005, Kewley & Ellison 2008, Hidalgo-Gámez & Ramírez-Fuentes 2009).

The method proposed by Pagel et al. (1979) is based on the variation of the strong oxygen lines with the oxygen abundance. Pagel et al. (1979) defined the "oxygen abundance parameter" $R_{23} = ([OII]\lambda 3727 + [OIII]\lambda\lambda 4959 + 5007)/H_\beta$, which increase with the oxygen abundance for values lower than 20% of the solar one and then reverses his behavior, decreasing with increasing abundance, due to the efficiency of oxygen as a cooling agent that lead to a decreasing in the strength of the oxygen emission lines at higher metallicities. Three different regions can be identified in the trend of R_{23} with the oxygen abundance (Pérez-Montero & Díaz, 2005): a lower branch ($12 + log(O/H) < 8.1$), in which R_{23} increase with increasing abundance, an upper branch ($12 + log(O/H) > 8.4$), in which the trend is opposite, and a turnover region ($8.1 < 12 + log(O/H) < 8.4$). While the upper and lower branches can be fitted by regression lines, the turnover region seems to be the most troublesome, in fact object with the same value of R_{23} can have very different oxygen abundances. The R_{23} parameter is affected by two main problems: the two-valued nature of the calibration and the dependence on the degree of ionization of the nebula.

To break the degeneracy that affects the metallicity for values of $12+log(O/H) \geq 8.0$, Díaz & Pérez-Montero (2000) proposed an alternative calibrator, based on the intensity of sulphur lines: $S23 = ([SII]\lambda\lambda 6717 + 6731 + [SIII]\lambda\lambda 9069 + 9532)/H_\beta$. The [SII] and [SIII] lines are analogous to the optical oxygen lines [OII] and [OIII], but the relation between the "Sulphur abundance parameter" S_{23} and the oxygen abundance remain single valued up to solar metallicities (Díaz & Pérez-Montero 2000 and Pérez-Montero & Díaz 2005). Moreover, because of their longer wavelength, sulphur lines are less sensitive to the effective temperature and ionization parameter of the nebula, and almost independent of reddening, since the [SII] and [SIII] lines can be measured nearby hydrogen recombination lines. Díaz & Pérez-Montero (2000) have attempted a calibration of oxygen abundance through the sulphur abundance parameter, obtaining the following empirical relation:

$$12 + log(O/H) = 1.53 logS_{23} + 8.27 \tag{5.1}$$

For the polar disk of NGC4650A, by using the emission line fluxes given in Tab. 5.1 and Tab. 5.2, we derived both R_{23} and S_{23} parameters, which are listed in Tab. 5.3. Since there are few measurements available for the Sulphur lines, we have obtained an average value of S_{23} for the polar disk, by using the following telluric corrected fluxes ratios: $[SII]\lambda 6717/H_\beta = 0.18$, $[SII]\lambda 6731/H_\beta = 0.2$, $[SIII]\lambda 9069/H_\beta = 0.43$ and $[SIII]\lambda 9532/H_\beta = 0.25$, obtaining $logS_{23} = 0.024 \pm 0.030$. The average oxygen abundance, derived by adopting the Eq. 5.1, is the following: $12 + log(O/H)_S = 8.3 \pm 0.2$.

Pilyugin (2001) realized that for fixed oxygen abundances the value of $X_{23} = logR_{23}$ varies with the excitation parameter $P = R_3/R_{23}$, where $R_3 = OIII[4959+5007]/H_\beta$, and proposed that this latter parameter could be used in the oxygen

abundance determination. This method, called "P-method", propose to use a more general relation of the type $O/H = f(P, R_{23})$, compared with the relation $O/H = f(R_{23})$ used in the R_{23} method. The equation related to this method is the following

$$12 + log(O/H)_P = \frac{R_{23} + 54.2 + 59.45P + 7.31P^2}{6.07 + 6.71P + 0.371P^2 + 0.243R_{23}} \tag{5.2}$$

where $P = R_3/R_{23}$. It can be used for oxygen abundance determination in moderately high-metallicity HII regions with undetectable or weak temperature-sensitive line ratios (Pilyugin, 2001).

We used also the "P-method" to derive the oxygen abundance in the polar disk of NGC4650A: the values of $12+log(O/H)_P$ at each distance from the galaxy center are listed in Tab. 5.3, and shown in Fig. 5.13 and Fig. 6.6. The average value of the oxygen abundance is $12 + log(O/H)_P = 8.2 \pm 0.2$, which is consistent with the values derived by using the Sulphur abundance parameter (Eq. 5.1).

The metallicities corresponding to each value of oxygen abundances given before have been estimated. We adopted $12 + log(O/H)_\odot = 8.83 = A_\odot$ and $Z_\odot = 0.02$ (Asplund et al., 2004). Given that $Z_{NGC4650A} \approx KZ_\odot$ and $K = 10^{[A_{NGC4650A} - A_\odot]}$, we obtain a metallicity for the HII regions of the polar disk in NGC4650A $Z \simeq 0.004$ which correspond to $Z \simeq (0.2 \pm 0.002)Z_\odot$.

Direct oxygen abundance measurements

The electron temperature is the fundamental parameter to directly derive the chemical abundances in the star-forming regions of galaxies. In a temperature-sensitive ion, with a well separated triplet of fine-structure terms, electron temperature and electron density (N_e), can be measured from the relative strengths of lines coming from excited levels at different energies above the ground state (see Osterbrock 1989; Allen 1984). As explained in detail below, the oxygen abundances are function of both the emission line fluxes and electron temperatures: this relation is the basis of the commonly known as *direct* method or T_e method. Usually, it happens that not all these lines can be observed in the spectra, or they are affected by large errors. Thus, some assumption were proposed for the temperature structure through the star-forming region: for HII galaxies it is assumed a *two-zone model* with a low ionization zone, where the OII, NII, NeII and SII lines are formed, and a high ionization zone where the OIII, NIII, NeIII and SIII lines are formed (see, e.g. Campbell et al. 1986; Garnett 1992). Photoionization models are then used to relate the temperature of the low ionization zone t_2 to t_3, the temperature of the high ionization zone (Pagel et al. 1992; Pérez-Montero & Díaz 2003; Pilyugin et al. 2006; Pilyugin 2007; Pilyugin et al. 2009).

For NGC4650A, we aim to derive the oxygen abundance of the polar disk directly by the estimate of the O^{++} and O^+ ions electron temperatures. According to Izotov et al. (2005) and Pilyugin et al. (2006), we have adopted the following

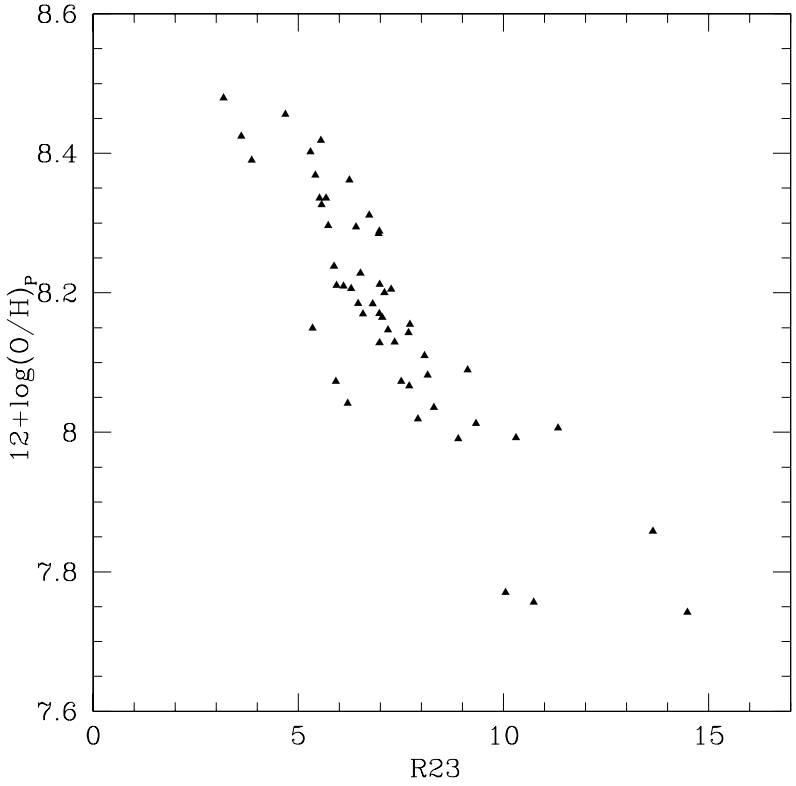

Figure 5.13: Oxygen abundance, obtained by using the empirical calibration introduced by Pilyugin (2001), versus oxygen abundance parameter R_{23} (see Sec. 5.5).

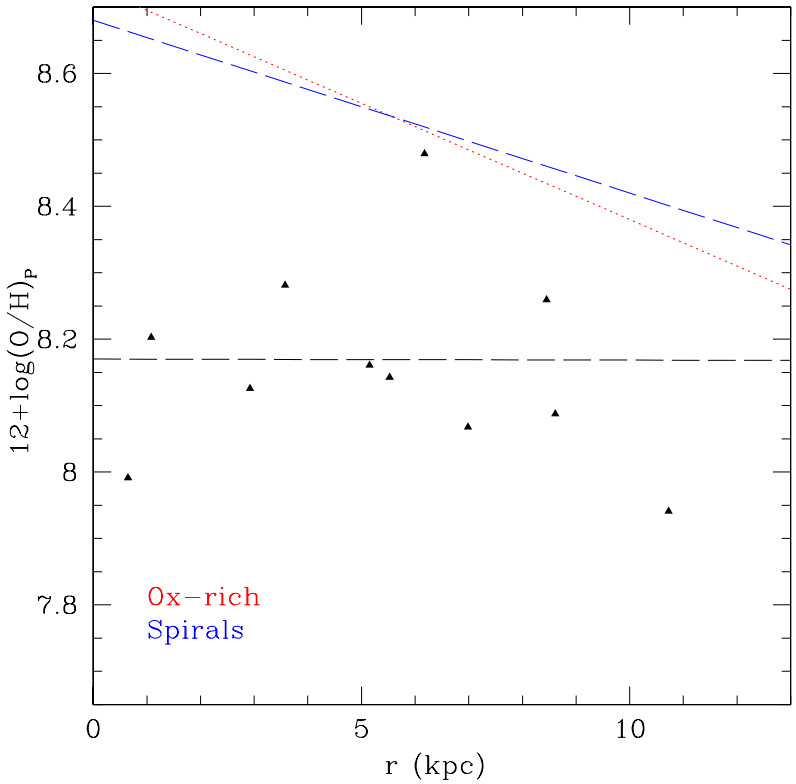

Figure 5.14: Oxygen abundance derived with empirical methods proposed by Pilyugin (2001) versus radius. The values in Tab. 5.3 were binned each 5 arcseconds. The superimposed lines are the linear best fit derived by Pilyugin et al. (2006); the red line represents the best fit to the abundance of oxygen-rich spirals, while the blue line is those related to ordinary spirals. The black line is the best fits obtained for NGC4650A.

equations for the determination of the oxygen abundances, which are based on a five-level atom approximation:

$$12 + log(OIII/H) = log([4959 + 5007]/H_\beta) + 6.2 + 1.251/t_3 - 0.55logt_3 - 0.014t_3 \quad (5.3)$$

$$12+log(OII/H) = log(\frac{[3727]}{H_\beta})+5.961+\frac{1.676}{t_2}-0.40logt_2-0.034t_2+log(1+1.35x_2) \quad (5.4)$$

where t_3 and t_2 are the electron temperatures within the [OIII] and [OII] zones respectively, in units of 10^4 K; $x_2 = 10^{-4} N_e t_2^{-0.5}$, where N_e is the electron density. The total oxygen abundance is $O/H = OIII/H + OII/H$.

The electron temperatures and the electron density, needed to solve the above relations, have been derived using the task TENDEM of the STSDAS package in IRAF, which solves the equations of the statistical equilibrium within the five-level atom approximation (De Robertis et al. 1987; Shaw & Dufour 1995). According to this model, both t_3 and t_2 are function of the electron density N_e and of the line ratios $R_{OIII} = [OIII]\lambda(4959 + 5007)/[OIII]\lambda4363$ and $R_{OII} = [OII]\lambda3727/[OII]\lambda7325$, respectively. For NGC4650A, N_e has been derived from the line ratio $[SII]\lambda6717/[SII]\lambda6731$, which has the average value of 0.83 ± 0.06, through the whole disk extension, for a default temperature of 10^4 K. This let to $N_e \sim 1217\ cm^{-3}$. Even though the auroral line $[OIII]\lambda4363$ is usually very weak, even in the metal-poor environments, the large collecting area of the 8m telescope and the high signal-to-noise spectra, let us to measure such emission line along the whole extension of the polar disk (see Tab. 5.1), which let us to estimate R_{OIII}. The electron temperature $t_3 = f(R_{OIII}, N_e)$ has been calculated by putting N_e and R_{OIII} as inputs in the TENDEM task: given the large spread of R_{OIII}, we adopted the average value in the following three bins, $0 \leq R \leq 20$ arcsec, $20 < R \leq 40$ arcsec, $40 < R \leq 60$ arcsec. The distribution of t_3 in each bin is shown in Fig. 5.15: the electron temperature is almost constant till about 40 arcsec and tends to increase at larger distances. In the same figure there are also plotted the values of t_2 (at the same distances) obtained by adopting the following empirical $t_2 - t_3$ relation, derived by Pilyugin et al. (2009): $t_2 = 0.264 + 0.835t_3$. The empirical $t_2 - t_3$ relation has been investigated and debated for a long time and several forms are given in the literature; that by Pilyugin et al. (2009) is the most recent work on this subject, where they derived the $t_2 - t_3$ relation in terms of the nebular $R_3 = [OIII]\lambda(4959 + 5007)/H_\beta$ and $R_2 = [OII]\lambda3727/H_\beta$ line fluxes. They found that such relation is valid for HII regions with a weak nebular R_3 lines ($logR_3 \geq 0.5$) and it turns to be consistent with those commonly used (see Fig. 14 in Pilyugin et al. (2009) paper and reference therein). The polar disk of NGC4650A, since $logR_3 = 0.5 \pm 0.2$ (this is the average value on the whole disk extension), is located in the upper validity limit of the $t_2 - t_3$ relation.

This is what is usually done since the auroral line $[OII]\lambda7325$ is too weak to obtain a good enough estimate of the electron temperature t_2. For the polar disk of NGC4650A, the line fluxes of $[OII]\lambda(7320+7330)$ are strong enough to be measured at about 30 arcsec and the average value of $[OII]\lambda(7320+7330)/H_\beta = 0.04 \pm 0.01$. The average value of the ratio
$R_{OII} = [OII]\lambda3727/[OII]\lambda7325$ is given as input in the TENDEM task, and we obtain $t_2 = (1.092 \pm 0.20) \times 10^4$ K, which is added to Fig. 5.15. This value is lower than that derived by using photoionization models, even if the observed and theoretical values of t_2 are consistent within errors: such difference could be due both to the uncertainties in the line fluxes measurements, made on so few and weak lines, and to the validity limit of the $t_2 - t_3$ relation.
To obtain the oxygen abundance for the polar disk, we decided to adopt both estimates for t_2, by using the average value inside 40 arcsec for that derived by photoionization models, which is $t_2^{mod} = (1.7 \pm 0.2) \times 10^4$ K, and, consistently, an average value for $t_3 = (2.0 \pm 0.2) \times 10^4$ K at the same distances.

By adopting the Eq. 5.3 and Eq. 5.4, the oxygen abundance $12 + log(O/H)_T$ for the polar disk is shown in Fig. 5.16 and listed in Tab. 5.4. By using the value of t_2 derived by direct measurements of OII line fluxes, the metallicity is higher with respect to that derived by using the value of t_2 from photoionization models: the average value is $12 + log(O/H)_{T_{obs}} = 8.4 \pm 0.1$ and $12 + log(O/H)_{T_{mod}} = 7.6 \pm 0.5$ for the two cases respectively. The large error, that are derived by propagating the emission line intensity errors listed in Tab. 5.1 and Tab. 5.2, which is about 0.5, let both estimates consistent.
It is important to point out that the oxygen abundance derived by direct measurements of OII line fluxes for t_2 is much more similar to the value derived by empirical methods, which is $12 + log(O/H) = 8.3$, than the value derived by using photoionization models for t_2: this may suggest that NGC4650A could be out of the range of validity of these models.

Discussion: use of the chemical analysis to constrain the galaxy formation

As discussed above, we derive the oxygen abundance, $12+log(O/H)$ to be 8.2 ± 0.1, by using both the empirical and direct methods. In the following sections we will discuss the results obtained by the present work, how they could reconcile with the predictions by theoretical models and, finally, we address the main conclusions of this study.

Results

Here we discuss how the average value of metallicity and its distribution along the polar disk compares with those typical for other late-type disk galaxies and PRGs.

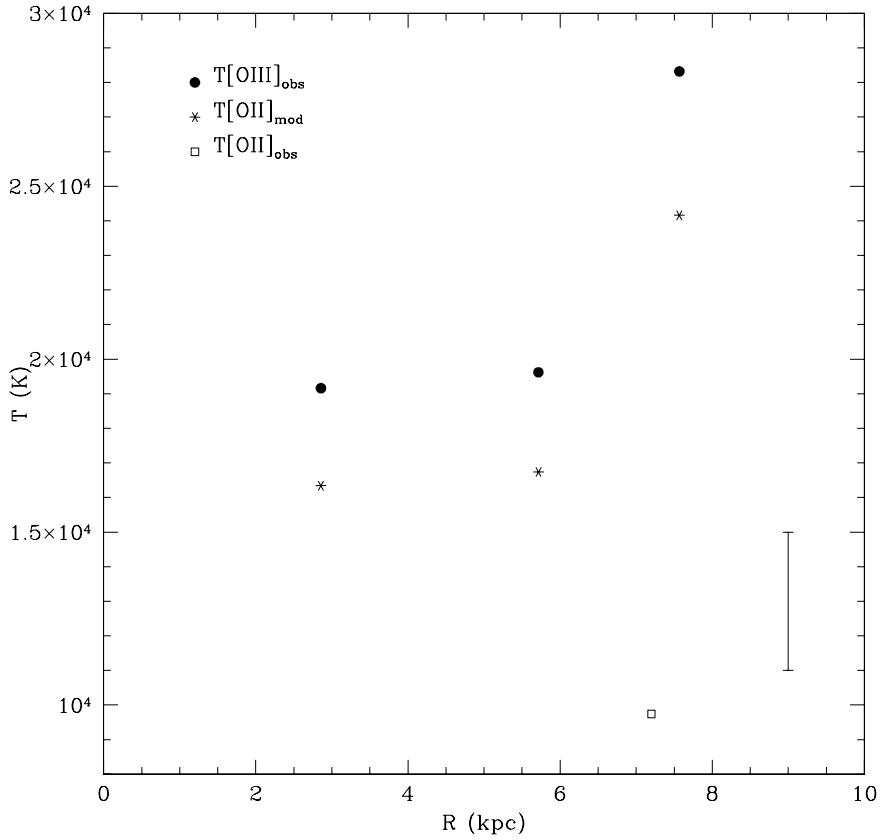

Figure 5.15: Electron temperature along the polar disk of NGC4650A. The filled circles correspond to the observed T[OIII], the starred points correspond to the T[OII] estimated by the photoionization model (see Sec. 5.5 for details), the open square corresponds to the average value of T[OII] directly estimated by the ratio $R_{OII} = OII[3727]/[7325]$. In the bottom left side of the plot the mean error is shown.

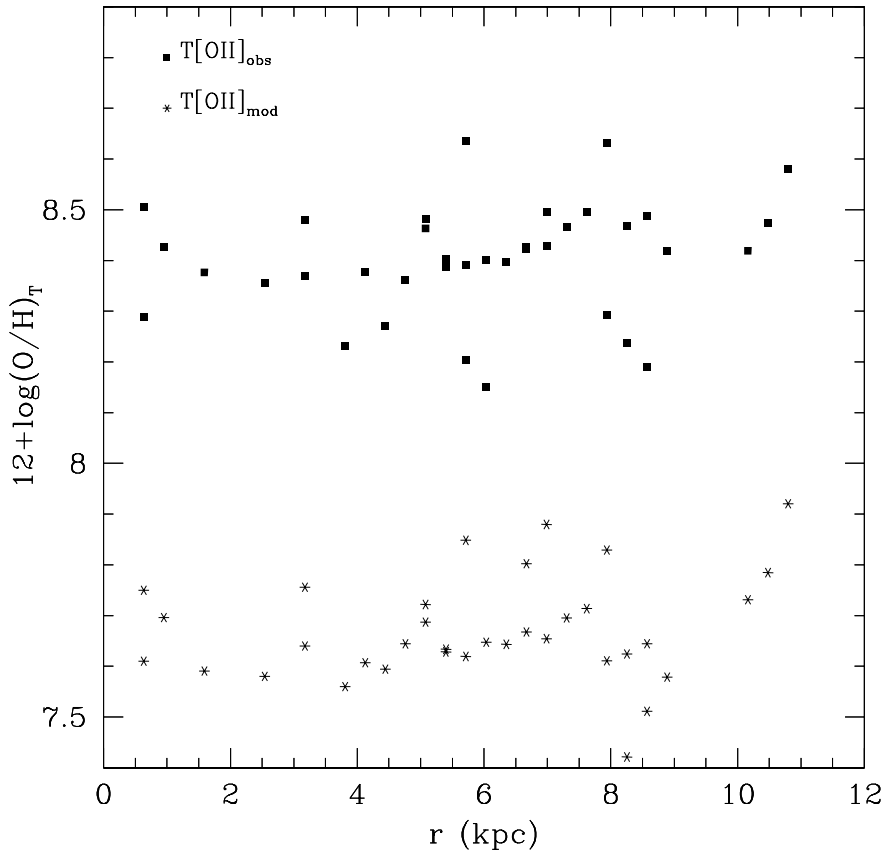

Figure 5.16: Oxygen abundance derived with direct method. Squares are the values derived by using the observed $T[OII]$ estimates; stars are those derived by using the $T[OII]$ from photoionization models. See Sec. 5.5 for details. The errors on oxygen abundance is 0.5.

- *Metallicity-Luminosity relation*

The mean values for the oxygen abundance along the polar disk, derived by the empirical (see Sec. 5.5) and direct methods (see Sec. 5.5), are compared with those for a sample of late-type disk galaxies by Kobulnicky & Zaritsky (1999), as function of the total luminosity (see Fig. 5.23). For all galaxies of the sample, and in particular for spiral galaxies, the total luminosity is that of the whole system, i.e. bulge plus disk, therefore also for NGC4650A we have accounted for the total luminosity of the galaxy ($M_B = -19.3$, evaluated by using the same value of H_0 used by Kobulnicky & Zaritsky (1999) in order to compare NGC4650A with galaxies in their sample), to which contributes both the central spheroid and the polar disk. We found that NGC4650A is located inside the spread of the data-points and contrary to its high luminosity it has metallicity lower than spiral galaxy disks of the same total luminosity. If we take into account the total luminosity of the polar disk alone ($M_B = -17$), NGC4650A falls in the region where HII and irregular galaxies are also found, characterized by lower luminosity and metallicities with respect to the spiral galaxies.

For what concerns the chemical abundances in PRGs, only few measurements are available in the literature. By using the direct method, very recently Pérez-Montero et al. (2009) have derived the chemical abundances of IIZw71, a blue compact dwarf galaxy also catalogued as a probable polar ring: consistently with its low luminosity, the metallicity of the brightest knots in the ring is lower with respect to that of NGC4650A. Through a similar study, Brosch et al. (2010) have derived the chemical abundances for the apparent ring galaxy SDSS J075234.33+292049.8, which has a more similar morphology to that observed in NGC4650A: the average value for the oxygen abundance along the polar structure is $12 + logO/H = 8.49 \pm 0.08$. As pointed out by authors, taking into account the ring brightness, such value is somewhat lower than that expected by the metallicity-luminosity relation. A spectroscopic study of the peculiar galaxy UGC5600, classified as probable PRG (Whitmore et al., 1990), by Shalyapina et al. (2002) reports a quasi-solar metallicity for such object, $12 + log(O/H) \sim 8.8 = 0.9 Z_{\odot}$, which is consistent with its high luminosity ($M_B = -19.4$), but it is larger with respect to the values of other PRGs given before.

- *Metallicity gradient along the polar disk*

The oxygen abundance in the polar disk of NGC4650A as a function of the radius derived by empirical and direct methods are shown in Fig. 6.6 and Fig. 5.16 respectively: both of them show that metallicity remains constant along the polar disk. This suggests that the star formation and metal enrichment in the polar structure of NGC4650A is not influenced by the stellar evolution of the older central spheroid, where the last burst of star formation occurred between 3 to 5 Gyrs ago (Iodice et al., 2002b): this turns also to be consistent with a later formation of the polar disk. The absence of any metallicity gradient is a typical behavior found in LSB galaxies (de Blok & van der Hulst, 1998), and also in the polar disk galaxy studied by Brosch et al. (2010), which has a very similar structure

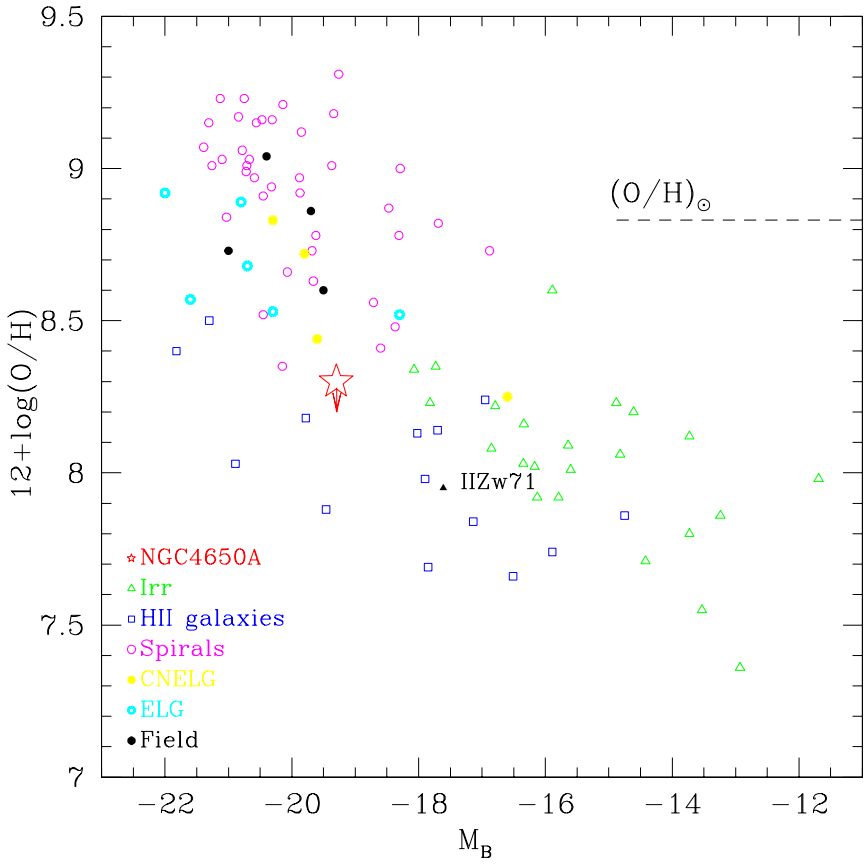

Figure 5.17: Oxygen abundance vs absolute blue magnitude for CNELGs (yellow filled circles), ELGs (cyan open circles), four field galaxies with emission lines (filled black circles), nearby dwarf irregulars (open triangles), local spiral galaxies (open circles), local HII galaxies (open squares), NGC4650A (star) and the polar disk galaxy IIZw71 (Pérez-Montero et al., 2009). The dashed line indicates the solar oxygen abundance. The arrow indicates the shift of the value of the oxygen abundance if we use the direct methods to evaluate it. The total B-band magnitude for NGC4650A ($M_B = -19.3$) has been evaluated by using the same value of H_0 used by Kobulnicky & Zaritsky (1999) in order to compare NGC4650A with galaxies in their sample

to NGC4650A. On the contrary, ordinary and oxygen-rich spiral galaxies show a decreasing abundance with increasing radii (see Fig. 6.6 and Pilyugin et al. 2006). These observed features in spiral disks are well explained by the infall models of galaxy formation which predict that they build up via accretion by growing inside-out (Matteucci & Francois 1989; Boissier & Prantzos 1999) and such process generates the observed gradients.

- *Star Formation Rate (SFR)*

We have derived the SFR for the polar disk, from the H_α luminosity using the expression given by Kennicutt (1998) $SFR(M_\odot/yr) = 7.9\times10^{-42}\times L(H_\alpha)(erg/s)$. We found that it is almost constant along the disk, within a large scatter of the datapoint. Therefore, given the average value of $L(H_\alpha) \simeq 3.8\times10^{39}$ erg/s we have obtained an average $SFR \sim 0.04M_\odot/yr$ and $SFR \sim 0.02M_\odot/yr$ for the North and South arms respectively. These values are quite similar to the total SFR derived for the HII regions of PRG IIZw71 (Pérez-Montero et al. 2009), which is $SFR \sim 0.035M_\odot/yr$. In order to make a comparison with SFR estimates for a sample of PRGs studied by Reshetnikov & Combes (1994), we have derived a mean value of the H_α flux by integrating within a rectangular aperture of $2.5'' \times 4.6''$ along each arm of the polar disk and we have obtained an average value of $SFR \sim 0.006M_\odot/yr/pc^2$. This value is consistent with the SFR of the HII regions in the PRGs studied by Reshetnikov & Combes (1994), where $0.001 \leq SFR \leq 0.31$. In particular, two PRGs of this sample, UGC7576 and UGC9796, where the polar structure is very similar to that of NGC4650A (i.e. exponential surface brightness profile, very blue colors, knotty appearance, prominent HII regions and a large amount of HI gas, all associated to this component and distributed as a disk in differential rotation; see Reshetnikov & Combes 1994 and Cox et al. 2006), have $SFR \sim 0.005M_\odot/yr/pc^2$. As already stressed by Reshetnikov & Combes (1994), the HII regions of the PRGs, including also NGC4650A, have SFR similar to late-type spiral galaxies (Kennicutt et al., 1987). In particular, by comparing the H_α luminosity versus the total B magnitude, the polar disk galaxies, NGC4650A, UGC7576 and UGC9796, are located in the same area where Sc-Irr galaxies are also found.

Taking into account that the polar disk is very young, since the last burst of star formation occurred less than 1 Gyr ago (Iodice et al., 2002b), we check if the present SFR of 0.06 $M_\odot/yr$, and even 2 and 3 times higher (i.e. $SFR = 0.12M_\odot/yr$ and $SFR = 0.18M_\odot/yr$), can give the estimated metallicity of $Z = 0.2Z_\odot$ and how strongly could increase the metallicity with time. We used a linearly declining SFR (Bruzual & Charlot, 2003a) $(t) = 2M_\star\tau^{-1}[1-(t/\tau)]$ (typically used for late-type galaxies), to estimate the expected stellar mass for the three different values of the SFR (0.06, 0.12 and 0.18 $M_\odot/yr$) and three epochs (0.8 Gyr, 1 Gyr and 2 Gyrs), obtaining stellar masses in the range $4\times10^9M_\odot \leq M_\star \leq 1\times10^{10}M_\odot$. The stellar mass ($M_\star \sim 4\times10^9M_\odot$) in the disk from NIR observations (Iodice et al., 2002b) falls within this range. Than, by using the mass-metallicity relation derived by Tremonti et al. (2004), where $12+log(O/H) = -1.492+1.847log(M_\star)-$

$0.08026(logM_\star)^2$, we found that $1.02Z_\odot \leq Z \leq 1.4Z_\odot$. This shows that the present SFR for the polar disk ($SFR = 0.06M_\odot yr^{-1}$) is able to increase the metallicity of about $0.2Z_\odot$ after 1Gyr. The derived values for Z are larger than $Z = (0.2 \pm 0.002)Z_\odot$, found by using the element abundances (see Sec.5.5): this differences could be attributed to the accretion of metal-poor gas, as discussed in detail in the following sections.

Theoretical predictions

How galaxies acquire their gas is an open issue in the models of galaxy formation and recent theoretical works have argued that cold accretion plays a major role. This idea is supported by many numerical simulations suggesting that this could be an important mechanism in the galaxy formation (Katz & White 1993; Katz et al. 1994; Kereš et al. 2005; Dekel & Birnboim 2006; Dekel & Birnboim 2008; Bournaud & Elmegreen 2009). Kereš et al. (2005) studied in detail the physics of the *cold mode* of gas accretion and one feature they found is that it is generally directed along filaments, allowing galaxies to draw gas from large distances.
Recently Ocvirk et al. (2008), using cosmological simulations, studied the metal enrichment of the intergalactic medium as a key ingredient in determining the transition mass from cold to hot dominated accretion. Their measurements turn to be consistent with the analytical prediction of Dekel & Birnboim (2006) in the low metallicity regime for the cold streams. The efficiency of radiative cooling decreases towards low metallicity, and at $Z/Z_\odot = 10^{-3}$ the cooling properties of the gas are those of a primordial mixture. Gas accretion is bimodal both in temperature and in metallicity: the cold accretion mode is associated with a combination of metal-poor filamentary accretion and dense metal-rich satellite galaxy disc surrounding, while the hot mode features has strong chemical heterogeneity and a radius-dependent metallicity.

More recent simulations of disk formation in a cosmological context performed by Agertz et al. (2009) revealed that the so called chain-galaxies and clump-clusters, found only at higher redshifts (Elmegreen et al., 2007), are a natural outcome of early epoch enhanced gas accretion from cold dense streams as well as tidally and ram-pressured stripped material from minor mergers and satellites. This freshly accreted cold gas settles into a large disk-like systems; simulations show that the interaction region between the new-formed disk and the cold streams can also result not aligned with the initial galactic disk: based on a very poor statistics, Agertz et al. (2009) suggest that this misalignment might not be typical, and it is due to a third cold stream that is perpendicular to the main filament. A more recent analysis by Dekel et al. (2009a) shows that the accretion of gas along misaligned filaments with respect to the disk plane are more common and it leaves traces down to low redshift. An almost polar filament can result just as an extreme case of such process and, as suggested by Agertz et al. (2009), it could be responsible for the formation of polar disks.

This scenario not only reproduces the observed morphology and global rotation of disks, but also finds a realistic metallicity gradient and SFR of $20 M_{\odot}/yr$. Agertz et al. (2009) found solar metallicity for the inner disk, while that in the clump forming region is only $\sim 1/10 Z_{\odot}$ due to the accretion of pristine gas in the cold streams mixing with stripped satellite gas. Therefore, the studies cited above suggest that the chemical abundance is one of the key parameters that can be estimated in a galaxy disk and directly compared with the theoretical predictions. This is the main goal of the present work: we studied the chemical abundances in the polar disk of NGC4650A in order to check the cold accretion scenario for this object.

Hydrodynamical simulations performed by Macciò et al. (2006) and Brook et al. (2008b) have shown that the formation of a polar disk galaxy can occur naturally in a hierarchical universe, where most low-mass galaxies are assembled through the accretion of cold gas infalling along a filamentary structures. According to Macciò et al. (2006), the polar disk forms from cold gas that flows along the extended $\sim 1 Mpc$ filament into the virialized dark matter halo. The gas streams into the center of the halo on an orbit that is offset from radial infall. As it reaches the center, it impacts with gas in the halo of the host galaxy and with the warm gas flowing along the opposite filament. Only the gas accreted perpendicular to the major axis of the potential can survive for more than a few dynamical lifetimes. Brook et al. (2008b) argued that polar disk galaxies are extreme examples of the misalignment of angular momentum that occurs during the hierarchical structure formation: an inner disk starts forming shortly after the last major merger at $z \sim 2$. Due to its gas rich nature, the galaxy rapidly forms a new disk whose angular momentum is determined by the merger orbital parameters. Later, gas continues to be accreted but in a plane that is almost perpendicular to the inner disk. At $z \sim 0.8$ the central galaxy is still forming stars in a disk, while the bulk of new star formation is in the highly inclined polar disk. By $z \sim 0.5$ the inner disk has exhausted its gas, while gas continues to fall onto the polar disk. From this point, star formation occurs exclusively in the polar disk, that remains stable for at least 3 Gyrs.
The formation mechanisms described above can self-consistently explain both morphology and kinematics of a polar disk galaxy and, in particular, all the observed features (like colors and color gradients, longevity, spiral arms, HI content and distribution) of the polar structure.

Summary and conclusions

The present study could be considered a step forward both to trace the formation history of NGC4650A and to give hints on the mechanisms at work during the building of a disk by cold accretion process.

As mentioned in the Sec.5.6, the new kinematic data obtained for the central spheroid (Iodice et al., 2006), together with the previous studies, set important

constraints on the possible formation mechanisms for NGC4650A. In particular, the merging scenario is ruled out because, according to simulations (e.g. Bournaud et al. 2005b), a high mass ratio of the two merging galaxies is required to form a massive and extended polar disk as observed in NGC 4650A: this would convert the intruder into an elliptical-like, not rotationally supported, stellar system. This is in contrast with the high maximum rotation velocity ($\sim 80 \div 100$ km/s) observed in the outer regions of the central spheroid (Iodice et al., 2006).

Both the high baryonic mass (star plus gas) in the polar structure and its large extension cannot reconcile with a polar ring formed via the gradual disruption of a dwarf satellite galaxy (as explained by Iodice et al. 2002b). Differently, a wide polar ring and/or disk (as observed in NGC4650A) may form both around a disk or an elliptical galaxy through the tidal accretion of gas stripped from a gas-rich donor, in the case of large relative velocity and large impact parameter and for a particular orbital configuration (e.g. Bournaud & Combes 2003b). Therefore, the two formation scenarios which can be really envisioned in the specific case of NGC4650A are the tidal accretion and the accretion of external primordial cold gas from cosmic web filaments (Macciò et al. 2006; Brook et al. 2008b). To this aim we have derived the metallicity and SFR for the polar disk in NGC4650A in order to compare them with those predicted by different formation scenarios.

The main results of the present work are (see also Sec. 6.25): *i*) the low value of the metallicity derived for the polar disk $Z = 0.2Z_{\odot}$, in spite of its high luminosity, $M_B = -19.3$ (see Fig. 5.23), *ii*) the lack of any metallicity gradient along the polar disk, which suggests that the metal enrichment is not influenced by the stellar evolution of the older central spheroid, *iii*) the metallicities expected for the present SFR at three different epochs, $1.02Z_{\odot} \leq Z \leq 1.4Z_{\odot}$, are higher than those measured from the element abundances and this is consistent with a later infall of metal-poor gas.

In the following we will address how these results reconcile with the predictions by theoretical models (see Sec. 5.5) and may discriminate between the two formation mechanisms.

If the polar ring/disk formed by the mass transfer from a gas-rich donor galaxy, the accreted material comes only from the outer and more metal-poor regions of the donor: is the observed metallicity for the polar component in NGC4650A consistent with the typical values for the outer disk of a bright spiral galaxy? According to Bresolin et al. (2009), the metallicity of very outer regions of a bright spiral is $0.2Z_{\odot} \leq Z \leq 1.1Z_{\odot}$: the observed value for NGC4650A, $Z = 0.2Z_{\odot}$, is close to the lower limit.

The cold accretion mechanism for disk formation predicts quite low metallicity ($Z = 0.1Z_{\odot}$) (Dekel & Birnboim 2006, Ocvirk et al. 2008, Agertz et al. 2009): such value refers to the time just after the accretion of a misaligned material, so it can be considered as initial value for Z before the subsequent enrichment.

How this may reconcile with the observed metallicity for NGC4650A?

We estimated that the present SFR for the polar disk ($SFR = 0.06 M_{\odot} yr^{-1}$)

is able to increase the metallicity of about 0.2 after 1Gyr (see Sec.6.25): taking into account that the polar structure is very young, less than 1Gyr (Iodice et al., 2002b), an initial value of $Z = 0.1Z_{\odot}$, at the time of polar disk formation, could be consistent with the today's observed metallicity.
This evidence may put some constraints also on the time-scales of the accretion process. The issue that need to be addressed is: how could a cosmic flow form a ring/disk only in the last Gyr, without forming it before? Given that the average age of 0.8 Gyr refers to the last burst of star formation, reasonably the gas accretion along the polar direction could have started much earlier and stars formed only recently, once enough gas mass has been accumulated in the polar disk. Earlier-on, two possible mechanisms may be proposed. One process that may happen is something similar to that suggested by Martig et al. (2009) for the quenching of star formation in early-type galaxies: given that star formation takes place in gravitationally unstable gas disks, the polar structure could have been stable for a while and this could have quenched its star formation activity, until the accumulated mass gas exceeds a stability threshold and star formation resumes.

Alternatively, according to the simulations by Brook et al. (2008b), the filament could have been there for several Gyrs with a relative low inclination, providing gas fuel to the star formation in the host galaxy first, about 3 Gyrs ago. Then large-scale tidal fields can let the disk/filament misalignment increase over the time till 80-90 degrees and start forming the polar structure during the last 1-2 Gyrs. This picture might be consistent not only with the relative young age of the polar disk, but also with the estimate of the last burst of star formation in the central spheroid (Iodice et al., 2002b).

One more hint for the cold accretion scenario comes from the fact that the metallicity expected by the present SFR turns to be higher than those directly measured by the chemical abundances. As suggested by Dalcanton (2007), both infall and outflow of gas can change a galaxy's metallicity: in the case of NGC4650A a possible explanations for this difference could be the infall of pristine gas, as suggested by (Finlator et al. 2007; Ellison et al. 2008).

The lack of abundance gradient in the polar disk, as typically observed also in LSB galaxies, suggests that the picture of a chemical evolution from inside-out, that well reproduce the observed features in spiral disks (Matteucci & Francois 1989, Boissier & Prantzos 1999), cannot be applied to these systems. In particular, observations for LSB galaxies are consistent with a quiescent and sporadic chemical evolution, but several explanation exist that supports such evidence (de Blok & van der Hulst, 1998). Among them, one suggestion is that the disk is still settling in its final configuration and the star formation is triggered by external infall of gas from larger radii: during this process, gas is slowly diffusing inward, causing star formation where conditions are favorable. As a consequence, the star formation is not self-propagating and the building-up of the disk would not give rise to an abundance gradient. The similarities between LSB galaxies and the polar disk in NGC4650A, including colors (Iodice et al., 2002c) and chemical abundances

(this work), together with the very young age of the polar disk, the presence of star forming regions towards larger radii, the warping structure of outer arms (Gallagher et al. 2002, Iodice et al. 2002c), and the constant SFR along the disk (this work), suggest that the infall of metal-poor gas, through a similar process described above, may reasonably fit all these observational evidences.

Given that, are there any other observational aspects that can help to disentangle in a non ambiguous way the two scenarios?

One important feature which characterize NGC4650A is the high baryonic (gas plus stars) mass in the polar structure: it is about $12 \times 10^9 M_\odot$, which is comparable with or even higher than the total luminous mass in the central spheroid (of about $5 \times 10^9 M_\odot$). In the accretion scenario, the total amount of accreted gas by the early-type object is about 10% of the gas in the disk donor galaxy, i.e. up to 10^9 $M_\odot$, so one would expect the accreted baryonic mass (stellar + gas) to be a fraction of that in the pre-existing galaxy, and not viceversa, as it is observed for NGC4650A. Furthermore, looking at the field around NGC4650A, the close luminous spiral NGC4650 may be considered as possible donor galaxy (Bournaud & Combes, 2003b), however the available observations on the HI content for this object show that NGC4650 is expected to be gas-poor (Arnaboldi et al. 1997; van Driel et al. 2002b). So, where the high quantity of HI gas in NGC4650A may come from? If the polar disk forms by the cold accretion of gas from filaments there is no limit to the accreted mass.

Given all the evidences shown above, we can infer that the cold accretion of gas by cosmic web filaments could well account for both the low metallicity, the lack of gradient and the high HI content in NGC4650A. An independent evidence which seems to support such scenario for the formation of polar disks comes from the discovery and study of an isolated polar disk galaxy, located in a wall between two voids (Stanonik et al., 2009): the large HI mass (at least comparable to the stellar mass of the central galaxy) and the general underdensity of the environment can be consistent with the cold flow accretion of gas as possible formation mechanism for this object.

The present work remarks how the use of the chemical analysis can give strong constraints on the galaxy formation, in particular, it has revealed an independent check of the cold accretion scenario for the formation of polar disk galaxies. This study also confirmed that this class of object needs to be treated differently from the polar ring galaxies, where the polar structure is more metal rich (like UGC5600, see Sec. 6.25) and a tidal accretion or a major merging process can reliable explain the observed properties (Bournaud & Combes, 2003b). Finally, given the similarities between polar disks and late-type disk galaxies, except for the different plane with respect to the central spheroid, the two classes of systems could share similar formation processes. Therefore, the study of polar disk galaxies assumes an important role in the wide framework of disk formation and evolution, in particular, for what concern the "rebuilding" of disks through accretion of gas from cosmic filaments, as predicted by hierarchical models of galaxy formation

(Steinmetz & Navarro, 2002).

Table 5.1: Observed and de-reddened emission lines fluxes relative to H_β in the $3300 - 6210$ Å wavelength range.

r (arcsec)[a]	$\frac{OII[3727]}{H_\beta}$		$\frac{H_\gamma[4340]}{H_\beta}$		$\frac{OIII[4363]}{H_\beta}$		$\frac{OIII[4959]}{H_\beta}$		$\frac{OIII[5007]}{H_\beta}$	
slit 1	F_{obs} ±0.05	F_{int} ±0.06	F_{obs} ±0.013	F_{int} ±0.015	F_{obs} ±0.004	F_{int} ±0.005	F_{obs} ±0.02	F_{int} ±0.02	F_{obs} ±0.03	F_{int} ±0.03
-44.1	5.95	7.76	...	...	0.058	0.066	0.52	0.51	1.83	1.77
-42.34	4.32	5.64	...	...	0.201	0.227	0.52	0.51	1.83	1.77
-40.57	4.01	5.22	0.392	0.445	0.182	0.205	0.58	0.57	1.97	1.91
-38.81	3.69	4.81	...	...	0.094	0.107	0.57	0.56	1.67	1.61
-37.04	3.61	4.71	0.438	0.497	0.096	0.109	0.80	0.78	1.91	1.85
-35.28	3.39	4.42	0.398	0.451	0.095	0.108	0.80	0.78	1.82	1.76
-33.52	3.42	4.45	0.329	0.373	0.064	0.073	0.79	0.78	1.87	1.81
-31.75	3.38	4.41	0.377	0.428	0.043	0.048	0.51	0.50	1.60	1.55
-29.99	3.47	4.52	0.423	0.480	0.038	0.043	0.54	0.52	1.58	1.53
-28.22	3.99	5.21	0.464	0.526	0.188	0.212	0.60	0.59	1.76	1.71
-17.64	4.06	5.29	0.400	0.454	0.105	0.119	1.05	1.03	3.11	3.01
-14.11	3.12	4.06	0.376	0.427	...	...	0.50	0.50	1.36	1.31
-3.528	4.35	5.67	...	...	...	...	0.81	0.80	2.51	2.43
26.46	...	...	0.348	0.395	...	...	...	...	...	...
28.22	...	...	0.540	0.613	...	...	...	...	...	...
37.04	3.39	4.42	...	...	...	...	1.79	1.75	5.33	5.16
38.81	3.94	5.13	...	...	...	...	1.92	1.88	6.85	6.63
45.86	2.41	3.14	...	...	...	...	0.24	0.24	0.51	0.49
47.63	4.33	5.64	...	...	0.030	0.034	0.21	0.20	0.37	0.36
49.39	3.70	4.82	...	...	...	...	0.20	0.20	0.33	0.32
slit 2										
-49.49	...	...	0.598	0.678	...	...	...	...	...	...
-33.52	1.97	2.57	0.555	0.630	...	...	0.19	0.19	0.43	0.42
-31.75	2.24	2.91	...	...	...	...	0.17	0.17	0.54	0.53
-3.528	2.54	3.31	...	...	...	...	0.88	0.86	2.89	2.80
5.292	3.59	4.69	0.233	0.264	...	...	0.80	0.78	2.69	2.60
8.82	3.28	4.28	...	...	...	...	0.43	0.42	1.27	1.23
17.64	3.15	4.11	0.594	0.674	...	...	0.92	0.90	2.15	2.08
21.17	2.22	2.90	...	...	...	...	0.88	0.86	2.56	2.48
22.93	3.27	4.26	0.386	0.438	...	...	0.51	0.50	1.58	1.53
24.7	2.44	3.19	0.387	0.439	...	...	0.93	0.91	2.71	2.62
26.46	3.08	4.01	0.442	0.501	...	...	0.83	0.82	2.51	2.43
28.22	4.13	5.38	0.444	0.504	...	...	0.75	0.73	2.27	2.19
29.99	3.32	4.33	0.472	0.535	...	...	0.64	0.62	1.91	1.85
31.75	5.96	7.77	0.423	0.480	...	...	0.83	0.81	2.22	2.15
33.51	...	...	0.540	0.613	...	...	...	...	...	...
44.1	2.57	3.35	...	...	...	...	0.88	0.86	2.84	2.75
45.86	4.14	5.40	0.427	0.484	0.129	0.146	0.09	0.09	0.43	0.42
47.63	2.02	2.64	...	...	0.537	0.606	0.73	0.71	2.27	2.19
49.39	...	...	0.384	0.436	...	...	...	...	...	...
56.45	3.46	4.51	...	...	...	...	1.04	1.02	3.72	3.60
58.21	3.93	5.13	...	...	0.162	0.183	1.15	1.13	4.18	4.05
59.98	4.92	6.41	...	...	...	...	1.68	1.65	6.63	6.42

[a]The negative values are for the northern regions of the spectra

Table 5.2: Observed and de-reddened emission lines fluxes relative to H_β in the $5600 - 11000$Å wavelength range

r (arcsec)[a]	$\frac{H_\alpha}{H_\beta}$[b]		$\frac{SII[6717]}{H_\beta}$		$\frac{SII[6731]}{H_\beta}$		$\frac{SIII[9069]}{H_\beta}$		$\frac{SIII[9532]}{H_\beta}$	
slit 1	F_{obs} ±0.02	F_{int} ±0.03	F_{obs} ±0.015	F_{int} ±0.011	F_{obs} ±0.016	F_{int} ±0.012	F_{obs} ±0.08	F_{int} ±0.06	F_{obs} ±0.15	F_{int} ±0.11
-38.81	...	...	...	...	...	...	...	...	0.05	0.03
-37.04	5.46	4.25	...	...	...	...	...	...	...	...
-35.28	3.85	2.99	...	...	...	...	...	...	0.017	0.010
-33.52	2.44	1.896	...	...	...	...	...	...	0.04	0.03
-31.75	0.930	0.724	...	...	...	...	...	...	...	...
-29.99	0.412	0.321	...	...	...	...	...	...	...	...
-26.46	...	...	...	...	...	...	...	...	0.05	0.03
-17.64	...	...	...	...	...	...	...	...	0.03	0.019
-15.88	...	...	...	...	...	...	...	...	0.06	0.03
-10.58	...	...	0.199	0.153	0.632	0.483	...	...	...	...
-8.82	...	...	0.426	0.329	0.577	0.441	0.052	0.0320	...	...
-7.06	...	...	0.84	0.646	0.935	0.714	0.0293	0.0178	...	...
-5.29	...	...	...	...	...	...	0.041	0.0252	...	...
-3.53	...	...	...	...	...	...	0.68	0.41	...	...
-1.76	...	...	...	...	...	...	0.266	0.162	...	...
0.0	...	...	1.39	1.07	1.31	1.00	...	...	...	...
1.76	...	...	1.48	1.14	0.609	0.465	0.33	0.202	...	...
3.53	...	...	0.686	0.529	0.460	0.351	...	...	...	...
5.29	...	...	0.136	0.105	0.422	0.322	...	...	...	...
7.06	...	...	0.0142	0.0109	0.377	0.288	0.041	0.0249	0.023	0.014
29.99	...	...	...	...	...	...	...	...	0.014	0.008
31.75	...	...	...	...	...	...	...	...	0.022	0.013
40.57	...	...	0.0340	0.0262	0.174	0.133	...	...	...	...
51.16	...	...	0.465	0.358	0.280	0.214	0.33	0.202	1.0	0.6
slit 2										
-45.86	...	...	...	...	...	...	...	...	0.11	0.06
-38.81	1.59	1.24	...	...	...	...	...	...	...	...
-37.04	5.48	4.26	...	...	...	...	...	...	...	...
-33.52	...	...	...	...	...	...	...	...	0.13	0.08
-22.93	0.874	0.680	...	...	...	...	...	...	...	...
-17.64	...	...	...	...	...	...	0.240	...	...	
-5.29	...	...	0.0536	0.0413	0.271	0.207	...	...	0.22	0.1319
-3.53	...	...	0.090	0.070	0.0551	0.0421	...	...	...	...
-1.76	...	...	0.962	0.741	0.0023	0.00177	...	...	0.17	0.10
0.0	...	...	0.0691	0.0533	0.113	0.087	...	...	...	...
1.76	...	...	...	...	...	...	...	...	0.13	0.08
3.53	...	...	...	...	...	...	0.55	0.33	0.3	0.17
5.29	...	...	...	...	...	...	0.36	0.218	...	...
8.82	...	...	0.583	0.449	0.87	0.658	1.59	0.97	2	1.3
10.58	...	...	...	...	...	...	0.67	0.41	0.3	0.20
19.4	...	...	...	...	...	...	...	...	0.18	0.10
21.17	...	...	...	...	...	...	0.54	0.33	...	...
24.7	1.63	1.26	0.159	0.123	1.15	0.88	...	...	0.18	0.11
26.46	0.290	0.226	...	...	...	...	...	...	...	...
28.22	0.0620	0.0482	...	...	...	...	...	...	0.15	0.09
29.99	0.0938	0.0730	...	...	...	...	0.51	0.311	...	...
31.75	3.82	2.97	0.118	0.091	0.291	0.222	...	...	0.09	0.05
33.52	5.47	4.25	0.204	0.157	0.216	0.165	...	...	0.23	0.13
35.28	...	...	0.096	0.074	0.237	0.181	...	...	...	...
38.81	...	...	...	...	...	...	0.43	0.259	...	...
42.34	...	...	...	...	...	...	...	...	...	...
56.45	...	...	0.091	0.070	0.230	0.175	...	...	...	...
58.21	...	...	...	...	...	...	...	...	0.22	0.13
59.98	...	...	0.077	0.0587	0.134	0.102	0.37	0.226	...	...

[a]The negative values are for the northern regions of the spectra
[b]H_α flux is corrected for corresponding [NII]λ6548 flux

Table 5.3: Oxygen and Sulphur abundance parameters and oxygen abundances for the polar disk in NGC4650A

r (arcsec)	R_{23} ($\pm$0.05)	$12 + log(O/H)_P$ ($\pm$0.2)
Slit 1		
-44.1	10.05	7.8
-42.34	7.91	8.0
-40.57	7.70	8.1
-38.81	6.98	8.1
-37.04	7.35	8.1
-35.28	6.97	8.2
-33.52	7.04	8.2
-31.75	6.45	8.2
-29.99	6.57	8.2
-28.22	7.50	8.1
-17.64	9.33	8.0
-14.11	5.87	8.2
-3.528	8.90	8.0
37.04	11.33	8.0
38.81	13.64	7.8
45.86	3.86	8.4
47.63	6.20	8.0
49.39	5.34	8.1
Slit 2		
-33.52	3.18	8.5
-31.75	3.61	8.4
-3.528	6.97	8.3
5.292	8.08	8.1
8.82	5.93	8.2
17.64	7.10	8.2
21.17	6.24	8.4
22.93	6.28	8.2
24.7	6.73	8.3
26.46	7.26	8.2
28.22	8.30	8.0
29.99	6.81	8.2
31.75	10.74	7.7
44.1	6.96	8.3
45.86	5.91	8.1
47.63	5.55	8.4
56.45	9.13	8.1
58.21	10.30	8.0
59.98	14.48	7.7

5.6 Chemical abundances of the PRGs UGC7576 and UGC9796: testing the formation scenario

Authors: Marilena Spavone, Enrichetta Iodice, Magda Arnaboldi, Giuseppe Longo and Ortwin Gerhard

Submitted to Astronomy & Astrophysics

Abstract

The study of the chemical abundances in the polar disk galaxy NGC4650A (Spavone et al., 2010) has been a step forward both in tracing the formation history of the galaxy and giving hints on the mechanisms at work during the building of disk by cold accretion process. It's now important to establish whether such results are typical for the class of polar disk galaxies as whole.

The present work aim to check the cold accretion of gas through a "cosmic filament" (Macciò et al., 2006) as a possible scenario for the formation of the polar structures in UGC7576 and UGC9796. If these form by cold accretion, we expect the HII regions abundances and metallicities to be lower than those of same-luminosity spiral disks, with values of $Z \sim 1/10\ Z_{\odot}$, as predicted by cosmological simulations (Agertz et al., 2009).

We have used deep long-slit spectra, obtained with DOLORES@TNG in the optical wavelengths, of the brightest HII regions associated with the polar structures to derive their chemical abundances and SFR. We used the *Empirical methods*, based on the intensities of easily observable lines, to derive the oxygen abundance $12 + log(O/H)$ of both galaxies. Such values are compared with those typical for different morphological galaxy types of comparable luminosity.

The average metallicity values for UGC7576 and UGC9796 are $Z = 0.4Z_{\odot}$ and $Z = 0.1Z_{\odot}$ respectively. Both values are lower than those measured for ordinary spirals of similar luminosity and UGC7576 presents no metallicity gradient along the polar structure. These data, toghether with other observed features, available for the two PRGs by previous works, have been compared with the predictions of simulations of both tidal accretion, cold accretion and merging, to disentangle between these scenarios.

Table 5.4: Oxygen abundances for the polar disk in NGC4650A derived by the T_e method

r (arcsec)	$12 + log(O/H)_{T_{mod}}$	$12 + log(O/H)_{T_{obs}}(\pm 0.1)$
Slit 1		
-44.10	7.83 ± 0.58	8.6
-42.34	7.71 ± 0.52	8.5
-40.57	7.69 ± 0.49	8.5
-38.81	7.65 ± 0.50	8.4
-37.04	7.67 ± 0.46	8.4
-35.28	7.64 ± 0.46	8.4
-33.52	7.65 ± 0.45	8.4
-31.75	7.62 ± 0.49	8.4
-29.99	7.63 ± 0.49	8.4
-28.22	7.69 ± 0.50	8.5
-17.64	7.76 ± 0.42	8.5
-14.11	7.58 ± 0.49	8.4
-3.53	7.75 ± 0.46	8.5
37.04	7.80 ± 0.33	8.4
38.81	7.88 ± 0.33	8.5
45.86	7.42 ± 0.58	8.2
47.63	7.64 ± 0.68	8.5
49.39	7.58 ± 0.67	8.4
Slit 2		
-33.52	7.34 ± 0.57	8.1
-31.75	7.39 ± 0.57	8.2
-3.53	7.61 ± 0.36	8.3
5.29	7.70 ± 0.42	8.4
8.82	7.59 ± 0.52	8.4
17.64	7.64 ± 0.42	8.4
21.17	7.56 ± 0.35	8.2
22.93	7.61 ± 0.48	8.4
24.70	7.59 ± 0.36	8.3
26.46	7.64 ± 0.40	8.4
28.22	7.72 ± 0.47	8.5
29.99	7.63 ± 0.46	8.4
31.75	7.85 ± 0.54	8.6
44.10	7.61 ± 0.36	8.3
45.86	7.62 ± 0.68	8.5
47.63	7.51 ± 0.35	8.2
56.45	7.73 ± 0.37	8.4
58.21	7.78 ± 0.38	8.5
59.98	7.92 ± 0.36	8.6

Introduction

How galaxies acquire their gas is an open issue in the models of galaxy formation: recent theoretical works, supported by many numerical simulations, have argued that cold accretion plays a major role (Katz & White 1993; Katz et al. 1994; Kereš et al. 2005; Dekel & Birnboim 2006; Dekel & Birnboim 2008; Bournaud & Elmegreen 2009).
Kereš et al. 2005 studied in detail the physics of the *cold mode* of gas accretion and they found that it is generally directed along filaments, allowing galaxies to draw gas from large distances. In particular, the cold accretion is a key mechanism to provide gas to disk galaxies (Brosch et al., 2010).

Recent simulations of disk formation in a cosmological context performed by Agertz et al. (2009) revealed that the so called chain-galaxies and clump-clusters, found only at higher redshifts (Elmegreen et al., 2007), are a natural outcome of early epoch enhanced gas accretion from cold dense streams as well as tidally and ram-pressured stripped material from minor mergers and satellites. This freshly accreted cold gas settles into a large disk-like systems. This scenario not only reproduce the observed morphology and global rotation of disks, but also find a realistic metallicity gradient and SFR of $20 M_{\odot}/yr$. Agertz et al. (2009) found solar metallicity for the inner disk, while that in the clump forming region is only $\sim 1/10 Z_{\odot}$ due to the accretion of pristine gas in the cold streams mixed with stripped satellite gas.

Simulations also show that the interaction region between the new-formed disk and the cold streams can also result not aligned with the initial galactic disk: based on a very poor statistics, Agertz et al. (2009) suggest that this misalignment might not be typical, and it is due to a third cold stream that is perpendicular to the main filament. More recent analysis show that the accretion of gas along misaligned filaments with respect to the disk plane are more common and it leaves traces down to low redshift (Dekel et al. 2009a; Roškar et al. 2010). An almost polar filament can result just as an extreme case of such process and, as suggested by Agertz et al. (2009), it could be responsible for the formation of polar disks.

Hydrodynamical simulations performed by Macciò et al. (2006) and Brook et al. (2008b) have shown that the formation of a polar disk galaxy can occur naturally in a hierarchical universe, where most low-mass galaxies are assembled through the accretion of cold gas infalling along a filamentary structures. According to Macciò et al. (2006), the polar disk forms from cold gas that flows along the extended $\sim 1 Mpc$ filament into the virialized dark matter halo. The gas streams into the center of the halo on an orbit that is offset from radial infall. As it reaches the center, it impacts with gas in the halo of the host galaxy and with the warm gas flowing along the

opposite filament. Only the gas accreted perpendicular to the major axis of the potential can survive for more than a few dynamical lifetimes.

Brook et al. (2008b) argued that polar disk galaxies are extreme examples of the misalignment of angular momentum that occurs during the hierarchical structure formation: an inner disk starts forming shortly after the last major merger at $z \sim 2$. Due to its gas rich nature, the galaxy rapidly forms a new disk whose angular momentum is determined by the merger orbital parameters. Later, gas continues to be accreted but in a plane that is almost perpendicular to the inner disk. At $z \sim 0.8$ the central galaxy is still forming stars in a disk, while the bulk of new star formation is in the highly inclined polar disk. By $z \sim 0.5$ the inner disk has exhausted its gas, while gas continues to fall onto the polar disk. From this point, star formation occurs exclusively in the polar disk, that remains stable for at least 3 Gyrs. The formation mechanisms described above can selfconsistently explain both morphology and kinematics of a polar disk galaxy. In particular, the predictions turn also to be consistent with many features (like colors and color gradients, longevity, spiral arms, HI content and distribution) observed for the polar disk galaxy NGC4650A.

This has been the best investigated object in the class of polar ring galaxies (PRGs) (Arnaboldi et al. 1997; Gallagher et al. 2002; Iodice et al. 2002a; Swaters & Rubin 2003; Bournaud & Combes 2003b; Iodice et al. 2006) in order to constrain many of the processes at work during galaxy interactions and merging. Very recently, Spavone et al. (2010), by using deep longslit spectroscopy with FORS2@ESO-VLT, have studied the abundance ratios and metallicities of the HII regions associated to the polar disk in NGC4650A, in order to test the cold accretion scenario for this object. The chemical abundance is one of the key parameters that can be estimated in a galaxy disk and directly compared with the theoretical predictions: infact, if the gas is essentially primordial it should have a very low abundance of heavy elements.

Main results obtained for NGC4650A show i) that it has metallicity lower than spiral galaxy disks of the same total luminosity, where $Z = 0.2Z_{\odot}$, which is consistent with values predicted for the formation of disks by cold accretion processes (Agertz et al., 2009); ii) the absence of any metallicity gradient along the polar disk, which suggests that the metal enrichment is not influenced by the stellar evolution of the older central spheroid and, thus, the disk was formed later by the infall of metal-poor gas from outside which is still forming the disk. The latter is also a characteristic found in LSB galaxies (de Blok & van der Hulst, 1998) and in some other PRGs (**?**). Such study has revealed an indirect and well-based check for the cold accretion scenario of disk formation: we would like to perform the same kind

of analysis on the two PRGs UGC7576 and UGC9796. The structure of these two objects is very similar to that of NGC4650A, which may suggest a similar formation mechanism: the polar structure is more extended with respect to the central spheroid, thus, as NGC4650A, they were classified as wide PRG (Whitmore et al., 1990); it is characterized by and exponential surface brightness profile, very blue colors, knotty appearance and a large amount of HI gas all associated to this component. The most relevant feature in UGC9796 is that the HI distribution resemble that of a disk in differential rotation, rather than a ring (Reshetnikov et al. 1994; Cox et al. 2006), like in NGC4650A (Arnaboldi et al., 1997). Given the new results obtained for NGC4650A it is now important to establish whether: the lack of Z gradient and low Z, and the inferred accretion of low-Z material after the formation of the central spheroid, are typical for the class of wide PRGs as a whole: to this aim we have studied the PRGs UGC7576 and UGC9796.

UGC7576

UGC7576 (Fig. 5.18) is a kinematically confirmed Polar Ring Galaxy (Whitmore et al., 1990) and its main properties are listed in Tab. 5.5. This object is at a distance of about 94 Mpc, based on $H_0 = 75\ km\ s^{-1}\ Mpc^{-1}$ and heliocentric radial velocity of $V = 7022\ km\ s^{-1}$, which implies that 1 arcsec = 0.45 kpc. The kinematic shows that the polar structure of UGC7576 is more similar to a ring rather than a disk, contrary to those of NGC4650A and UGC9796. Reshetnikov et al. (1994) studied the global morphology of UGC7576 and they were able to distinguish three components: *i*) the main central body with elliptical isophotes, *ii*) a narrow polar ring crossing the central region of the main galaxy, *iii*) a faint outer envelope. The gradient of the surface brightness distribution of the central galaxy decrease at $r \geq 20''$, while both B-V and V-R color indices slightly decrease with radius.

The distribution of color indices is sligthly asymmetric, suggesting that the polar ring is projected not exactly on the nucleus but with a small NW displacement. The color asymmetry correlates with the asymmetry in the hydrogen distribution (Schechter et al., 1984). Moreover, the plane of the disk reveals a warping, which suggests that the ring has not settled yet in the equilibrium plane.

Surface brightness distribution along the major axis of the ring is very symmetric and the surface brightness is approximately constant ($\mu_B \sim 24.3$) up to $r \sim 35''$, then falls abruptly. Also the colors have no evident changes within the region of constant brightness.

UGC7576 is also embedded in a faint outer envelope, whose major axis position angle coincides with the position angle of the polar ring and this

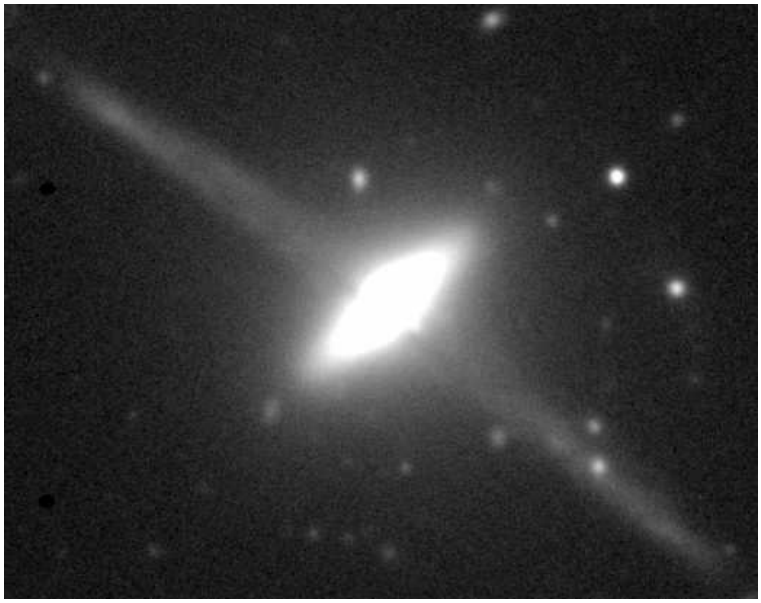

Figure 5.18: R-band image of the Polar Ring Galaxy UGC7576

suggests a common origin for both components (Reshetnikov et al., 1994).

Reshetnikov & Combes (1994) studied the kinematics of UGC7576: their H_α rotation curve turns to be consistent with the HI rotation curve obtained by Schechter et al. (1984). Both curves are straight lines with the same gradient, probably because the ring is an edge-on narrow annulus. This characteristic, together with the great amount of neutral hydrogen associated to the polar ring, found by Mould et al. (1982), indicates a large mass-to-light ratio.

UGC9796

UGC9796 (Fig. 5.19), also known as IIZw 73, is at a distance of about 72 Mpc based on $H_0 = 75\ km\ s^{-1}\ Mpc^{-1}$ and heliocentric radial velocity of $V = 5406\ km\ s^{-1}$, which implies that 1 arcsec = 0.35 kpc. It has one of the most non-polar PRG. Its apparent major axis infact is only 65° from the major axis of the central S0 rotationally supported galaxy and this implies a rapid rate of differential precession. The polar structure is less symmetric than in UGC7576 and the distribution of the colors is also asymmetric, with the NE side considerably redder than the SW side. The color asymmetry coincides with the asymmetry of the HI. The HI gas is all associated to the polar structure, which thus contains as many baryons as the host galaxy (Schechter et al., 1984), and shows a central hole at about 25″. The huge

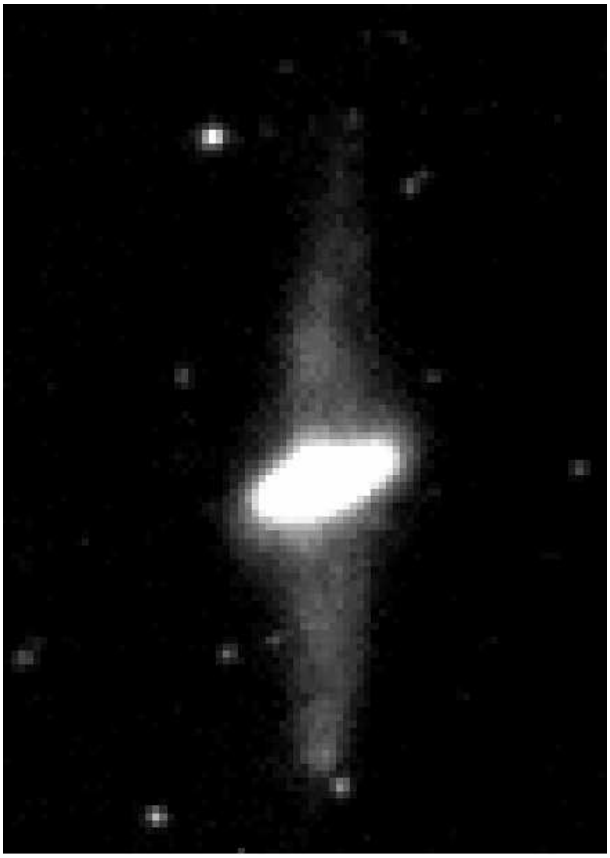

Figure 5.19: Optical image of the Polar Ring Galaxy UGC9796, obtained by the authors at TNG telescope.

mass-to-light ratio of $M_{dyn}/L_B \simeq 50$ in solar units, lead Cox et al. (2006) to conclude that most of the mass in this system is dark. As in the case of UGC7576, the H_α rotation curve (Reshetnikov & Combes, 1994) is in good agreement with the HI rotation curve (Schechter et al., 1984). The shape of the rotation curve indicates that this component is actually a differentially rotating disk, rather than a ring, very similar to the polar disk in NGC4650A.

In Tab. 5.5 we summarize some properties of UGC7576 and UGC9796, compared with those of NGC4650A.

Observation and data reduction

The spectra analyzed in this work were obtained with DOLORES@TNG (Device Optimized for the LOw RESolution), in visitor mode during the observing run A21TAC-54 (on May 2010). DOLORES is installed at the

Table 5.5: Global properties of UGC7576 and UGC9796 compared to those observed for NGC4650A.

Parameter	UGC7576	UGC9796	NGC4650A
R.A. (J2000)	12h27m41.8s	15h15m56.3s	12h44m49.0s
Decl. (J2000)	+28d41m53s	+43d10m00s	-40d42m52s
Helio. radial velocity	7022 km/s	5406 km/s	2880 km/s
Redshift	0.02342	0.01832	0.009607
Distance	94 Mpc	72 Mpc	38 Mpc
Central galaxy			
M_B	-19.15	-17.93	-18.83
B-V	+0.84	+0.92	+0.78
V-R	+0.46	+0.55	
Polar structure			
M_B	-17.5	-17.0	-17.0
$M(HI)(M_\odot)$	2.7×10^9	2.6×10^9	8.0×10^9
$M(HI)/L_B$	0.6	1.5	4
B-V	+0.70	+0.57	+0.26
μ_B	24.3	24.5	22.6
R_{25}	13.6	10.8	7.0
r_{max}	$40''$	$60''$	$40''$

Nasmyth B focus of the TNG and is equipped with the E2V 4240 CCD with an angular resolution of $0''.252\ pix^{-1}$.
The adopted slit was $2''$ wide and it was aligned along the polar disks of the two galaxies UGC7576 and UGC9796, at $P.A. = 53°$ and $P.A. = 16°$ respectively (see Fig. 6.2), in order to include the most luminous HII regions in the polar disks. The total integration time for each object is 4 hrs, with an average seeing of $1''.2$.

At the systemic velocities of UGC7576 and UGC9796, to cover the redshifted emission lines of $[OII]\lambda3727$, $[H_\gamma]\lambda4340$, $[OIII]\lambda4363$, $[OIII]\lambda\lambda4959, 5007$, $[H_\beta]\lambda4861$ and $[H_\alpha]\lambda6563$, the grism LR-B was used in the $3600 - 6800$Å wavelength range, with a dispersion of 2.52 Å/pix.

The data reduction was carried out using the CCDRED package in the IRAF[4] (*Image Reduction and Analysis Facility*) environment. The main strategy adopted for each data-set included dark subtraction[5], flat-fielding correction, sky subtraction and rejection of bad pixels. Wavelength calibra-

[4]IRAF is distributed by the National Optical Astronomy Observatories, which is operated by the Associated Universities for Research in Astronomy, Inc. under cooperative agreement with the National Science Foundation.

[5]Bias frame is included in the Dark frame.

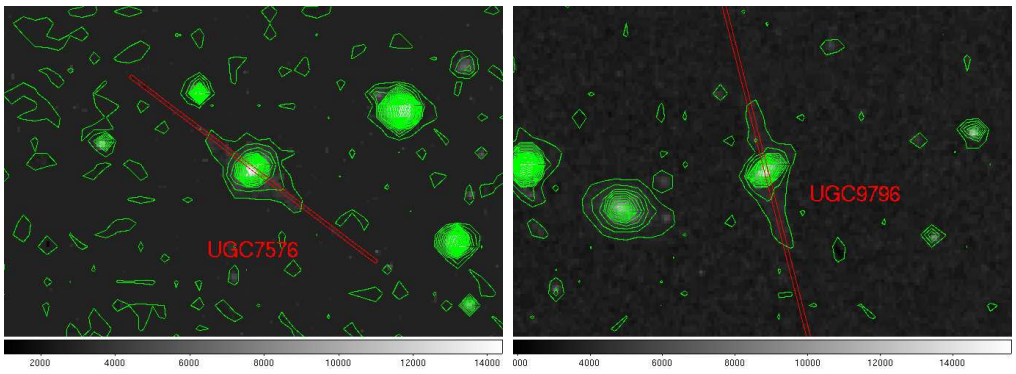

Figure 5.20: Optical image of UGC7576 (left) and UGC9796 (right), with superimposed slits used to acquire data analyzed in this work.

tion was achieved by means of comparison spectra of Hg+Ne lamps acquired for each observing night, using the IRAF TWODSPEC.LONGSLIT package. The sky spectrum was extracted at the outer edges of the slit, for $r \geq 30$ arcsec from the galaxy center, where the surface brightness is fainter than $24 mag/arcsec^2$, and subtracted off each row of the two dimensional spectra by using the IRAF task BACKGROUND in the TWODSPEC.LONGSLIT package. On average, a sky subtraction better than 1% was achieved. The sky-subtracted frames were co-added to a final median averaged 2D spectrum.

The final step of the data-processing is the flux calibration of each 2D spectra, by using observations of the standard star Feige66 and the standard tasks in IRAF (STANDARD, SENSFUNC and CALIBRATE). To perform the flux calibration we extracted a 1-D spectrum of the standard star to find the calibration function; then we extracted a set of 1-D spectra of the galaxy summing up a number of lines corresponding to the slit width. Since the slit width was $2''$ and the scale of the instrument was $0.252''/pix$, we collapsed eight lines to obtain each 1-D spectrum. Finally we applied the flux calibration to this collection of spectra.

The wavelength and flux-calibrated spectra are shown in Fig. 5.21 and Fig. 5.22.

The fluxes of the above mentioned emission lines were measured using the IRAF SPLOT routine, that provides an interactive facility to display and analyze spectra. We evaluated flux and equivalent width by marking two continuum points around the line to be measured. The linear continuum is subtracted and the flux is determined by simply integrating the line intensity over the local fitted continuum. The errors on these quantities have been calculated, following Pérez-Montero & Díaz (2003), by the relation

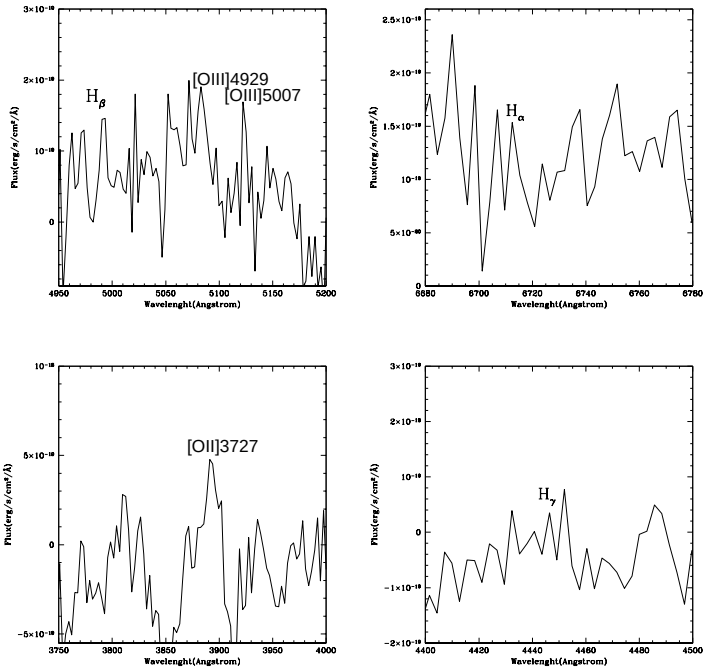

Figure 5.21: Spectrum of UGC7576.

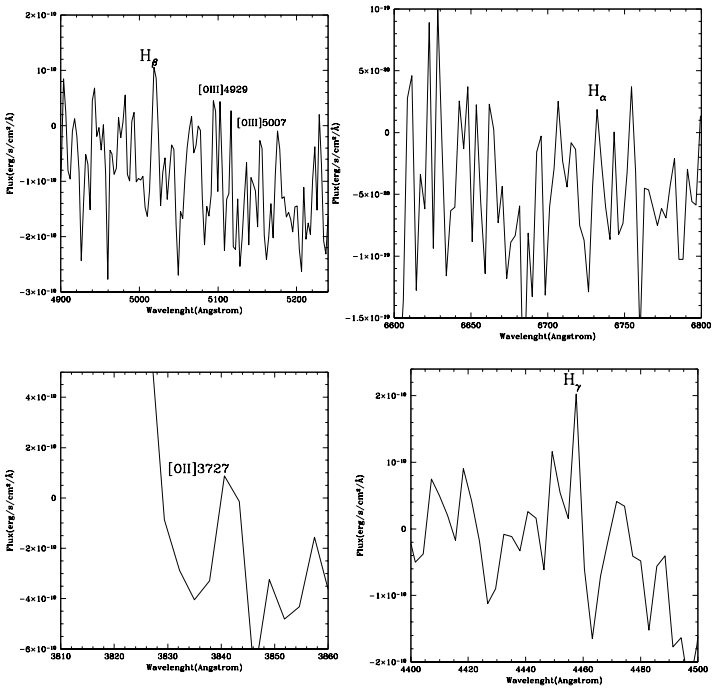

Figure 5.22: Spectrum of UGC9796.

$\sigma_1 = \sigma_c N^{1/2}[1 + EW/(N\Delta)]^{1/2}$, were σ_1 is the error in the line flux, σ_c is the standard deviation in a box near the measured line and represents the error in the continuum definition, N is the number of pixels used to measure the flux, EW is the equivalent width of the line and Δ is the wavelength dispersion in Å/pixel.

Reddening correction

Reduced and flux calibrated spectra and the measured emission line intensities were corrected for the reddening, which account both for that intrinsic to the source and to the Milky Way. By comparing the intrinsic Balmer decrement $H_\alpha/H_\beta = 2.89$, we derived the visual extinction $A(V)$ and the color excess $E(B-V)$, by adopting the mean extinction curve by Cardelli et al. (1989) $A(\lambda)/A(V) = a(x)+b(x)R_V$, where $R_V[\equiv\ A(V)/E(B-V)] = 3.1$ and $x = 1/\lambda$. All the emission lines in our spectra are in the *optical/NIR* range (see Cardelli et al. 1989), so we used the average R_V-dependent extinction law derived for these intervals to perform the reddening correction.

We derived the average observed Balmer decrements for both galaxies, which are the following:
$(H_\alpha/H_\beta)_{UGC7576} = 3.18 \pm\ 2.10$
$(H_\alpha/H_\beta)_{UGC9796} = 2.24 \pm\ 1.30$
while the color excess obtained by using these observed decrements are:
$[E(B-V)]_{UGC7576} = 0.09 \pm\ 0.36$
$[E(B-V)]_{UGC9796} = -0.25 \pm\ 0.92.$
Such values of E(B-V) are used to derive the extinction A_λ, through the Cardelli's law. Finally, the corrected fluxes are given by
$F^\lambda_{int}/F^{H_\beta}_{int} = F^\lambda_{obs}/F^{H_\beta}_{obs} 10^{0.4[A_\lambda - A_{H_\beta}]}$.

Empirical oxygen abundances determination

The analysis of nebular spectra in HII regions is the best tool for the determination of chemical abundances in spiral and irregular galaxies. The abundances of several elements can be determined by using strong emission lines clearly visible in the spectra.

The main aim of this work is to measure the *Oxygen abundance parameter* $R_{23} = ([OII]\lambda 3727 + [OIII]\lambda\lambda 4959 + 5007)/H_\beta$ (Pagel et al., 1979), and consequently the oxygen abundance $12 + log(O/H)$ and the metallicity of the HII regions in the polar disks of UGC7576 and UGC9796, as already done by Spavone et al. (2010) for NGC4650A.

The *Empirical methods* are based on the cooling properties of ionized nebulae which translate into a relation between emission-line intensities and oxygen abundance. Several abundance calibrators have been proposed based on different emission-line ratios: R_{23} (Pagel et al., 1979), S_{23} (Díaz & Pérez-Montero, 2000); among the other, in this work we used the so called P-method introduced by Pilyugin (2001).

Pilyugin (2001) realized that for fixed oxygen abundances the value of $X_{23} = logR_{23}$ varies with the excitation parameter $P = R_3/R_{23}$, where $R_3 = OIII[4959{+}5007]/H_\beta$, and proposed that this latter parameter could be used in the oxygen abundance determination. This method, called "P-method", propose to use a more general relation of the type $O/H = f(P, R_{23})$, compared with the relation $O/H = f(R_{23})$ used in the R_{23} method. The equation related to this method is the following

$$12 + log(O/H)_P = \frac{R_{23} + 54.2 + 59.45P + 7.31P^2}{6.07 + 6.71P + 0.371P^2 + 0.243R_{23}} \tag{5.5}$$

where $P = R_3/R_{23}$. It can be used for oxygen abundance determination in moderately high-metallicity HII regions with undetectable or weak temperature-sensitive line ratios Pilyugin (2001).

The average values of oxygen abundance obtained for UGC7576 and UGC9796 are $12 + log(O/H)_P = 8.5 \pm 0.5$ and $12 + log(O/H)_P = 7.7 \pm 1$ respectively (see Tab. 5.6). Moreover, for UGC7576 it has been possible to measure the oxygen abundance $12 + log(O/H)_P$ at different distances from the center of the galaxy and the values are shown in Fig. 6.6.

Table 5.6: Oxygen abundances and metallicities of UGC7576 and UGC9796 compared to those observed for NGC4650A.

Parameter	UGC7576	UGC9796	NGC4650A
$12 + log(O/H)$	8.5 ± 0.5	7.7 ± 1	8.2 ± 0.2
$Z/Z_\odot$	0.4 ± 0.002	0.1 ± 0.001	0.2 ± 0.002

Metallicity and SFR estimates

We derive the oxygen abundance $12{+}log(O/H)$ for UGC7576 and UGC9796, by using the empirical P-method (Pilyugin, 2001). We found $12{+}log(O/H) = 8.46 \pm 1.69$ for UGC7576 and $12 + log(O/H) = 7.75 \pm 3.23$ for UGC9796. The metallicities corresponding to each value of oxygen abundances given before have been estimated. We adopted $12 + log(O/H)_\odot = 8.83 = A_\odot$

and $Z_\odot = 0.02$ (Asplund et al., 2004). Given that $Z \approx KZ_\odot$, $K_{UGC7576} = 10^{[A_{UGC7576} - A_\odot]}$ and $K_{UGC7576} = 10^{[A_{UGC9796} - A_\odot]}$, we obtain metallicities for the HII regions of the polar disk in UGC7576 and UGC9796 $Z \simeq 0.008$ and $Z \simeq 0.002$ which correspond respectively to $Z \simeq (0.4 \pm 0.002)Z_\odot$ and $Z \simeq (0.1 \pm 0.001)Z_\odot$ (see Tab. 5.6).

Metallicity-luminosity relation

The mean values for the oxygen abundance along the polar structure of UGC7576 and UGC9796, derived by the empirical method (see sec. 5.6), are compared with those for a sample of late-type disk galaxies by Kobulnicky & Zaritsky (1999), as function of the total luminosity. To this aim, we adopted the total bulge plus disk luminosities $M_B = -19.8$ for UGC7576 and $M_B = -19.4$ for UGC9796, by using $H_0 = 50$ km/s/Mpc as in Kobulnicky & Zaritsky (1999). Results are shown in Fig. 5.23.

We found that UGC7576 is located in the region where spiral galaxies are found, and, contrary to its high luminosity, it has metallicity lower than spiral galaxy disks of the same total luminosity and it is consistent with that observed for NGC4650A.

UGC9796 instead is even more metal-poor than UGC7576 and NGC4650A, in fact it is located in the region where HII and irregular galaxies are also found, characterized by lower luminosities and metallicities with respect to the spiral galaxies.

We also compare our new results with those obtained by Pérez-Montero et al. (2009) for IIZw71, a blue compact dwarf galaxy also catalogued as a probable polar ring: consistently with its low luminosity, the metallicity of the brightest knots in the ring of IIZw71 is lower with respect to that of UGC7576, but it is slightly higher than those of UGC9796. Taking into account the total magnitude, such values are somewhat lower than that expected by the metallicity-luminosity relation.

Star formation rate

We have derived the SFR for the polar structures of UGC7576 and UGC9796, from the H_α luminosity using the expression given by Kennicutt (1998) $SFR = 7.9 \times 10^{-42} \times L(H_\alpha)$. We found that it is almost constant along the disks of both galaxies, within a large scatter of the datapoint. Therefore, given the average values of $L(H_\alpha) \simeq 2.36 \times 10^{36}$ erg/s for UGC7576 and $L(H_\alpha) \simeq 5.33 \times 10^{35}$ erg/s for UGC9796, we have obtained an average $SFR \sim 1.9 \times 10^{-5} M_\odot/yr$ and $SFR \sim 4.2 \times 10^{-6} M_\odot/yr$ respectively. These values are significantly lower than those obtained for NGC4650A (Spavone

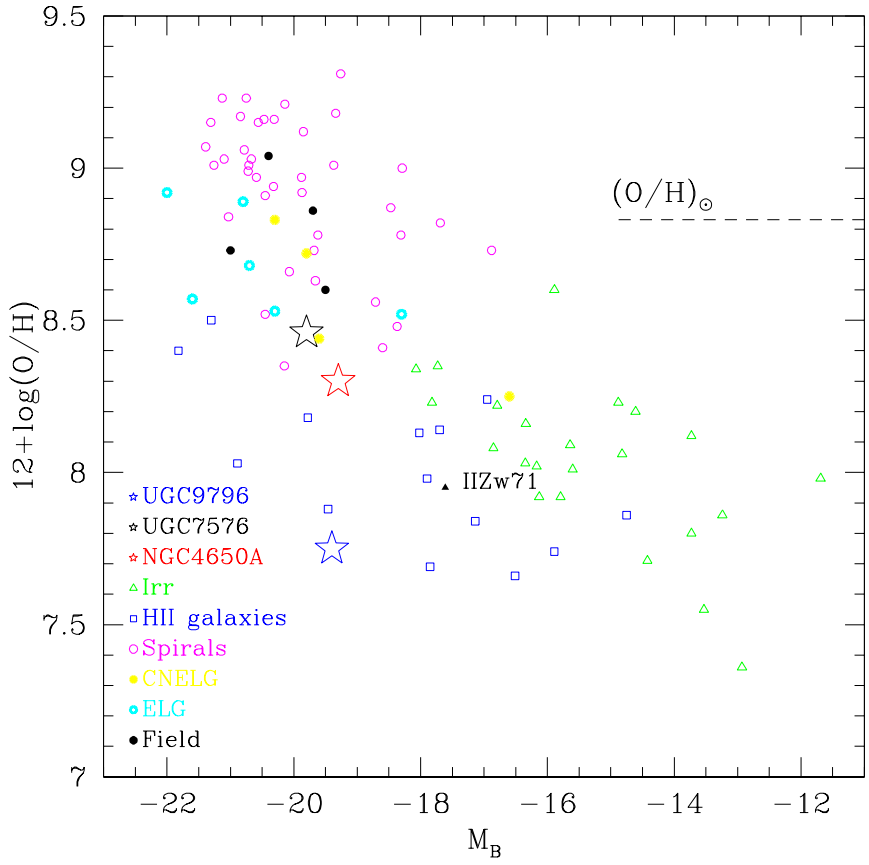

Figure 5.23: Oxygen abundance vs absolute blue magnitude for CNELGs (yellow filled circles), ELGs (cyan open circles), four field galaxies with emission lines (filled black circles), nearby dwarf irregulars (open triangles), local spiral galaxies (open circles), local HII galaxies (open squares), NGC4650A (red star) (Spavone et al. 2010), the polar disk galaxy IIZw71 (Perez-Montero et al.2009), UGC7576 (black star) and UGC9796 (blue star) (this work). The dashed line indicates the solar oxygen abundance. The total B-band magnitude for NGC4650A, UGC7576 and UGC9796 ($M_B = -19.3$, $M_B = -19.8$ and $M_B = -19.4$) have been evaluated by using the same value of H_0 used by Kobulnicky et al. (1999) in order to compare our galaxies with those in their sample

et al., 2010), which is $SFR \sim 0.06 M_{\odot}/yr$ and IIZw71 (Pérez-Montero et al., 2009), which is $SFR \sim 0.035 M_{\odot}/yr$.

Taking into account that the polar structure in both PRGs is very young, since the last burst of star formation occurred less than 1 Gyr ago (Reshetnikov & Combes, 1994), we check if the present SFR and even 2 and 3 times higher (i.e. $SFR = 3.8 \times 10^{-5} M_{\odot}/yr$, $SFR = 5.7 \times 10^{-5} M_{\odot}/yr$ and $SFR = 8.4 \times 10^{-6} M_{\odot}/yr$, $SFR = 1.26 \times 10^{-5} M_{\odot}/yr$), can give the estimated metallicities of $Z = 0.4 Z_{\odot}$ (for UGC7576) and $Z = 0.1 Z_{\odot}$ (for UGC9796) and how strongly could increase the metallicity with time.

Given the presence of star forming regions in the polar disk of NGC4650A, Spavone et al. (2010) used a constant SFR law for this object. In the case of UGC7576 and UGC9796, taking into account the difference of magnitude of the H_{α} fluxes and consequently of the SFR of these galaxies with respect to NGC4650A and the absence of star forming clumps, we used an exponentially declining SFR, typically used for late-type galaxies, that started several Gyrs ago (we assume $t_0 = 8 Gyrs$) and with a decay timescale of $\tau = 2 Gyrs$, $SFR(t) = M_{\star} \tau^{-1} exp[-(t_0 - t)/\tau)]$, where t is the lookback time (Bruzual & Charlot, 2003a). Than, by using the mass-metallicity relation derived by Tremonti et al. (2004), where $12 + log(O/H) = -1.492 + 1.847 log(M_{\star}) - 0.08026 (log M_{\star})^2$, we found that for UGC7576 $0.5 Z_{\odot} \leq Z \leq 1 Z_{\odot}$ and for UGC9796 $0.05 Z_{\odot} \leq Z \leq 0.45 Z_{\odot}$. This shows that the present SFR for the polar structures is able to increase the metallicity of about 0.15 $Z_{\odot}$ for UGC7576 and 0.05 $Z_{\odot}$ for UGC9796, after 1Gyr. The derived values for Z are larger than $Z = 0.4 \pm 0.002 Z_{\odot}$ and $Z = 0.1 \pm 0.001 Z_{\odot}$, found by using the element abundances (see Sec.5.6): this differences could be attributed to the accretion of metal-poor gas, as discussed in detail in sec. 5.6.

Metallicity gradient along the polar structure of UGC7576

The oxygen abundance in the polar ring of UGC7576 as a function of the radius derived by empirical methods is shown in Fig. 6.6: the plot shows that the gradient in the metallicity remains almost constant along the polar ring. It is only slightly declining, differently from what it is observed for spiral galaxies, where there is a very steep gradient in metallicity. The absence of metallicity gradient is a typical behaviour found in LSB galaxies (de Blok & van der Hulst, 1998), and also in the polar disk galaxy studied by Brosch et al. (2010) and in NGC4650A (Spavone et al., 2010). This suggests that, as already pointed out for NGC4650A (Spavone et al., 2010), the star formation and the metal enrichment in the polar structure is not influenced by the stellar evolution of the central spheroid and that the polar ring was formed later. As also suggested by Rupke et al. (2010), numerical simulations predict

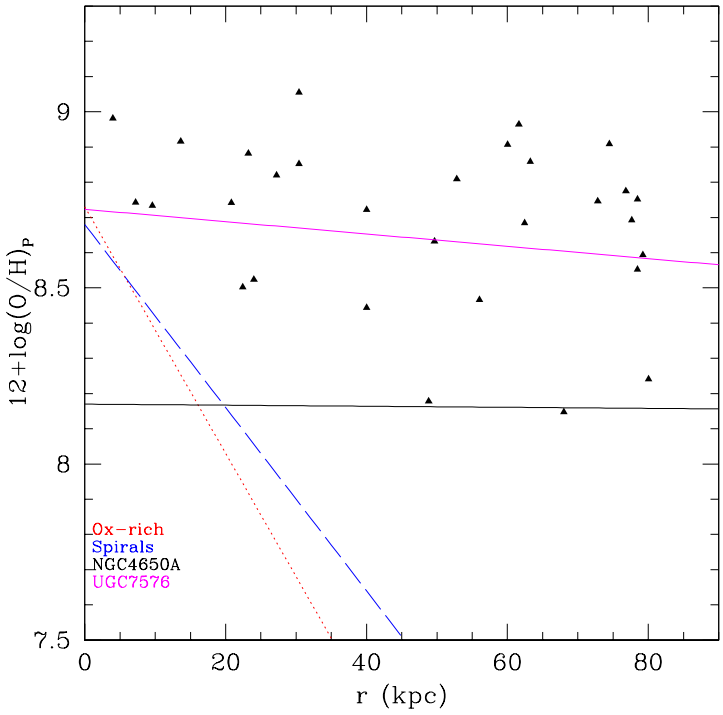

Figure 5.24: Oxygen abundance derived with P- method, proposed by Pilyugin (2001), versus radius. The superimposed lines are the linear best fit derived by Pilyugin et al. (2006); the red line represents the best fit to the abundance of oxygen-rich spirals, while the blue line is those related to ordinary spirals. The black line is the best fit obtained for NGC4650A, while the magenta line is the best fit obtained for UGC7576.

that the absence of metallicity gradient is accounted for by inflow of low metallicity gas from the outskirts.

On the contrary, ordinary and oxygen-rich spiral galaxies show a decreasing abundance with increasing radii (see Fig. 6.6 and Pilyugin et al. 2006). These observed features in spiral disks are well explained by the infall models of galaxy formation which predict that they build up via accretion by growing inside-out (Matteucci & Francois 1989; Boissier & Prantzos 1999) and such process generates the observed gradients.

Formation history for UGC7576 and UGC9796: discussion and conclusions

Galaxies with a polar ring/disk have ever had a special role in the studies of physical processes at work during galaxy interactions and merging, even if in the last years a lot of steps forward have been made to understand the formation and evolution of such systems (Spavone et al., 2010), the debate on the origin of PRGs is still open. In order to account both for the featureless morphology of the central spheroidal galaxy and for the more complex structure of the polar ring/disk, up to date three main formation processes have been proposed: *i)* a major dissipative merger; *ii)* tidal accretion of material (gas and/or stars) by outside; *iii)* cold accretion of pristine gas along a filament.

In the merging scenario, the PRG results from a "polar" merger of two disk galaxies with unequal mass, (Bekki 1997; Bekki 1998a; Bournaud et al. 2005b). In the accretion scenario, the polar ring/disk may form by a) the disruption of a dwarf companion galaxy orbitating around an early-type system, or by b) the tidal accretion of gas stripping from a disk galaxy outskirts, captured by an early-type galaxy on a parabolic encounter (Reshetnikov & Sotnikova 1997; Bournaud & Combes 2003b; Hancock et al. 2009). Both major merger and accretion scenarios are able to account for many observed PRGs morphologies and kinematics, such as the existence of both wide and narrow rings, helical rings and double rings (Whitmore et al., 1990).
The cold accretion scenario has been proposed very recently for the formation of a wide disk-like polar rings (see Sec. 5.6): a long-lived polar structure may form through cold gas accretion along a filament, extended for ~ 1 Mpc, into the virialized dark matter halo (Macciò et al., 2006). In this formation scenario, there is no limits to the mass of the accreted material, thus a very massive polar disk may develop either around a stellar disk or a spheroid.

As suggested by the previous studies on PRGs, and in particular on NGC4650A (Spavone et al. 2010, Iodice et al. 2006), the critical physical parameters that let to discriminate among the three formation scenarios are 1) the baryonic mass (stars plus gas) observed in the polar structure with respect to that in the central spheroid; 2) the kinematics along both the equatorial and meridian planes; 3) the metallicity and SFR in the polar structure. In the tidal accretion scenario the total amount of accreted gas by the early-type object is about 10% of the gas in the disk donor galaxy, i.e. up to $10^9 M_\odot$. In the case of NGC4650A, the polar structure is characterized by an high baryonic mass, of about $12 \times 10^9 M_\odot$, which is comparable with or even higher than the total luminous mass in the central spheroid (of about $5 \times 10^9 M_\odot$):

this feature let to exclude the formation of the polar disk throught the tidal accretion of gas and stars by an external donor galaxy (Bournaud & Combes, 2003b). Furthermore, both the high baryonic mass in the polar structure and its large extension cannot reconcile with a polar ring formed via the gradual disruption of a dwarf satellite galaxy (as explained by Iodice et al. 2002a).

In the merging scenario, the morphology and kinematics of the merger remnants depends on the merging initial orbital parameters and the initial mass ratio of the two galaxies (Bournaud et al., 2005b). In the case of NGC4650A, this scenario is ruled out because, according to simulations (e.g. Bournaud et al. 2005b), a high mass ratio of the two merging galaxies is required to form a massive and extended polar disk as observed in NGC 4650A: this would convert the intruder into an elliptical-like, not rotationally supported, stellar system. This is in contrast with the high maximum rotation velocity ($\sim 80 \div 100$ km/s) observed in the outer regions of the central spheroid (Iodice et al., 2006).

If the polar structure, both around an elliptical and disk galaxy, forms by the cold accretion of gas from filaments there is no limit to the accreted mass. Moreover, due to the inflow of pristine gas, the metallicity is lower with respect to that observed in galaxies of comparable total luminosity, and its value derived by the present SFR is higher than those directly measured by the chemical abundances. Spavone et al. (2010) have found that such predictions turn to be consistent with observations in the polar disk galaxy NGC4650A, yielding to the conclusion that the cold accretion of gas by cosmic web filaments is the most realistic formation scenario for this object.

By studying the chemical abundances in the polar structure of UGC7576 and UGC9697, in the present work we aim to test the cold accretion scenario for these objects. The main results are as follows (see also Sec. 5.6): 1) both PRGs have on average lower metallicity with respect to that of same-luminosity spiral disks, in particular, for UGC7576 $Z = 0.4Z_{\odot}$ and for UGC9796 $Z = 0.1Z_{\odot}$; 2) the metallicity expected for the present SFR at three different epochs are higher than those measured from the element abundaces, and they varies in the range $0.5Z_{\odot} \leq Z \leq 1Z_{\odot}$ for UGC7576 and $0.05Z_{\odot} \leq Z \leq 0.45Z_{\odot}$ for UGC9796; 3) for UGC7576, the metallicity remains almost constant along the polar structure.

In the following, we will address how these results reconcile with the theoretical predictions for the cold accretion process and discuss how the SFR and metallicity derived in this work, togheter with the other two key parameters, i.e. the baryonic mass and kinematics, available by previous studies on these objects, may help to discriminate among the three formation scenarios, in non ambiguous way as done for NGC4650A. All these quantities, for both the PRGs studied in this work and for NGC4650A, are summarized

in Tab. 5.7.

The cold accretion mechanism for disk formation predicts quite low metallicity ($Z = 0.1Z_{\odot}$) (Dekel & Birnboim 2006, Ocvirk et al. 2008, Agertz et al. 2009): such value refers to the time just after the accretion of a misaligned material, so it can be considered as initial value for Z before the subsequent enrichment. How this may reconcile with the observed metallicity for UGC7576 and UGC9796?

We estimated that the present SFR for the polar structure is $SFR = 1.9\times10^{-5}M_{\odot}yr^{-1}$ for UGC7576 and $SFR = 4.2\times10^{-6}M_{\odot}yr^{-1}$ for UGC9796: these values are able to increase the metallicity of about $0.15Z_{\odot}$ for UGC7576 and $0.05Z_{\odot}$ for UGC9796 after 1Gyr (see Sec.5.6): taking into account that the polar structure is very young, less than 1Gyr (Reshetnikov et al., 1994), an initial value of $Z = 0.1Z_{\odot}$, at the time of polar structure formation, could be consistent with the today's observed metallicity. Therefore, the cold accretion of gas can be a possible formation scenario for both the PRGs UGC7576 and UGC9796. One more hint for the cold accretion scenario comes from the fact that the metallicity expected by the present SFR for both PRGs turns to be higher than those directly measured by the chemical abundances: as already suggested for NGC4650A (Spavone et al., 2010), a possible explanation for this observed feature could be the infall of pristine gas (Finlator et al. 2007; Ellison et al. 2008).
Moreover, in the case of UGC7576, the lack of abundance gradient along the polar structure is consistent with the prediction of recent numerical simulations by Rupke et al. (2010) and Kewley & Ellison (2008); they observe flatter metallicity gradients than those observed in typical spiral galaxies, due to the radial inflow of low metallicity gas from outside.

As first important result of this work, we found that the observed metallicity and SFR in both PRGs UGC7576 and UGC9796 turn to be consistent with the predictions for a polar structure formed by the cold accretion of gas. Given that, we will discuss if, by taking into account all the critical parameters available for these objects (see Tab.5.7), we can disentangle between the cold accretion and the other possible formation scenarios for both PRGs.

According to simulations of merging scenario (Bournaud et al., 2005b), a high mass ratio of the two colliding galaxies is required to form massive and extended polar structures as observed in UGC7576 and UGC9796: this would convert the intruder galaxy in an elliptical-like not rotationally suppoted object. Since this is in contrast with the high maximum rotation velocities observed (see Reshetnikov & Combes 1994 and Tab. 5.7) in UGC7576 ($\sim 212km/s$) and UGC9796 ($\sim\ 157km/s$), the merging scenario is ruled out for both galaxies.

The high baryonic (gas+stars) masses, the large extentions of the polar structure and the low metallicity observed in these PRGs are not accounted for in the formation of polar rings through the disruption of a dwarf galaxy, which are characterized by higher metallicities ($1/9Z_{\odot} \div 1/3Z_{\odot}$) and lower HI masses ($\sim 10^7 M_{\odot}$; Galametz et al. 2009 and Bekki 2008).

Differently, the tidal accretion scenario, in which gas is stripped from a gas-rich donor in a partcular orbital configuration (Bournaud & Combes, 2003b), is able to produce wide polar rings and/or disks both around a disk or an elliptical galaxy. In order to consider the accretion hypothesis, we studied the field around these galaxies to see if there are any objects as possible donor galaxy candidates: inside a radius of about 5 times the diameter of both PRGs, as suggested by Brocca et al. (1997), we find that UGC7576 has no close companions, while UGC9796, that is in a small group, has 5 companions (Cox et al., 2006). Therefore, while also the tidal accretion scenario is ruled out for UGC7576, it needs to be envisioned in the case of UGC9796. The VLA images show that UGC9796 and the close companion galaxy MCG+07-31-049 (labeled as 1 in Fig. 5.25) could be in the orbital configuration needed to form a polar structure through an accretion event (Bournaud & Combes, 2003b): infact, the HI gas in UGC9796, which is all associated with the polar structure, has the outer contours warped away from the poles and, in the SE regions, it extends towards MCG+07-31-049, which has HI distribution extending in a direction perpendicular to that of UGC9796.

In the tidal accretion process, the total amount of accreted gas is about 10% of the gas in the disk donor galaxy and it comes only from the outer and more metal-poor regions of the donor galaxy. All the companion galaxies of UGC9796 have an amount of HI gas ($\sim 10^9 M_{\odot}$) comparable with those of this PRG (Cox et al., 2006), but, according to Bresolin et al. (2009), the metallicity of the outer regions of bright spiral galaxies is $0.2Z_{\odot} \leq Z \leq 1.1Z_{\odot}$ and the observed value for UGC9796, $Z = 0.1 \pm 0.001 Z_{\odot}$, is below the lower limit.

Given all the evidences shown above, we can give the following conclusions for this work.
The cold accretion of gas by cosmic web filaments could well account for both the low metallicity, the lack of gradient and the high HI content in UGC7576. Moreover, the general underdensity of the environment where this galaxy is, can be consistent with the cold flow accretion of gas as the possible formation mechanism for this object.
For UGC9796 instead, the scenario is slightly more complex. In fact, the low metallicity estimated, even lower than those observed in the outskirts of spiral galaxies, together with the range of metallicities expected given the present SFR, are consistent with the formation of disks through cold accretion

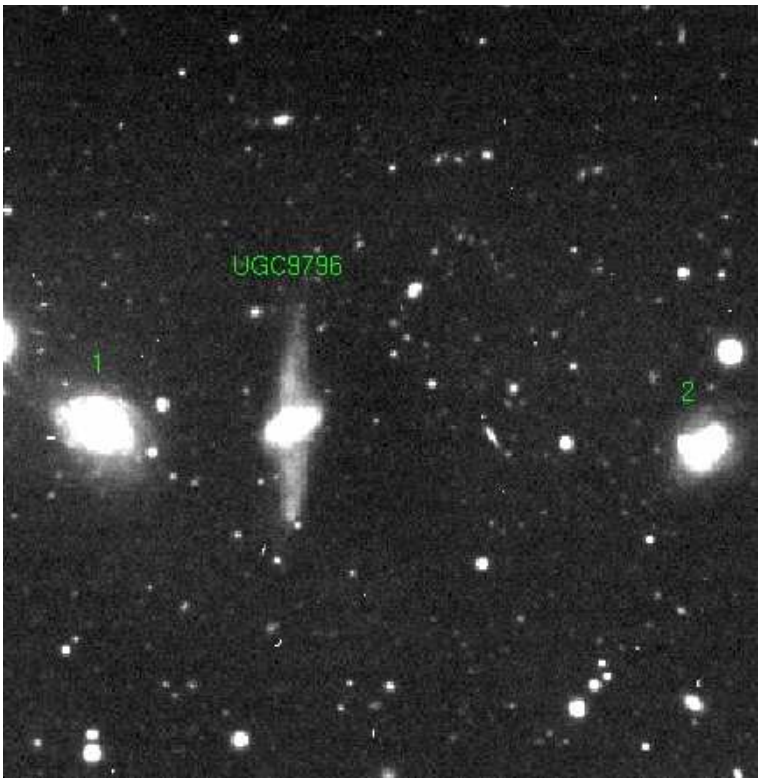

Figure 5.25: Optical image of UGC9796 and its two nearest companion galaxies, MCG +07-31-049 (number 1) and CGPG 1514.2+4320 (number 2).

Table 5.7: Discriminant parameters between different formation scenarios

PRG	M_b^{HG} ($M_\odot$)	M_b^{PD} ($M_\odot$)	V_{eq} (km/s)	V_{eq}/V_{PD}	σ_0 (km/s)	M_b^{HG}/M_b^{PD}	v/σ	Z_{est} ($Z_\odot$)	Z_{exp} ($Z_\odot$)
UGC7576	7.86×10^9	2.88×10^9	212	0.96	116	2.73	1.8	(0.4 ± 0.002)	$(0.5 \div 1)$
UGC9796	1.0×10^{10}	3.05×10^9	157	1.08	73	3.28	2.15	(0.1 ± 0.001)	$(0.05 \div 0.45)$
NGC4650A	5×10^9	12×10^9	90	0.75	70	0.42	1.28	(0.2 ± 0.002)	$(1.02 \div 1.4)$

mechanisms (Dekel & Birnboim 2006, Ocvirk et al. 2008 and Agertz et al. 2009). On the other hand, the tidal accretion scenario cannot be ruled out, given that the galaxy MCG +07-31-049, with its high amount of HI and its orbital configuration, could be a good candidate donor for UGC9796.

CHAPTER 6

The merging scenario

As already mentioned, the mutual tidal capture of two disk galaxies during a close, planar passage was first illustrated by Toomre & Toomre (1972) who, by performing a numerical integration of the restricted three body problem, produced computer simulations of galaxy interactions that were able to reproduce the observed peculiar structures. They also gave an indication of the terrible strength of inelastic effects in slower encounters estimating that the relative orbit of NGC4038/39 had decayed from $e = 0.8$ to $e = 0.5$ as a result of the most recent passage, and that even more severe orbital decays seemed necessary to account for the half-dozen objects which they described as resembling "a single luminous ball, from which protrude several tentacles or filaments".

Evidence began to collect that disk galaxies might be surrounded by massive dark halos; it was noted that such halos would increase the merger cross-sections of visible galaxies (Toomre, 1977). The simplest N-body simulations modeled the encounters of a pair of spherical galaxies, but these experiments are perhaps best viewed as reproducing the dynamics of dark halos.

6.1 Spherical systems

N-body models shed light on the mechanisms responsible for rapid orbital decay. In head-on collisions, decay results from the gravitational compression arising when two galaxies nearly coincide; this compression causes a slightly

greater axial force to be felt between them as they try to separate than they experienced at corresponding distances during their approach. By stirring up the material in each galaxy at the expense of their orbital energy, this mechanism brings about the rapid merger of even the most centrally concentrated systems in only a few passages. In off-axis collisions, the collective response is dominated by those particles which orbit within their respective galaxies in the same direction as the two galaxies pass each other. Such particles are again promoted onto less-bound orbits, receiving both binding energy and angular momentum from the relative motion of the two galaxies, and producing tail-like structures. Orbital decay is more rapid if the victim galaxies rotate internally in the same direction as their passage, since more of their constituents then match the angular speed of the perturber.

It seems unlikely that any bound pair of galaxies can forever escape merging. In some cases the decay time-scale may be quite long, and it can become difficult to delineate the conditions leading to an eventual merger. However, parabolic encounters between identical spherical galaxies with half-mass radii greater than their pericentric separation generally lead to rapid capture and merger on the subsequent orbital passage.

Fluctuating gravitational fields during the merging process tend to transfer binding energy between different components of the system, but such fluctuations damp down before a complete redistributon takes place. This *incomplete* violent relaxation only partly erases the original ordering of material in binding energy; the centers and outskirts of merger remnant remain dominated by particles from the respective centers and outskirts of the victim galaxies. Thus radial population gradients present in the progenitors may well survive the merging process.

After a merger, the remnant relaxes progressively outward on a time scale comparable to the local crossing time. Outside the relaxed region at any typical instant there is material falling back onto the remnant for the first time on long-period, loosely-bound orbits. Still further out, lay bound particles which have become unbound during the merger. Multiple passages before merger generate more complicated structures since each passage launches a fresh outward surge of loosely-bound mass. The amount of material that escapes depends on the structure of the victim galaxies as well as on the parameters of their encounter. In general, the escaping material comes from the outskirts of the original galaxies; truncated victims generally lose only a few percent of their mass after merging in parabolic encounters.

The material that does not quite escape eventually phase-mixes to form an extended envelope around the body of the remnant. Simple arguments based on continuity of the energy distribution imply that this envelope will have a $\rho \propto r^{-4}$ density profile. Insofar as such a density profile provides a fair

approximation, in projection, to the outer parts of a de Vaucouleurs law, the continuity of the distribution function may help explain why de Vaucouleurs profiles are frequently produced in mergers, as well as in other situations involving violent relaxation.

To the extent that a small amount of mass lost can be neglected, the overall scale of a merger remnant may be estimated by a straightforward energy argument. The simplest version describes the merger following a parabolic encounter of two identical galaxies; in this case the total mass and binding energy of the remnant are just twice the mass and binding energy of a single victim. Then the gravitational radius $r_g = GM^2/U$, mean velocity dispersion and characteristic surface density of the remnant must be respectively double, equal and half the corresponding values for the victims. However, these relations are only valid for the remnant as a whole; energy conservation alone does not predict the central properties of merger remnants, nor how different components become distributed in multicomponent remnants.

The cores of merger remnants are constrained by the Liouville theorem $df^{(N)}/dt = 0$, where $f^{(N)}$ is the N-particle distribution function, since a system with a de Vaucouleurs profile requires an infinite peak in phase-space density. Thus if the victim galaxies have finite cores, the remnant they produce must also have a finite core. In practice, mergers of spherical isotropic galaxies seem to produce only a modest decrease in the maximum coarse-grained phase-space density. Remnants generally have core radii comparable to those of the victim galaxies, but their central densities and velocity dispersions are often higher.

Mergers of spherical galaxies produce remnants with fairly simple shapes and kinematics. Head-on encounters result in prolate remnants with anysotropic velocity dispersions, whereas if the encounter is not quite head-on, the result is a slowly-tumbling triaxial object. Encounters with a pericentric separation $R_p \geq 0.5R_h$, where R_h is the victim half-mass radius, generally result in nearly oblate remnants with figures supported largely by internal rotation. This last outcome might appear to dispute the notion that slowly rotating elliptical galaxies are formed by mergers, since it may seem unlikely that progenitors falling from separations of $\sim$ 1 Mpc would frequently pass within only $\sim$ 1 or 2 kpc of each other on their first plunge. However, hierarchical clustering generally favors rather close encounters. In addition, extended dark halos take up much of the orbital angular momentum. An effect left only implicit in the early single-component studies.

6.2 Disk/Halo systems

Dark matter has been included in more recent models of merging disk systems to support approximately flat rotation curves, to help prevent violent bar instabilities and otherwise make the simulations more realistic. Over the past decade, the particle number N has increased by two orders of magnitude, but perhaps the most significant difference between the latest models and their predecessors is the scale of the halos modelled. In the earlier calculations, halos of approximately the same mass and radial extent as the visible disks were employed, obviously insufficient to maintain flat rotation curves out to the radii seen in some galaxies. Halos used in some recent calculations have four or more times the mass and several times the radial extent of the luminous components.

The dynamics of encounters between such galaxies are largely governed by the interactions of their extended dark halos; consequently even passages in which the *visible* components completely miss each other at first can lead to rapid orbital decay. Roughly speaking, a pair of spherical, interpenetrating dark halos interact as if they were single component systems: the orbital angular momentum of the two halos is transferred to internal degrees of freedom, imparting spin and creating broad tidal tails. More tightly bound components, such as embedded disks and/or bulges, are not much braked by the tidal forces retarding the dark matter; instead, these components lose orbital angular momentum mostly by interacting with their own surrounding halos, once the latter have been decelerated. It is the interaction between such extended dark halos that brings the two galaxies to a halt and subsequent merger while the luminous tails extracted from their disks are still well-defined.

As in mergers of spherical systems, the incomplete violent relaxation of disk/halo models only blurs the original ordering in binding energy; the tightly bound components which contained most of the luminosity in the original galaxies will be found near the center of the merger remnant. Luminous material dominates the central regions of the merger remnants precisely because the dense luminous parts of the infalling galaxies remain largely undisturbed until they finally encounter each other and merge within a now-common envelope of halo material. This ends any concern that mergers between galaxies with larger dark halos might mix up the dark and luminous components, producing diffuse, extended remnants with extremely low surface brightnesses.

Thus, even if the two galaxies originally encountered each other on a parabolic orbit, the luminous regions typically find each other only after their relative orbit has become more tightly bound. As a result, the luminous stuff

tends to have a substantially higher velocity dispersion in a disk/halo remnant than it did in the initial galaxies. In parabolic mergers of composite bulge/disk/halo systems, the velocity dispersions of those particles belonging to the bulges are $\sim 40\%$ higher in the final remnant than in the initial galaxies. It seems likely that this effect might well remove the objection that disk galaxy merger remnants should have markedly lower velocity dispersions than elliptical galaxies of the same total luminosity. Actual observations indicate that merger remnants have velocity dispersions consistent with normal elliptical of the same luminosity.

A more interesting challenge to the simple slogan that "merging disk galaxies make ellipticals" comes from the expected core radii of merger remnants. In fact, central disk phase-space densities are lower than the peak phase-space densities of many lower luminosity ellipticals. Moreover, the violence needed to convert a pair of dynamically cold disks to a hot, spheroidal remnant must involve a good deal of vacuum together with the disk phase fluid, further lowering the grained phasepace density. Thus merging disk galaxies cannot form the cores of ellipticals unless they contain either substantial preexisting bulges or else sufficient interstellar material to build such cores dissipatively.

As a matter of fact, the shapes and kinematics of the remnants of disk/halo galaxy mergers are much more complex and diverse than those produced by mergers of spherical systems, but certain generalizations can still be made. Just as for spherical systems, mergers from high angular momentum orbits tend to produce oblate, rapidly-rotating remnants, while those resulting from head-on encounters are prolate. But this is more true for the halos of remnants than for their luminous contents; orbital decays tends to leave the latter with but a small part of the orbital angular momentum they possessed originally. In many of the numerical experiments, the final encounters of the most tightly bound components are observed to be nearly head-on, producing remnants with nearly prolate centers supported largely by particles on box orbits.

Remnants with rapidly rotating luminous components can result from direct or nearly direct encounters which allow the spin and orbital angular momenta of the original disks to reinforce each other. Such remnants have nearly oblate figures and owe much of their flattening to rotational support. The significant streaming motions in these remnants are due to the many particles in direct minor-axis tube orbits. Highly flattened remnants can also be produced by nearly retrograde encounters, but here the comparable numbers of particles on direct and retrograde minor-axis tube orbits give resulting objects little, if any, net streaming motion.

Encounters between more inclined disks tend to produce rounder, more

slowly-rotating remnants with more luminous material on major-axis tube orbits. In some cases, the initial spins of the disks are "remembered" in the sense that circulation about the major axis in one direction is favored over circulation in the other direction; such differential population of the various orbit families can result in large misalignments between the spin and minor axes. Studies of elliptical galaxies suggest that most of them have small kinematic misalignments, while a minority have spin vectors nearly parallel to their major axes; this may still prove a serious obstacle to the production of ellipticals by mergers of inclined disk galaxies.

Finally, some experiments yield merger remnants with intrinsic axial twists or rapid figure rotation. The long-term stability of such configurations remains an open question; effects related to the diffusion of chaotic orbits, for example, may only show up on time scales so long that they are completely obscured by the "particle noise" in the potentials of existing N-body models.

6.3 Gas dynamics in merging disk galaxies

If pressure forces are small, the gas in interacting galaxies follows the same trajectories as the stars, but shocks can transfer momentum between parcels of gas and thereby drive it off the stellar track. Early works suggested that global shocks could sweep the gas from spiral galaxies during fast interpenetrating collisions, producing gas-poor disks resembling S0 galaxies, but this idea did not survive revised estimates of collision rates. Unless the encounter geometry is just right, the fraction of gas removed by direct impacts cannot be large. But tidal forces in slow passages can perturb the gas and stars alike over most of the disk, and if large-scale shocks develop in the gas, its flow may diverge markedly from that of the disk stars.

Self-consistent models of interacting gas-rich spirals suggest that the most common result of such tidal perturbations is indeed not to eject the interstellar material but to drive a large fraction of it close to the center of each galaxy. One (but not the only) way this can happen is for the perturbed stellar disk to form a bar; gravitational torques between the bar and the shocked gas rob the latter of its angular momentum and so allow it to flow inward. If the encounter is a close one, the shocks generated are extremely strong and a substantial fraction of the gas in the disk can flow inwards on a dynamical time scale. This inward-driven gas typically collects in a rotating ring or "blob" with dimensions of $\leq 1kpc$.

Only when two galaxies undergo a final, nearly head-on collision will hydrodynamic forces between these newly built gas blobs come into play. Such final encounters result from orbital decay in bound pairs of galaxies. In

the present context, the central gas blobs loose orbital angular momentum to the surrounding stellar stuff. Their eventual coalescence cancels out much of their residual spin about different exes. Thus experimental merger remnants are often left with massive central gas clouds containing $\geq 50\%$ of the gas initially spread throughout the victim disks. The linear dimensions of these clouds, corresponding to a few hundred parsec, are comparable to the spatial resolution of the calculations.

The ultimate fate of gas in merging galaxies is still more difficult to predict. Observations imply that compression in large-scale shocks and in the dense gas clouds may convert a substantial fraction of the gas to stars on a $\sim 10^8 yr$ time scale. It seems likely that energy released by stellar or nonthermal activity could blow out most of the remaining gas, thus producing the "super-winds" seen in some infrared luminous galaxies. Such outflows may well strip merger remnants of their cool interstellar gas, create x-ray coronae around some ellipticals, or even transport metals back to the intercluster medium.

If the time scale for star formation significantly exceeds the remnant's central dynamical time scale, the gas may settle into a relatively thin central disk. Such a disk has been reported in numerical models of merging spiral galaxies. Because the gas must loose so much angular momentum to arrive where we find it, the small amount of spin it retains may not be well correlated with the rotation of the merger remnant as a whole. Indeed, the above mentioned models contain *counter-rotating* gas disks, spinning in the opposite direction from the rest of the remnant.

Subsequent star formation would leave a compact stellar disk with kinematics unlike the rest of the galaxy, perhaps resembling the "kinematically decoupled cores" found in elliptical galaxies (Spavone et al. 2006 and references therein). Counter-rotating systems can be produced by purely stellar-dynamical mergers, and apparent counter-rotation may also result from projection effects in triaxial systems with streaming motions. However, the line profiles of some systems indicate that their disks are dynamically "cold"; such disks were probably assembled in gaseous form.

6.4 Compact Groups of Galaxies

Isolated galaxies are quite uncommon in the universe; galaxies in fact tend to form complex structures like groups and clusters. Usually such systems of galaxies are distributed with relatively low density, but it is rather common to detect doublet or triplet of galaxies with small angular separation. There are also some structures in which galaxies are in "critical conditions": the so

called *Compact Groups of Galaxies*.

Compact groups are small, relatively isolated, system of typically four or five galaxies in a very compact configuration on the sky. The detection of such groups is very important to study galaxy interactions in such extreme conditions; theories on the formation and evolution of galaxies in fact predict that frequency and intensity of interaction processes, strongly depend on the density of the environment in which galaxies are. For this reason, Compact Groups are considered the ideal ground where to study galaxy interaction processes such as dynamical friction, tidal interactions and merging.

Such groups do not necessarily form a distinct class, but may instead be extreme examples of systems having a range of galaxy density and population. Because of this, the properties of the groups in any particular sample may be strongly influenced by the criteria used to define the sample. For this reason, it is necessary to define specific, quantitative, criteria for their identification. These criteria define the minimum number and magnitude range of the galaxies, and also consider the galaxy spatial distribution.

The use of quantitative selection criteria was pioneered by Rose (1977) who searched for groups that have three or more galaxies that are brighter than a limiting magnitude of 17.5, and that have a projected surface density enhancement of a factor of 1000 compared to the surrounding background galaxy density. Searching an area of 7.5% of the sky, he found 170 triplets, 33 quartets, and 2 quintets. Unfortunately, the sample received little follow-up studies. Sulentic (1983) re-examined the 35 Rose groups which contain four or more galaxies and found that only a third actually satisfied the assumed selection criteria. This is testimony to the difficulty of visual searches. A more fundamental problem is that the fixed magnitude limit in the selection criteria makes the sample susceptible to strong distance-dependent biases.

To try to reduce such effects, Hickson (1982) adopted a relative magnitude criterion, selecting systems of four or more galaxies whose magnitudes differ by less than 3.0. A distance independent (to first order) compactness criterion was employed: $\mu_G < 26$, where μ_G is the mean surface brightness of the group calculated by distributing the flux of the member galaxies over the smallest circular area containing their geometric centers. To avoid including the cores of rich clusters, an isolation criterion was necessary so as to reject the group if a non-member galaxy, not more than 3 mag fainter than the brightest member, occurred within three radii of the center of the circle (A non-member galaxy is a galaxy which if included in the group would cause the group to fail one or more of the selection criteria). From a search of 67% of the sky (all the POSS prints), and using magnitudes estimated from the POSS red prints, exactly 100 groups (hereafter HCG's) were found satisfying these criteria, summarized below:

1. $n \geq 4$ with $m \leq m_b + 3$
2. $R_N \geq 3R_G$
3. $\mu_G < 26$

where n is the number of galaxies in the group, m is the red magnitude of the faintest member of the group, m_b is the red magnitude of the brightest member of the group, R_G is the radius of the smallest circle containing the centers of the group members, μ_G is the mean surface brightness within this circle and R_N is the distance between the center of the circle and the nearest galaxy, not belonging to the group, satisfying the same magnitude criterium.

However, a sample selected on the basis of the surface brightness is affected by both geometric and kinematic selection effects. The former occurs because non-spherical systems will be preferentially selected if they are oriented to present a smaller cross-sectional area, the latter because we will preferentially select systems which, owing to galaxy orbital motion, are momentarily in a more compact state (transient compact configurations). Thus, a compact group might result from a chance alignment or transient configuration within a loose group.

Other biases arise from the subjective nature of the search procedure. Because of the difficulty of identifying faint groups, the HCG catalog starts to become significantly incomplete at an integrated magnitude of about 13. A more subtle effect results from the difficulty of recognizing low-surface-brightness groups. Because of this, the catalog also becomes incomplete at surface brightnesses fainter than 24 (Hickson, 1982). Yet another effect is that groups may be more noticeable if the magnitude spread of their members is small. Thus, the catalog may also be incomplete for magnitude intervals greater than about 1.5. These effects are of critical importance in statistical analysis of the sample. One immediate conclusion is that the actual number of groups which satisfy the selection criteria may be considerably larger than the number found by a subjective search.

6.4.1 Spatial distribution and environment

The space distribution and environment of compact groups provide important clues to their nature. HCGs median redshift is $z = 0.03$, well beyond the Virgo cluster, and further studies reveal that they are uniformly distributed and show no preference for rich clusters. However, galaxies in rich clusters have different kinematic and morphological features with respect to thos in compact groups, thus it is reasonable to argue that small clumps of galaxies in rich clusters are not compact groups. Vennik et al. (1993) found that

mani HCGs are associated to loose groups; this was a clear indication that compact groups are preferentially found in low density environments.

Vennik et al. (1993) compared the space distribution of luminous matter near some compact groups and loose groups of galaxies, finding that all the studied groups have a similar projected density distribution and that all compact groups are not isolated but rather small condensations within loose groups. Moreover, by analyzing surface brightness profiles, we also found that loose groups hosting compact groups tend to have higher space density of luminous matter than normal ones. The true nature of this excess is not clear: it would be *genetic* (compact groups form only in loose groups with higher density) or *evolutionary* (the formation of a compact group within a loose group produce a "bulge" in the inner regions of the loose group).

It is also important to establish whether galaxies in compact groups are different from their neighbors. Kindl (1990) found that compact groups contain a fraction of late-type galaxies (spirals and irregulars) significantly lower than the surrounding structures. This result is particularly important to understand the physical nature of compact groups. Moreover, independent studies have found significant differences between galaxies in compact groups and those in other environments.

6.4.2 Structure and morphology

Further indications about the nature of compact groups can be derived from the spatial distribution and luminosities of the member galaxies. In fact, if they are projection effects or transient configurations, the luminosity functions should be similar to those of field galaxies and the galaxies spatial distribution should be consistent with a random one. If instead they are physically bound systems, the luminosity profiles and the spatial distribution should reveal features showing their different origin and evolution.

Shapes and orientations

Rose (1977) determined that the ellipticities in his sample were consistent with a random distribution of galaxies. Using the larger HCG sample, Hickson et al. (1984) reached the conclusion that groups are typically more elongated than it would be a random distribution of galaxies. An immediate consequence of this result is that compact groups cannot easily be explained as random projections or chance crossings, as this would largely erase any inherent ellipticity of a parent loose group. These conclusions, however, are not unique, in fact Hickson et al. (1984) also found the shapes to be consistent with those observed in dynamical simulations of compact groups seen in

projection as subgroups within loose groups. In addition, one must always be concerned about possible selection biases. It may be that highly elongated groups are more easily noticed in visual searches. If the intrinsic shapes of compact groups are related to their formation process, one might expect to see a relationship between the orientation angle of a group and the environment. Palumbo et al. (1993) examined the environments of the HCGs, and found that the orientations of the major axes of the groups were consistent with an isotropic distribution.

If compact groups are not simply projection effects, they might be expected to show a centrally-concentrated surface density profile, as is seen in clusters of galaxies. Although the number of galaxies in individual compact groups is small, with a large sample it is possible to estimate a mean profile. By scaling and superimposing the HCGs, Hickson et al. (1984) found evidence for central concentration. Further studies also find a consistent density profile for all groups, without any scaling; this is particularly interesting, in fact this would not be expected if most groups are chance alignments within loose groups. It also implies that compact groups have a unique scale, which seems counter to the concept of hierarchical clustering. However this arises as a result of a minimum mass density and velocity dispersion that is required for the groups to be virialized.

Morphological types in compact groups

Several studies of the morphological types of galaxies in compact groups have been performed and most of them agree that the fraction of early type galaxies, f_s is significantly less in compact groups ($f_s \simeq 0.5$) than in the field ($f_s \simeq 0.8$). Moreover, it appears also that most compact groups are composed by galaxies of the same morphological type, in contrast with a random distribution. Such concordance could result from a correlation of morphological type with some other property of the group. The strongest such correlation found to date is between morphological type and velocity dispersion (see Fig. 6.1); groups with higher velocity dispersions contain fewer late-type (gas-rich) galaxies (Shaker et al., 1998). They also tend to be more luminous.

This result should be an evidence of the elliptical galaxies formation through the merging of disk galaxies. The merging of two late type galaxies in fact, lead to the formation of an early type galaxy with luminosity widely higher than those of the initial galaxies. Thus, elliptical dominated compact groups should be the result of previous merging events. In the simple hypothesis that the luminous matter is a good tracer of the group gravitational potential, the low velocity dispersion, the small dimensions and the high spa-

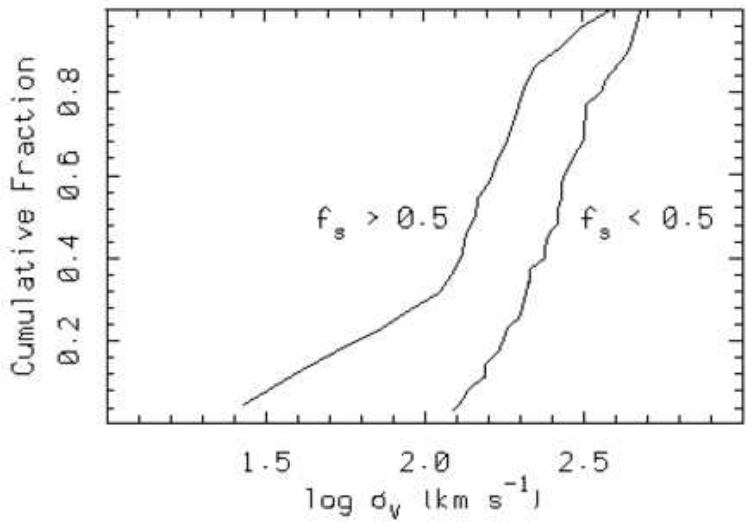

Figure 6.1: Morphology-velocity correlation for compact groups.

tial density, suggest the presence of a high merging rate in compact groups that should therefore be considered as a favourite place for the formation of elliptical galaxies.

The morphology-density relation seen in clusters and loose groups is not the dominant correlation in compact groups, and this suggests that the velocity dispersion is more fundamental, i.e. of greater physical relevance to the formation and evolution of galaxies in compact groups, than is apparent physical density.

There is much evidence that interactions are occurring in a large fraction of galaxies in compact groups. The strongest direct support comes from kinematical studies, showing that two thirds of the observed HCG spiral galaxies have peculiar rotation curves. These show asymmetry, irregularity and in some cases extreme distortion, all typical signs of strong gravitational interaction.

Zepf & Whitmore (1993) found that elliptical galaxies in compact groups tend to have lower internal velocity dispersions than do ellipticals in other environments having the same effective radii, absolute magnitudes and colors. They therefore do not lay on the fundamental plane defined by other elliptical galaxies. This discrepancy correlates with isophote shape in that those galaxies that have "disky" or irregular isophotes tend to have lower velocity dispersion. Zepf & Whitmore (1993) report that HCG elliptical galaxies are less likely to have "boxy" isophotes, and more likely to have irregular isophotes. Such effects are consistent with results of simulations of tidal encounters

Compact groups are considered *second generation structures*: given that most groups are not isolated, but rather small structures within loose groups and clusters, and that their relaxation times are about 10^8 yrs, it is likely that they are recent aggregations of material. The first generation of these objects should be destroyed by rapid merging processes and stripping of dark matter haloes, with a subsequent production of relics that appear as early type galaxies surrounded by extended dark matter haloes.

A consequence of this scenario is a distinction between early and late type galaxies in compact groups; elliptical galaxies must be highly evolved objects, while late type galaxies, that are recent aggregations, poorly influence the dynamics of the group.

Luminosity function

One of the best studied property of galaxies is the *luminosity function*, defined as the number of galaxies per volume unit, per magnitude range and eventually per morphological type. The luminosity functions obtained by grouping galaxies in the three main morphological types (ellipticals, spirals and lenticulars) show clear differences; ellipticals and lenticulars tend to cluster in the central high density regions of clusters, while spirals are placed in the outer and low density regions. These considerations lead to the conclusion that the luminosity function should depend on the density of the environment. The most representative relation for the cumulative luminosity function was proposed by Schechter (1976):

$$\phi(L)dL = \phi^*(L/L^*)^\alpha e^{(-L/L^*)} d(L/L^*) \tag{6.1}$$

where L^* is a characteristic luminosity, ϕ^* is the galaxy density per magnitude unit at the luminosity L^* and α is a constant indicating the slope of the relation at low luminosities.

The standard technique for the determination of the luminosity function weights each galaxy by V_m/V, where V is the volume of the smallest geocentric sphere containing the group, and V_m is the volume of the largest such sphere within which the group could have been detected. Using this approach a luminosity function for HCG galaxies similar to that of field galaxies has been obtained.

However, standard calculations do not address the selection effects of the HCG sample. For example, the luminosity range within an individual group is limited by the 3-mag range of the selection criteria. Because of this, fainter galaxies within compact groups are not included in the catalog. In order to account for such biases we need to use a modelling technique in which galaxies are drawn from a trial luminosity function and assigned

to groups. Redshifts are given to each group according to the observed distribution, and groups that failed to meet the HCG selection criteria are rejected. The luminosity distribution of the resulting galaxy sample is then compared to the observations and the process repeated with different trial luminosity functions. The best-fit luminosity function obtained in this way is deficient in faint galaxies, although a normal field-galaxy luminosity function cannot be definitively excluded.

6.4.3 Far Infrared Emission

Simulations show that, during strong galactic interactions, gas and dust dissipate angular momentum and become more centrally concentrated, so favoring non thermal nuclear activities (such as Active Galactic Nuclei, AGN) due to the infall of gaseous material in the central black holes. This process gives rise to the production of violent burst of star formation, that affect both colors and luminosities at radio, optical and infrared wavelengths.

At the FIR wavelengths the observed fluxes are mainly due to thermal emission of dust grains, warmed up by the interstellar radiation field. Merging or interacting galaxies, usually show an infrared excess, due to the presence of an anomalous number of regions of starburst that lead to an increase of temperature and density of the surrounding interstellar medium. For this reason FIR emission is considered a good indicator of galaxy interaction. The warming of the gas due to the ultraviolet (UV) emission of young and massive stars, lead to an excess of FIR luminosity.

Surprisingly, while this excess has been confirmed for interacting pair of galaxies and for clusters, it has not yet been detected in compact groups (Allam et al., 1996). By using IRAS[1] data, Merluzzi et al. (2000) proposed that the lack of a FIR excess could be due to the peculiar density of the surrounding environment of compact groups, in which are particularly efficient many processes, such as gas stripping, that could suppress star formation. Moreover, the non homogeneity of the sample can make meaningless the comparison with other objects; galaxies in Hickson compact groups in fact have different morphological, photometric and kinematical properties.

6.4.4 Star formation and nuclear activity

Many evidences show that tidal interactions play an important role in the enhancement of star formation activity in galaxies. Compact groups, with

[1]The Infrared Astronomical Satellite, was the first observatory to perform an all-sky survey at infrared wavelengths

their high galaxies density and significant signs of interaction, could be the ideal laboratory to study such effects; many of them in fact contain galaxies hosting active galactic nuclei.

As already said, the general degree of star formation activity in compact groups of galaxies, can be derived from infrared observations. The first studies of this kind were mainly based on IRAS data.

Hickson et al. (1989) by using low angular resolution data in the far infrared, obtained with IRAS satellite, detected sources in 40 HCGs and concluded that the ratio of far-infrared-to-optical luminosity is greater by about a factor of two in compact group galaxies, compared to that of isolated galaxies. This result was disputed by Sulentic & de Mello Rabaca (1993) who argued that the low spatial resolution of the data made the assignment of infrared flux to individual galaxies ambiguous. They concluded that redistribution of the flux could result in little or no infrared enhancement.

The resolution problem can be avoided by considering the infrared colors of the sources instead of the infrared/optical ratio. Zepf & Whitmore (1993) compared the ratio of $60\mu m$ to $100\mu m$ fluxes of compact group galaxies with those of isolated galaxies and also with those of galaxies believed to be currently merging. He found that the compact group sample was significantly different from both other samples, and estimated that about two thirds of the compact group galaxies had warm colors (larger $60/100\mu m$ ratios) similar to those of merging galaxies.

A different approach to interpreting the infrared results was taken by Menon (1991) who emphasized that the strong correlation between radio and infrared radiation indicates that these likely originate from a common region. In compact group spirals the radio emission is primarily nuclear whereas in isolated spirals it originates in the disk. If this is also true for the infrared flux, there must be an enhancement of the infrared/optical ratio, in the nuclear region, of more than an order of magnitude.

However, by using the correlation between radio and infrared emission found for field galaxies and clusters, Hickson et al. (1989) showed, even if in a non direct way, that galaxies in compact groups tend to be overluminous in the infrared. Further studies of the IRAS data with higher angular resolution confirmed these results.

This idea is also supported by further observations in which CO[2] emission is detected in 55 of the 70 HCG's galaxies selected on the basis of IRAS data. The infrared luminosty-H_2 mass ratio derived with these observations

[2]The CO emission at 2.6 mm is an indicator of the molecular hydrogen content in a galaxy.

showed an enhancement which correlates with the projected nearest-neighbor distance.

Further indications are provided by radio continuum studies. Nonthermal emission from spiral galaxies can arise from both disk and nuclear sources. Disk emission is predominantly due to supernova remnants and is thus related to the star formation rate. Nuclear emission can arise both from star formation and from an active nucleus. Observations of spiral galaxies in Hickson compact groups show that overall they typically show less continuum emission than those in isolated environments, a fact which is consistent with the neutral hydrogen observations. However, when considering the nuclear regions alone, the radio emission is found to be an order of magnitude higher compared to isolated spirals. The implication is that star formation and/or AGN activity is substantially enhanced in the nuclear regions of many compact group spiral galaxies. This is generally consistent with a picture in which galaxy interactions remove gas from the outer regions of galaxies, while simultaneously allowing gas to flow inwards toward the nucleus, resulting in enhanced star formation in the nuclear region, and possibly fueling an active nucleus.

Although there are clear examples of tidal interactions stimulating disk radio emission in some compact groups, statistical evidences for a link between interactions and radio emission in compact groups have been only recently found. If interactions are stimulating nuclear radio emission, one would expect the radio luminosity to be correlated with some index describing the degree of interaction such as the projected distance to the nearest neighbor. Evidences supporting this hypothesis were found observing that early type galaxies having high radio/optical emission ratio showed an excess of nearby galaxies. A similar effect was also observed in spiral galaxies in compact groups.

Further analysis of compact groups revealed that elliptical and S0 galaxies detected at a wavelength of 20 cm had closer neighbors than the undetected galaxies. The effect was not found for spiral galaxies, but if one considers only the detected galaxies, there is a significant correlation between radio-to-optical luminosity and nearest neighbor distance for both early and late type galaxies.

Continuum radio emission has also been detected in a number of HCG elliptical galaxies. Unlike those found in cluster ellipticals, the radio sources are low-luminosity and compact. Where spectral indices are available, they indicate that the radio emission arises from an AGN rather than from starburst activity. In the HCG sample, there is a significant preference for radio-loud elliptical galaxies to be first-ranked optically. The probability of radio emission does not correlate with absolute luminosity, but instead correlates with

relative luminosity within a group. Spiral HCG galaxies do not show this effect. Although the tendency of radio galaxies in rich clusters to be first-ranked has been known for many years, it is surprising to find a similar effect in small groups, where both the number of galaxies and luminosity range are small, the gravitational potential well is much less clearly defined, and it is unlikely that any individual galaxy holds a central location. It is difficult to imagine any explanation for this result in which the compact group is not a true physical system. It would appear that, regardless of absolute luminosity, only the first-ranked (presumably the most massive in the group) elliptical galaxy can develop a radio source.

6.4.5 Diffuse light

During strong interactions, stars stripped from galaxies by tidal forces can accumulate into the potential well of the group and may be detected as diffuse light. Rose (1977), found no evidence for diffuse light in his groups, and was lead to the conclusion that most of his groups must be transient configurations. Other studies instead revealed the presence of ionized gas and common haloes around many compact groups. While the expected diffuse light should be detectable with modern techniques, it would generally be very faint. Estimates of the total amount of diffuse light in the detected groups are rather uncertain as they depend sensitively on subtraction of the galactic light, and the sky background. Deeper photometry and improved image processing techniques may yet reveal diffuse light in other compact groups

6.4.6 Cool gas

The mass and distribution of cool galactic and intergalactic gas, can be obtained from observations of the 21-cm line of neutral hydrogen. Studies of large samples of compact groups found a median HI mass of $2.2 \times 10^{10} M_{\odot}$. The conclusion of such studies is that compact groups are typically deficient in neutral hydrogen by about a factor of two compared to loose groups. This effect is consistent with similar deficit in continuum radio emission seen in the disks of compact group spiral galaxies, and suggests that interactions in compact groups has removed much of the gas from the galaxies (Menon, 1991). Simulations suggest that in addition to an outflow of gas, inflow also occurs which may fuel nuclear star-formation, as suggested by the strongly-enhanced radio emission seen in the nuclear regions of compact group spiral galaxies.

High resolution studies of individual galaxies show that the gas is not confined to the galaxies. In many groups, the radio emission originates from a common envelope surrounding the group, while in other there are signs of tidal distortions. These results strongly indicate that at least these compact groups are physically dense systems and not chance alignments or transient configurations in loose groups. They also show that many groups have evolved to the point that gas contained within individual galaxies has been distributed throughout the group.

6.4.7 Hot gas

X ray observations revealed the presence of great amount of ionized gas within groups and clusters of galaxies. These observations allow the estimation of the amount, distribution, temperature and metallicity of the gas. X ray properties of poor clusters and compact groups are similar to those of rich clusters. Moreover, in many compact groups, the X emission is diffuse rather than concentrated on individual galaxies.

The presence of an hot gas halo is related to the depth of the potential well; for this reason, poor structures such as compact groups, would be not able to keep diffuse hot gas. Further investigations in fact revealed that most of this emission is associated with a shock front generated by galaxy interactions rather than gas trapped in the group potential well.

ROSAT observations revealed massive hot gas envelopes surrounding some compact groups (like HCG62) and showed that these systems are dominated by dark matter. Subsequent investigations detected X-rays from 18 additional compact groups, either from individual galaxies, or from diffuse gas. These studies showed that the physical properties of individual systems span a wide range, but that the ratio of gas-to-stellar mass is significantly lower than in rich clusters. Moreover, the detected compact groups all contained a majority of early-type galaxies and no spiral-rich groups were detected. This result is consistent with the fact that X-ray-selected groups and loose groups tend to be spiral poor, and led to the suggestion that spiral-rich compact groups might not be physically dense systems at all.

6.5 Hickson 62. I. Kinematics of NGC4778.

Authors: Marilena Spavone, Enrichetta Iodice, Giuseppe Longo, Maurizio Paolillo and Silvia Sodani

Published on Astronomy & Astrophysics, 457, 493S

Abstract

Detailed studies of the photometric and kinematical properties of compact groups of galaxies are crucial to understand the physics of galaxy interactions and to shed light on some aspects of galaxy formation and evolution. In this paper we present a kinematical and photometrical study of a member, NGC4778, of the nearest (z=0.0137) compact group: Hickson 62. The aim of this work was to investigate the existence of kinematical anomalies in the brightest group member, NGC4778 in order to constrain the dynamical status and the formation history of the group. We used long-slit spectra obtained with FORS1 at VLT, to measure line-of-sight velocity distributions by means of the Fourier Correlation Quotient method, and to derive the galaxy rotation curve and velocity dispersion profile. Our analysis reveals that Hickson 62a, also known as NGC4778, is an S0 galaxy with kinematical and morphological peculiarities, both in its central regions ($r < 5''$) and in the outer halo. In the central regions, the rotation curve shows the existence of a kinematically decoupled stellar component, offset with respect to the photometric center. In the outer halo we find an asymmetric rotation curve and a velocity dispersion profile showing a rise on the SW side, in direction of the galaxy NGC4776. The nuclear counterrotation, the distorted kinematics in the outer halo and the X-ray properties of the group suggest that NGC4778 may be the product of a recent minor merger, more reliable with a small late-type galaxy.

Introduction

Poor groups of galaxies are the most common cosmic structures and contain a large fraction of the galaxies present in the universe (Tully & Fisher 1987, Eke et al. 2004). At a difference with rich clusters, they span a wide range of densities, from loose groups, having spatial density of baryonic matter slightly above that of the field, to compact ones having densities comparable or higher than those encountered in the cores of the richest clusters. For this reason, they are the ideal ground where to test all scenarios for galaxy

formation and evolution and where to pinpoint the details of the physics controlling galaxy interactions.

Loose groups having masses in the range $10^{13} - 10^{14}$ $M_{\odot}$, almost certainly are still collapsing and are therefore crucial to uncover the formation processes shaping cosmic structures (Zabludoff & Mulchaey, 1998). Many factors converge in identifying compact groups as good candidates to be one of the regions where some of this processes occur. In first place, their high spatial density of luminous matter and small velocity dispersions imply dynamical lifetimes of the order of a fraction of the Hubble time. This leading to the possibility that the groups observed in the present time and in the local universe are second generation objects, just accreting new members from the loose groups of galaxies in which almost always they are embedded (Vennik et al., 1993). Second, compact groups are numerous and contain a non negligible fraction of the baryonic matter in the nearby universe (Pildis et al., 1996). Therefore, whatever is their ultimate fate, they are bound to have an impact on the observable properties of galaxies and cosmic structures.

As it was stressed in Mendes de Oliveira et al. (2003) (hereafter M03), the influence of environmental effects on the internal dynamics and matter distribution of compact group galaxies has not yet been clearly established, mostly due to lack of reliable kinematic data. Extensive kinematical studies of both the stars and gas in galaxies belonging to compact groups (Rubin et al. 1991; Nishiura et al. 2000; M03; Rampazzo et al. 1998; Bonfanti et al. 1999) all suggest that peculiar kinematical behaviors are much more common ($\sim 75\%$) than in the field.

Moreover, M03 showed that velocity fields of the ionized gas component in galaxies belonging to compact groups are often significantly affected by non-circular motions, local asymmetries and misalignments between the kinematic and stellar axes. These peculiarities, however, tend to smooth out if the rotation curve is derived by averaging the velocity fields of the galaxies over large regions. If these averaged values are used, a large fraction ($\sim 80\%$) of the HCG members follow the same Tully-Fisher (TF) relationship of field galaxies (M03). This may indicate that the haloes of compact group galaxies have not been significantly stripped inside their optical size. However, according to M03, the remaining 20% of the galaxies, including the lowest-mass systems, present significant anomalies which could be explained by assuming that compact group galaxies have smaller dark halos than their field counterparts, due to tidal truncation. A result which finds support in numerical simulations (cf. Governato et al. (1991)) and has important consequences on the groups dynamical lifetimes.

In spite of the vast literature existing, due both to the limited statistics and to the problems encountered in disentangling true groups from optical

ones as well as in deprojecting the measured kinematic and photometric quantities, our understanding of the dynamical and evolutionary status of compact groups still presents quite a few gaps. Gaps which can be filled only through detailed multitechnique and multiwavelength analysis of individual cases. In this respect, the dynamical and evolutive status of a group two observables are crucial: the detailed kinematics of the individual galaxies and the structure of the diffuse hot gas halo. In this paper and in Paper II (Sodani et al. 2006) we present a study of the compact group of galaxies Hickson 62 based on archival optical, spectroscopic and X-ray data extracted from the ESO and the Chandra archives.

In this first paper we focus mainly on the peculiar kinematics and on the photometry of the dominant galaxy NGC4778 (Hickson 62a), while in Paper II we shall discuss the diffuse X ray halo embedding at least two of the group components. This paper is structured as follows: in Section 6.5 we discuss the main characteristics of Hickson 62, in Section 6.5 we describe the observations and the data reduction procedure. The photometric properties of NGC4778 are presented in Section 6.9 and the kinematics in 6.5. Finally, we draw our conclusions in 6.5. Throughout this paper we shall adopt a distance of 60.9 Mpc based on $H_0 = 70$ km s^{-1}Mpc^{-1} and an heliocentric radial velocity $V = 4260$ km s^{-1}, this implies 1 arcsec = 0.29 kpc.

HCG62

Hickson 62 is a quartet of accordant early type galaxies at a redshift of 0.0137 (Hickson et al., 1988). It also belongs to the loose group LGG 313 (Rood & Struble 1994; Tovmassian 2001) containing at least 13 galaxies within a distance of $\sim$ 200 Kpc. The group is dominated by the pair NGC4778 (also known as HCG 62a) and NGC4776 (HCG 62b), having a projected separation of only 8 Kpc. NGC4778 formerly classified as an E3 galaxy, is now classified as an S0 with a bright compact nucleus, as already noticed by J. Herschel (1811), and subsequently discovered to be a low luminosity AGN (Fukazawa et al. 2001 and Coziol et al. 1998). Both NGC4776 and NGC4761 (HCG62c) are classified as peculiar S0's. Finally, NGC4764 (HCG62d) is a faint E2 galaxy slightly more distant from the center of the action. The main photometric and morphological characteristics of the group galaxies are summarized in Table 6.5.

The compact group is also embedded in a bright X-ray halo which extends out to 200 kpc, revealing the presence of a deep common gravitational well centered on NGC 4778. The high resolution Chandra images also showed the presence of large cavities in the gaseous halo due to the interaction of

	NGC4778 (HCG62a)	NGC4776 (HCG62b)	NGC4761 (HCG62c)	NGC4764 (HCG62d)
R.A.$_{J2000}$	12 53 06	12 53 05	12 53 10	12 53 06.6
δ_{J2000}	-09 12 14	-09 12 00	-09 11 55	-09 15 28
Type	S0	S0	S0	E2
Size (arcsec)	52.3×34.3	44.2×33.3	24.6×12.3	19.9×16.8
Redshift	0.0142	0.01188	0.01478	0.01392
m_v	13.47	14.04	14..86	15.98
m_b	13.79	14.21	15.00	16.30
m_r	11.25	12.04	13.59	14.11
Ext.	0.227	0.227	0.224	0.217

Table 6.1: Summary of the properties of the Hickson 62 members. Data are taken from Nasa/IPAC Extragalactic Database.

relativistic plasma with the hot IGM, a sign of recent activity due to the NGC 4778 central AGN (Vrtilek et al., 2002).

NGC4778 has been the target of several studies. Long slit spectroscopy has been obtained at different position angles. Bettoni et al. (1995) and Rampazzo et al. (1998), positioned the slit along the line joining the nuclei of NGC4778 and NGC4776 (P.A.=127°) and their results lead to the conclusion that the pair NGC4778/4776 is not interacting and the kinematical peculiarities observed in NGC4778 are likely due to an interaction with NGC4761. In fact, the velocity dispersion and rotation curves of NGC4776 are well behaved and appear unperturbed, while the velocity dispersion profile of NGC4778 shows a relatively sharp increase to the SE, suggestive of the presence of a perturber.

Observations and data reduction

Spectroscopic data

The spectroscopic data were extracted from the European Southern Observatory (ESO) public archive[3]. They have been obtained with the FORS1 spectrograph at VLT-UT1. The detector is a 2048 × 2048 pxl Tektronix CCD, with a scale of $0.2''$ pixel^{-1} (with the standard resolution collimator). The data, consisting in four set of spectra, were acquired with a slit $1.6''$ wide and $6'.8$ long, using the GRIS-600V grism with a dispersion of 49 Å mm^{-1}, corresponding to 1.18 Å pxl^{-1}, in the $4650-7100$ Å wavelength range. The spectra

[3]http://archive.eso.org/

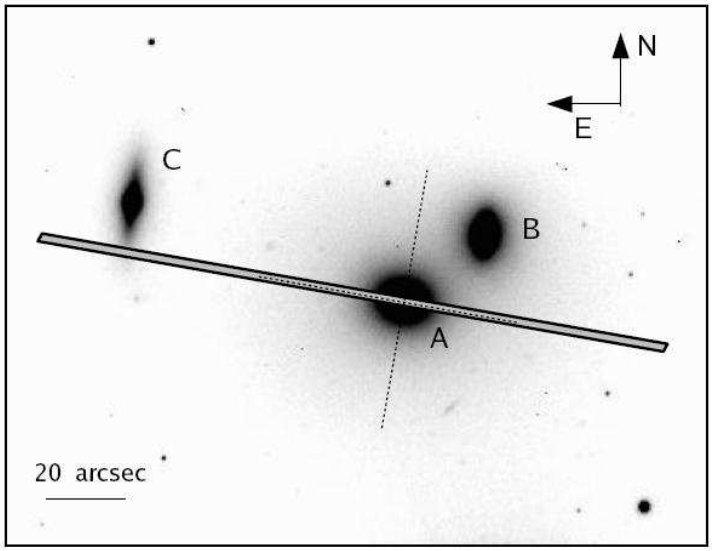

Figure 6.2: B band image of HCG62 with the slit overlayed. The dashed lines overlayed on the slit represent the directions along which we have extracted the light profiles presented in fig.6.6.

were acquired along the photometric major axis (PA=80°) of NGC4778 and, by chance, they also intercepted NGC4761 in a direction parallel to its minor axis, slightly offcentered to SE side with respect to the nucleus (see Fig.6.2).

The total integration time of the spectra is 2700 s and the average seeing turned out to be $1''$. A set of spectra of standard template F stars, were also acquired with the same configuration.

Individual frames were pre-reduced using the standard MIDAS image processing package; the wavelength calibration was made using the IRAF TWODSPEC.LONGSLIT package and a set of He-Ar-Ne lamp spectra, taken for each observing night. The spectral resolution turned out to be 2.8 Å (FWHM), equivalent to a velocity resolution of $\sigma \simeq 60\ kms^{-1}$. Sky subtraction was performed using a narrow region at both edges of the slit where there was minimum galaxy contamination. Finally, all exposures were co-added in a final median averaged 2D spectrum (cf. Fig.6.3).

The final steps of spectral processing consisted of *i*) binning the spectra along the spatial direction in order to achieve a signal-to-noise $(S/N) \geq 50$ at all radii (which is the S/N measured at the last data points, while the central pixels have S/N about 3 times larger), leaving no more than 2 data points within the seeing disk; *ii*) removing the galaxy continuum by fitting a fourth order polynomial (for a detailed description of the procedures see

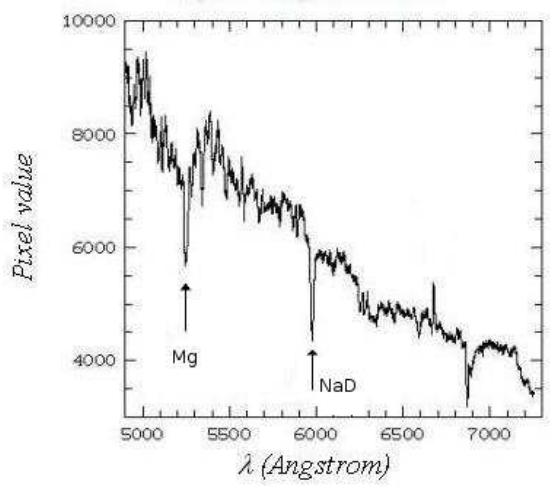

Figure 6.3: Observed spectrum of NGC4778. The main absorption features used for the kinematical analysis are marked.

Bender et al. 1994).

Imaging data for NGC4778

We also extracted from the ESO archive CCD images of Hickson 62 obtained with FORS1 at ESO VLT-UT1 in the Jonson B and R bands. The CCD was the same used for the spectra, and the exposure times were 240 seconds and 180 seconds in the B and R band, respectively. All images were taken in fairly good (i.e. FWHM $\simeq 1''$) seeing conditions. The raw CCD frames were pre-processed using the MIDAS image processing package and standard techniques for de-biasing and flat-fielding. Unfortunately, standard stars were not available to perform absolute photometric calibration and we were forced to adopt the tabulated zero point, namely: 27.594 $\pm$ 0.045 and 27.939 $\pm$ 0.025 for the B and R band, respectively. We used the IRAF-ELLIPSE task on the B band image to perform the isophotal analysis, to derive the effective parameters (the effective radius turns out to be $R_e = 13\pm\ 1\ arcsec$), and to derive the diskyness parameter, ellipticity and position angle for the NGC4778 isophotes.

Photometry of NGC4778

Here we describe and discuss the main features in the light distribution of NGC4778, in order to better understand the kinematical properties described

in section 6.5 and to examine some possible connection between photometry and kinematics.

In Fig.6.4 (top panel) we show the results of the isophotal analysis of NGC4778. For $2'' \leq r \leq 12''$, the ellipticity (ϵ), Position Angle (P.A.) and diskyness (a_4/a) are approximately constant, thus indicating that in the intermediate regions of the galaxy the isophotes are almost round, co-axial and do not significantly deviate from purely elliptical shape (Bender et al., 1994).

At larger radii (for $r \geq 12'' \sim R_e$), isophotes present increasing flattening and become more boxy (i.e. $a_4/a < 0$). Also, the P.A. changes of about $\sim 30°$. These results are consistent with those of Mendesdeoliveira (1992). Looking in more detail the nuclear regions (Fig.6.4 bottom panel), between $1'' \leq r < 2.5''$ (outside the seeing disk), a small twisting ($\sim 10°$) and an increasing flattening is observed. In the same regions a_4/a is significantly larger than zero.

In Fig.6.5 we show the average $B-R$ color profile of NGC4778. The galaxy has bluer colors in the central regions and, more precisely, we note an inversion of the trend of the color profile beyond $5''$. Even though colors may be affected by systematic errors due to the adopted calibration zero point, the mean color profile of NGC4778 is consistent with the range of values typical for early-type galaxies ($1.65 \leq B-R \leq 1.8$ Fukugita et al. 1995) and for spheroidal galaxies in compact groups ($0.9 \leq B-R \leq 1.7$ for the Es and $1.5 \leq B-R \leq 1.8$ for the S0; see Zepf et al. 1991).

The model of the luminosity distribution of NGC4778

We performed the 2-Dimensional model of the NGC4778 light distribution through the super-position of a spheroidal central component and an exponential disk (Iodice et al. 2001; Byun & Freeman 1995). The projected light of the spheroidal component follows the generalized de Vaucouleurs law (Caon et al., 1993):

$$\mu_b(x,y) = \mu_e + k\left[\left(\frac{r_b}{R_e}\right)^{1/n} - 1\right] \tag{6.2}$$

with $k = 2.17n - 0.355$, $r_b = [x^2 + y^2/q_b^2]^{1/2}$, while q_b, μ_e and R_e are the *apparent axial ratio*, the *effective surface brightness* and the *effective radius* respectively. The projected light distribution of the exponential disk (Freeman, 1970b) is given by

$$\mu_d(x,y) = \mu_0 + 1.086\left(\frac{r_d}{r_h}\right) \tag{6.3}$$

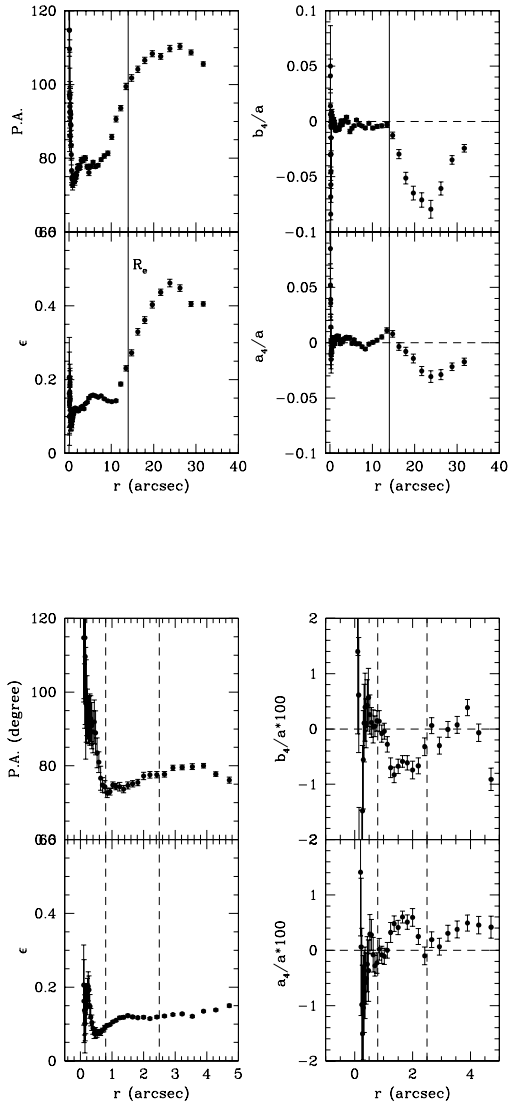

Figure 6.4: Top panel - Ellipticity, position angle (P.A.) and diskiness for NGC4778. The solid line indicates R_e. The trends of all parameters are different from those of $r < R_e$. Bottom panel - The same as above for the nuclear region of NGC4778. The first dashed line indicates the limit over which the data points are not affected by the seeing. The second dashed line marks the region discussed in the text.

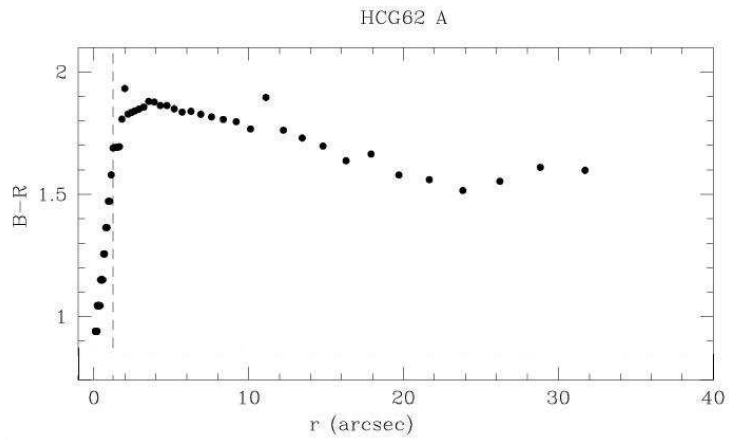

Figure 6.5: Mean B-R color profile of NGC4778. The dashed line indicates the limit of reliability of the photometry.

with $r_d = [x^2 + y^2/q_d^2]^{1/2}$, and where q_d μ_0 and r_h are the *apparent axial ratio*, *the central surface brightness* and the *scalelength* of the disk respectively.

We used: i) a model made by a bulge-like component with a Sersic law $r^{1/n}$; ii) a model made by the superposition of a bulge-like component with an $r^{1/n}$ light distribution, and an exponential disk. To take into account the systematic effect of the seeing that influence the model parameters, we masked the central area of the galaxy (within the seeing).

The better agreement of the second model with the data, strongly supports the conclusion that NGC4778 is a misclassified S0 galaxy. The structural parameters derived from the fit are: $\mu_b = 23.48 \pm 0.01$, $r_h = 21.9 \pm 0.2$ arcsec, $\mu_e = 22.55 \pm 0.01$, $r_e = 4.60 \pm 0.04$ and $n = 1.49 \pm 0.01$, leading to a bulge-to-disk ratio, $L_B/L_D \simeq 0.24$.

Fig. 6.6 shows the comparison between the observed and calculated light profiles in the B band. Residuals show that, in the SE and NE directions the fitted profiles are in agreement with the observed one. In the NW and SW directions instead, the residuals show that the observed light profile is brighter than the fitted one, due to light contamination from NGC4776. Notice that the region between $1''$ and $5''$ from the center, the fit does not reproduce the observed light profile thus suggesting the presence of an additional component for which the light distribution does not follow an $r^{1/n}$ law (Jog & Maybhate, 2006).

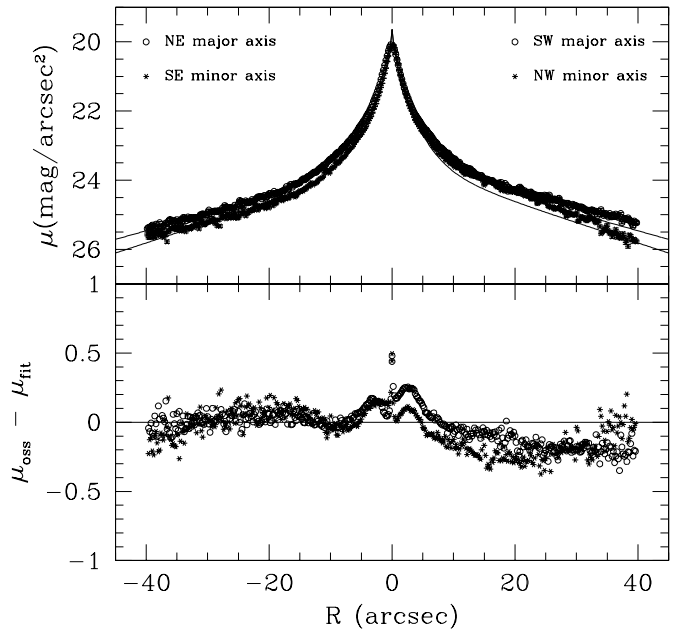

Figure 6.6: Top panel - 2-D fit of NGC4778 light distribution. The observed light profiles along the major (open circles), and minor axis (asterisk), are compared with those derived by the fit (continuous line). Bottom panel - Residuals between the observed and the fitted light profiles.

Line-Of-Sight Velocity Distribution of HCG62

The *Line-Of-Sight Velocity Distribution* (LOSVD) was then derived from the continuum-removed spectra using the Fourier Correlation Quotient (FCQ) method (Bender 1990; Bender et al. 1994). We assumed the LOSVD to be described by a Gaussian function and derived the line-of-sight rotational velocity v and the velocity dispersion σ. Main sources of statistical and systematics errors are the template mismatching and inaccurate continuum removal (the problem of error estimate was analyzed in detail by Bender et al. (1994), Mehlert et al. (2000) and Gerhard (1993)). The errors on each kinematic data-point were derived from photon statistics and CCD read-out noise and were calibrated via Monte Carlo simulations: noise is added to the template star, it is broadened according to the observed values of σ, the output kinematical values were compared with the input ones.

In Fig.6.7 (top panel) we show the line-of-sight radial velocity curve and the velocity dispersions profile for both NGC4778 and NGC4761. As the uncalibrated light profile through the slit (see Fig.6.7 bottom panel) also shows, the whole kinematic profile extends up to about 60 arcsec ($\sim$ 17 kpc) from the galaxy center, which is about $4R_e$ and the contribution of NGC4761 to the whole spectrum is always about 20%. For the study of NGC4778 we therefore extracted a region in the spectra of 50 arcsec from the galaxy center.

Kinematics of NGC4778

The rotation curve and the radial velocity dispersion profile along the major axis of NGC4778 are shown in Fig. 6.8. The kinematic profiles reveal two important features: *i)* a counter-rotation in the nuclear region, for $r \leq 2.5''$; *ii)* at large galactocentric distances (for $r > 2.5''$) the rotation curve and velocity dispersion are asymmetric with respect to the galaxy center. Note that the central value is chosen in order to obtain the rotation curve symmetric within $3''$. Given that, the dynamical center of the curves does not correspond to the photometric one, the point of maximum signal to noise ratio, which is offset by $2''$ in the NE direction.

On the whole, the galaxy presents significant rotation. An increasing rotation is measured starting from $r \sim 3''$: on the NE side, the rotation reaches a value of about 70 km/s at $r \sim 13''$ ($\sim R_e$) and then it remain nearly constant out to about $35''$ ($\sim 2R_e$). At larger radii, as we have already seen in the last section, the spectrum is contaminated by the light coming from the galaxy NGC4761, therefore the value of 200 km/s detected for $r = 55''$ cannot be due to the typical motion of the stars in NGC4778. On the SW side, the velocity increases reaching its maximum value of 80 km/s

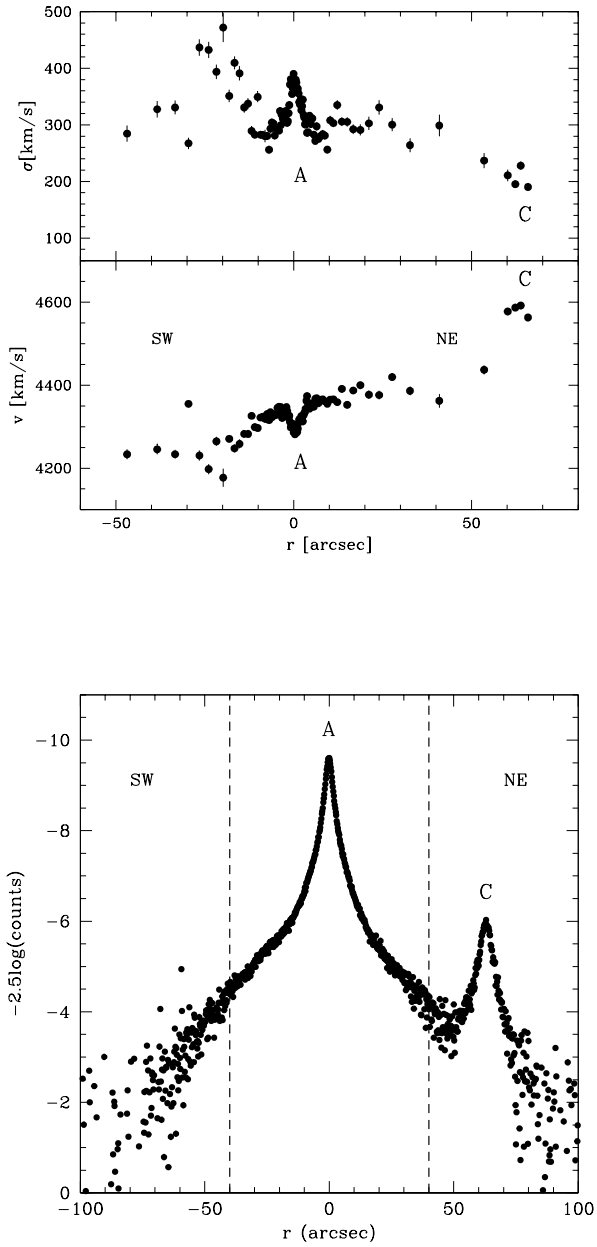

Figure 6.7: Top panel - Rotation curve and velocity dispersion profile derived for the whole slit length, which include both galaxies NGC4778 and NGC4761 (labelled on the plot as A and C respectively). Bottom panel - Uncalibrated light profile through the slit, which includes both galaxies NGC4778 and NGC4761; the dashed lines indicates the region of the spectrum used to derive the kinematics.

at $r \sim 20''(\sim 1.4R_e)$; at larger radii we observe a drop in the velocity which becomes consistent with zero at $r > 35''(\sim 2.5R_e)$.

The velocity dispersion decreases from the maximum value of about $380km/s$ in the center of the galaxy, to a value of $280-300\ km/s$ for $r > 5''$, remaining nearly constant, within the errors, up to $2R_e$. Both on the SW and on the NE side, for $3'' \leq r \leq 5''$, the velocity dispersion decreases from 380 km/s to 280-300 km/s at $r \sim 5''$. At larger radii, the velocity dispersion increases on the SW side, and reaches the maximum value of about 420 km/s (at $r \sim 20'' - 25''$), and then decreases reaching values consistent with those observed on the NE side.

Looking in more detail the nuclear region, for $r \leq 2.5''$ we detect an inversion of the velocity gradient towards the center, with a maximum value of the velocity of $20 - 30\ km/s$, with respect to the outer radii. This inversion within the central regions with respect to the overall trend, reveals the presence of a counter-rotating decoupled core. In correspondence with the inversion of the velocity gradient, the velocity dispersion profile shows an hint for a local minimum (see Fig.6.8 bottom panel).

Photometry versus kinematics

In Fig.6.9 we plot the comparison of the light profile along the slit in the NE and SW directions, where data-points were binned to reach a minimum signal-to-noise of 50. For $r > 3''$, where the kinematic shows a clear asymmetry, the light profile along the slit results unperturbed. This suggests that the peculiarities in the outer kinematical properties may be attributed to perturbed motion of the stars in NGC4778, rather than to a contamination by the light from surrounding galaxies. In particular, on the SW side, the increase detected at $r \sim 20''$ in both the rotation curve and the velocity dispersion profile, is likely due to dynamical effects rather than to a projection effect. Gravitational interactions, in fact, lead to the distortion of the orbits and a tidal heating of the stars surrounding the interacting objects (cf. Combes et al. 1995). For $r \geq 12'' \sim R_e$, where the kinematic profiles on the SW side also shows abrupt variations, we detect an increasing flattening and twisting of the isophotes.

In order to check whether the observed flattening could be attributed to the rotation or not, we evaluated the *anisotropy parameter* $(v/\sigma)^*$. The anisotropy parameter $(v/\sigma)^*$ is defined as the ratio between the observed value of (v/σ) and the theoretical value for an isotropic oblate rotator $(v/\sigma)_t = [\epsilon/(1-\epsilon)^{1/2}]$ (Binney, 1978), where ϵ is the observed ellipticity. For NGC4778, at $r \sim 2R_e$ $(\sim 30'')$, where $\epsilon \sim 0.4$, we estimate $(v/\sigma)^* \sim 0.66$. Comparing this result with those obtained by Bender et al. (1994) for a sample of

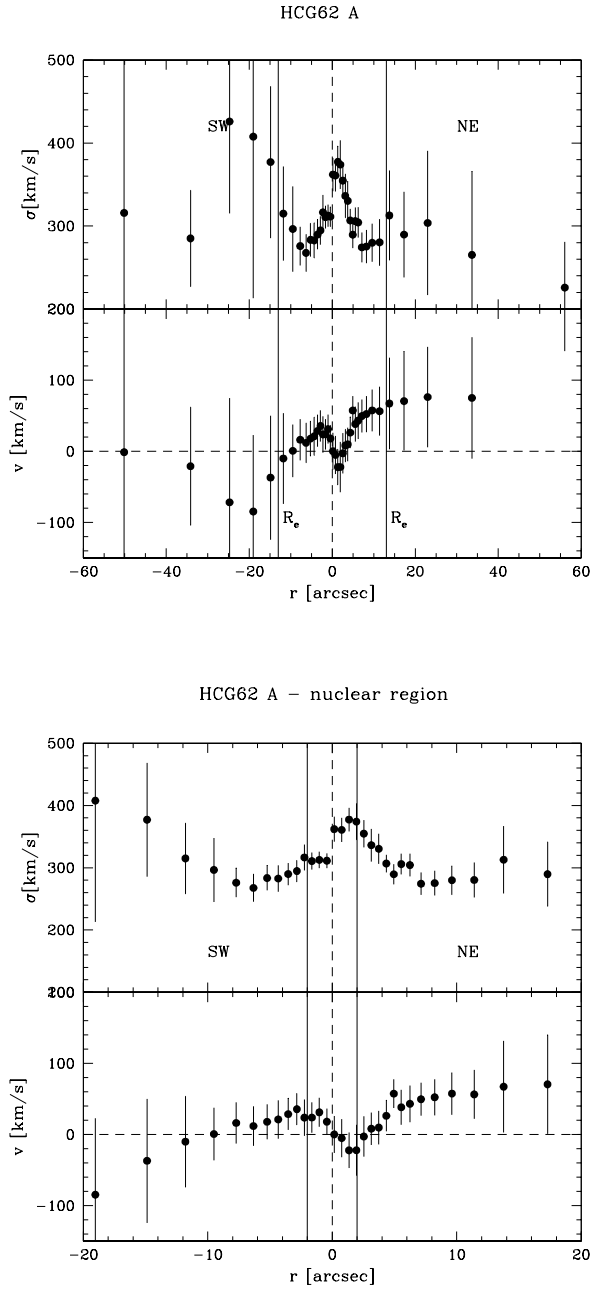

Figure 6.8: Rotation curve and velocity dispersion profile derived for NGC4778 for the whole galaxy extension (top panel) and for the nuclear regions (bottom panel) The vertical solid lines marks the regions discussed in the text.

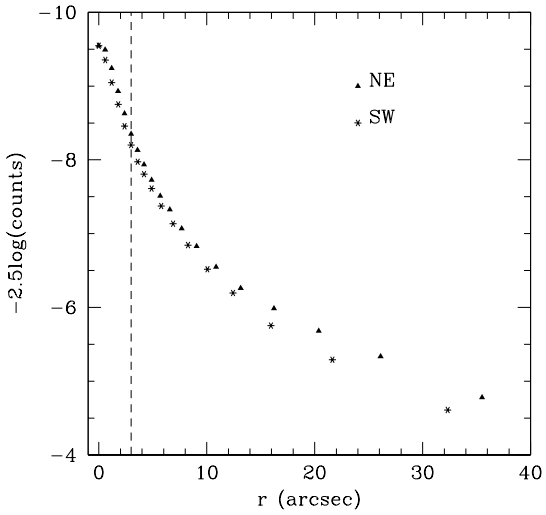

Figure 6.9: Comparison of the uncalibrated light profile along the slit in the NE and SW directions. The data-points were binned to reach a minimum signal-to-noise of 50.

44 elliptical galaxies, we find that in the $M_B - log(v/\sigma)^*$ plane[4], NGC4778 is located among the rotationally supported galaxies (see Fig.18 of Bender et al. 1994).

In the nuclear regions, where kinematic shows a decoupled component with an inversion of the velocity gradient, we have $a_4/a > 0$, which indicates the presence of disky isophotes (see Fig.6.4 bottom panel).

Discussion and conclusion

We have analyzed high signal-to-noise spectra along the major axis of the dominant galaxy of the Hickson Compact Group HCG62. On the whole, the observed kinematics and photometry of NGC4778 is consistent with that of an S0 galaxy.

-*Nuclear regions*- The higher resolution data enabled us to detect the signature of the nucleus of NGC4778: inside $3''$ we observe an inversion in the velocity profile gradient, which also correspond to some anomalous photometric features, such as bluer colors, and twisting in the position angle

[4] M_B is the total magnitude in the B band, derived from the apparent magnitude within the isophote at $2R_e$

of the isophotes. These features strongly suggest the existence of a small core ($\sim 600\ pc$) kinematically decoupled from the whole galaxy. Such anomalous Kinematically Decoupled Cores (KDC) are common in early-type galaxies and show very similar features to those observed in the nuclear regions of HCG62a: the velocity profile is characterized by a central asymmetry, to which corresponds an unusual central isophotal flattening (see Krajnović & Jaffe 2004).

Similar behavior are observed for instance in NGC3623, belonging to the Leo Triplet (Afanasiev & Sil'chenko, 2005). The central region of this galaxy, in fact, shows the presence of a chemically distinct core, a relic of a star formation burst, due to interactions, that is shaped as a cold stellar disk with a radius of $\sim 250-350\ pc$. Like NGC4778, NGC3623 also shows a drop in the stellar velocity dispersion in the nucleus. Numerical simulations (Bournaud & Combes, 2003b) predict that peculiar nuclear components may be the result of an interaction event between two galaxies. Both major merging and accretion of external material may induce that some gas does flow in to the nuclear regions of the remnant and quickly forms a small concentration of new stars that maintain the original angular momentum of the initial galaxy, counter-rotate with respect to the host galaxy. Furthermore, N-body simulations including gas, stars and star formation, suggest that galaxies can develop a central velocity dispersion drop due to nuclear gas inflow, then subsequent star formation and the appearance of young luminous stars born from dynamically cold gas (Wozniak & Champavert, 2006).

-*Formation and evolution*- Our data are in good agreement with those obtained by Rampazzo et al. (1998) along the direction connecting the nuclei of NGC4778 and NGC4776 (P.A.= 128°). They also found that the rotation curve is not symmetric with respect to the center of NGC4778, with a rapid increase in the SE direction at about 15″ from the center. The velocity dispersion increases on both sides, reaching a maximum at about 10″ from the center on the SW side. Given that the close galaxy NGC4776 is located on the NW, they suggested that *i)* the rapid variation of the rotation curve and the sharp increase of the velocity dispersion in the SE direction is a real effect, reliable due to a dynamical perturbation; *ii)* while the rise towards NGC4776 (on the NW side) could be partly an artifact due to the apparent superposition of the galaxies. The new kinematics along the SW side (presented in this work) further suggest that the South side of NGC4778 is dynamically perturbed.

As we have discussed in the section 6.5, the rotation curve of NGC4778 is not symmetric with respect to the center, and this is a feature observed in many other compact groups (Bonfanti et al., 1999). According to the literature, many compact groups mainly composed by early-type galaxies, like

HCG62, show several morphological signature of interactions, and for all of them the apparent kinematical interactions are not explainable as a mere optical superposition. This conclusion is strongly supported by the simulations performed by Combes et al. (1995), which show that the peculiarities observed in many rotation curves of galaxies belonging to compact groups are due to intrinsic effects and not to contamination along the line of sight. Our results are also in agreement with the estimates coming from merger simulations (Combes et al., 1995), that predict asymmetry in the kinematical profiles and a distinction between the photometric and the dynamical center.

The asymmetry and the shape of the rotation curve and velocity dispersion profile of NGC4778 do not find correlation with the photometric features of the galaxy, except for the bluer colors in the central region. The absence of correlation between the dynamical and the morphological peculiarities suggests that the dynamical properties of the HCG galaxies may be due to a minor merger event. In fact, as showed by Nishiura et al. (2000), weak galaxy collisions could not perturb the galaxy rotation curves, but morphological deformations could be induced in the outer parts of the galaxy (tidal tails, bridges etc), while minor mergers could perturb the rotation curves in the inner regions, especially for gas-poor early-type galaxies, without causing morphological peculiarities.

We have estimated the mass-to-light (M/L) ratio of NGC4778 in order to derive some constraints on the amount of dark matter in HCG62. Since the kinematical profiles are not symmetric, for the calculation of the M/L ratio, we have used the value of v_{max} and σ_{max} taken from the unperturbed side (NE) of the curves. Moreover, in absence of an accurate photometric calibration, we used as total B magnitude the value provided by NED, $m_b = 13.79$. Choosing the values $v_{max} \simeq 80\ km/s$, $\sigma_{max} \simeq 270\ km/s$ and $R_{max} = 34$ arcsec ($\simeq 10\ Kpc \simeq 2R_e$), by using the virial theorem $(M/L)_{vir} \simeq \frac{2R\ (\sigma^2+v^2)}{(L\ G)}$, we obtain $M/L \simeq 20.6$. This abnormally high mass-to-light ratio is compatible with a recent merging which has induced a tidal heating in the center of NGC4778, thus leading to a velocity dispersion which is too high with respect to the actual mass of the galaxy. This result however presents conflicting aspects. In fact, while such behavior is predicted by numerical simulations (Combes et al., 1995), a detailed study of the x-ray diffuse halo detected in the central regions of the group leads to a very similar virial estimate of M/L. A more detailed discussion of this point will be presented in Sodani et al. 2006.

The velocity dispersion of HCGs are generally higher than would be expected given their visible mass (even if the discordant galaxies are ignored):

this can also be explained if the bulk of the mass is in a non visible form (Hickson, 1997). Moreover, ROSAT observations revealed a massive hydrogen envelope surrounding HCG62, and showed that this group is dominated by dark matter. Both N-body and hydrodynamic simulations indicate that the dark matter halos of individual galaxies merge first, creating a massive envelope within which the visible galaxies move (Barnes 1984, Bode et al. 1993). Kinematic studies of loose groups (e.g. Puche & Carignan 1991) indicate that the dark matter is concentrated around the individual optical galaxies. In contrast, the X-ray observations indicate that in most compact groups, the gas and dark matter are more extended and are decoupled from the galaxies. This may be consistent with a M/L 30% to 50% lower in compact groups respect to isolated galaxies (Rubin et al., 1991).

The hierarchical mergers of cluster galaxies might power the emission line gas in the center of the group members (Valluri & Anupama, 1996): according to the merger scenario, in order to power emission-line nebulae, the merger must include a galaxy or a group of galaxies that are late-types and which bring with them cold gas. The observed H_α emission in NGC4778, and also in NGC4776 and NGC4761, further support the idea that this galaxy has recently experienced a merger event.

The overall scenario depicting NGC4778 as the product of a recent merger, as emerges by previous discussion, is consistent with the results obtained from X-ray observations. The presence of an extended X-ray halo is consistent with scenarios describing current compact group as the result of a first generation of mergers, where the dominant galaxy sits at the bottom of a large common gravitational well. The presence of two X-ray cavities in the hot gaseous halo located on symmetrically with respect to NGC4778 also indicate that the AGN residing in the galaxy core, must have undergone a recent (a few 10^7 yr, Bîrzan et al. 2004) active phase during which the radio-emitting relativistic plasma has created two low density regions within the hot IGM. It is commonly believed that such activity can be triggered by merging events, which increases the accretion rate onto the central massive black hole (Cattaneo et al., 2005). These fits a scenario in which NGC4778 underwent a merger sometime in the past which produced the counter-rotating core and triggered the nuclear activity. However the low incidence of strong, type I AGN activity in interacting galaxies suggests that a delay of several 10^8 years is generally expected until the peak of the AGN fase (Canalizo et al. 2006, Grogin et al. 2005, however see also Koulouridis et al. 2006). In the case of NGC4778 we can derive a lower limit of 10^7 yr for such delay from the age of the cavities. On the other end, an upper limit is represented by the age of the merger which, given the typical dynamical timescales of Compact Groups, can be estimated in 10^8 yr. This result agrees with the estimate

that AGNs have duty cycles of the order of 10^{7-8} years.

6.6 Shakhbazian Groups of Galaxies

In 1973 the Armenian astronomer R.K. Shakhbazian observed a cluster of red objects by using the *Palomar Sky Atlas*. This consisted of 17 apparently stellar objects in an area of $\sim 1'$ and initially it was classified as a stellar cluster. Later on, in 1973, by observing the spectra of 5 objects in this system it became clear that there were galaxies at a redshift z = 0.1168.

This compact group of galaxies was called *Shakhbazian I* and was described by Shakhbazian as a "compact group of compact galaxies" composed by very red objects. In the same year it started a systematic research of other compact clusters of compact galaxies (CCCG) with the same features observed in *Shakhbazian I*. This research lead to the publication, by Shakhbazyan (1973), of a list of 377 group candidates, the so called "Shakhbazian groups".

6.6.1 Selection criteria

In the following are listed the selection criteria used by Shakhbazian to identify his groups:

1. The number of galaxies in each group must be comprised between 5 and 15;
2. The apparent magnitude of individual galaxies must be in the range $14 \leq \mu$ 19;
3. The groups are "compact", so the projected distances between galaxies must be $3 \div 5$ times the typical diameter of a galaxy;
4. Almost all galaxies in a group must be extremely red;
5. Galaxies belonging to a group must be relatively compact (high surface brightness and no diffuse edges);
6. The group must be isolated in the projected space.

The selection was done visually, and these criteria introduce some bias towards systems with higher percentage of elliptical and lenticular galaxies, due to the selection in color, and a high contamination by stars, due to the compactness criterion for galaxies.

6.6.2 Mean properties

Early photometric and spectroscopic investigations suggest that Shakhbazian groups are mainly composed by massive ($\sim 10^{11} M_\odot$), luminous ($M_v \sim -22.1$) and very red ($+1 \leq \ B - V \leq \ +2$) elliptical and lenticular galaxies, that move away both from the diameter-luminosity and color-magnitude relation. They have a very compact aspect, making them easly mistaken as stars, in fact, their deprojected density is about $10^{4 \div 5}$ gal Mpc^{-3}. Measures of velocity dispersion give very low values, even lower than their statistical errors, due to the low statistic. The mass to light ratios for many groups are comparable or even lower than those of "normal ellipticals", indicating the absence of dark matter haloes, while spiral and blue elliptical galaxies are nearly absent. Most of the Shakhbazian's groups are classified in three morphological types:

1. Centrally concentrated groups;
2. Elongated groups with "chain" shape;
3. Off-centered groups.

Mass to light ratios for these groups are estimated by using the *virial mass*[5] ($M_v \sim \ 10^{12} \div \ 10^{13} M_\odot$) and the total luminosity ($L \sim \ 10^{12} L_\odot$); the values obtained turn to be lower than those derived for clusters of galaxies and giant ellipticals (respectively $\sim \ 100$ and $\sim \ 50$), leading to the conclusion that these structures have no dark matter haloes. The estimated *crossing times*[6] ($t_{cr} \sim \ 10^{8 \div 9}$ yr) are much lower than the Hubble time[7], giving the possibility to these structures to dynamically evolve in $\sim \ 1$ Gyr.

More recent and accurate measurements, allow to better understand the main characteristic of these groups of galaxies, even if their true nature is still matter of debate. These recent measurements confirmed the great abundance of elliptical galaxies in Shakhbazian's groups, but not their peculiarity in mass, luminosity and color, putting them again in the color-magnitude diagram: galaxies in these groups, although very luminous, are non peculiar el-

[5] In astronomy, the virial mass has different meanings depending on the context. In the context of Dark matter halos of galaxies or galaxy clusters, Virial mass refers to the mass within the virial radius r_{vir}, a radius within which a spherical "top hat" density perturbation destined to become a galaxy is collapsing. In other contexts, it may refer to the mass inferred from the rotation curve or velocity dispersion of a bound collection of stars as determined by assuming the virial theorem applies.

[6] The time it takes a particle to travel from one point in its orbit to another point 180 degrees away.

[7] The inverse of the Hubble constant and a crude measure of the universe's age.

lipticals. Moreover, also velocity dispersion and mass to light ratios measurements converge towards values similar to those found for Hickson compact groups and loose groups ($\sigma \sim 200 \div 250 kms^{-1}$, $M/L \sim 100 \div 200 M_{\odot}/L_{\odot}$).

The axial ratios distribution of SHK's groups, with a mean value of $< b/a >= 0.5$, shows that these groups tend to be very prolate structures. They are often found between two close clusters and tend to form a "bridge" between them, and this could be the reason for the very prolate configuration.

6.7 Characterizing Shakhbazian Groups of Galaxies

Authors: Silvio Barbati, Giuseppe Longo, Maurizio Paolillo, Marilena Spavone

In preparation

Abstract

Poor groups of galaxies are the most common cosmic structures. However, due to the poor statistics, projection effects and the lack of accurate kinematics, our understanding of the dynamical and evolutionary status of compact groups is still limited. In our recent study of the Shakhbazian (SHK) sample, after confirming the physical nature of most groups, we reached the conclusion that their peculiar properties with respect to those of the well known Hickson sample are due to the contamination of the SHK sample from more extended and/or massive structures embedding them. This suggests that they are second generation structures, whose peculiar properties are driven by the environment in which they form. In order to confirm this, we propose to perform MOS observations of a sample of 10 compact galaxy groups in order to obtain a controlled sample and constrain mass, dynamical status and evolutionary timescales, together with the spectral properties of their members.

Introduction

Poor groups of galaxies are the most common cosmic structures and contain a large fraction of the galaxies present in the universe (Tully & Fisher 1987, Eke et al. 2004). At odd with rich clusters, they span a wide range of densities, from loose groups, having spatial density of baryonic matter slightly above that of the field, to compact ones having densities comparable or higher than those encountered in the cores of the richest clusters. For this reason, they are the ideal ground where to test galaxy formation and evolution scenarios and where to pinpoint the details of the physics controlling galaxy interactions. The best studied sample of compact groups to date is the one included in the Hickson catalogue (Hickson, 1982). Hickson compact groups have much higher spiral fractions than expected from the universal morphology-density relation (Mamon, 1986). Conversely, these compact groups are spiral poor relative to other systems of the same velocity dispersion, but with a strong

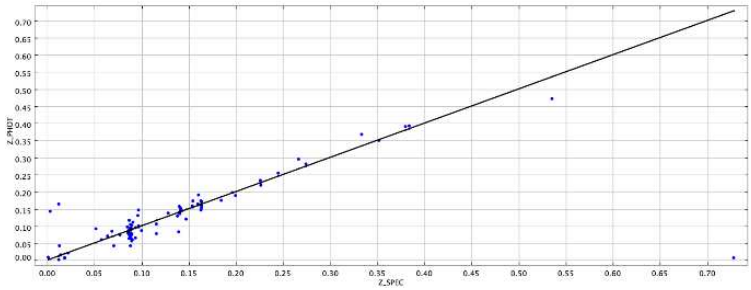

Figure 6.10: Photometric versus SDSS spectroscopic redshifts for galaxies in the SHK 348 region. The plot shows all objects within 3 Mpc, from the group centroid, with available SDSS spectroscopic redshift. Only a few compact group members, i.e. within the central 200 kpc, have spectroscopic redshift.

inverse correlation of spiral fractions and velocity dispersion (Hickson et al. 1988, Weinmann et al. 2006).

The Hickson sample, however, is biased towards extremely high values of matter density and therefore it allows to investigate only the close-to-final stage of the complex dynamical process which rules the evolution of galaxy groups from their accretion to their final collapse into a single massive merger remnant. The density range bridging the field to these almost coalesced structures is still poorly explored, mainly due to the difficulties encountered in constructing reliable samples of 'physically bound', low multiplicity groups.

Shakhbazian groups of galaxies

The Shakhbazian Groups of Galaxies, (SHKGs) in spite of having been originally selected as "compact groups of compact galaxies", due to the less restrictive selection criteria adopted by their discoverers (see sec. 6.6), have been shown to sample a large range of spatial densities (Shakhbazyan 1973, Baier & Tiersch 1979, Stoll et al. 1993, Stoll et al. 1997). In an ongoing effort to study the low density regime of cosmic structures in the local Universe we have performed a systematic study of all the SHKGs covered by the Sloan Digital Sky Survey. Unfortunately only a minority of SHKGs have measured spectroscopic redshifts, and often only for one or two galaxies in each group. However, using accurate photometric redshifts, derived with neural network tools by D'Abrusco et al. (2007) ($\sigma_{z_{phot}} \simeq 0.02$, Fig. 6.10) and a series of diagnostics which are detailed in Capozzi et al. (2009) we found that $> 80\%$ of these groups are real structures.

This result is intriguing in light of the fact that SHKGs are missing in other catalogues of galaxy groups. Only 2 SHK groups in the SDSS are in common with the Hickson sample. The overlap with other published studies of galaxy groups is also extremely poor (e.g. SDSS: Tago et al. 2007, Berlind et al. 2006; 2dF: Eke et al. 2004, Plionis et al. 2007; UZC: Focardi & Kelm 2002; also see Lee et al. 2004). This is most probably due to the fact that they are not as isolated and thus are entirely missed by detection algorithms looking for isolated and compact structures. Also, studies of groups in the SDSS have been based so far on the spectroscopic dataset, which is highly incomplete for environments as dense as the Shakhbazian groups. In our work we found that only a minority ($< 10\%$) of candidate group members belong to the SDSS spectroscopic sample.

From the morphological point of view, Baier & Tiersch (1979) showed that SHKGs, as expected from their selection criteria, are on average rich in early type (E/S0) galaxies (77% against 51% in HCGs and 40% in the field), which are on average very red ($B - V \geq 1.0$ and $R - K = 2.9$, Tovmassian et al. 2007). Using photometric criteria (e.g. Strateva et al. 2001), we studied the morphological content of SHKGs and found that more than 90% of the SHKGs have indeed Early-Type fractions $f(E) > 0.6$. The overabundance of Early-Type galaxies is however confined to the group core since when we consider the morphological content of the local environment ($150 < r < 1000$ kpc) and background ($2 < r < 3$ Mpc) we observe that the Early-Type morphological fraction decreases outward (see Fig. 6.11, right panel). Following the same approach, we also estimated $f(E)$ for a subsample composed of all HCGs with $z_{spec} \geq 0.03$, located within the SDSS. When compared with our subsample of HCGs, we find that SHKGs have somewhat higher values of $f(E)$ (see Fig. 6.11, left panel), especially considering that our HCG subsample is biased toward high Early-Type fractions ($f(E) \sim 40\%$ vs 30% in the complete HCGs sample).

In order to investigate the properties of SHKGs, in terms of compactness and isolation, we compared our estimate of the group richness measured within 150 kpc (N_{150}) and within 500 kpc (N_{500}) (Fig. 6.12). Our analysis shows that SHKGs present heterogeneous properties ranging from objects with $N_{500} \simeq N_{150}$, i.e. fairly compact and isolated groups, to more extended structures for which $N_{500} > N_{150}$. Using the *extension index* $EI = N_{500}/N_{150}$ we divide the sample in *compact* ($EI \leq 1.5$) and *extended* ($EI \geq 1.5$) groups (Fig. 6.13). A trend for the SHKGs can be observed with increasing richness (Fig. 6.13, left panel): rich SHKGs (with $N_{150} \geq 7$) are mostly embedded within extended structures (EI ≥ 1.5), while poorer ones ($N_{150} < 7$) are a mixture of isolated and more extended objects (likely [core+halo] configurations). On the other hand we find that the analyzed HCGs are dominated by

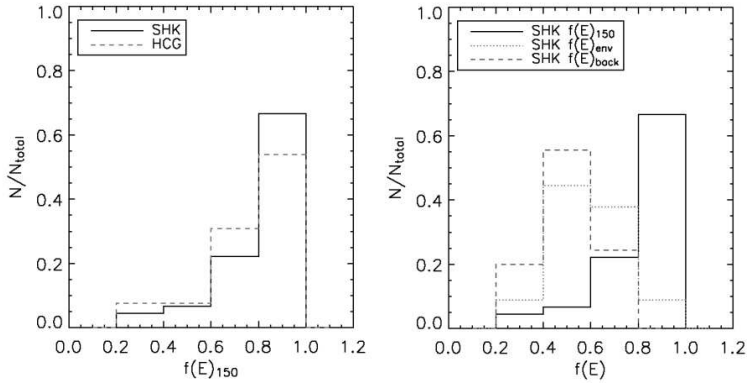

Figure 6.11: **Left panel:** normalized f(E) distributions for the inner regions of the SHKGs (solid line), and of the HCGs (dotted line). **Right panel:** Early-Type fraction distributions for SHKGs in the core ($r < 150$ kpc, solid line), local environment ($150 < r < 1000$ kpc, dotted line) and background ($2 < r < 3$ Mpc, dashed line).

concentrated structure (Fig. 6.13, right panel), as expected from the stricter isolation selection criteria used to identify them: less than 15% of the sample has an extension index larger than 2, to be compared with $> 40\%$ for SHKGs. Also note that rich SHKGs have, on average, high Early-type fractions.

Our analysis thus suggests that, contrary to what previously thought (see for instance Tiersch et al. 2002), SHKGs are an extremely heterogeneous class of objects which includes both cores of rich, extended structures and compact, isolated groups. The differences with HCGs are mainly due to the contamination of the sample by richer extended structures which have no counterpart in the analyzed HCG sample.

Similarly, while the large fraction of Early-Type gas-poor galaxies found in SHKGs could partly explain the fact that enhanced FIR emission was detected in only a small fraction ($\sim 7\%$) of them (Tovmassian et al., 1999) in contrast to the more pronounced excess found in HCGs ($> 60\%$), again note that the SHK sample is biased toward larger Early-Type fractions due to the contamination of rich, extended systems (Fig. 6.12, 6.13).

A further comparison with the properties of the well studied Hickson sample reveals that velocity dispersion of SHKGs (where available) appear to be generally higher (≥ 300 km/s, Fig. 6.14) and crossing times smaller ($t_c \sim 90$ Myr), than those of most compact groups. However neglecting the presence of an extended halo inevitably leads to underestimates of the crossing times (e.g. Zandivarez et al. 2003).

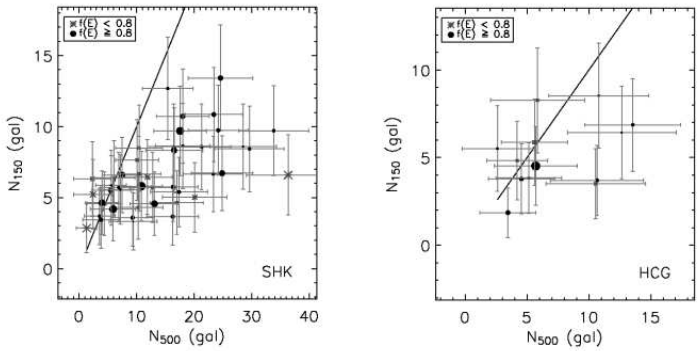

Figure 6.12: Background subtracted group richness estimated within 150 kpc versus background subtracted richness within 500 kpc. The line shows the expected locus for isolated compact groups. Groups with $f(E) < 0.8$ and $f(E) \geq 0.8$ are plotted, respectively, as grey asterisks and black dots. The size of the symbols is scaled according to the group redshift. **Left panel:** Shakhbazian groups. **Right panel:** Hickson groups.

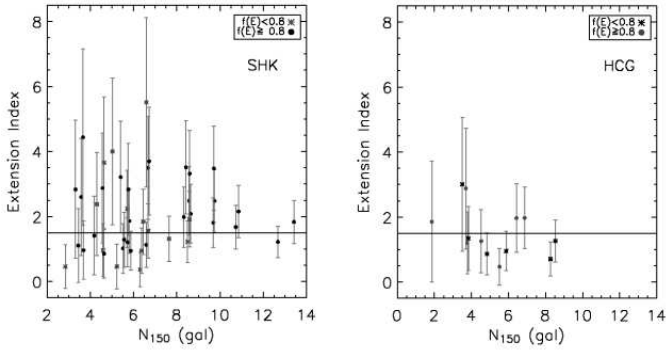

Figure 6.13: Extension index vs N_{150} for SHKs (left panel) and HCGs (right panel). Solid line for extension index = 1.5 is plotted. Groups with $f(E) < 0.8$ and $f(E) \geq 0.8$ are plotted, respectively, as grey asterisks and black dots.

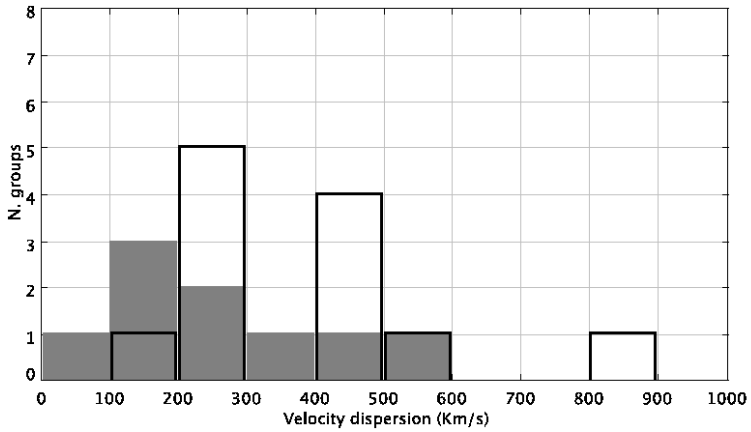

Figure 6.14: We observe a tentative evidence that more concentrated SHK groups (grey filled histogram) have lower velocity dispersion than less concentrated ones (open black histogram), thus suggesting that the total mass plays a significant role in the evolution of these structures. However the small statistics does not allow to draw significant conclusions, especially when groups with less reliable velocity dispersion estimates ($\sim 2/3$ of the total) are removed from the sample. Furthermore the subsample of SHK groups with measured velocity dispersions is strongly biased toward rich/extended structures.

Aim of the work

SHKGs have not been intensely investigated and still little is known about their properties and state of evolution. Available data for SHKGs are of poor quality: the few detailed works available in literature are devoted to the rich end of the catalogue, and 3/4 of the groups with robust velocity dispersion belong to the extended subsample. Most of the claims (relatively high velocity dispersions, short crossing times, etc.) have hence to be revisited, since they are biased towards richer structures, which are possibly also the more massive ones and reside in peculiar environments.

To this aim, we have acquired data, with two accepted proposal at Telescopio Nazionale Galileo (TNG), to obtain redshift measurements for ~ 10 SHK groups overlapping the area covered by the SDSS, selected in order to uniformly sample the different sub-populations present in this heterogeneous catalogue, and which are confirmed 3D overdensities according to our photometric redshift estimates. We stress that the size of the sample is chosen in order to obtain statistically robust conclusions, removing the selection biases that affected many results published so far, through a candidate selection method based on a homogeneous analysis of a large SDSS sample. Furthermore, the number of proposed targets will allow to double the number of groups with robust velocity dispersion estimates and mainly sample the lower richness systems which have been poorly probed so far, while still keeping the observing time within reasonable limits. Our sample will be integrated with the few Shakhbazian (~ 7) groups in the SDSS for which accurate velocity dispersion measurements are already available in literature.

Observation and data reduction

We obtained spectra for all galaxies brighter than $r = 20$ within $\sim 5' \simeq 500$ kpc from the group center and within $z_{phot} =< z_{phot} > \pm 3\sigma$, thus deriving redshifts for more than 20 objects per group. This will allow to constrain the velocity dispersion of these structures and to estimate their virial radii. Accurate and homogeneous estimates of their richness, crossing times, masses and M/L ratios will hence be feasible, which will allow to put strict constrains on the dark matter content, dynamical timescales and evolutionary state of these structures. Furthermore, using photometric redshift we are able to effectively identify candidate targets for MOS spectroscopy, thus maximizing the observing efficiency. Furthermore, recent works (e.g. de la Rosa et al. 2007) have shown that the ages and metallicity of elliptical galaxies in Fossil Groups are different from those of HCGs, thus indicating the need to revise

the current belief that such compact groups will evolve in a massive merger remnant. These findings challenge the standard hierarchical model as applied to low redshift systems and in this context it is vital to understand which place SHK groups occupy in the evolutionary path of small scale structures.

We will hence be able to: i) obtain redshift estimates for groups without literature data, sampling the different sub-populations identified based on our richness and concentration criteria; ii) confirm the galaxy membership of the groups, which is currently based on photometric estimates for most of the objects; iii) study the dynamical status of the group and derive dynamical mass estimates; iv) study the stellar population of the member galaxies through comparison of H_β and $[Mg/Fe]$ diagnostics with population synthesis models, in order to infer ages and metallicities of the dominant early-type population as done by de la Rosa et al. (2007) for HCGs, as well as the degree of activity from emission line measurements.

The knowledge of the redshift and velocity dispersion is crucial to derive the evolutionary timescales and constrain the mechanism that led to the formation of structures with such an high fraction of early-type galaxies. In particular we intend to investigate the relationship between the intrinsic properties of the group (mass, M/L ratio, extended dark matter halos, f(E), etc.) and those of the surrounding environment, in order to understand if these groups are part of a continuous sequence leading to the formation of richer and more evolved structures or they represent different evolutionary paths.

To achieve the scientific goals of the project we used DOLORES on the TNG telescope to obtain low resolution MOS and long slit spectroscopy of > 20 galaxies for each group of our sample. The TNG provided an acceptable efficiency and instrumental setup to complete our program in a limited number of nights, since our groups are relatively close $z < 0.2$.

Data reduction has been performed with standard astronomical software (IRAF, MIDAS) to obtain galaxy redshift through cross-correlation with available templates. Population synthesis models (STARLIGHT, SSP-MILES) have been used to study the stellar populations of target galaxies. We also used self-written code to include the resulting data in our study of large scale structures through the analysis of massive multi-wavelength datasets (e.g. SDSS).

Preliminary results

SHK groups probe an environment with characteristics which are intermediate between those of loose and very compact groups. We analyzed Multi

Table 6.2: Main results for SHK's group

SHK	R_{vir} (kpc)	L ($L_\odot$)	M/L	σ (km/s)	z_{mean}	z_{median}	z	$\tau_{TOV}(10^6 yr)$	$\tau(10^6 yr)$	N (gal)	IE
10	281	1.19×10^{11}	32	540	0.146	0.1346	0.1346	35	59	5	3.43
71	247	4.79×10^{10}	77	480	0.1129	0.1131	0.1133	26	40	6	1.52
75	475	1.23×10^{11}	87	660	0.1652	0.1657	0.1652	37	73	5	3.94
80	105	1.02×10^{11}	10	480	0.1295	0.1302	0.1307	17	31	5	2.04
259	143	1.27×10^{11}	17	450	0.1515	0.1519	0.1518	17	34	7	1.1

Object Spectra (MOS) of a subsample of SHK's group, extracted from the whole set of observation obtained at TNG, in order to identify possible group members in photometric redshift space and to derive, for each group, several individual properties (richness, size, mean photometric redshift, fraction of red galaxies, etc.). In Tab. 6.2 are summarized the main results obtained.

Group properties

We estimated the mean and median spectroscopic redshift by using the biweight method. This study confirmed that the majority of groups are physical entities with richness in the range 3-13 galaxies, and properties ranging between those of loose and compact groups. Moreover, we also confirm that the more extended structures represent a mixture of core+halo configurations and cores of rich clusters.

Richness

We derived, for all SHK groups, richness estimates within 150 and 500 kpc; in Fig. 6.15 we compare our richness estimates with those performed by Tovmassian et al. (2006) for their sample of SHK's groups. We find that all the analyzed groups fall in the region where $N_{500} > N_{150}$, i.e. these are on an average richer structures.

Mass-to-luminosity ratio

Our values of M/L (Fig. 6.16) are consistent with Tovmassian et al. (2006), who show that SHK groups appear to be embedded into large, loose structures. The mean values of M/L, consistent with what found in HCGs $M/L \sim 35$, is sensibly lower than what usually observed in rich clusters ($M/L \sim 210$). However, we find that groups near the diagonal in this plot and with lower M/L are less massive with respect to those with an higher M/L. We thus confirm the distinction in two classes of groups, already discussed by Capozzi et al. (2009), one composed by a pure core structure and another one of core+halo structures.

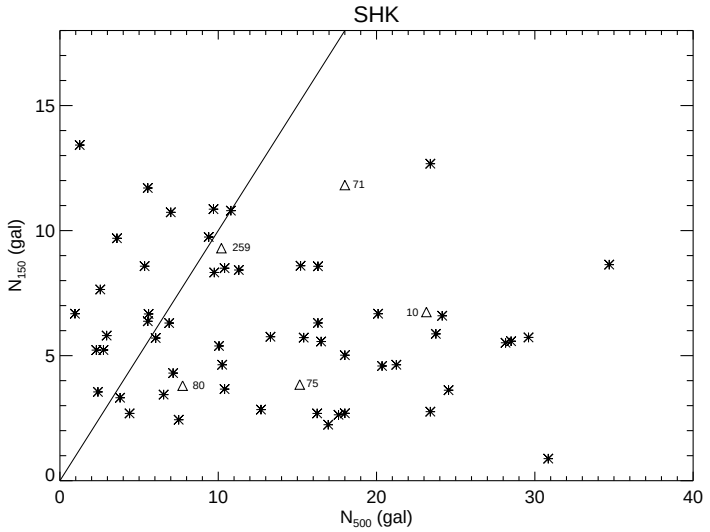

Figure 6.15: Comparison between our richness measurements and those performed by Tovmassian et al. (2006)

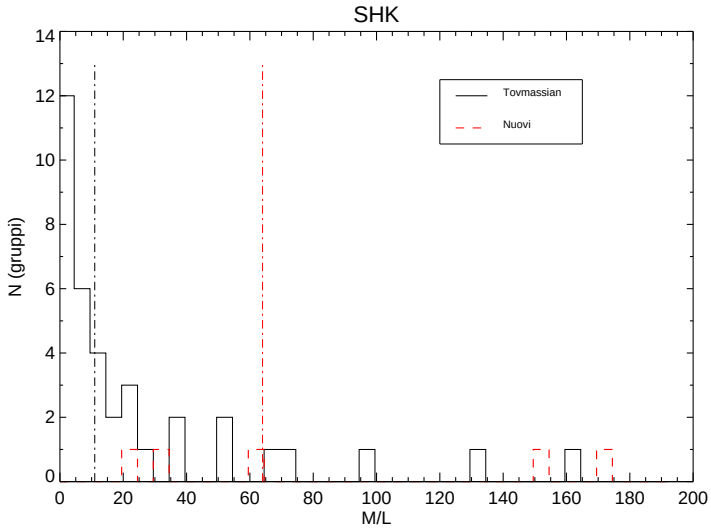

Figure 6.16: Comparison between the mass to light ratio measurements in our sample and those performed by Tovmassian et al. (2006)

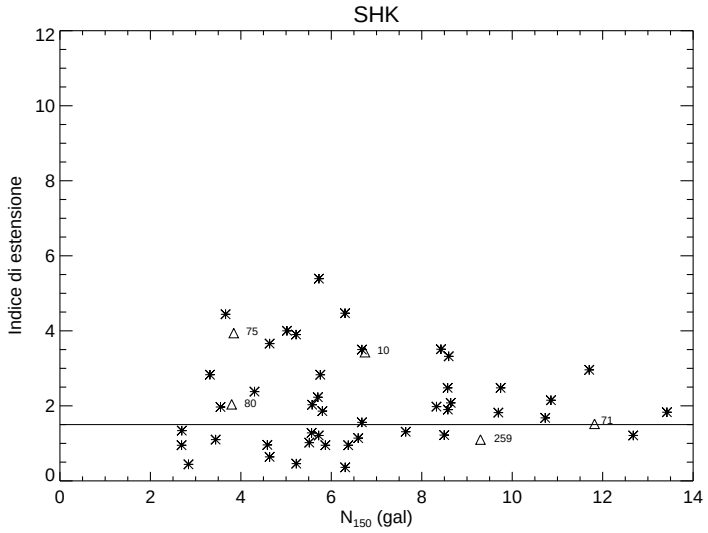

Figure 6.17: Extention index versus N_{150} for SHK groups. Solid line for extention index = 1.5 is plotted.

Extension

We divided the sample in *compact* and *extended* groups, depending on their *extention index* defined as $EI = N_{500}/N_{150}$ (see Fig. 6.17).

We find that the majority of rich groups ($N_{150} \geq 7$) is embedded within extended structures ($EI \geq 1.5$), while poorer structures (with $N_{150} < 7$) are a mixture of compact and extended objects, likely core+halo configurations, as already discussed in above.

Mass and velocity dispersion

In Fig. 6.18 we show the correlation between EI and the velocity dispersion of our groups.

We find that extended groups have on average a higher velocity dispersion, and are on average more massive, than isolated groups, suggesting that our SHK groups sample includes rich extended systems.

We also compare our estimates of the velocity dispersions with those performed by Tovmassian et al. (2006), finding that groups in our sample have higher velocity dispersions and are more massive (see Fig. 6.19 and 6.20). This could also be due to the fact that Tovmassian et al. (2006) estimated the velocity dispersion only in the very central regions, where σ is lower, while in our measurements we use also the outer halo.

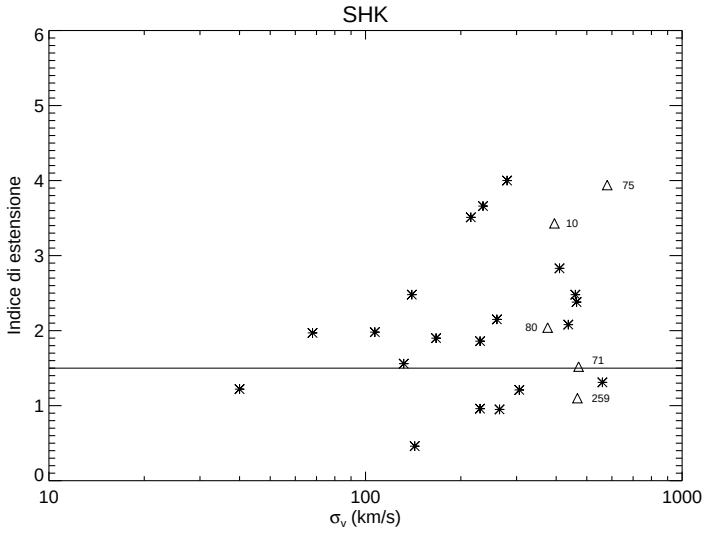

Figure 6.18: Extention index versus σ for SHK groups. A logarithmic scale on x-axis is used.

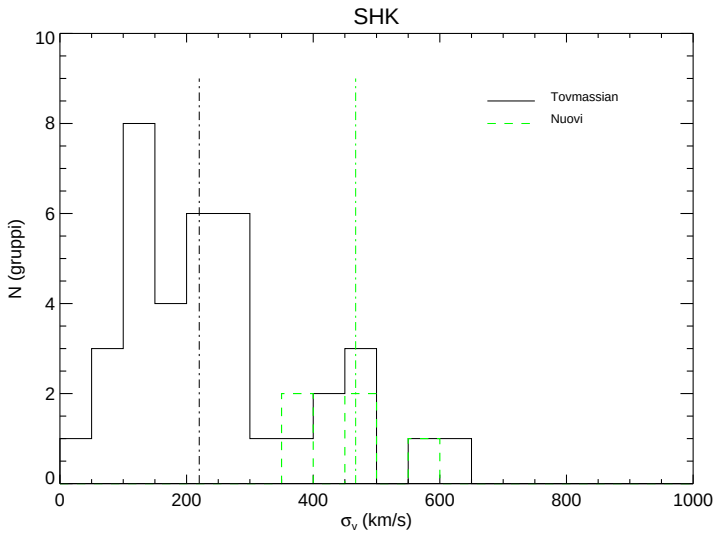

Figure 6.19: Comparison between the velocity dispersion of groups in our sample and those estimated by Tovmassian et al. (2006).

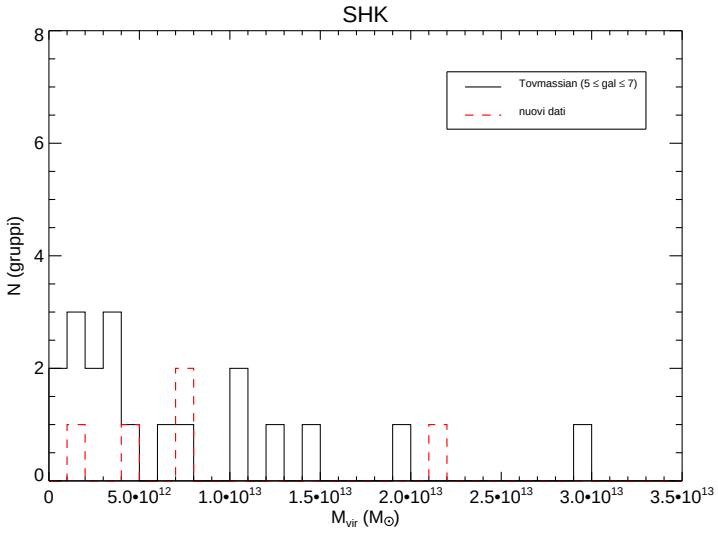

Figure 6.20: Comparison between the masses of groups in our sample and those estimated by Tovmassian et al. (2006).

6.8 The role of dry mergers in galaxy formation

Recent investigations of the role of dry mergers in the build up of massive galaxies within the cold dark matter paradigm (Khochfar & Silk, 2009), reveal a nearly constant dry merger rate of $\sim 6 \times 10^{-5} Mpc^{-3} Gyr^{-1}$ at $z \leq 1$ and a steep decline at larger z. Less than half of these mergers are between two galaxies that are morphologically classified as early-types, and the other half is mostly between an early- and late-type galaxy. Latter are prime candidates for the origin of tidal features around red elliptical galaxies.

Mergers are fundamental to the cold dark matter paradigm of structure formation. They not only drive mass evolution by merging smaller dark matter haloes into larger ones, but they also change the morphology of galaxies from late to early-type (e.g. Toomre & Toomre 1972; Barnes & Hernquist 1992), and drive gas to the center of the merger remnant that triggers star formation and active galactic nucleus (AGN) activity.

Early structural studies (Bender et al., 1992) hinted at the mass-dependent importance of dissipation during their formation: massive elliptical galaxies are mainly formed from dry mergers of early-type galaxies, while less massive ones show mixed mergers between an elliptical and a spiral galaxy. Only elliptical galaxies well below $L_\star$ are predominantly formed by wet mergers from two spiral galaxies. Ia has also been argued that the strong size evolu-

tion of massive early-type galaxies provides evidence for dry merging. In an attempt to model the size-evolution of early-type galaxies, Khochfar & Silk (2006) showed that the amount of dissipation during mergers can account for the observed size evolution. In their model, dry mergers result in remnants with larger sizes than remnants from gaseous mergers of the same mass. Similar results have been reported from numerical simulations of mergers with varying degrees of gas fractions by Cox et al. (2006).

The existence of a characteristic mass scale, below which the cooling time t_{cool} of a collapsing gas cloud is shorter than its dynamical time t_{dyn}, allowing for efficient collapse on a dynamical time-scale and subsequent star formation. In massive dark matter haloes with $M_{DM} > 10^{12} M_{\odot}$, one generally finds $t_{cool} \gg t_{dyn}$ and that shock heating of the collapsing gas supports the formation of a hot, static atmosphere at the halo virial temperature (Birnboim & Dekel, 2003).

From an observational point of view, the existence of a bimodality in the properties of the galaxy population, occurring at a mass scale of $M_{\star} > 3 \times 10^{10} M_{\odot}$, lends support to the notion of a transition in the mode of galaxy formation (Dekel & Birnboim, 2006). Hence, one expects that dry merging will occur when cooling is sufficiently delayed at masses above a transition mass scale and if the reservoir of cold gas in the galaxy is used up by star formation before the merger happens.

It's then likely that most elliptical galaxies formed through nearly dissipationless, or "dry", mergers of red, bulge-dominated galaxies rather than mergers of spiral disks. Even if mergers between early-type galaxies are statistically unlikely, as the median field galaxy is an Sb spiral, most mergers likely occur in groups, in which the early-type galaxy fraction is much higher than in the general field. Furthermore, semianalytical models of galaxy formation have predicted that the most recent mergers of bright ellipticals were between gas-poor, bulge-dominated galaxies, and several studies have shown that such merging is consistent with the observed fundamental plane relation. Finally, mergers between red galaxies may be common in young, unvirialized galaxy clusters at $z \sim 1$.

6.8.1 Morphological signatures

Mergers between gas-poor, bulge-dominated galaxies are generally more difficult to recognize than mergers between gas-rich disks. Elliptical-elliptical mergers do not develop prominent tidal tails dotted with star-forming regions but are instead characterized by the ejection of broad "fans" of stars and, in certain cases, an asymmetric deformation (off-centering) of the inner isophotes (Combes et al., 1995). Tails may develop if one of the progenitors

rotates or has a disk component (Combes et al., 1995), but as there is no cold, young component, these are expected to be more diffuse than those seen in encounters between late-type galaxies.

When two hot stellar systems collide, the central parts of the merger remnant quickly settle in a new equilibrium configuration, whereas the material in the outer parts, where dynamical timescales are long, gradually becomes more diffuse. The surface brightness of tidal features associated with this type of merger is comparatively low; the features consist of old, red stellar populations and have higher M/L ratios than the blue tails associated with mergers of late-type galaxies. Furthermore, they are typically more diffuse, due to the lack of a cold disk in the progenitors. After the merger, the evidence of the past encounter becomes increasingly difficult to detect as dynamical evolution reduces the surface brightness further.

Models predict also kinematic features, such as U-shaped velocity profiles in the pair components and a velocity dispersion enhancement between the galaxies (Combes et al., 1995). The origin of U-shaped rotation curves comes from the truncation of the faint envelopes towards the companion, and the corresponding velocities approaching the center of mass velocity. Simulations show that this effect is intrinsic, and not due to contamination along the line of sight.

6.9 CSL-1: a prototype of dry merger caught in the act

Authors: Maurizio Paolillo, Giovanni Covone, Carlo Nipoti, Marilena Spavone, Massimo Capaccioli, Giuseppe Longo, Andrea Cimatti and Luca Ciotti

In preparation

Abstract

On January 2006, the Hubble Space Telescope (HST) observed the peculiar double extragalactic object CSL-1; the high resolution image show that the object is a pair of interacting giant elliptical galaxies at redshift z = 0.46. In this paper we present a detailed structural and morphological study of the main properties of this system in order to test whether the *Dry merger* is a possible scenario for CSL-1. To reach this scientific goal we use medium to high resolution observations obtained with FORS1@VLT, HST/ASC and TNG@DOLORES.

Introduction

Mergers play an important role in the formation and evolution of galaxies in the cold dark matter paradigm of structure formation. They not only drive mass evolution by merging smaller dark matter haloes into larger ones, but they also change the morphology of galaxies from late to early-type (Toomre & Toomre, 1972), drive gas to the center of the merger remnant that triggers star formation and and active galactic nucleus (AGN) activity.

Minor merging events, in which the mass ratio is lower than 1/3, are important for $L_\star$ galaxies, while major merging are considered one of the most important physical mechanism in the assemblement of the present day massive elliptical galaxies.

Early structural studies of elliptical galaxies by Bender et al. (1992) already hinted at the mass-dependent importance of dissipation during their formation. In a first systematic study of the morphology of merging pairs in a CDM galaxy formation model, Khochfar & Burkert (2003) could show that massive elliptical galaxies are mainly formed from dry mergers of early-type galaxies, while less massive ones show mixed mergers between an elliptical and a spiral galaxy. Only elliptical galaxies well below $L_\star$ are predominantly formed by wet mergers from two spiral galaxies.

Subsequent work on the role of dry mergers revealed that they can explain the formation of slow rotating boxy ellipticals, that they lie on the fundamental plane, follow the $M_\star - \sigma$ relation and that they could possibly explain the formation of a stellar density core in the center of the remnant due to a binary black hole merger.

Recent numerical models (Eliche-Moral et al., 2010) predict that wet major mergers have controlled the massive early type galaxies buildup since $z \sim 1$, although dry and mixed mergers have also played an essential role in it. The bulk of this assembly took place at $0.7 < z < 1$, being nearly frozen at $z \leq 0.7$ due to the negligible number of major mergers occurred per massive early type galaxies since then. The models also suggest that major mergers have been the main driver for the observational migration of mass from the massive end of the blue galaxy cloud to that of the red sequence in the last $\sim 8Gyr$.

But why it is important to catch in act such events?
First of all, it makes possible a detailed comparison with simulations, allowing us to test our knowledge of these phenomena. Then, we have clues to understand how the scaling relations (Fundamental Planes, Photometric Plane) are affected by this class of mergers: do progenitor galaxies follow the same scaling relations as the resulting galaxies appear to follow in the local universe?

However, debate on the role of dry merging in the formation of massive early type galaxies is still open.

In this paper we present a detailed analysis of a dry merging event at intermediate redshift, involving two very similar elliptical galaxies, with nearly equal luminosity $L \simeq L_\star$. The merging system (previously known as CSL1 Sazhin et al. 2003) is found in the Capodimonte Deep Field, OACDF (Alcalá et al., 2004).

Throughout this paper we shall adopt for CSL-1 a distance of about 1851 Mpc based on $H_0 = 75\ km\ s^{-1}\ Mpc^{-1}$ and an heliocentric radial velocity $V = 138804 \pm 1499 km\ s^{-1}$, which implies that $1 arcsec \sim 9 kpc$.

Observations and data reduction

HST observations

Milliarcsecond-resolution deep images of CSL-1 were collected in January 2006 using the ACS/WFC on Hubble Space Telescope. The object was observed for 6 HST orbit in the F814W band (comparable to Johnson-Cousins I-band), yelding and effective exposure time of ~ 14000 seconds. The obser-

Table 6.3: General properties of CSL-1

Parameter	Value	Ref.
Morphological type	G Pair	NED[a]
R.A. (J2000)	12h23m30.6s	NED
Dec. (J2000)	-12d38m57s	NED
Helio. Radial Velocity	138804 km/s	NED
Redshift	0.463	NED
Distance	1851 Mpc	
V Magnitude	20.7	NED

[a]NASA/IPAC Extragalactic Database

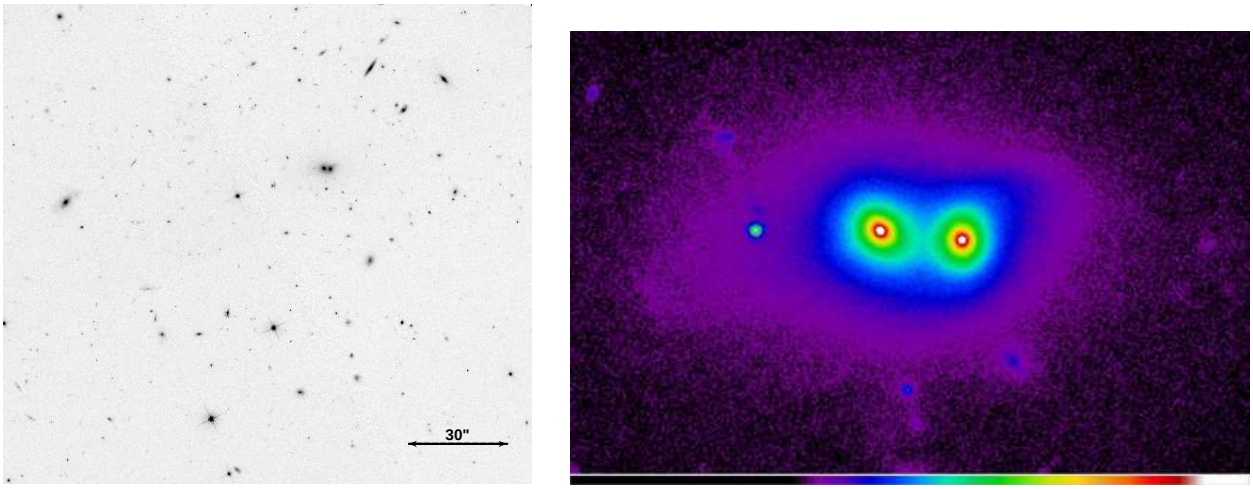

Figure 6.21: Left: The HST image of the CSL-1 region in the F814W band. Right: CSL-1 image in pseudocolor.

vations were performed adopting a 1/3 pixel dither pattern, to allow sub-pixel sampling of the HST PSF and cosmic ray rejection. All 6 orbits were combined through the Multidrizzle software Koekemoer et al. (2002) using a 1/2 pixel (0.025 arcsec/pixel) resampling pattern. In Fig. 6.21 we show the final stacked image of the whole field and a close-up on the CSL-1 system.

Spectroscopy

The spectra used in this work were acquired with FORS1@UT1 spectrograph on the ESO Very Large Telescope (VLT), in March 2005, under Director's Discretionary Time (proposal 274.A-5039).FORS1 was equipped with the E2V CCDs with an angular resolution of $0.25''pixel^{-1}$. The adopted slit was

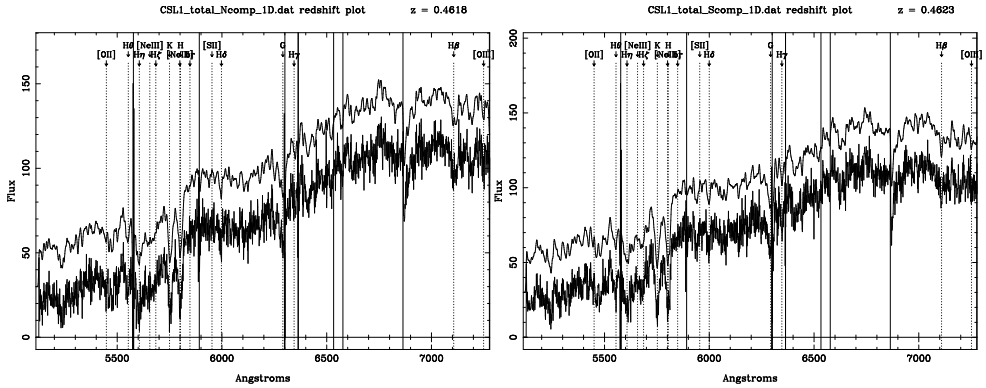

Figure 6.22: Spectra of the E (left) and W (right) components of CSL-1. The raw spectrum is shown on the bottom while a slightly smoothed version is showed above it. Flux normalization is arbitrary.

1.0″ wide and spectra were acquired setting the slit across the centers of the two components of CSL-1 at $P.A. = 130°$ (see Fig. 1 in Sazhin et al. (2003)). The grism 600V+GG435 was used, in the wavelength range $4430 \leq \lambda \leq 7370$, with a dispersion of 49 Å/mm, and the observations were split into several exposure, to avoid saturation and to allow for a better removal of the bad pixels and cosmic rays, and the total integration time was 4740 s.

The risk of cross-contamination between the spectra of the two components was minimized by retaining only the six frames with an average S/N of 12 and a point-spread function FWHM of < 1 arcsec for a total exposure time of 4740 s.

The data reduction was carried out using the CCDRED package in the IRAF[8] (*Image Reduction and Analysis Facility*) environment. The main strategy adopted for each data-set included dark subtraction[9], flatfielding correction, sky subtraction and rejection of bad pixels. Finally, all frames were registered and co-added to form the final science frames. Wavelength calibration was achieved by means of comparison spectra of Ne-Ar lamps acquired during the observing run, using the IRAF TWODSPEC.LONGSLIT package. The sky spectrum was extracted at the outer edges of the slit and subtracted off each row of two-dimensional spectra by using the IRAF task BACKGROUND in the TWODSPEC.LONGSLIT package. The sky-subtracted frames were co-added to a final median averaged 2D spectrum.The spectra are of the two components are shown in Fig. 6.22.

[8]IRAF is distributed by the National Optical Astronomy Observatories, which is operated by the Associated Universities for Research in Astronomy, Inc. under cooperative agreement with the National Science Foundation.

[9]Bias frame is included in the Dark frame.

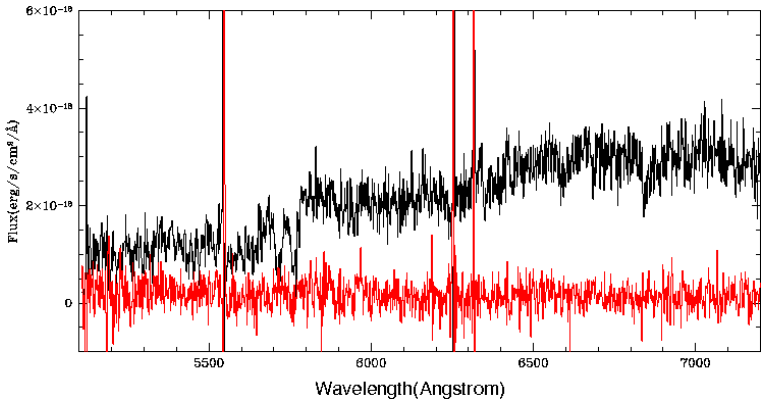

Figure 6.23: Flux calibrated spectra of the two components of CSL-1.

The final step of data processing is the flux calibration of each 2D spectra, by using observations of the standard star EG247 and the standard IRAF tasks (STANDARD, SENSFUNC and CALIBRATE). To perform the flux calibration, we extracted 1D spectrum of the standard star to find the calibration function, then we extracted a set of 1D spectra of the galaxies summing up a number of lines corresponding to the slit width. Since the slit width was 1.0″ and the scale of the instrument was $0.2''/pixel$, we collapsed five lines to obtain each 1D spectrum. Finally we applied the flux calibration to this collection of spectra. The wavelength and flux-calibrated spectra are shown in Fig. 6.23.

Photometry: morphology, light distribution and structural parameters

Radial profiles

Radial profiles of both the E and W components were extracted (Fig. 6.24) avoiding the overlap region where the cross contamination is more severe. Furthermore a second profile was extracted removing a slice of $\sim 80\,\mathrm{deg}$ coinciding with the tidal tails shown in Figure 6.25. The resulting profiles including and excluding the tidal tail regions is shown in Figure 6.24.

2-Dimensional model of the light distribution

We performed a 2-dimensional model of the light distribution in the HST F814W band. To this aim, we used the GALFIT task (Peng et al., 2002),

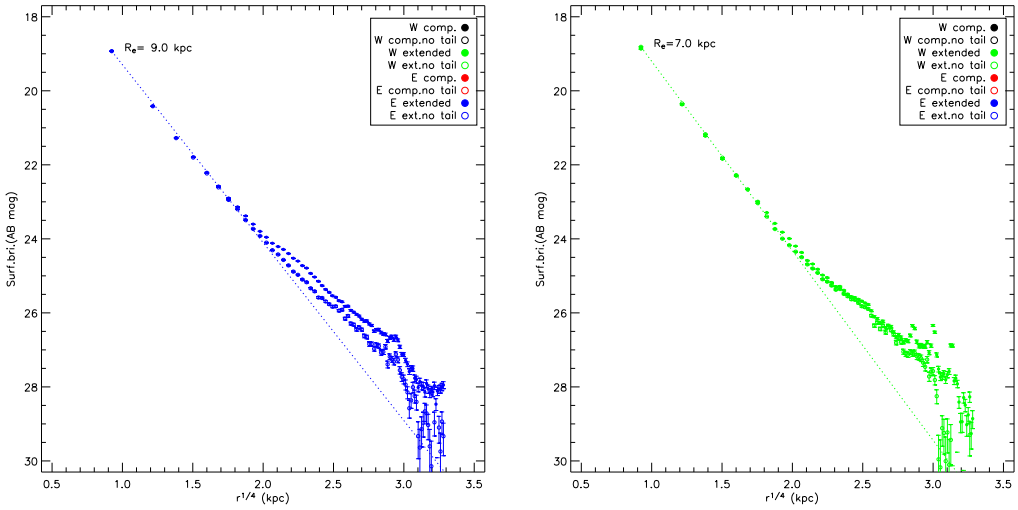

Figure 6.24: Radial profiles of the E (left) and W (right) components of CSL-1. An $r^{1/4}$ profile with the best fit R_e is shown for comparison.

Table 6.4: 2D fitting results from F814W ACS images

Parameter	E component	W component
R_{eff} (kpc)	10.6	7.9
Sersic index n	6.1	5.8
$\bar{\mu}_e$	21.8	21.4
M_{tot}^{model}	-23.5	-23.3
b/a	0.8	0.9
$P.A.$	54.3	-11.1
$Disky(+)/boxy(-)$	0.16	0.06

using the error maps generated with Multidrizzle as weights and masking nearby sources detected with SExtractor. As a first attempt and according to the morphological classification given for CSL-1 (see Tab.6.3) as a pair of Elliptical galaxies, the galaxy light is modelled through a single Sersic law (Sersic, 1968).

We fit the two objects with two Sersic (Sersic, 1968) light profiles, obtaining the best fit values reported in Table 6.4. The residual image, presented in Fig.6.25, clearly shows the presence of warped structures in the CSL-1 outskirts, most probably tidal tails due to the interaction between the two galaxies.

We used *GALFIT* to study the structure of the galaxies in CSL-1, with the main aim to estimate their structural parameters, in order to obtain the

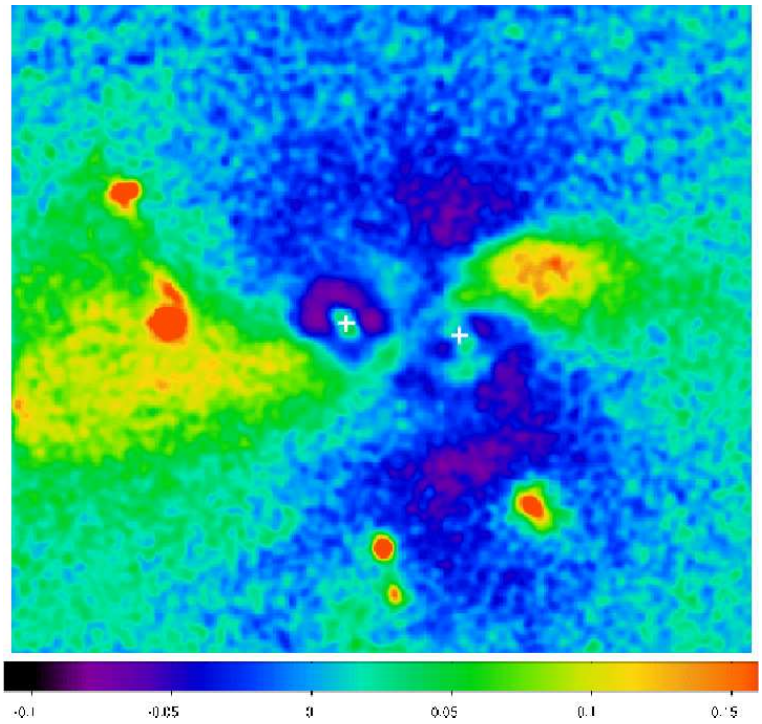

Figure 6.25: The normalized residuals (residuals/model) obtained by subtracting from the HST images a model consisting of two Sersic light profiles. Crosses mark the centroids of the two galaxies.

photometric and the fundamental plane for this system and to compare them with the properties of elliptical galaxies.

We used the *GALFIT* best-fit parameters to compare them with the properties of elliptical galaxies. The results are shown in Figure 6.26 for the Faber-Jackson relation and the Kormendy relation.

These figures show that the two component of CSL1 are placed on the scaling relations of elliptical galaxies and are located in the region where "bulge dominated ellipticals" are found.

Radial velocity and internal velocity dispersion

A cross-correlation analysis of the two spectra based on the CaII (H and K), H_β, H_δ and H_γ lines and the G band, yields a velocity difference between the two components of $\Delta\ v = 14 \pm 30$ km/s, which reduces to $0 \pm\ 20$ km/s if we exclude the H_β line which is affected by residual instrumental effects.

To measure the internal velocity dispersion of the two components we used the ppxf software by Cappellari & Emsellem (2004). We adopted the K stellar templates from the Indo-US Coudé spectrograph, which has an accuracy of $\sigma\ \sim\ 22$ km/s. Fitting only v and σ, we derive $\sigma_E = 260 \pm\ 9$ km/s and $\sigma_W = 220 \pm\ 7$ km/s for the E and W components respectively. Excluding bright sky lines and telluric features we find $\sigma_E = 257 \pm\ 10$ km/s and $\sigma_W = 195 \pm\ 8$, while using only a selected line set we obtain $\sigma_E = 262 \pm\ 13$ km/s and $\sigma_W = 182 \pm\ 8$.

Stellar population synthesis

In order to obtain light-weighted measurement of age and mean content of the stellar populations in each of the two merging galaxies, we used the software STARLIGHT (Cid Fernandes et al., 2005) on the VLT spectra. We obtained the results shown in Fig. 6.27.

The main result coming from this plots is that the bulk of the star formation happened approximately at $1 \times\ 10^{10}$ Gyr.

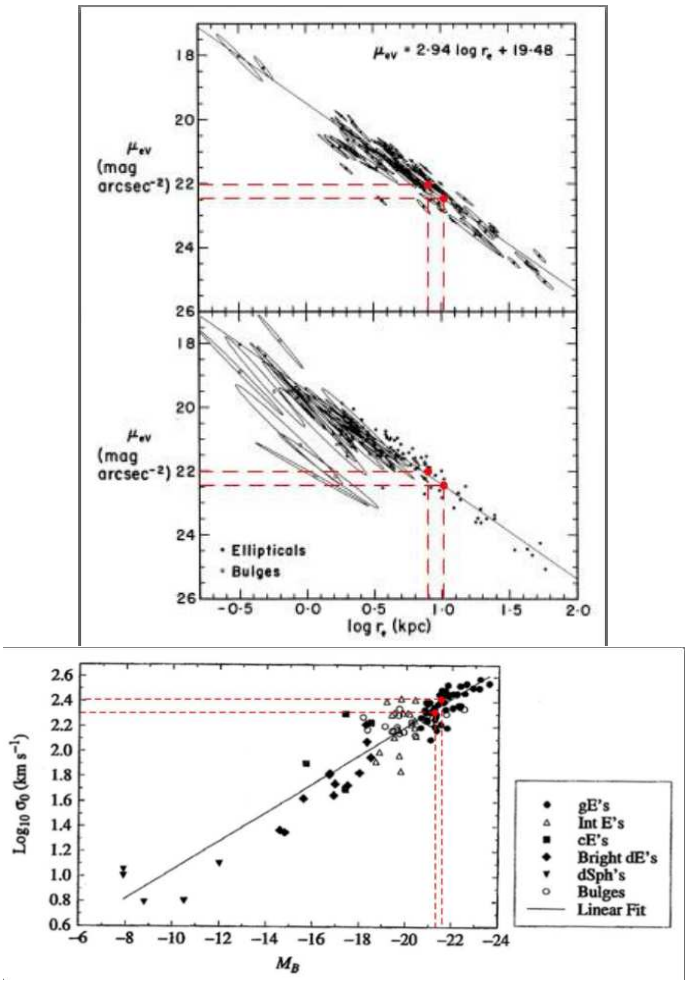

Figure 6.26: The CSL1 components on the Kormendy (left), adapted from Hamabe & Kormendy (1987) and Faber-Jackson (right), adapted from Faber & Jackson (1976) relations.

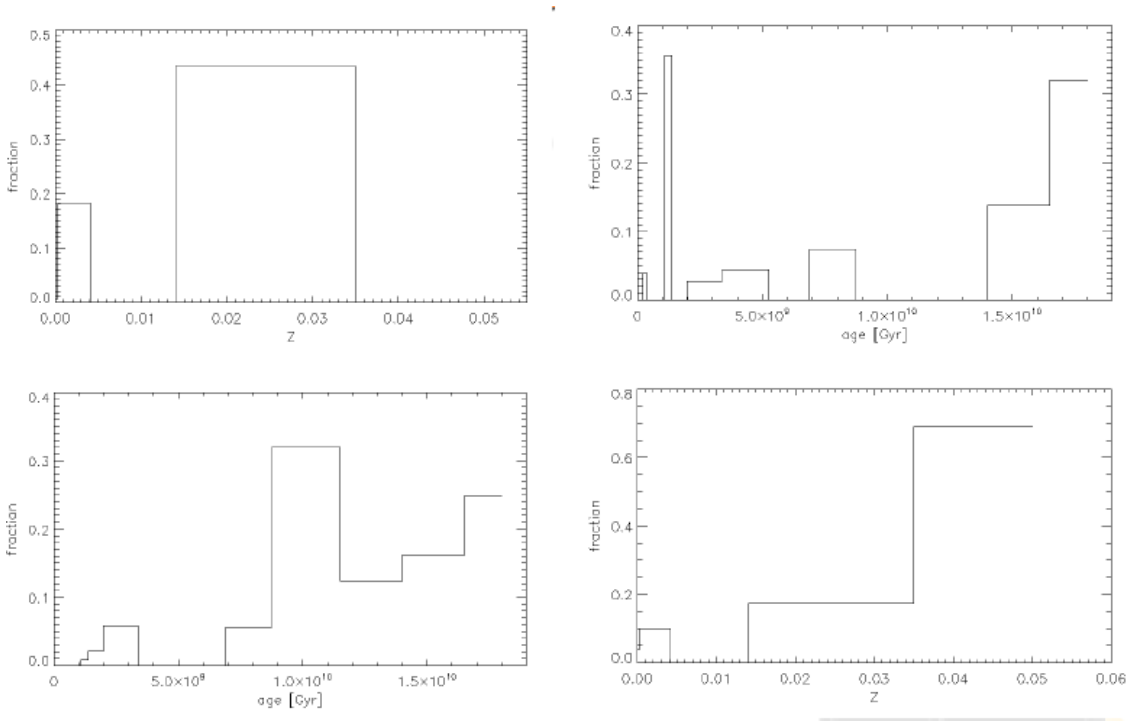

Figure 6.27: The four panels show the age and the metallicity distribution for the E (left) and W (right) galaxies respectively. Quantities were derived by fitting the VLT optical spectra with the software STARLIGHT.

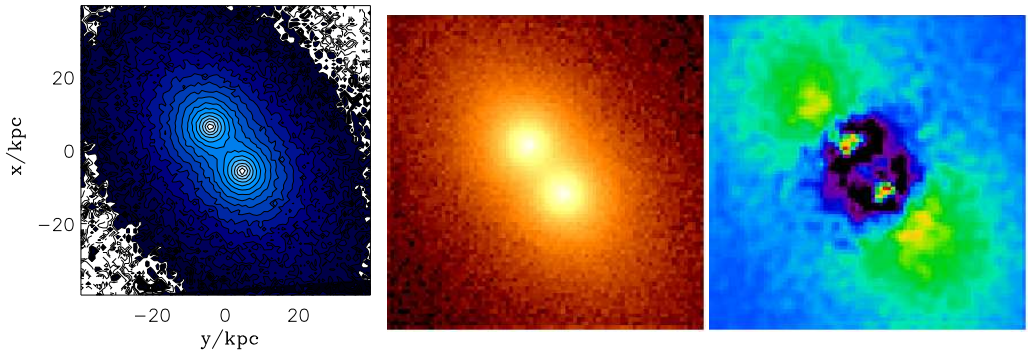

Figure 6.28: One of our simulations (left two panels) and residuals obtained from a 2D Sersic fit (rightmost panel).

Comparison with simulations: testing the dry-merger scenario

We also performed a set of simulations with different initial configurations and compared them to our data. Results are shown if Fig. 6.28 and 6.29, Fig. 6.30 and 6.31.

CSL1 is clearly an interacting system, given the small separation between the two components, relative line of sight velocities comparable with zero and evident tidal tails. However, at the present stage, none of our simulation is able to reproduce the observed residuals and surface brightness profiles. A possible responsible for this effect could be the rotation of both galaxies in the plane of the sky, that can lead to a phase displacement thus forming the observed tails.

We are also analyzing the environment of CSL1, estimating the number counts in the CSL1 field (see Fig. 6.32) by using different SExtractor threshold, and comparing it with the OAC-DF and HDF counts.

There are no evident bumps in this plot, indicating the presence of over-densities in the field, except for a small indication around 19. We can then conclude that CSL1 is in a low density environment, probably near a small group.

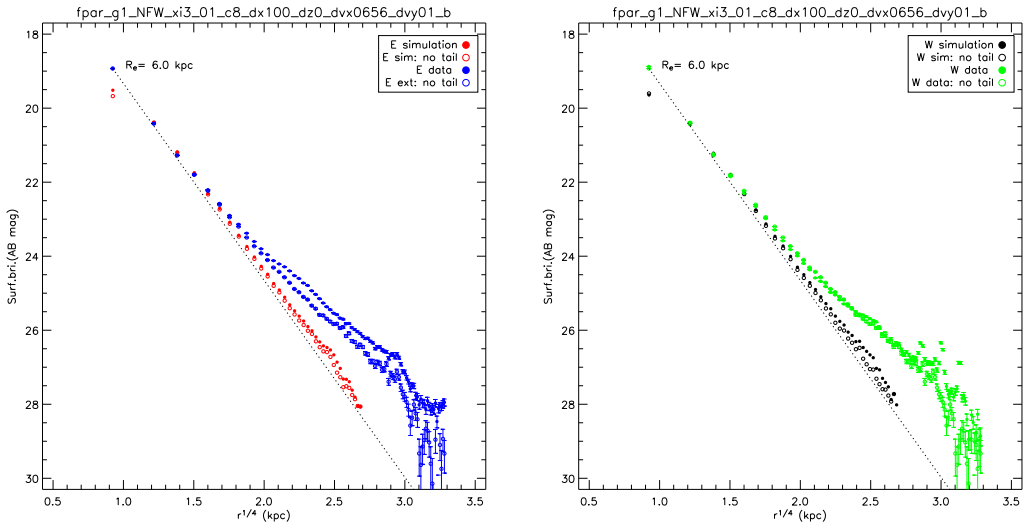

Figure 6.29: Radial profiles of the E and W components of the simulations shown above, compared with the actual data

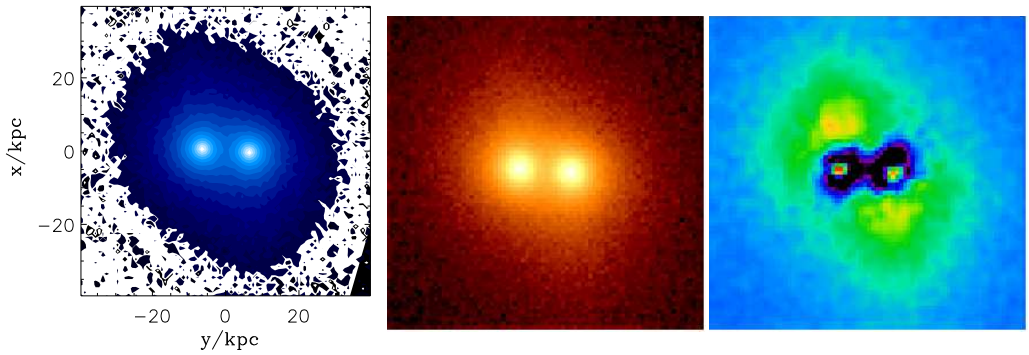

Figure 6.30: One of our simulations (left two panels) and residuals obtained from a 2D Sersic fit (rightmost panel).

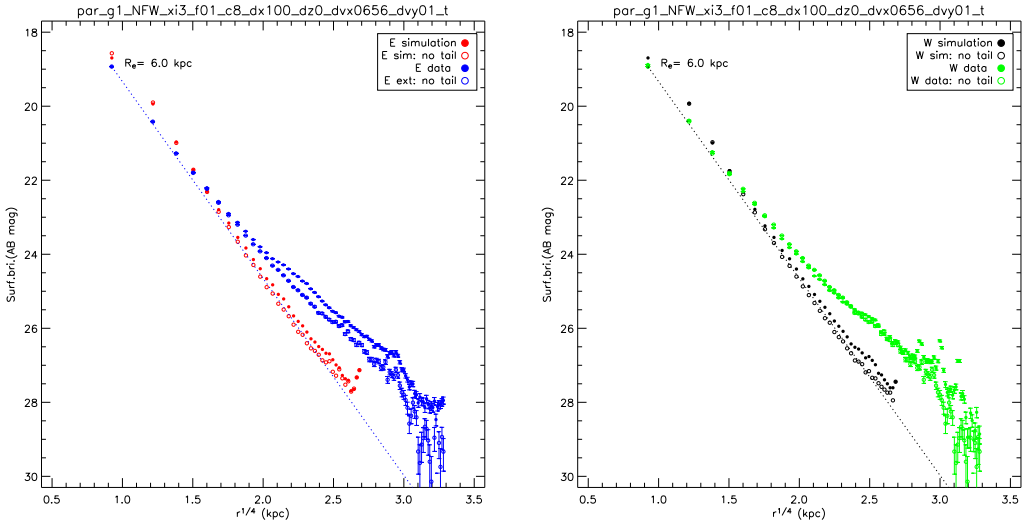

Figure 6.31: Radial profiles of the E and W components of the simulations shown above, compared with the actual data

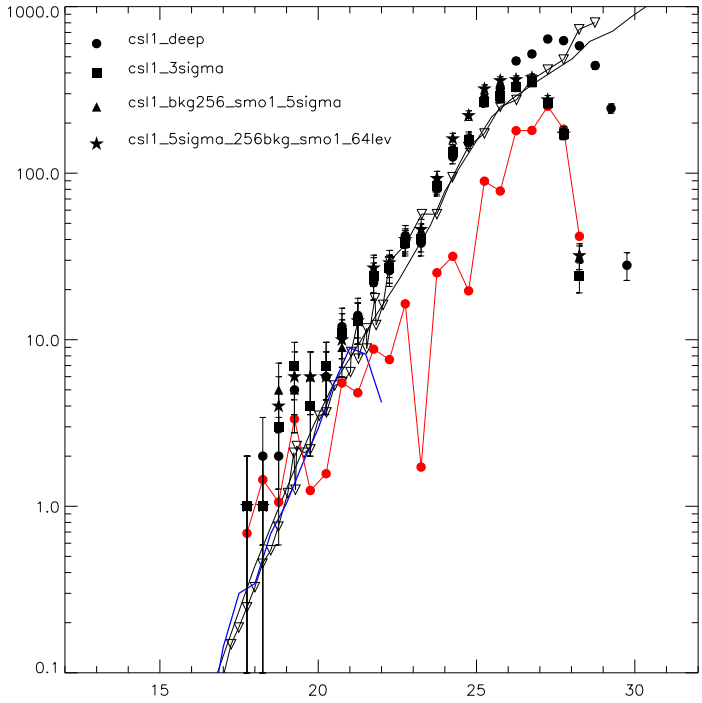

Figure 6.32: Galaxy number counts in the CSL-1 field using different SExtractor theresholds, and compared to OAC-DF and HDF counts.

CHAPTER 7

Conclusions

Since 1950 it was clear that galaxies were not "island universe" but that they interact with their neighbors. The observations in fact show that about 6 % of galaxies in the Universe are obviously peculiar, in the sense that they cannot be associated with any standard galaxy type and are tidally distorted.

Galaxies can interact with their neighbors in many different ways and through a large variety of mechanisms. In this work I presented a detailed analisys of a sample of peculiar and interacting galaxies selected, on the basis of their peculiarities, in order to reproduce the three main interaction processes: *Tidal accretion*, *Cold accretion* and *Merging*.
Other types of interactions, such as smooth accretion, ram pressure stripping and so on, are equally important in the growth of galaxies. The relative share of all processes depends on the environments and it drives many morphological features (bars, polar rings and so on).

But, why it is important to study galaxy interaction?

One of the major open issues in modern cosmology is to understand how galaxies formed and evolved. It is likely that the formation and evolution of galaxies are dominated by two main processes: *i*) the assembly of luminous and dark matter through accretion and mergers, and *ii*) the conversion of baryonic and non-baryonic matter into stars. The "Cold Dark Matter" (CDM) scenario for galaxy formation is based on the hierarchical mass assembly (Cole et al., 2000a) which predicts that the observed galaxies and their dark halo were formed through a repeated merging process of smaller systems.

This is the reason why the study of galaxy interactions and merging has

received an ever increasing attention in recent years, both on the observational and theoretical sides. Many galaxies show the presence of components with decoupled angular momentum, and this can be explained only with the occurrence of a second event in the formation of the galaxy. Several theoretical works based on numerical simulations, have tested some plausible scenarios for the origin of the decoupled matter: either gas accretion from infall processes, or merger with gas-rich galaxies, or accretion of external cold gas from cosmic web filaments.

To constrain the dynamical status and the formation history of a galaxy, detailed studies of its kinematical and photometric properties are fundamental. A comparison of these properties with the predictions of numerical simulations is also necessary to try to address the most plausible formation scenario for each studied object.

This is exactly the approach that I used in the present work: detailed studies of the main properties (photometry, kinematic, metallicity etc.) of the analyzed galaxies have been presented. All the obtained measurements have been compared with the prediction of numerical simulations for the formation and evolution of galaxies through different mechanism.

In the framework of the "Tidal accretion" scenario, the "host galaxy" can accrete gas from external sources, such as a gas-rich "donor galaxy". The tidal accretion scenario accounts for a large variety of polar structures; many simulations show that the accretion produces warped rings and transient features (see Bournaud & Combes 2003b), if the involved galaxies are in a particular orbital configuration. However, in this scenario the host galaxy can accrete only 10% of the gas in the donor, i.e. only the outer regions.

Recent theoretical works (Macciò et al., 2006) have argued that external gas can also be accreted from cosmic web filaments extended for ~ 1 Mpc into the virialized dark matter halo of the galaxy. In this scenario, differently from the tidal accretion, there is no limit to the mass of the accreted material. Moreover, the gas flowing through these filaments, turns to be pristine; for this reason this scenario was called "Cold accretion".

Finally, colliding galaxies also tend to merge with another and the final outcome after some violent convulsions is another kind of galaxy: an elliptical. During this period, the gas in these galaxies can be ignited violently in a starburst creating stars at rates hundreds of times greater than normal. Galaxy "merging" is fundamental to building up structure in the universe and explains many of the peculiar features of young galaxies.

The first object studied in the present work is the minor axis dust lane galaxy NGC1947 (see Chapter 4). This galaxy is peculiar because it shows the presence of two components with different angular momentum, in fact gas and dust rotate along the minor axis while stars rotate along the major

axis. The presence of these decoupled components is the clue that the galaxy is not the result of a single protogalactic cloud collapse, but that it has experienced a second event. To investigate the nature of this interaction event, I performed a detailed study of both photometry and kinematic of NGC1947. Looking at the kinematic profiles, I found that, while on average the stellar rotation curve along the minor axis is almost flat (stars do not rotate in this direction), the gas component presents a significant rotation along both axis, indicating that the gas is in a warped structure.
The optical and infrared photometry indicates that the dust lane has a concentric ring-like structure, with three other dust lanes parallel to the principal one, differently from what is usually observed for these kind of galaxies.
Putting together all the above evidences, I analyzed the possible formation scenarios for NGC1947 to try to disentangle in a non ambiguous way between them. From a morphological point of view, the galaxy does not present signs of a significant interaction, such as tidal tails, shells an so on; this suggests that the interaction event would have occurred very long ago ($\sim$ 10 Gyrs), but this is not consistent with the estimate of the age of the last burst of star formation, that is 1 Gyr. Moreover, the warping of the gas indicates that the interaction occurred recently, given that the gas has not yet settled in an equilibrium plane. Simulations by Bournaud & Combes (2003b) instead, predict the formation of polar structures through tidal accretion if the involved galaxies, and in particular their HI gas, are in a particular orbital configuration. Since I found, in the field around NGC1947, an early type spiral (ESO 085-GA088) with HI distribution in the orbital configuration needed to form a polar ring (of gas) through an accretion event, i.e. perpendicular to that of NGC1947, I can address the recent polar accretion from a gas rich donor galaxy as the most probable interaction event in the formation history of NGC1947.

The second peculiar galaxy analyzed in this thesis, is the Polar Disk Galaxy NGC4650A. This is considered the prototype for polar ring galaxies and it has been one of the best investigated object.
NGC4650A has a very luminous central spheroid with an exponential luminosity profile, in which stars rotate in a disk with high rotational velocities. The polar structure is very young with regions of star formation; stars and gas are distributed in a disk, rather than in a ring, and the disk and the central spheroid coexist at small radii. The galaxy has also a great amount of HI, all associated to the polar structure and 4 times more extended than the optical disk.
The two possible formation scenarios for PRGs, proposed till some years ago, involve the interaction of two galaxies, and are the tidal accretion of gas from a donor galaxy and the merging along a polar direction of two disk

galaxies. Both scenarios are able to account for the main morphologies of PRGs and an to produce a central galaxy similar to an early-type. The accretion scenario fails in reproducing extended disk-like polar structure, while the merging scenario fails to form a massive polar disk around an HG with rotation velocity as those observed in NGC4650A. In fact, in a merging scenario a high mass ratio is required to form a massive polar disk as observed in NGC4650A, and according to simulations of galaxy mergers this would convert the intruder in an elliptical-like, not rotationally supported, stellar system, while the kinematics shows that this is not the case of NGC4650A. Recent theoretical works have argued the most realistic way to form a polar disk as in NGC4650A might be the cold accretion.
If the polar disk forms by accretion from cosmic web filaments of external cold gas, we expect metallicities similar to those of late-type galaxies. In order to test this new scenario, I used high resolution spectroscopy, both in the near infrared and in the optical, to study the abundance ratios and metallicities of HII regions associated to the polar disk in NGC4650A. I used both "empirical" (Pagel et al. 1979, Díaz & Pérez-Montero 2000 and Pilyugin 2001) and "direct" (Garnett, 1992) methods to estimate the oxygen abundance, then converted in metallicity, of the polar disk in NGC4650A.
By comparing the abundance of the polar disk with those of galaxies of different morphological type, but same luminosity, NGC4650A has metallicity lower than spiral galaxy disks of the same total luminosity. Taking into account the value of the present star formation rate ($0.06 M_{\odot}/yr$), estimated by using the intensity of the H_{α} line, the metallicity obtained is consistent with those predicted by cold accretion mechanism for disk formation. Moreover, the oxygen abundance for the disk of NGC4650A is fairly constant along the disk. In contrast to the situation of spiral galaxies, where the metal enrichment happen from outside to inside, no steep metallicity gradient has been found for this PRG; this means that the metal enrichment is not influenced by the older central spheroid and that the disk was formed later. The metallicity expected for the present SFR is on average higher than those measured from the element abundance and this is consistent with a diluition of the gas due to the infall of metal poor gas from outside.

As a follow up of this work, I performed a similar study on two other PRGs, UGC7576 and UGC9796. I analyzed TNG spectra along the polar structures of these galaxies and, by using only empirical methods, I estimated the oxygen abundances and metallicities for both galaxies. Also in this case, the PRGs have metallicities of $0.4 Z_{\odot}$ and $0.1 Z_{\odot}$, lower than those of spiral disks of same total luminosities. UGC7576 also present an almost flat metallicity gradient, consistent, as already discussed for NGC4650A, with an inflow of metal poor gas in the galaxy. Furthermore, this object is also

isolated and the absence of a close companion lead to the exclusion of the tidal accretion of gas from a donor galaxy for UGC7576. UGC9796 is instead in a small group, with 5 close companion galaxies. Since all these galaxies have an amount of HI gas comparable with those of UGC9796, we cannot definitely rule out the tidal accretion hypothesis. The merging scenario is instead ruled out for both UGC7576 and UGC9796, because both galaxies have rotationally supported central spheroids and massive and extended polar structures; to form such structures through a merging event, high mass ratios are required and a similar merging would destroy the ordered motions of the stars in the central galaxies, converting them in elliptical-like not rotationally supported objects, contrary to what we observe from the kinematic of UGC7576 and UGC9796.

The merging scenario has been tested by analyzing a Compact Group of Galaxies belonging to the Hickson's catalog, HCG62. Galaxies in these groups are in a very compact configuration, with a small separation and have very low velocity dispersion. These features are very important because, taking into account that theories on the formation and evolution of galaxies predict that the intensity and frequency of interactions strongly depend on the density of the environment in which they are, compact group are considered the ideal ground where to test the merging scenario. For these reasons, I performed a study of the photometric and kinematical properties of the 4 galaxies in the group and in particular for the dominant galaxy NGC4778. This study has revealed the presence of a kinematically decoupled and counterrotating core inside NGC4778, and the photometry shows also that the isophotes in the central regions are more flattened and present a twisting of the position angle.
Numerical simulations predict the formation of a kinematically decoupled core as a consequence of a merging, because gas and stars fall into the potential well of the host galaxy, maintaining the angular momentum of the primal galaxy (Bournaud & Combes, 2003b). Moreover, we found an absence of correlation between photometric and kinematical anomalies; this absence of correlation allow to conclude that the event that NGC4778 has experienced is a "minor merging". In fact, while weak interactions do not perturb the kinematics but can lead to morphological deformations in the outer regions, the minor merger could perturb the kinematics in the inner regions (Nishiura et al., 2000).

The "dry merging" scenario has also been investigated, by studying the interacting pair of galaxies known as CSL1. HST, VLT and TNG data have been used to study this interacting system of early type galaxies; the main properties of this system have been investigated by using both imaging and spectroscopy, and numerical simulations of dry merging between early type

galaxies have been performed. Even if the work is still in progress, main conclusions can be drawn. Luminosity profiles for both galaxies of CSL1 are not well reproduced by a single Sersic law, as one would expect given their classification as early type galaxies, but by a spheroid plus a disk component. The residuals of the subtraction of the 2D model to the image of CSL1 show the presence of two extended tails, of the shape typically predicted for dry merging events. However, both galaxies in CSL1 are located, in the scaling relations, in the region where massive and bulge dominated ellipticals are found.

Finally, I also performed a structural and morphological analysis of a sample of Shakhbazian groups, with the main goal to characterize them. Poor groups of galaxies are the most common cosmic structures and Shakhbazian groups represent second generation structures whose evolution and morphological content depends on the environment in which they form. MOS and long-slit observations of a sample of compact galaxy groups in order to constrain their mass, dynamical status and evolutionary timescales. Also this work is still in progress, but the main results and conclusions for this work are the following: the estimates of the mass/luminosity ratios of this sample are consistent with those of the Hickson's groups and there is also a correlation between richness and extention and M/L ratio. In fact, groups with lower M/L are those composed only by a core and have lower mass, while groups with higher M/L are core+halo structures, and then have higher mass.

Publications & Proposals

Referred papers

- **Spavone, M.**; Iodice, E.; Arnaboldi, M.; Gerhard, O.; Saglia, R.; Longo, G., "Chemical Abundances in the Polar Disk of NGC 4650A: Implications for Cold Accretion Scenario", 2010, The Astrophysical Journal, Volume 714, Issue 2, pp. 1081-1095

- **Spavone, M.**; Iodice, E.; Calvi, R.; Bettoni, D.; Galletta, G.; Longo, G.; Mazzei, P.; Minervini, G., "Revisiting the formation history of the minor-axis dust lane galaxy NGC 1947", 2009, Monthly Notices of the Royal Astronomical Society, Volume 393, Issue 1, pp. 317-328

- **Spavone, M.**; Iodice, E.; Longo, G.; Paolillo, M.; Sodani, S., "Hickson 62. I. Kinematics of NGC 4778", 2006, Astronomy and Astrophysics, Volume 457, Issue 2, October II 2006, pp.493-500

- **Spavone, M.**; Iodice, E.; Arnaboldi, M.; Longo, G.; Gerhard, O., "Chemical abundances of the PRGs UGC7576 and UGC9796: testing the formation scenario", 2010, Submitted to Astronomy & Astrophysics.

- M. Paolillo; G. Covone; C. Nipoti; **M. Spavone**; M. Capaccioli; G. Longo; A.Cimatti; L. Ciotti, "A prototype dry-merger caught in the act", in preparation

Conference proceedings

- **Spavone, M.**; Iodice, E.; Longo, G.; Paolillo, M., "A kinematically decoupled component in NGC4778", 2007, "1st Workshop of Astronomy and Astrophysics for Students" held in Naples (ITALY) on April 19-20, 2006. Published by INFN-Naples, eds. N.R. Napolitano & M. Paolillo, p.109

- Sodani, S.; de Filippis, E.; Paolillo, M.; Longo, G.; **Spavone, M.**, "An X-ray investigation of Hickson 62", 2007, "1st Workshop of Astronomy and Astrophysics for Students" held in Naples (ITALY) on April 19-20, 2006. Published by INFN-Naples, eds. N.R. Napolitano & M. Paolillo, p.113

- **Spavone, M.**; Iodice, E.; Longo, G.; Paolillo, M., "The complex kinematics of galaxies in Hickson 62", 2005, Astron. Nachr., 326, 512-512

- **Spavone, M.**; Iodice, E.; Arnaboldi, M; Gerhard, O.; Saglia, R.; and Longo, G.; "Metallicity of the Polar Disk in NGC4650A: Constraints for Cold Accretion Scenario", 2010, American Institute of Physics Conference Series, 1240, 173 (Hunting for the dark: the hidden side of galaxy formation. AIP Conference Proceedings, Volume 1240, pp. 173-174 (2010)).

- **Spavone, M.**; "Chemical Abundances in the Polar Disk of NGC 4650A: Implications for Cold Accretion Scenario", 2010, Mem. S.A.It., 75, 282

Other publications

- Dennefeld, M.; Arevalo, M. J.; Brozek, T.; Candian, A.; Cardoso, C.; Leyder, J. C.; Harutyunyan, A.; Pursimo, T.; Johansson, J.; Misgeld, I.; Monguio, M.; **Spavone, M.**, "Supernova 2008dq", 2008, Central Bureau Electronic Telegrams, 1421, 1

- "Conoscere il suono, la natura, l'universo" a cura di M. Campanino, 2007, Fondazione IDIS-Cittá Della Scienza, Ed. CUEN

Accepted proposals

- Proposal for Observations at TNG telescope (Canary Island), "Characterizing Compact Group of Galaxies", AOT18 (Co-I)

- Proposal for Observations at TNG telescope (Canary Island), "Characterizing Compact Group of Galaxies", AOT19 (Co-I)
- Proposal for Observations at TNG telescope (Canary island), "Chemical abundances of PRGs UGC7576 and UGC9796: implication for the cold accretion by filaments" AOT21 (Co-I and observer in charge)

Bibliography

Afanasiev, V. L. & Sil'chenko, O. K. 2005, A&A, 429, 825

Agertz, O., Teyssier, R., & Moore, B. 2009, MNRAS, 397, L64

Alcalá, J. M., Pannella, M., Puddu, E., Radovich, M., Silvotti, R., Arnaboldi, M., Capaccioli, M., Covone, G., Dall'Ora, M., De Lucia, G., Grado, A., Longo, G., Mercurio, A., Musella, I., Napolitano, N., Pavlov, M., Rifatto, A., Ripepi, V., & Scaramella, R. 2004, A&A, 428, 339

Allam, S., Assendorp, R., Longo, G., Braun, M., & Richter, G. 1996, A&A, 117, 39

Allen, R. J. 1984, The Observatory, 104, 61

Alpher, R. A. & Herman, R. C. 1950, Reviews of Modern Physics, 22, 153

Arnaboldi, M., Freeman, K. C., Sackett, P. D., Sparke, L. S., & Capaccioli, M. 1995, planss, 43, 1377

Arnaboldi, M. & Galletta, G. 1993, A&A, 268, 411

Arnaboldi, M., Oosterloo, T., Combes, F., Freeman, K. C., & Koribalski, B. 1997, AJ, 113, 585

Arnaboldi, M. & Sparke, L. S. 1994, AJ, 107, 958

Arp, H. 1966, ApJS, 14, 1

Asplund, M., Grevesse, N., Sauval, A. J., Allende Prieto, C., & Kiselman, D. 2004, A&A, 417, 751

Baier, F. W. & Tiersch, H. 1979, Astrophysics, 15, 24

Barnes, J. 1984, MNRAS, 208, 873

Barnes, J. E. 2002, MNRAS, 333, 481

Barnes, J. E. & Hernquist, L. 1992, ARA&A, 30, 705

Bekki, K. 1997, ApJL, 490, L37+

—. 1998a, ApJ, 499, 635

—. 1998b, ApJL, 502, L133+

—. 2008, ApJL, 680, L29

Bender, R. 1990, A&A, 229, 441

Bender, R., Burstein, D., & Faber, S. M. 1992, ApJ, 399, 462

Bender, R., Saglia, R. P., & Gerhard, O. E. 1994, MNRAS, 269, 785

Berlind, A. A., Frieman, J., Weinberg, D. H., Blanton, M. R., Warren, M. S., Abazajian, K., Scranton, R., Hogg, D. W., Scoccimarro, R., Bahcall, N. A., Brinkmann, J., Gott, III, J. R., Kleinman, S. J., Krzesinski, J., Lee, B. C., Miller, C. J., Nitta, A., Schneider, D. P., Tucker, D. L., & Zehavi, I. 2006, ApJS, 167, 1

Bertola, F., Bettoni, D., Danziger, J., Sadler, E., Sparke, L., & de Zeeuw, T. 1991, ApJ, 373, 369

Bertola, F., Bettoni, D., Rusconi, L., & Sedmak, G. 1984, AJ, 89, 356

Bertola, F. & Galletta, G. 1978, ApJL, 226, L115

Bertola, F., Galletta, G., & Zeilinger, W. W. 1992, A&A, 254, 89

Bettoni, D., Buson, L. M., Maira, L., & Bertola, F. 1995, in Astronomical Society of the Pacific Conference Series, Vol. 70, Groups of Galaxies, ed. O.-G. Richter & K. Borne, 95–+

Bettoni, D., Galletta, G., García-Burillo, S., & Rodríguez-Franco, A. 2001, A&A, 374, 421

Binney, J. 1978, MNRAS, 183, 779

Binney, J. & Tremaine, S. 1987, Galactic dynamics, ed. Binney, J. & Tremaine, S.

Birnboim, Y. & Dekel, A. 2003, MNRAS, 345, 349

Bîrzan, L., Rafferty, D. A., McNamara, B. R., Wise, M. W., & Nulsen, P. E. J. 2004, Apj, 607, 800

Bode, P. W., Cohn, H. N., & Lugger, P. M. 1993, ApJ, 416, 17

Boissier, S. & Prantzos, N. 1999, MNRAS, 307, 857

Bonfanti, P., Simien, F., Rampazzo, R., & Prugniel, P. 1999, A&AS, 139, 483

Bournaud, F. & Combes, F. 2003a, A&A, 401, 817

—. 2003b, A&A, 401, 817

Bournaud, F. & Elmegreen, B. G. 2009, ApJL, 694, L158

Bournaud, F., Jog, C. J., & Combes, F. 2005a, A&A, 437, 69

—. 2005b, A&A, 437, 69

—. 2007, A&A, 476, 1179

Bresolin, F., Ryan-Weber, E., Kennicutt, R. C., & Goddard, Q. 2009, ApJ, 695, 580

Brocca, C., Bettoni, D., & Galletta, G. 1997, A&A, 326, 907

Brook, C. B., Governato, F., Quinn, T., Wadsley, J., Brooks, A. M., Willman, B., Stilp, A., & Jonsson, P. 2008a, ArXiv e-prints, 802

—. 2008b, ApJ, 689, 678

Brook, C. B., Kawata, D., Gibson, B. K., & Freeman, K. C. 2004, ApJ, 612, 894

Brosch, N., Kniazev, A. Y., Moiseev, A., & Pustilnik, S. A. 2010, MNRAS, 401, 2067

Bruzual, G. & Charlot, S. 2003a, MNRAS, 344, 1000

—. 2003b, MNRAS, 344, 1000

Bundy, K., Fukugita, M., Ellis, R. S., Kodama, T., & Conselice, C. J. 2004, ApJL, 601, L123

Buttiglione, S., Arnaboldi, M., & Iodice, E. 2006, Memorie della Societa Astronomica Italiana Supplementi, 9, 317

Byun, Y. I. & Freeman, K. C. 1995, ApJ, 448, 563

Campbell, A., Terlevich, R., & Melnick, J. 1986, MNRAS, 223, 811

Canalizo, G., Stockton, A., Brotherton, M. S., & Lacy, M. 2006, nar, 50, 650

Caon, N., Capaccioli, M., & D'Onofrio, M. 1993, MNRAS, 265, 1013

Capozzi, D., de Filippis, E., Paolillo, M., D'Abrusco, R., & Longo, G. 2009, MNRAS, 396, 900

Cappellari, M. & Emsellem, E. 2004, PASP, 116, 138

Cardelli, J. A., Clayton, G. C., & Mathis, J. S. 1989, ApJ, 345, 245

Carollo, C. M., Danziger, I. J., & Buson, L. 1993, MNRAS, 265, 553

Cattaneo, A., Combes, F., Colombi, S., Bertin, E., & Melchior, A. 2005, MNRAS, 359, 1237

Chandrasekhar, S. 1943, ApJ, 97, 255

Cid Fernandes, R., Mateus, A., Sodré, L., Stasińska, G., & Gomes, J. M. 2005, MNRAS, 358, 363

Cole, S., Lacey, C. G., Baugh, C. M., & Frenk, C. S. 2000a, MNRAS, 319, 168

—. 2000b, MNRAS, 319, 168

Combes, F. & Arnaboldi, M. 1996, A&A, 305, 763

Combes, F., Rampazzo, R., Bonfanti, P. P., Prugniel, P., & Sulentic, J. W. 1995, A&A, 297, 37

Conselice, C. J., Bershady, M. A., Dickinson, M., & Papovich, C. 2003a, AJ, 126, 1183

—. 2003b, AJ, 126, 1183

Covington, M., Dekel, A., Cox, T. J., Jonsson, P., & Primack, J. R. 2008, MNRAS, 384, 94

Cox, A. L., Sparke, L. S., & van Moorsel, G. 2006, AJ, 131, 828

Coziol, R., Ribeiro, A. L. B., de Carvalho, R. R., & Capelato, H. V. 1998, ApJ, 493, 563

D'Abrusco, R., Staiano, A., Longo, G., Brescia, M., Paolillo, M., De Filippis, E., & Tagliaferri, R. 2007, ApJ, 663, 752

Dalcanton, J. J. 2007, ApJ, 658, 941

Davé, R., Cen, R., Ostriker, J. P., Bryan, G. L., Hernquist, L., Katz, N., Weinberg, D. H., Norman, M. L., & O'Shea, B. 2001, ApJ, 552, 473

de Blok, W. J. G., Bosma, A., & McGaugh, S. 2003, MNRAS, 340, 657

de Blok, W. J. G. & van der Hulst, J. M. 1998, A&A, 335, 421

de la Rosa, I. G., de Carvalho, R. R., Vazdekis, A., & Barbuy, B. 2007, AJ, 133, 330

De Lucia, G., Springel, V., White, S. D. M., Croton, D., & Kauffmann, G. 2006, MNRAS, 366, 499

De Propris, R., Conselice, C. J., Liske, J., Driver, S. P., Patton, D. R., Graham, A. W., & Allen, P. D. 2007, ApJ, 666, 212

De Robertis, M. M., Dufour, R. J., & Hunt, R. W. 1987, JRASC, 81, 195

de Vaucouleurs, G., de Vaucouleurs, A., & Corwin, H. G. 1976, 2nd reference catalogue of bright galaxies containing information on 4364 galaxies with reference to papers published between 1964 and 1975 (University of Texas Monographs in Astronomy, Austin: University of Texas Press, 1976)

Dekel, A. & Birnboim, Y. 2006, MNRAS, 368, 2

—. 2008, MNRAS, 383, 119

Dekel, A., Birnboim, Y., Engel, G., Freundlich, J., Goerdt, T., Mumcuoglu, M., Neistein, E., Pichon, C., Teyssier, R., & Zinger, E. 2009a, Nature, 457, 451

Dekel, A., Sari, R., & Ceverino, D. 2009b, ApJ, 703, 785

Díaz, A. I. & Pérez-Montero, E. 2000, MNRAS, 312, 130

Djorgovski, S. & Davis, M. 1987, ApJ, 313, 59

Dupraz, C. & Combes, F. 1985, in Lecture Notes in Physics, Berlin Springer Verlag, Vol. 232, New Aspects of Galaxy Photometry, ed. J.-L. Nieto, 151–154

Efstathiou, G., Ellis, R. S., & Carter, D. 1982, MNRAS, 201, 975

Eke, V. R., Frenk, C. S., Baugh, C. M., Cole, S., Norberg, P., Peacock, J. A., Baldry, I. K., Bland-Hawthorn, J., Bridges, T., Cannon, R., Colless, M., Collins, C., Couch, W., Dalton, G., de Propris, R., Driver, S. P., Efstathiou, G., Ellis, R. S., Glazebrook, K., Jackson, C. A., Lahav, O., Lewis, I., Lumsden, S., Maddox, S. J., Madgwick, D., Peterson, B. A., Sutherland, W., & Taylor, K. 2004, MNRAS, 355, 769

Eliche-Moral, M. C., Prieto, M., Gallego, J., & Zamorano, J. 2010, ArXiv e-prints

Ellison, S. L., Patton, D. R., Simard, L., & McConnachie, A. W. 2008, ApJL, 672, L107

Elmegreen, D. M., Elmegreen, B. G., Ravindranath, S., & Coe, D. A. 2007, ApJ, 658, 763

Faber, S. M. & Jackson, R. E. 1976, ApJ, 204, 668

Finlator, K., Davé, R., & Oppenheimer, B. D. 2007, MNRAS, 376, 1861

Focardi, P. & Kelm, B. 2002, A&A, 391, 35

Freeman, K. C. 1970a, ApJ, 160, 811

—. 1970b, ApJ, 160, 811

Fukazawa, Y., Nakazawa, K., Isobe, N., Makishima, K., Matsushita, K., Ohashi, T., & Kamae, T. 2001, ApJL, 546, L87

Fukugita, M., Shimasaku, K., & Ichikawa, T. 1995, PASP, 107, 945

Galametz, M., Madden, S., Galliano, F., Hony, S., Schuller, F., Beelen, A., Bendo, G., Sauvage, M., Lundgren, A., & Billot, N. 2009, A&A, 508, 645

Gallagher, J. S., Sparke, L. S., Matthews, L. D., Frattare, L. M., English, J., Kinney, A. L., Iodice, E., & Arnaboldi, M. 2002, ApJ, 568, 199

Galletta, G. 1996, in Astronomical Society of the Pacific Conference Series, Vol. 91, IAU Colloq. 157: Barred Galaxies, ed. R. Buta, D. A. Crocker, & B. G. Elmegreen, 429–+

Galletta, G., Sage, L. J., & Sparke, L. S. 1997, MNRAS, 284, 773

Gamow, G. 1946, Physical Review, 70, 572

Garnett, D. R. 1992, AJ, 103, 1330

Genel, S., Genzel, R., Bouché, N., Sternberg, A., Naab, T., Schreiber, N. M. F., Shapiro, K. L., Tacconi, L. J., Lutz, D., Cresci, G., Buschkamp, P., Davies, R. I., & Hicks, E. K. S. 2008, ApJ, 688, 789

Gerhard, O. E. 1993, MNRAS, 265, 213

Governato, F., Bhatia, R., & Chincarini, G. 1991, ApJL, 371, L15

Grogin, N. A., Conselice, C. J., Chatzichristou, E., Alexander, D. M., Bauer, F. E., Hornschemeier, A. E., Jogee, S., Koekemoer, A. M., Laidler, V. G., Livio, M., Lucas, R. A., Paolillo, M., Ravindranath, S., Schreier, E. J., Simmons, B. D., & Urry, C. M. 2005, ApJL, 627, L97

Hahn, O., Teyssier, R., & Carollo, C. M. 2010, MNRAS, 405, 274

Hamabe, M. & Kormendy, J. 1987, in IAU Symposium, Vol. 127, Structure and Dynamics of Elliptical Galaxies, ed. P. T. de Zeeuw, 379–+

Hancock, M., Smith, B. J., Struck, C., Giroux, M. L., & Hurlock, S. 2009, AJ, 137, 4643

Hawarden, T. G., Longmore, A. J., Tritton, S. B., Elson, R. A. W., & Corwin, Jr., H. G. 1981, MNRAS, 196, 747

Heisler, J., Merritt, D., & Schwarzschild, M. 1982, ApJ, 258, 490

Hernquist, L. & Weil, M. L. 1993, MNRAS, 261, 804

Hickson, P. 1982, ApJ, 255, 382

—. 1997, ARAA, 35, 357

Hickson, P., Kindl, E., & Huchra, J. P. 1988, ApJ, 331, 64

Hickson, P., Menon, T. K., Palumbo, G. G. C., & Persic, M. 1989, ApJ, 341, 679

Hickson, P., Ninkov, Z., Huchra, J. P., & Mamon, G. A. 1984, in Clusters and Groups of Galaxies. International Meeting held in Trieste, Italy, September 13-16, 1983. Editors, F. Mardirossian, G. Giuricin, M. Mezzetti; Publisher, D. Reidel Pub. Co., Dordrecht, Holland, Boston, MA, Hingham, MA, U.S.A. Sold and distributed in the U.S.A. and Canada by Kluwer Academic Publishers, 1984. LC # QB858.7 .C58 1984. ISBN # 9027717729. P.367, 1984, ed. F. Mardirossian, G. Giuricin, & M. Mezzetti, 367–+

Hidalgo-Gámez, A. M. & Ramírez-Fuentes, D. 2009, AJ, 137, 169

Hubble, E. 1929, Proceedings of the National Academy of Science, 15, 168

Hubble, E. P. 1936, Realm of the Nebulae, ed. Hubble, E. P.

Iodice, E., Arnaboldi, M., De Lucia, G., Gallagher, III, J. S., Sparke, L. S., & Freeman, K. C. 2002a, AJ, 123, 195

Iodice, E., Arnaboldi, M., Napolitano, N. R., Oosterloo, T. A., & Józsa, G. I. G. 2008, in Astronomical Society of the Pacific Conference Series, Vol. 396, Astronomical Society of the Pacific Conference Series, ed. J. G. Funes & E. M. Corsini, 483–+

Iodice, E., Arnaboldi, M., Saglia, R. P., Sparke, L. S., Gerhard, O., Gallagher, J. S., Combes, F., Bournaud, F., Capaccioli, M., & Freeman, K. C. 2006, ApJ, 643, 200

Iodice, E., Arnaboldi, M., Sparke, L. S., Buta, R., Freeman, K. C., & Capaccioli, M. 2004, A&A, 418, 41

Iodice, E., Arnaboldi, M., Sparke, L. S., & Freeman, K. C. 2002b, A&A, 391, 117

Iodice, E., Arnaboldi, M., Sparke, L. S., Gallagher, J. S., & Freeman, K. C. 2002c, A&A, 391, 103

Iodice, E., D'Onofrio, M., & Capaccioli, M. 2001, ApSS, 276, 869

Izotov, Y. I., Thuan, T. X., & Guseva, N. G. 2005, ApJ, 632, 210

Jog, C. J. & Maybhate, A. 2006, MNRAS, 370, 891

Kartaltepe, J. S., Sanders, D. B., Scoville, N. Z., Calzetti, D., Capak, P., Koekemoer, A., Mobasher, B., Murayama, T., Salvato, M., Sasaki, S. S., & Taniguchi, Y. 2007, ApJS, 172, 320

Katz, N., Quinn, T., Bertschinger, E., & Gelb, J. M. 1994, MNRAS, 270, L71+

Katz, N. & White, S. D. M. 1993, ApJ, 412, 455

Kennicutt, Jr., R. C. 1998, ARA&A, 36, 189

Kennicutt, Jr., R. C., Edgar, B. K., & Hodge, P. W. 1989, ApJ, 337, 761

Kennicutt, Jr., R. C., Roettiger, K. A., Keel, W. C., van der Hulst, J. M., & Hummel, E. 1987, AJ, 93, 1011

Keres, D. 2008, in COSPAR, Plenary Meeting, Vol. 37, 37th COSPAR Scientific Assembly, 1496–+

Kereš, D., Katz, N., Weinberg, D. H., & Davé, R. 2005, MNRAS, 363, 2

Kewley, L. J. & Ellison, S. L. 2008, ApJ, 681, 1183

Khochfar, S. & Burkert, A. 2003, ApJL, 597, L117

Khochfar, S. & Silk, J. 2006, ApJL, 648, L21

—. 2009, MNRAS, 397, 506

Kindl, E. 1990, PhD thesis, British Columbia Univ., Vancouver.

Kobulnicky, H. A. & Kewley, L. J. 2004, ApJ, 617, 240

Kobulnicky, H. A. & Zaritsky, D. 1999, ApJ, 511, 118

Koekemoer, A. M., Fruchter, A. S., Hook, R. N., & Hack, W. 2002, in The 2002 HST Calibration Workshop : Hubble after the Installation of the ACS and the NICMOS Cooling System, ed. S. Arribas, A. Koekemoer, & B. Whitmore, 337–+

Koulouridis, E., Plionis, M., Chavushyan, V., Dultzin-Hacyan, D., Krongold, Y., & Goudis, C. 2006, ApJ, 639, 37

Krajnović, D. & Jaffe, W. 2004, A&A, 428, 877

Lee, B. C., Allam, S. S., Tucker, D. L., Annis, J., Johnston, D. E., Scranton, R., Acebo, Y., Bahcall, N. A., Bartelmann, M., Böhringer, H., Ellman, N., Grebel, E. K., Infante, L., Loveday, J., McKay, T. A., Prada, F., Schneider, D. P., Stoughton, C., Szalay, A. S., Vogeley, M. S., Voges, W., & Yanny, B. 2004, AJ, 127, 1811

Lin, C. C. & Shu, F. H. 1964, ApJ, 140, 646

Lin, L., Koo, D. C., Willmer, C. N. A., Patton, D. R., Conselice, C. J., Yan, R., Coil, A. L., Cooper, M. C., Davis, M., Faber, S. M., Gerke, B. F., Guhathakurta, P., & Newman, J. A. 2004, ApJL, 617, L9

Lotz, J. M., Davis, M., Faber, S. M., Guhathakurta, P., Gwyn, S., Huang, J., Koo, D. C., Le Floc'h, E., Lin, L., Newman, J., Noeske, K., Papovich, C., Willmer, C. N. A., Coil, A., Conselice, C. J., Cooper, M., Hopkins, A. M., Metevier, A., Primack, J., Rieke, G., & Weiner, B. J. 2008, ApJ, 672, 177

Lynds, R. & Toomre, A. 1976, ApJ, 209, 382

Macciò, A. V., Governato, F., & Horellou, C. 2005, MNRAS, 359, 941

Macciò, A. V., Moore, B., & Stadel, J. 2006, ApJL, 636, L25

Malin, D. F. & Carter, D. 1980, Nature, 285, 643

Mamon, G. A. 1986, ApJ, 307, 426

Martig, M., Bournaud, F., Teyssier, R., & Dekel, A. 2009, ApJ, 707, 250

Matteucci, F. & Francois, P. 1989, MNRAS, 239, 885

Mazzei, P. & Curir, A. 2003, ApJ, 591, 784

Mazzei, P., Curir, A., & Bonoli, C. 1995, AJ, 110, 559

Mazzei, P., Xu, C., & de Zotti, G. 1992, A&A, 256, 45

Mehlert, D., Saglia, R. P., Bender, R., & Wegner, G. 2000, A&AS, 141, 449

Mendes de Oliveira, C., Amram, P., Plana, H., & Balkowski, C. 2003, AJ, 126, 2635

Mendesdeoliveira, C. 1992, PhD thesis, British Columbia Univ.

Menon, T. K. 1991, ApJ, 372, 419

Merluzzi, P., Shaker, A. A., & Longo, G. 2000, in Astronomical Society of the Pacific Conference Series, Vol. 209, IAU Colloq. 174: Small Galaxy Groups, ed. M. J. Valtonen & C. Flynn, 205–+

Moellenhoff, C. 1982, A&A, 108, 130

Mould, J., Balick, B., Bothun, G., & Aaronson, M. 1982, ApJL, 260, L37

Naab, T., Johansson, P. H., Ostriker, J. P., & Efstathiou, G. 2007, ApJ, 658, 710

Napolitano, N. R., Capaccioli, M., Romanowsky, A. J., Douglas, N. G., Merrifield, M. R., Kuijken, K., Arnaboldi, M., Gerhard, O., & Freeman, K. C. 2005, MNRAS, 357, 691

Navarro, J. F., Frenk, C. S., & White, S. D. M. 1997, ApJ, 490, 493

Nishiura, S., Shimada, M., Ohyama, Y., Murayama, T., & Taniguchi, Y. 2000, AJ, 120, 1691

Ocvirk, P., Pichon, C., & Teyssier, R. 2008, MNRAS, 390, 1326

Oosterloo, T. A., Morganti, R., Sadler, E. M., Vergani, D., & Caldwell, N. 2002, AJ, 123, 729

Osterbrock, D. E. 1989, Astrophysics of gaseous nebulae and active galactic nuclei, ed. Osterbrock, D. E.

Pagel, B. E. J., Edmunds, M. G., Blackwell, D. E., Chun, M. S., & Smith, G. 1979, MNRAS, 189, 95

Pagel, B. E. J., Simonson, E. A., Terlevich, R. J., & Edmunds, M. G. 1992, MNRAS, 255, 325

Palumbo, G. G. C., Saracco, P., Mendes de Oliveira, C., Hickson, P., Tornatore, V., & Baiesi-Pillastrini, G. C. 1993, ApJ, 405, 413

Peebles, P. J. E. 1982, ApJL, 263, L1

Peng, C. Y., Ho, L. C., Impey, C. D., & Rix, H.-W. 2002, AJ, 124, 266

Pérez-Montero, E. & Díaz, A. I. 2003, MNRAS, 346, 105

—. 2005, MNRAS, 361, 1063

Pérez-Montero, E., García-Benito, R., Díaz, A. I., Pérez, E., & Kehrig, C. 2009, A&A, 497, 53

Persson, S. E., Murphy, D. C., Krzeminski, W., Roth, M., & Rieke, M. J. 1998, AJ, 116, 2475

Pildis, R. A., Evrard, A. E., & Bregman, J. N. 1996, AJ, 112, 378

Pilyugin, L. S. 2001, A&A, 369, 594

—. 2007, MNRAS, 375, 685

Pilyugin, L. S., Mattsson, L., Vílchez, J. M., & Cedrés, B. 2009, MNRAS, 398, 485

Pilyugin, L. S., Thuan, T. X., & Vílchez, J. M. 2006, MNRAS, 367, 1139

Plionis, M., Ragone, C., & Basilakos, S. 2007, in Groups of Galaxies in the Nearby Universe, ed. I. Saviane, V. D. Ivanov, & J. Borissova, 285–+

Puche, D. & Carignan, C. 1991, ApJ, 378, 487

Quinn, T. 1991, in Warped Disks and Inclined Rings around Galaxies, ed. S. Casertano, P. D. Sackett, & F. H. Briggs, 143–+

Rampazzo, R., Covino, S., Trinchieri, G., & Reduzzi, L. 1998, A&A, 330, 423

Reshetnikov, V., Bournaud, F., Combes, F., Faúndez-Abans, M., de Oliveira-Abans, M., van Driel, W., & Schneider, S. E. 2005, A&A, 431, 503

Reshetnikov, V. & Sotnikova, N. 1997, A&A, 325, 933

Reshetnikov, V. P. & Combes, F. 1994, A&A, 291, 57

Reshetnikov, V. P., Faúndez-Abans, M., & de Oliveira-Abans, M. 2002, A&A, 383, 390

Reshetnikov, V. P., Hagen-Thorn, V. A., & Yakovleva, V. A. 1994, A&A, 290, 693

Richter, O.-G., Sackett, P. D., & Sparke, L. S. 1994, AJ, 107, 99

Robertson, B. E. & Bullock, J. S. 2008, ApJL, 685, L27

Rood, H. J. & Struble, M. F. 1994, PASP, 106, 413

Rose, J. A. 1977, ApJ, 211, 311

Rossa, J., Laine, S., van der Marel, R. P., Mihos, J. C., Hibbard, J. E., Böker, T., & Zabludoff, A. I. 2007, AJ, 134, 2124

Roškar, R., Debattista, V. P., Brooks, A. M., Quinn, T. R., Brook, C. B., Governato, F., Dalcanton, J. J., & Wadsley, J. 2010, MNRAS, 408, 783

Roškar, R., Debattista, V. P., Stinson, G. S., Quinn, T. R., Kaufmann, T., & Wadsley, J. 2008, ApJ, 675, L65

Rubin, V. C., Ford, W. K. J., & . Thonnard, N. 1980, ApJ, 238, 471

Rubin, V. C., Hunter, D. A., & Ford, Jr., W. K. 1991, ApJS, 76, 153

Rupke, D. S. N., Kewley, L. J., & Barnes, J. E. 2010, ApJL, 710, L156

Sackett, P. D., Rix, H., Jarvis, B. J., & Freeman, K. C. 1994, ApJ, 436, 629

Sackett, P. D. & Sparke, L. S. 1990, ApJ, 361, 408

Sage, L. J. & Galletta, G. 1993, ApJ, 419, 544

Salpeter, E. E. 1955, ApJ, 121, 161

Sandage, A. & Tammann, G. A. 1987, A revised Shapley-Ames Catalog of bright galaxies (Carnegie Institution of Washington Publication, Washington: Carnegie Institution, 1987, 2nd ed.)

Sargent, W. L. W., Schechter, P. L., Boksenberg, A., & Shortridge, K. 1977, ApJ, 212, 326

Sazhin, M., Longo, G., Capaccioli, M., Alcalá, J. M., Silvotti, R., Covone, G., Khovanskaya, O., Pavlov, M., Pannella, M., Radovich, M., & Testa, V. 2003, MNRAS, 343, 353

Schechter, P. 1976, ApJ, 203, 297

Schechter, P. L., Sancisi, R., van Woerden, H., & Lynds, C. R. 1984, MNRAS, 208, 111

Schinnerer, E. & Scoville, N. 2002, ApJL, 577, L103

Schweizer, F., Seitzer, P., Faber, S. M., Burstein, D., Dalle Ore, C. M., & Gonzalez, J. J. 1990, ApJL, 364, L33

Schweizer, F., Whitmore, B. C., & Rubin, V. C. 1983, AJ, 88, 909

Semelin, B. & Combes, F. 2005, A&A, 441, 55

Serra, P., Trager, S. C., Oosterloo, T. A., & Morganti, R. 2007, ArXiv e-prints, 712

Sersic, J. L. 1968, Atlas de galaxias australes (Cordoba, Argentina: Observatorio Astronomico, 1968)

Shaker, A. A., Longo, G., & Merluzzi, P. 1998, Astronomische Nachrichten, 319, 167

Shakhbazyan, R. K. 1973, Astrophysics, 9, 296

Shalyapina, L. V., Moiseev, A. V., & Yakovleva, V. A. 2002, Astronomy Letters, 28, 443

Shaw, R. A. & Dufour, R. J. 1995, PASP, 107, 896

Spavone, M., Iodice, E., Arnaboldi, M., Gerhard, O., Saglia, R., & Longo, G. 2010, ApJ, 714, 1081

Spavone, M., Iodice, E., Calvi, R., Bettoni, D., Galletta, G., Longo, G., Mazzei, P., & Minervini, G. 2009, MNRAS, 393, 317

Spavone, M., Iodice, E., Longo, G., Paolillo, M., & Sodani, S. 2006, A&A, 457, 493

Spergel, D. N., Verde, L., Peiris, H. V., Komatsu, E., Nolta, M. R., Bennett, C. L., Halpern, M., Hinshaw, G., Jarosik, N., Kogut, A., Limon, M., Meyer, S. S., Page, L., Tucker, G. S., Weiland, J. L., Wollack, E., & Wright, E. L. 2003, ApJS, 148, 175

Springel, V. & Hernquist, L. 2005, ApJL, 622, L9

Stanonik, K., Platen, E., Aragón-Calvo, M. A., van Gorkom, J. H., van de Weygaert, R., van der Hulst, J. M., & Peebles, P. J. E. 2009, ApJL, 696, L6

Steiman-Cameron, T. 1991, in Warped Disks and Inclined Rings around Galaxies, ed. S. Casertano, P. D. Sackett, & F. H. Briggs, 131–+

Steinmetz, M. & Navarro, J. F. 2002, NA, 7, 155

Stickel, M., Lemke, D., Klaas, U., Krause, O., & Egner, S. 2004, A&A, 422, 39

Stoll, D., Tiersch, H., & Cordis, L. 1997, Astronomische Nachrichten, 318, 149

Stoll, D., Tiersch, H., Oleak, H., Baier, F., & MacGillivray, H. T. 1993, Astronomische Nachrichten, 314, 225

Strateva, I., Ivezić, Ž., Knapp, G. R., Narayanan, V. K., Strauss, M. A., Gunn, J. E., Lupton, R. H., Schlegel, D., Bahcall, N. A., Brinkmann, J., Brunner, R. J., Budavári, T., Csabai, I., Castander, F. J., Doi, M., Fukugita, M., Győry, Z., Hamabe, M., Hennessy, G., Ichikawa, T., Kunszt, P. Z., Lamb, D. Q., McKay, T. A., Okamura, S., Racusin, J., Sekiguchi, M., Schneider, D. P., Shimasaku, K., & York, D. 2001, AJ, 122, 1861

Sulentic, J. W. 1983, ApJ, 270, 417

Sulentic, J. W. & de Mello Rabaca, D. F. 1993, ApJ, 410, 520

Swaters, R. A. & Rubin, V. C. 2003, ApJL, 587, L23

Tago, E., Einasto, J., Saar, E., Tempel, E., Einasto, M., Vennik, J., & Muelle, V. 2007, VizieR Online Data Catalog, 347, 90927

Thakar, A. R. & Ryden, B. S. 1996, ApJ, 461, 55

—. 1998, ApJ, 506, 93

Tiersch, H., Tovmassian, H. M., Stoll, D., Amirkhanian, A. S., Neizvestny, S., Böhringer, H., & MacGillivray, H. T. 2002, A&A, 392, 33

Toomre, A. 1964, ApJ, 139, 1217

Toomre, A. 1977, in Evolution of Galaxies and Stellar Populations, ed. B. M. Tinsley & R. B. Larson, 401–+

Toomre, A. & Toomre, J. 1972, ApJ, 178, 623

Tovmassian, H., Plionis, M., & Torres-Papaqui, J. P. 2006, A&A, 456, 839

Tovmassian, H. M. 2001, PASP, 113, 543

Tovmassian, H. M., Chavushyan, V. H., Verkhodanov, O. V., & Tiersch, H. 1999, ApJ, 523, 87

Tovmassian, H. M., Tiersch, H., Tovmassian, G. H., Chavushyan, V. H., Neizvestny, S., Pramskij, A. G., Torres-Papaqui, J. P., & Rozas, M. 2007, RMxAA, 43, 45

Tremaine, S. 1990, The origin of central cluster galaxies., ed. Wielen, R., 394–405

Tremonti, C. A., Heckman, T. M., Kauffmann, G., Brinchmann, J., Charlot, S., White, S. D. M., Seibert, M., Peng, E. W., Schlegel, D. J., Uomoto, A., Fukugita, M., & Brinkmann, J. 2004, ApJ, 613, 898

Tully, R. B. & Fisher, J. R. 1987, skytel, 74, 612

Valluri, M. & Anupama, G. C. 1996, AJ, 112, 1390

van Driel, W., Combes, F., Arnaboldi, M., & Sparke, L. S. 2002a, A&A, 386, 140

—. 2002b, A&A, 386, 140

Vennik, J., Richter, G. M., & Longo, G. 1993, Astronomische Nachrichten, 314, 393

Vrtilek, J. M., Grego, L., David, L. P., Ponman, T. J., Forman, W., Jones, C., & Harris, D. E. 2002, APS Meeting Abstracts, 17107

Weinmann, S. M., van den Bosch, F. C., Yang, X., & Mo, H. J. 2006, MNRAS, 366, 2

Whitmore, B. C., Lucas, R. A., McElroy, D. B., Steiman-Cameron, T. Y., Sackett, P. D., & Olling, R. P. 1990, AJ, 100, 1489

Whitmore, B. C., McElroy, D. B., & Schweizer, F. 1987, ApJ, 314, 439

Wozniak, H. & Champavert, N. 2006, mnras, 369, 853

Zabludoff, A. I. & Mulchaey, J. S. 1998, ApJL, 498, L5+

Zandivarez, A., Domínguez, M. J. L., Ragone, C. J., Muriel, H., & Martínez, H. J. 2003, MNRAS, 340, 1400

Zavala, J., Okamoto, T., & Frenk, C. S. 2008, MNRAS, 387, 364

Zel'Dovich, Y. B. 1970, A&A, 5, 84

Zepf, S. E. & Whitmore, B. C. 1993, ApJ, 418, 72

Zepf, S. E., Whitmore, B. C., & Levison, H. F. 1991, ApJ, 383, 524

Zwicky, F. 1933, Helvetica Physica Acta, 6, 110